Development of a multi-stage purification process for serum-derived exosomes and evaluation of their regenerative capacity

Candice de Boer

Thesis Presented for the Degree of

DOCTOR OF PHILOSOPHY

in the Department of Surgery

UNIVERSITY OF CAPE TOWN

December 2019

Supervisor: Associate Professor Neil Davies

DECLARATION

I, Candice de Boer, hereby declare that the work on which this dissertation/thesis is based is my original work (except where acknowledgements indicate otherwise) and that neither the whole work nor any part of it has been, is being, or is to be submitted for another degree in this or any other university.

I empower the university to reproduce for the purpose of research either the whole or any portion of the contents in any manner whatsoever.

Signature: Signed by candidate

Date: 2019-12-06

DEDICATION

I dedicate this thesis to my parents. Thanks to my late Dad (Mark), who always believed in me and supported my academic journey. Thanks to my dearest Mom (Catherine), for her endless love, strength, support and encouragement which have inspired me to pursue and complete this research.

ACKNOWLEDGEMENTS

First and foremost, I would like to thank God for His guidance and strength to complete this PhD. It has been a tough project requiring commitment, perseverance and resilience.

I express my immense gratitude to my supervisor, Assoc Prof Neil Davies, for his guidance, wisdom, time and support in navigating this complex research field. Thank you for always being there to give your scientific expertise to approach and solve the challenges that came with the PhD.

I am grateful to the National Research Foundation for financial support and to UCT for the travel grants. I want to thank the Parry Trust for financial assistance, especially in the last year of my PhD.

I would like to thank everyone from the Cardiovascular Research Unit at UCT for a productive work environment, and their friendly smiles and encouragement. Thank you to Helen Ilsley for helping to manage the laboratory, assisting with cell proliferation experiments and processing the histological sections. Special thanks to my lab family, Kyle, Carla, Emma, Ellen and Sli; I appreciate the care and support throughout my PhD, and the coffee and cake breaks.

Thank you to Prof David Marais and Dr Dee Blackhurst from the Division of Chemical Pathology at UCT, for advising me on density gradients and for the permission to use their laboratory for all my density gradient isolations which were paramount for my project. It was tremendous assistance for my PhD research. Dee was so welcoming with a constant kindness and I enjoyed being part of the ‘Purple Lab’ family.

I am grateful to Prof Jonathan Blackburn and Dr Bridget Calder from the Department of Integrative Biomedical Sciences at UCT, for the acquisition of the mass spectrometry data. Thank you to Bridget for also analysing this data.

Thank you to Prof Kathy Myburgh from the University of Stellenbosch, for allowing me to use their NTA machine. I am grateful to fellow exosome researcher, Jason Lovett, for teaching me how to use the NTA and being an understanding sounding board of the difficulties in the exosome field. It was encouraging to be able to discuss the exosome field with fellow South African researchers.

I am grateful to Prof Sandrine Lecour from the Hatter Institute at UCT, for the use of their Lipoprint® System. Thank you to Dr Nicholas Woudberg for conducting the Lipoprint experiment with my samples. I am also thankful to the Hatter Institute for allowing me to use their -80°C freezer.

Thank you to my friends for their continued support and encouragement.

Last but not least, I'm grateful for the support I have received from my family throughout this long journey. I especially thank my sisters, Michelle Thöle-de Boer and Kristy-Lyn Barry, for always being there for me and encouraging me through the difficult times. To my late Dad, Mark de Boer, thank you for being one of my biggest supporters in achieving my academic goals. I know you would be so proud of me and you are with me in spirit. No words can express the love and constant support my precious Mom, Catherine de Boer, has provided me with throughout my life and education. Thank you, Mommy, for having faith in me even when things seemed difficult. Your constant upliftment motivated me to complete my PhD thesis!

TABLE OF CONTENTS

ABBREVIATIONS

ACTN4	alpha-actinin-4
ADAM10	a disintegrin and metalloproteinase domain-containing protein 10
AFM	atomic force microscopy
Ago2	argonaute-2
Alix	programmed cell death 6-interacting protein
APES	3-aminopropyltriethoxysilane
ApoA1	apolipoprotein A1
ApoB	apolipoprotein B
ApoB100	apolipoprotein B100
ApoB48	apolipoprotein B48
BACE1	beta-secretase 1
bFGF	basic fibroblast growth factor
BRCA2	breast cancer gene 2
CAP-1	carcinoembryonic antigen peptide-1
CD5L	CD5 antigen-like
CFSE	carboxyfluorescein succinimidyl diacetate ester
CRISPR/Cas9	clustered regularly interspaced short palindromic repeats/CRISPR associated protein 9
DELFIA	dissociation-enhanced lanthanide fluorescence immunoassay
DEPA	Dose, Efficiency, Purity, Activation
DG	density gradient
DG SEC	density gradient and size exclusion chromatography
DG UC	density gradient and ultracentrifugation
DNA	deoxyribonucleic acid
ECM	extracellular matrix
EDTA	ethylenediaminetetraacetic acid
ELISA	enzyme-linked immunosorbent assay

Eps15	epidermal growth factor receptor substrate 15
ESCRT	endosomal sorting complexes required for transport
EV	extracellular vesicle
FBS	foetal bovine serum
FPLC	fast protein liquid chromatography
GAPDH	glyceraldehyde-3-phosphate dehydrogenase
GC	Golgi complex
GM-CSF	granulocyte macrophage colony stimulating factor
GO	gene ontology
GSK-3β	glycogen synthase kinase 3 beta
GTP	guanosine triphosphate
H&E	haematoxylin and eosin
HdFb	human dermal fibroblast
HDL	high-density lipoprotein
HLA-DR	human leukocyte antigen-DR isotype
HMC-1	human mast cell line-1
HMEC	human microvascular endothelial cells
Hrs	hepatocyte growth factor-regulated tyrosine kinase substrate
HSP70	heat shock protein 70
HUVEC	human umbilical vein endothelial cell
IDL	intermediate-density lipoprotein
IFN-γ	interferon gamma
IGF-1R	insulin-like growth factor-1 receptor
IL	interleukin
ILV	intraluminal vesicle
IMMT	mitochondrial inner membrane mitofilin
IP	immunoprecipitation
ISEV	International Society for Extracellular Vesicles
ISG15	interferon-stimulated gene 15
KBr	potassium bromide

KRAS-MEK	kirsten rat sarcoma viral oncogene homolog-mitogen-activated protein kinase kinase
Lamp2B	lysosome-associated membrane protein 2B
LC-MS/MS	liquid chromatography with tandem mass spectrometry
LDL	low-density lipoprotein
LGALS3BP	galectin-3-binding protein
LMP1	latent membrane protein 1
MAGE3	melanoma-associated antigen 3
MAPK1	mitogen-activated protein kinase-1
Mfge8	milk fat globule EGF factor 8
MHC	major histocompatibility complex
MI	myocardial infarction
miRNA	microRNA
MISEV2014	minimal information for studies of extracellular vesicles 2014
mRNA	messenger RNA
MSC	mesenchymal stem cell
MTA1	metastasis-associated protein 1
MVB	multivesicular body
MVP	major vault protein
MWM	molecular weight marker
NF-κB/STAT3	nuclear factor kappa-light-chain-enhancer of activated B cells/signal transducer and activator of transcription 3
NKG2D	natural killer group 2D
NOTCH1	Notch homolog 1, translocation-associated
NTA	nanoparticle tracking analysis
PBS	phosphate buffered saline
PCR	polymerase chain reaction
PDGF-BB	platelet-derived growth factor-BB
PEG	polyethylene glycol
PGE1	prostaglandin E1
PI3K/Akt	phosphatidylinositol 3-kinase/protein kinase B

PPP	platelet-poor plasma
PRF	platelet-rich fibrin
PROSPR	PRotein Organic Solvent Precipitation
PRP	platelet-rich plasma
PTEN	phosphatase and tensin homologue
PVDF	polyvinylidene difluoride
RECIST	Response Evaluation Criteria In Solid Tumours
RER	rough endoplasmic reticulum
RIPC	remote ischemic preconditioning
RNA	ribonucleic acid
RNAi	RNA interference
RT	room temperature
RT-qPCR	quantitative reverse transcription polymerase chain reaction
RVG	rabies virus glycoprotein
SCID	severe combined immunodeficient
SD	standard deviation
SDCBP	syntenin-1
SEC	size exclusion chromatography
SEM	scanning electron microscope
shRNA	short hairpin RNA
siRNA	short interfering RNA
SMA	smooth muscle actin
STAM	signal transducing adaptor molecule
TBS-T	tris buffered saline-tween
TEM	transmission electron microscopy
TGF-β1	transforming growth factor beta 1
TLR	toll like receptor
TNF-α	tumour necrosis factor alpha
TSG101	tumour suppressor gene 101
UC	ultracentrifugation

UC DG	ultracentrifugation and density gradient
UC DG SEC	ultracentrifugation, density gradient and size exclusion chromatography
VEGF	vascular endothelial growth factor
VEGFR2	vascular endothelial growth factor receptor 2
VLDL	very low-density lipoprotein
Vps4	vacuolar protein sorting-associated protein 4
WPBTS	Western Province Blood Transfusion Service
YAP	yes-associated protein
ZWP	curcuma zedoaria

LIST OF FIGURES

LIST OF TABLES

LIST OF APPENDICES

ABSTRACT

Exosomes are secreted membrane vesicles (30-100 nm) found in tissue culture media and various body fluids that have potential as therapeutics and disease biomarkers. Current literature has reported regenerative benefits for blood-derived exosomes but the majority of these studies purified exosomes using ultracentrifugation (UC), a method that has been found to have high levels of protein contamination. Here the regenerative capacity of exosomes isolated by size exclusion chromatography (SEC), a method shown to reduce protein contamination, from human serum was assessed.

SEC isolates were found to contain suitably sized vesicles and exosomal markers (CD9, CD81 and TSG101). These isolates allowed for cellular uptake of a range of fluorescent labels and enhanced cellular fibroblast proliferation and endothelial sprout formation in a 3D spheroid-based angiogenesis assay. Further to this, functionality was shown to be retained after incubation of the isolates for 21 days at 37°C. Though a promising indication of regenerative potential, it was found that the isolates contained significant levels of ApoB containing lipoproteins (up to 15 µg ApoB/ml). It was shown that these lipoproteins were predominately the very low and intermediate-density lipoproteins.

It was found that low-density lipoprotein can impact exosome uptake studies that use fluorescent nucleic acid, protein and lipid dyes. As a substantial extraneous lipoprotein content could also interfere with other downstream applications and analyses such as proteomic analysis, a multi-step purification method was developed. A simple 3-step density gradient (DG) UC was introduced prior to SEC that incorporated a high-density iodixanol cushion overlaid by a 18% iodixanol step containing UC concentrated human serum that was then overlaid with 6% iodixanol. This DG relied on flotation to remove lipoproteins. After the multi-step purification (UC DG SEC) ApoB and ApoA1 were not detectable by enzyme-linked immunosorbent assay and western blotting respectively. The UC DG SEC isolates were positive for CD9 and TSG101 and morphologically, as viewed by transmission electron microscopy, had the canonical exosome shape and size. Nanoparticle tracking analysis showed that though exosome marker levels were similar, there were 100 times more particles in SEC purified isolates relative to those from UC DG SEC, emphasising the extent of lipoprotein removal.

Proteomic analysis identified 224 proteins in UC DG SEC isolates relative to the 135 from SEC, with substantial increases in exosome-associated proteins and reductions in lipoproteins. The UC DG SEC exosomes still elicited a significant increase in cell proliferation of human dermal fibroblasts but no increase in endothelial sprout formation. After subcutaneous implantation in a rat model, the highly purified exosomes potentially increased an angiogenic response.

In conclusion, we show that serum SEC-derived exosomes with much reduced protein content do have regenerative properties but contain contaminating lipoproteins. Our new isolation technique isolated purer serum exosomes that retained cell proliferation stimulation and potentially enhanced an *in vivo* angiogenic response. This approach should render the isolated exosomes more suitable for biomarker discovery, molecular composition determination and biological function analysis.

CHAPTER 1: LITERATURE REVIEW

1.1 Exosomes

Eukaryotic cells communicate with each other using three types of signalling processes: (1) through direct interaction or through the release of soluble factors in processes such as: (2) paracrine signalling (communication over short distances by the release of these factors) and (3) endocrine signalling (communication over long distances) (Yáñez-Mó *et al.*, 2015). These soluble factors include hormones, growth factors, cytokines and exosomes. Exosomes provide a protective vehicle to transport different biomolecules that include proteins, nucleic acids and lipids. Over the last decade these have begun to be intensively investigated for their capacity to participate in intercellular communication. In 1946, Chargaff and West initially isolated procoagulant membrane-derived vesicles from blood using centrifugation at 31 000 g (Chargaff and West, 1946). Several decades later Wolf referred to this plasma pellet as “platelet dust” due to particles present in the pellet with a diameter of 20-50 nm (Wolf, 1967). In 1983-1984, in studies investigating the differentiation of sheep reticulocytes, vesicles were detected being released by multivesicular bodies (MVBs) which could then fuse with the cell membrane (Pan and Johnstone, 1983, Harding *et al.*, 1984). By 1987, these vesicles of endosomal origin were termed ‘exosomes’ and their initially hypothesised function was to remove non-essential proteins from cells (Johnstone *et al.*, 1987). Almost 10 years later, exosomes from EpsteinBarr virus transformed B lymphocytes were found to elicit a T cell response which suggested a functional role of exosomes in antigen presentation *in vivo* (Raposo *et al.*, 1996). Exosomes started to receive much greater attention from 2007, when messenger RNA (mRNA) and microRNA (miRNA) were detected within them, indicating they assist generally in intercellular communication (Valadi *et al.*, 2007). A recent survey of the literature for English language articles from 2000-2016 using the search terms “exosome” and/or “microvesicle” found that research is increasing exponentially with less than 1% of the 5480 identified papers published in 2000 and more than 20% in 2016 (Roy *et al.*, 2018).

Exosomes are secreted membrane vesicles which are found in body fluids such as blood, urine, saliva and cerebrospinal fluid. Other secreted vesicles include microvesicles, ectosomes, membrane particles, viruses and apoptotic bodies. Exosomes originate from MVBs, whereas the other secreted vesicles derive from the plasma membrane and have larger diameters of 100-1000

nm (Kowal *et al.*, 2014). Exosomes from different cell lines have similar properties in terms of their lipid bilayer (7-9 nm wide), diameter (30-100 nm) and they have densities between 1.13 g/ml-1.19 g/ml (Huang *et al.*, 2015). However, though the above are presently considered characteristic of exosomes, a recent cryo-transmission electron microscopy (TEM)-based study of exosomes derived from a single human mast cell line (HMC-1) of a defined density of 1.12 g/ml found a wide range of morphologies in addition to spherical 40-100 nm vesicles that included vesicles within vesicles, oval vesicles and even tubular vesicles (Zabeo *et al.*, 2017). Similar results have been reported for exosomes from a range of body fluids emphasises both the complexity of them as a class of vesicles and the uncertainties presently associated with them (Yuana *et al.*, 2013, Zonneveld *et al.*, 2014).

1.2 Properties of exosomes

1.2.1 Formation of exosomes

Many mammalian cells engulf a portion of their plasma membrane to form an early endosomal structure that will mature into a MVB (van Niel *et al.*, 2006). Exosomes are the intraluminal vesicles (ILVs) present inside the MVBs that are released by the cell. In brief, there is an inward budding of the cell's membrane forming the endosome. During this process the cell's transmembrane and peripheral membrane proteins become a part of the endosome's membrane. Repeated steps of the inward budding of the endosome results in a MVB containing ILVs and as the endosome matures these ILVs increase in number. Once these vesicles are released into the extracellular space they are termed exosomes (Figure 1.1). An important question is whether only specific MVBs fuse with plasma membrane to release the exosomes or all of them are involved. One study found specific trafficking of MVBs as they showed that cholesterol rich MVBs were preferentially able to fuse with the plasma membrane, detected by immunoelectron microscopy, which resulted in the release of major histocompatibility complex (MHC) class II containing exosomes (Raposo *et al.*, 1996). Further to this, exosome secretion can be controlled and decreased by reducing MVB concentration via ISGylation, which refers to the function of interferon-stimulated gene 15 (ISG15) conjugating to cytoplasmic and nuclear proteins analogous to ubiquitin modification (Villarroya-Beltri *et al.*, 2016). The components responsible for ISGylation in HEK293 cells were overexpressed and the effect on exosome secretion monitored by quantifying exosome markers CD63, tumour suppressor gene 101 (TSG101) and CD81. This

mainly mediated and stimulated the co-localisation of MVBs with lysosomes and activated aggregation and degradation of MVB proteins resulting in the decrease of exosome secretion (Villarroya-Beltri *et al.*, 2016).

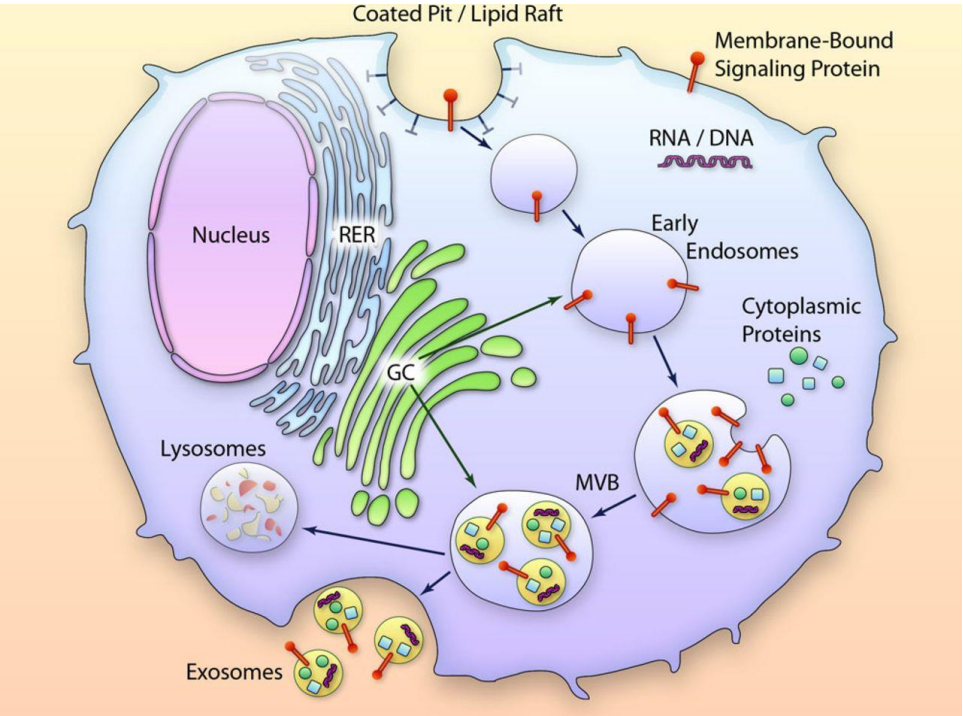

Figure 1.1: Formation of exosomes. Exosomes are formed from late endosomes and bud off from the plasma membrane. GC (Golgi complex); MVB (multivesicular body); RER (rough endoplasmic reticulum). Figure from (Waldenström and Ronquist, 2014) with permission.

The mechanisms involved in exosome biogenesis are not fully understood but the endosomal sorting complexes required for transport (ESCRT) machinery which form four complexes (ESCRT 0, I, II, III) and associated proteins (vacuolar protein sorting-associated protein 4 (Vps4) and programmed cell death 6-interacting protein (Alix)) appear to be important in the process (Colombo *et al.*, 2014). The ESCRT-0 complex recognises and sequesters ubiquitinated proteins to certain domains in the endosomal membrane. These mono-ubiquitinated proteins are identified by hepatocyte growth factor-regulated tyrosine kinase substrate (Hrs) which forms part of another protein complex with signal transducing adaptor molecule (STAM), epidermal growth factor receptor substrate 15 (Eps15) and clathrin (Babst, 2005, van Niel *et al.*, 2006). The ESCRT-I

complex contains TSG101 which is recruited by Hrs to further recognise ubiquitinated proteins. After membrane budding, which appears to be controlled by ESCRT-I and -II complexes, the sequestered cargo is incorporated into the buds. The ESCRT-III complex is recruited through ESCRT-II or Alix, a protein associated with ESCRT. The buds form ILVs and the ESCRT-III complex drives the ILV separation and uses ATPase Vps4 for recycling itself or for more budding (Wollert *et al.*, 2009, Hurley, 2010). There is indirect evidence for the above mechanisms as exosomes isolated from various cell or biofluid sources contain these various ESCRT components and ubiquitinated proteins, such as Alix and TSG101 mentioned, which are regarded as exosome markers (Liang *et al.*, 2013).

There are minimal studies that directly interrogate ESCRTs in exosome biogenesis. One study conducted an RNA interference (RNAi) screen targeting 23 ESCRT components and associated proteins in MHC-II expressing HeLa cells (Colombo *et al.*, 2013). After short hairpin RNA (shRNA) silencing, they trapped the exosomes with anti-CD63 coated beads and quantified them using flow cytometry detecting exosomal markers CD81 and human leukocyte antigen-DR isotype (HLA-DR) (associated with MHC-II). Only 7 ESCRT proteins fell within the criteria that they effected exosome secretion of those containing CD63 and either CD81 or MHC-II. Inhibiting the ESCRT-0 and -I components (Hrs, STAM1 and TSG101) decreased exosome secretion, whereas inhibiting the ESCRT-III component Vps4B increased exosome secretion. The down regulation of Alix resulted in upregulation of MHC-II content and increased the relative amounts of larger exosomes indicative of Alix's involvement in regulation of the nature of exosomes (Colombo *et al.*, 2013). It has also been reported that Alix, syntenin and syndecan control breast cancer cell (MCF-7)-derived exosome secretion as the knock-down of Alix or syntenin inhibited exosome secretion, western blot confirmed reduction in Alix and syntenin coupled with down regulation of syndecan and exosome markers CD63 and heat shock protein 70 (HSP70) (Baietti *et al.*, 2012). These apparent discrepancies between researchers further indicates the complexity of exosome secretion and Alix association and that it may depend on the cell type.

Although research has suggested ECSRT involvement in the biogenesis of exosomes, it is difficult to ascertain the absolute involvement of ESCRT proteins as they have multiple important cellular functions too. For example ESCRT-III and Vps4 are required for the final cell division step in cytokinesis to separate the membranes as depleting ESCRT-III and Vps4 proteins diminishes abscission (Morita *et al.*, 2010).

Complicating matters further, MVBs still form even after the removal of ESCRT subunits (Stuffers *et al.*, 2009) and non-ubiquitinated proteins have become cargo within ILVs (Theos *et al.*, 2006), suggesting there are ESCRT independent mechanisms for exosome biogenesis. For example, ceramide assists exosome biogenesis by initiating the membrane invagination which is helped by its cone-shaped structure (Trajkovic *et al.*, 2008). Tetraspanins associating with cytosolic and transmembrane proteins are suggested to be another possible ESCRT-independent pathway. CD63 is another possible candidate as it has been shown to be involved in the biogenesis of ILVs in melanosomes (van Niel *et al.*, 2011) and in HeLa cells (Edgar *et al.*, 2014) via knockdown. A possible mechanism might be that CD63 could play a role in deforming the membrane to separate the lipid microdomains or by recruiting other ESCRT-independent components (Edgar *et al.*, 2014). The exosome secretion and the movement between membranes relies on Rab GTPases, Rab27a, Rab27b, Rab11 and Rab35 to help release exosomes once the MVB fuses to the plasma membrane (Ostrowski *et al.*, 2010, Blanc and Vidal, 2017).

Although research has illuminated some parts of the process of exosome formation, the precise mechanism of exosome formation and selection of cargo is still unclear. Moreover, the diverse literature highlights how complex exosome biogenesis is, though with the substantial increase in exosome research, it can be hoped that a more detailed understanding into exosome formation will eventually be obtained.

1.2.2 Membrane composition

Exosomes are comprised of a lipid bilayer and studies largely report on the lipids contained within this bilayer; however, it is possible that trace amounts of lipids could be captured within vesicles during ILV formation (Skotland *et al.*, 2019). Ceramides, phosphatidylcholines, phosphatidylserines and sphingomyelins are exosomal lipid components (Haraszti *et al.*, 2016). A recent review of exosome lipid composition found that out of eight studies of cell-derived exosomes, there was a two to three fold increase of cholesterol, sphingolipid, glycosphingolipids, and phosphatidylserine content in exosomes compared to the cells (Skotland *et al.*, 2019). This higher lipid order of exosomes resembles that of lipid rafts, which are lipid dense domains in the plasma membrane that are detergent resistant and contain proteins, suggesting exosomes can be derived from lipid rafts (de Gassart *et al.*, 2003). Research into mesenchymal stem cell (MSC) (Tan *et al.*, 2013) and cancer cells (Staubach *et al.*, 2009) has provided more direct evidence that exosomes can be derived from lipid rafts. The ligands, transferrin and cholera-toxin B chain, that are present in receptor-mediated endocytosis and lipid rafts respectively, were labelled and

tracked in MSCs (Tan *et al.*, 2013). As both labelled ligands were detected within exosomes, this strongly suggests that they are derived from endocytosis that occurs at the lipid raft microdomains in the plasma membrane. For the breast cancer cell line, exosomes were isolated from MCF-7 cells using ultracentrifugation (UC) and the lipid rafts from the exosomes were isolated using affinity purification with a bait protein (MUC1-M2 fusion protein) (Staubach *et al.*, 2009). Mass spectrometry confirmed the presence of the lipid raft proteins (flotillin-1, prohibitin, G protein and annexin A2).

Lipid rafts are suggested to play a role in various cellular functions including signalling, protein/lipid transport and pathogen entry (Munro, 2003). A study supporting this role used synthetic exosome-like nanoparticles to investigate the role of lipids and avoiding the influence of exosome proteins (Beloribi *et al.*, 2012). Synthetic nanoparticles were constructed with lipid formulations of the SOJ-6 human tumour cells as these exosomes, isolated using UC and sucrose density gradient, were previously seen to induce cell death of the SOJ-6 tumour cells (Ristorcelli *et al.*, 2008). Ristorcelli *et al.* speculated that the tumour-derived exosomes may exert their function through autocrine signalling, promoting the phosphatidylinositol 3-kinase/protein kinase B (PI3K/Akt) survival pathway or inducing apoptosis through activation of phosphatase and tensin homologue (PTEN) and glycogen synthase kinase 3 beta (GSK-3β). Beloribi *et al.* found the synthetic exosomes, rich in lipid forming raft microdomains also decreased proliferation of the SOJ-6 cells and the activation of cell death was caused by inhibition of the Notch pathway through interaction with the synthetic exosomes lipid microdomains (Beloribi *et al.*, 2012).

The exosome bilayer membrane is important in protecting the cargo from degradation during circulation through the body (Revenfeld *et al.*, 2014) and the membrane composition of allogenic exosomes may also provide a mechanism to deliver therapeutic drugs as they are not likely to cause an immune response (Wu *et al.*, 2017). It has been suggested that the exosomal membrane is important for signalling to target cells to uptake and fuse with the exosomes (Vishnubhatla *et al.*, 2014). This is a critical area as a key function of exosomes, as mentioned above, is believed to be to allow cells to communicate and interact with one another (Minciacchi *et al.*, 2015). Integral to the communication function is the encapsulation and protection of signals within the lipid membrane and the fusion or engulfment of the membrane (Sahoo and Losordo, 2014). Exosome uptake is thought to occur mainly by endocytosis including micropinocytosis, phagocytosis and receptor/raft mediated endocytosis; direct membrane fusion can also occur (McKelvey *et al.*, 2015). An acidic pH (pH 6.0) might favour the fusion mechanism, as a study showed an increase in cancer-derived exosome release and fusion internalisation at an acidic pH

compared to neutral pH (pH 7.4) when analysed using spectrofluorometry and confocal microscopy with a lipid fluorescent probe (Parolini *et al.*, 2009). Furthermore, bone marrow dendritic cell-derived exosomes have been observed entering other dendritic cells either by endocytosis or fusion with endocytosis detected using exosomes labelled with pHrodo which fluoresced red at phagosome pH and fusion was detected using a de-quenching assay where lipophilic dye R18 was used to label exosomes and once they fused with lipid membranes, fluorescence increased proportionally to fusion (Montecalvo *et al.*, 2012). U87 MG cancer cell-derived exosomes have been shown to be internalised into human umbilical vein endothelial cells (HUVECs) and U87 MG cells using lipid raft-mediated endocytosis, indicated by the inhibition of exosome uptake using either methyl-β-cyclodextrin or simvastatin which reduced cellular membrane cholesterol and intracellular cholesterol respectively (Svensson *et al.*, 2013). Furthermore, internalisation was shown to be regulated by caveolin-1 as determined with caveolin-1 knock out cells.

A major difficulty with determining exosome formation and composition is their apparent complexity. For example, a recent study detected three different types of MSC extracellular vesicles (EVs) ascertained by their differing affinities of their membrane lipids for cholera toxin B chain, annexin V and shiga toxin B subunit (Lai *et al.*, 2016). Confocal microscopy showed the 3 sub-types were derived from various subcellular components with the cholera toxin B chain-, annexin V-, and shiga toxin B subunit-binding EVs detected within the plasma membrane, cytoplasm and nucleus respectively. It has been suggested in one paper that the cholera toxin B chain-binding EVs were considered 'true' exosomes (Lai and Lim, 2019) as they contained the exosome enriched proteins, CD81, CD9, Alix and TSG101 and are derived from endosomes, whereas the other two EV subtypes did not i.e. annexin V EVs were likely from cytoplasmic membrane organelles. Further complexity was shown by the lack of RNA in cholera toxin B chain-binding EVs, which could indicate RNA cargo loading may not involve lipid rafts associated with exosome formation (Lai *et al.*, 2016). However, the shiga toxin B subunit-binding EVs contained 53% of total EV RNA compared to >0.5% for the other two subtypes, inferring nuclear vesiculation may load RNA into EVs. The lack of RNA in the considered 'true' exosomes (cholera toxin B chain-binding exosomes) highlights the discrepancies in exosome research as numerous papers claim the presence of nucleic acids within exosomes (Ohshima *et al.*, 2010, Fernando *et al.*, 2017, Li *et al.*, 2018a) and the various EV subtypes could influence different cellular functions.

The membrane contents of exosomes may also be governed by the extracellular milieu they find themselves in, with urinary exosomes found to contain a higher cholesterol content compared to

PC-3 cancer cell-derived exosomes, which would be expected to confer a greater stability within the biofluid (Llorente *et al.*, 2013, Skotland *et al.*, 2017). It should be noted that a significant issue with studying exosomal lipids is the lack of an optimal exosome isolation method, as any lipid droplets, lipoproteins or mitochondria co-isolated with the exosomes could lead to incorrect conclusions drawn about the lipid content of exosomes. Reports of exosomes containing high cholesteryl ester and/or triacylglycerol concentrations could indicate contaminating lipid droplets are present (van Meer *et al.*, 2008). Biofluids such as plasma have a high content of lipoproteins which may further exacerbate the problem (Simonsen, 2017); however, isolating exosomes from cell culture is also not free from this issue as lipid droplets and mitochondria could leak into the conditioned media used for exosome isolations (Skotland *et al.*, 2019).

Exosomes contain various transmembrane proteins, such as tetraspanins (CD9, CD63, CD81), integrins, lipid raft-associated protein (flotillin), or cell adhesion molecules (Lötvall *et al.*, 2014). Tetraspanins are involved in numerous biological process such as motility, invasion, membrane fusion or regulating cellular signalling (Andreu and Yáñez-Mó, 2014). Some studies have investigated the function of exosome membrane proteins such as tetraspanins. One such study found that modified exosomes with decreased CD9 and increased CD151 content promoted the invasion of prostate RWPE1 cells (Brzozowski *et al.*, 2018). Furthermore, CD63 has been found to regulate the packaging of latent membrane protein 1 (LMP1), which is an Epstein-Barr virus-encoded oncoprotein, into exosomes. LMP1 associates with CD63 for exosome secretion and LMP1 packaging into exosomes requires CD63 as immuno-isolation or clustered regularly interspaced short palindromic repeats/CRISPR associated protein 9 (CRISPR/Cas9) knockout of CD63 lead to a decrease in LMP1 secreted exosomes and LMP1 packaging into exosomes (Hurwitz *et al.*, 2017). Continued investigation of exosome tetraspanins may lead to discerning cellular mechanisms and exosome trafficking to target diseases such as cancer.

1.2.3 Exosomal cargo

Exosomes contain proteins from the cytosol, cellular membrane, endocytic pathway and a scarce amount of proteins coming from the nucleus, rough endoplasmic reticulum (RER) and Golgi complex (GC). Cytosolic proteins enriched in exosomes include membrane transport and fusion proteins (GTPases and annexins), heat shock proteins (HSP70 and HSP90) and proteins involved in creating MVBs (Alix and TSG101) (Kowal *et al.*, 2014, Abramowicz *et al.*, 2018). Exosomes also contain mRNA, miRNA, cytokines and DNA (Huang *et al.*, 2015). A substantial amount of cell-free DNA is located within plasma exosomes (Fernando *et al.*, 2017) and the RNAs are

protected from RNases due to their encapsulation in a cholesterol-rich phospholipid bilayer (Chen *et al.*, 2010b). ExoCarta (http://www.exocarta.org) or Vesiclepedia (http://www.microvesicles.org) list all the proteins and RNAs that have been discovered and reported in exosomes (Tsao *et al.*, 2014).

Part of the cargo present within exosomes seems to depend on the cell source. For example, antigen presenting cells such as macrophages, B cells and dendritic cells will specifically express MHC-II molecules which present the antigen to CD4+ T cells for activation to recruit effector cells, whereas all cells will express MHC-I (except for red blood cells), with variable expression among cell type and influenced by inflammatory conditions, which present peptide antigens to CD8+ T cells (Wieczorek *et al.*, 2017). It has been shown that exosomes secreted from antigen presenting cells include these MHC-II molecules suggesting their role in local immune defence. Human monocyte-derived dendritic cells, classified as an antigen presenting cell, secrete exosomes containing both MHC-I and -II molecules (Admyre *et al.*, 2003, Lynch *et al.*, 2009). Moreover exosomes, isolated using UC and dynabead immunoprecipitation, from human bronchoalveolar lavage fluid contain MHC-II (Admyre *et al.*, 2003); suggesting they were secreted by antigen presenting cells. Furthermore, breast cancer-derived exosomes can transfer metastasis-associated protein 1 (MTA1), expressed in metastatic cells, to promote breast cancer progression by altering the hypoxia and oestrogen receptor signalling environment (Hannafon *et al.*, 2019).

Proteins that are involved during exosome biogenesis may become exosomal cargo, discussed earlier in section 1.2.1, but some of these proteins may also mediate other protein or RNA loading into exosomes. These include ESCRT components and tetraspanins. ESCRT components, TSG101 (Sundquist *et al.*, 2004), Vps4 (Wei *et al.*, 2015), and Alix (Iavello *et al.*, 2016) found within exosomes may control some cargo loading into exosomes. TSG101 binds ubiquitylated proteins during MVB formation (Sundquist *et al.*, 2004) and exosomes have been found to contain ubiquitinated proteins. Fifty ubiquitinated proteins were identified from myeloid suppressor cell-derived exosomes using mass spectrometry and bioinformatics analysis; hence, ubiquitination is another possible cargo loading mechanism (Burke *et al.*, 2014). Using RNAi against Alix resulted in a significant reduction in exosome cargo syndecan, CD63 and HSP70, which suggests its role in packaging certain cargo (Baietti *et al.*, 2012). The lipid membrane of exosomes may also direct protein cargo loading as a study found that reticulocyte-derived exosomal proteins (exosomes isolated using UC and sucrose gradient), Lyn, flotillin-1 and stomatin were associated with the lipid domain (Triton X-100 insoluble fractions) of the exosomal membrane inferring their lipid raft association for being sorted into exosomes (de Gassart *et al.*, 2003). Cytosolic proteins were

found to be randomly engulfed into exosomes by the inward budding of the MVBs membrane (Colombo *et al.*, 2014) but cytosolic proteins such as annexin and Rab may stimulate the fusion of MVB with the cell membrane and the release of exosomes (Beach *et al.*, 2014).

Several lines of research have indicated that particular miRNAs are sorted into exosomes. It has been identified that kirsten rat sarcoma viral oncogene homolog-mitogen-activated protein kinase kinase (KRAS-MEK) signalling controls protein argonaute-2 (Ago2) secretion into exosomes and it was suggested that the regulation of Ago2 controls the secretion of specific miRNAs into exosomes (McKenzie *et al.*, 2016). A deep sequencing approach and analysis of public data including microarray and quantitative reverse transcription polymerase chain reaction (RT-qPCR) arrays found that miR-451 was the most enriched in HEK293T cell-derived exosomes and 6 out of 8 datasets of various cell types, such as dendritic cells, Jurkat J77, Raji and breast cancer cells suggesting that cell lines selectively choose specific RNAs for exosome packaging (Guduric-Fuchs *et al.*, 2012). Gastric cancer cell line AZ-P7a-derived exosomes were enriched in the let-7 miRNA family, whereas other exosomes derived from other cancer lines (lung, colorectal, stomach) were not (Ohshima *et al.*, 2010). Other mechanisms apart from Ago2 for sorting miRNAs into exosomes have been reported. Neutral sphyngomyelinase 2 appears to be involved in directing miRNA into exosomes as up-regulated exosomal miRNA was detected after the overexpression of neutral sphyngomyelinase 2 in a breast cancer cell line (Kosaka *et al.*, 2013). An elegant study showed that a substantial portion of miRNA in exosomes from T-lymphocytes were positive for the short sequence GGAG in their 3' half (Villarroya-Beltri *et al.*, 2013). Further to this, it was found that this sorting due to sequence was dependent on heterogeneous nuclear ribonucleoprotein A2B1 and that sumoaylation (addition of small ubiquitin-like modifiers) of the protein was required.

Researchers have been striving to identify cargo components that would be suitable markers for all exosomes whether cellular or body fluid-derived by identifying a conserved exosome protein. However, this has proved challenging as indicated by discrepancies in literature, for instance, it has been found that CD9 and CD81 were conserved in 4 human prostate cell lines and 5 human breast cell lines (Yoshioka *et al.*, 2013). However, they found TSG101, Rab-5b and CD63 were detected at different concentrations depending on the cell source. In contrast, according to ExoCarta, CD9 (1), CD63 (7), TSG101 (11) and CD81 (24) are amongst the top 25 proteins identified in exosomes, and Rab-5b (86) was not. There are also issues of standardisation in the exosome field as the choice of exosome isolation technique influences mass spectrometry results used to determine exosome cargo (Kowal *et al.*, 2016). One such study compared the proteins

from LIM1863 cancer cell-derived exosomes isolated using UC, density gradient separation, and immunoaffinity capture (Tauro *et al.*, 2012). They found nearly two times higher concentration of Alix, TSG101, CD9 and CD81 using the immunoaffinity capture method. Furthermore, the isolation method can influence the mRNA profile detected from exosomes. Using gene expression microarray profiling, there were very different results for OptiPrep™ density gradient separation, UC and precipitation methods (ExoQuick-TC™) with correlation values as low as 0.40 (Spearman rho-values) (Van Deun *et al.*, 2014). These results highlight the variation and complexity in exosomes both as a consequence of cell source and isolation procedure, which can influence downstream RNA profiling of the exosomes.

MSCs are and have been intensively investigated as therapeutic agents for a wide range of pathologies with more than 600 clinical trials employing MSCs due to their potential therapeutic effects at www.clinicaltrials.gov (Phinney and Pittenger, 2017). It is generally understood at present that any potential therapeutic outcome is largely a consequence of paracrine activity and so their exosomes have received particular attention. The therapeutic use of MSC-derived exosomes will be discussed later in section 1.5 and 1.6.1. The composition of MSC-derived exosomes protein and genetic make-up have been reported in ExoCarta and so far, already 938 genes have been reported (protein, mRNA and miRNA data) (Table 1.1). Some of the MSC-derived exosomes proteins include ribosomal protein S16, histone cluster 1, nidogen 1 and ribosomal protein L23.

The research into exosomes as biomarkers has been extensive over the last 5-10 years and will be very briefly outlined below. There are comprehensive reviews (Properzi *et al.*, 2013, Barile and Vassalli, 2017, Nedaeinia *et al.*, 2017, Huang and Deng, 2019). Although less proteins have been identified in plasma and serum-derived exosomes compared to MSC-derived (Table 1.1), their cargoes are also of great interest due their potential to be biomarkers as a result of their high concentration in body fluids and their stability (Jabalee *et al.*, 2018). There are reported potential EV miRNA biomarkers in body fluids such as plasma (miR-21 and miR-1246 for human breast cancer (Hannafon *et al.*, 2016), miR-103a-3p and miR-30e-3p for malignant pleural mesothelioma (Cavalleri *et al.*, 2017), miR-122-5p and miR-300-3p (detected in rats) for transient ischemic attack (Li *et al.*, 2018a)); serum (miR-141 for prostate cancer (Li *et al.*, 2016c), miR-200b and miR-200c for epithelial ovarian cancer (Meng *et al.*, 2016), miR155 for human hematologic malignancies (Caivano *et al.*, 2017)) and urine (miR-21-5p for urothelial carcinoma (Matsuzaki *et al.*, 2017)). Furthermore, plasma EVs may have the potential to diagnose glioblastoma due to their substantially higher concentration in patients, detected using nanoparticle tracking analysis

(NTA), which significantly decreased after tumour removal (Osti *et al.*, 2019), strongly suggesting the viable tumour cells released substantial numbers of exosomes into the plasma. A recent study further highlighting the potential of plasma exosomes as biomarkers showed that plasma exosomes from patients with pancreaticobiliary cancers contained a significant portion of tumour DNA with multiple mutations detected such as Notch homolog 1, translocation-associated (NOTCH1) and breast cancer gene 2 (BRCA2) (San Lucas *et al.*, 2016). These studies highlight the importance of analysing the cargo within blood-derived exosomes to understand the function of exosomes as well as finding novel biomarkers for diseases. Exosome cargo can also be indicative of their functional activity with proteins such as HSP70 being implicated in cardioprotection (Vicencio *et al.*, 2015) (see section 1.7.4.1).

Table 1.1: Number of exosome genes (protein, mRNA and miRNA data) detected in various sources and reported in ExoCarta as of January 2019

Source of exosomes	Number of genes reported in ExoCarta
Mesenchymal stem cell	938
Plasma	214
Serum	119

1.3 Exosome isolation methods

1.3.1 Ultracentrifugation

UC was originally seen as the 'gold' standard to isolate exosomes. In 2016, UC had been used by 81% of researchers (Gardiner *et al.*, 2016). Multiple centrifugation steps are used to separate particles according to their buoyant density (Contreras-Naranjo *et al.*, 2017, Konoshenko *et al.*, 2018). Large particles with a buoyant density higher than exosomes such as cells, apoptotic bodies, larger vesicles, cell debris, are removed initially with a standard centrifugation (<20 000 g). UC is then used to isolate exosomes at (100 000-200 000 g) for 1-3 hours. The rotor type, centrifugation time, viscosity of the sample and k factor will affect the outcome of the isolation (Momen-Heravi *et al.*, 2012, Cvjetkovic *et al.*, 2014). The time of UC is important as UC of HMC-1 cell conditioned media in a Type 70 Ti fixed angle, showed that 70 minutes didn't isolate all the exosomes and 4 hours resulted in contaminating soluble proteins in the exosome pellet

(Cvjetkovic *et al.*, 2014). As biofluids are more viscous than cell culture media they can be diluted to improve isolation efficiency. The disadvantages of UC include the high centrifugation speeds, long isolation time and the protein contamination (Table 1.2) (Baranyai *et al.*, 2015). In proteomic research, co-isolation of protein aggregates and proteins is a major issue. Exosomes can be further purified by either repeated UC, sucrose density gradient, or microfiltration with pores <0.45 µm. However, additional purification steps result in a decrease in exosome yield (Théry *et al.*, 2006, Konoshenko *et al.*, 2018).

1.3.2 Precipitation

In 2016, precipitation had been used by 14% of researchers (Gardiner *et al.*, 2016) and increased in 2017 to 26.4% (Konoshenko *et al.*, 2018). Polyethylene glycol (PEG) is a volume-excluding polymer used to exclude the particles from the solution by decreasing its solubility. This method is modified from viral studies (Leberman, 1966). The polymer solution is mixed and incubated with the samples; which are subsequently pelleted down at 1500 g and resuspended in phosphate buffered saline (PBS) (Abramowicz *et al.*, 2016). There are numerous commercially available exosome isolation kits which are based on using PEG precipitation: ExoQuick™ (System Biosciences), Exo-spin™ (Cell Guidance Systems), Total Exosome Isolation reagent (Invitrogen), ExoPrep (HansaBioMed), Exosome Purification Kit (Norgen Biotek) and miRCURY Exosome Isolation Kit (Exiqon). Commercial isolation kits are less time consuming, do not need an UC, have a physiological pH range and are simple to use (Contreras-Naranjo *et al.*, 2017). For a more economical option, PEG 6000 can be used which gives similar results to commercial reagents when miRNAs were studied in serum exosomes (Andreu *et al.*, 2016).

A major drawback is that PEG is not specific to isolating exosomes; contaminating proteins, protein aggregates and other particles are also isolated (Lobb *et al.*, 2015). Particle purity is calculated by the ratio of particle number to protein concentration (Webber and Clayton, 2013). Studies have shown precipitation has a high concentration of particles; however, the particle purity is low due to the contaminants present (Baranyai *et al.*, 2015). Contaminants are more abundant when isolated from plasma due to the excess albumin present. Precipitation is lower in particle purity compared to UC even though UC yields a low concentration of particles (Lobb *et al.*, 2015). It has been shown that UC isolates were more enriched for serum and cell culture-derived exosome markers than those precipitated using commercial kits (ExoQuick and TEI) even though particle concentration was lower, as determined by NTA and protein concentration (Tang *et al.*, 2017). Yet another study found that UC had more albumin contamination and less exosomes than

ExoQuick (Caradec *et al.*, 2014). These differences are due to the different UC methods implemented. The second study only used one UC spin with a 30% sucrose cushion, whereas the first study used two UC spins which removed more contaminating proteins; however, the yield of exosomes decreased. Further purification steps appear to be required when using PEG precipitation.

1.3.3 Filtration

Filtration is often used before other exosome isolation methods (UC or size exclusion chromatography (SEC) see section 1.3.6) to remove cells and large EVs. The filters are either polyvinylidene difluoride (PVDF) or polycarbonate with a pore size ∽50-450 nm (Muller *et al.*, 2014, Contreras-Naranjo *et al.*, 2017). Contaminating plasma protein concentration decreases when filtration (0.2 µm) or SEC is used with UC (Muller *et al.*, 2014). Ultrafiltration, using 100 kDa or 10 kDa filters, has been explored to isolate exosomes free from protein contamination without having to use UC. The disadvantage of using ultrafiltration is that exosomes can become trapped in the filter, or shear, as well as the filter becoming clogged (Liga *et al.*, 2015). Hence, filters have a short lifespan and can lead to a decrease in exosome concentrations or increased unplanned contamination (Table 1.2).

Centrifugal filters can be used to concentrate exosomes or the biofluid before exosome isolation. There are various pore sizes and membrane types. A study compared five centrifugal filters when concentrating exosomes isolated using SEC from plasma or urine (Amicon Ultra-2 10k (Merck Millipore), Amicon Ultra-2 100k (Merck Millipore), Vivaspin 2 PES 10k (Sartorius Stedim Biotech GmbH), Vivaspin 2 CTA 10k (Sartorius Stedim Biotech GmbH) and Vivaspin 2 Hydrosart 10k (Sartorius Stedim Biotech GmbH)) (Vergauwen *et al.*, 2017). The 10 kDa regenerated cellulose membrane filters (Amicon 10k RC) isolated the highest yield (±3.6x10^{12} particles/ml) of exosomes. The 100 kDa Amicon filter decreased the exosome concentration compared to the 10 kDa; however, the other membranes had substantial loss of 80% and the particle loss was even higher than that for the 100 kDa Amicon filter.

1.3.4 Density gradients

Density gradient centrifugation is a popular isolation method technique and the gradient can be created in two ways: continuous density gradient (density increases gradually from the top either formed by centrifugation or beforehand) or discontinuous density gradient (density increases in discrete steps) (Konoshenko *et al.*, 2018). After a long high-speed centrifugation, the particles

separate according to their densities. The floatation density of exosomes is 1.1-1.2 g/ml (Théry *et al.*, 2006, Li *et al.*, 2017b) and either sucrose or iodixanol density gradients (OptiPrep) can be used. Reports have found that an OptiPrep gradient separates exosomes from viruses better than sucrose (Cantin *et al.*, 2008). OptiPrep density gradient UC isolates a purer concentration of exosomes than by either UC alone or the ExoQuick and Total Exosome Isolation precipitation methods (Van Deun *et al.*, 2014). They showed the density gradient isolated exosomes had an increase in exosome markers (Alix, HSP70, TSG101 and CD63), a decrease in contaminating proteins (extracellular Ago2 complexes) and a specific mRNA profile related to cellular functions. Their gradient was discontinuous ((40% (4 ml), 20% (4 ml), 10% (4 ml), 3.5% (3.5 ml)) and 1 ml of conditioned cell culture media was overlaid. A gradient is usually spun for >18 hours and >100 000 g at 4°C which is time consuming and the high velocity of UC may rupture the EVs (Van Deun *et al.*, 2014). Another study found that adding a density gradient after UC and miRCURY kit of human serum removed the contaminating human serum proteins; however, even with increasing the total protein the exosome markers (CD81 and TSG101) were not detected using western blotting (Buschmann *et al.*, 2018) again indicating loss due to multiple step isolations. Actually, a potential drawback for density gradients alone is a low yield of exosomes, where a 5-40% OptiPrep density gradient isolated only 0.3 µg of exosomes from 10^6 Rab27B-expressing MCF-7 cells compared to 0.7 µg using UC and 5 µg using precipitating agents (Van Deun *et al.*, 2014). It is to be noted, that the density gradient would have isolated purer exosomes resulting in a lower protein concentration. Overall the disadvantages of density gradients are the low yield of exosomes, long isolation time, laborious method and potential loss of exosomal biological function (Table 1.2).

1.3.5 Immunoaffinity purification

Affinity purification selectively isolates exosomes using exosome related antibodies attached to differing devices (enzyme-linked immunosorbent assay (ELISA) plates, immuno beads and microfluidic plates) (Abramowicz *et al.*, 2016). A microfluidic device such as the immuno-chip captures the exosomes based on their surface markers (Chen *et al.*, 2010a). There are a set of micro-channels engraved into a structure designed to separate and specifically isolate the exosomes. The first immuno-chip using CD63 isolated and purified exosomal RNA within 1 hour using 100-400 µl of serum. The RNA extracted was enough for potential use in diagnosing tumour cancer. A low cost approach that has been developed is ExoChip, a microfluid device made from polydimethylsiloxane with CD63 antibodies (Kanwar *et al.*, 2014). The exosomes were quantified using a plate reader after being stained with fluorescent carbocyanine dye and had an exosome

protein yield of 15-18 μg and 10-15 ng of total nucleic acids. This device has potential for diagnosing cancers as there was a significant increase in fluorescence from five pancreatic cancer patients compared to five healthy patients. Microfluidics has the potential in clinical settings to diagnose diseases based on quickly characterising their exosomes. However, though these devices are useful for analysing exosomes containing specific proteins they are not necessarily suitable for broader based exosome research which concern applies to any immune-based approach.

Immunoprecipitation (IP) is a widely used small scale immunoaffinity technique for isolating biological agents through precipitation of a solid phase attached to the targeting antibody. An early study directed at exosome purification was the isolation of B-lymphocyte-derived exosomes by targeting human MHC-II (Clayton *et al.*, 2001) with anti-MHC-II antibodies attached to paramagnetic beads. Subsequently, the isolated exosomes were analysed by flow cytometry and were found to contain immunological molecules MHC class-I and II, B7.1 (CD80) and B7.2 (CD86) and ICAM-1 (CD54), as well as B cell marker CD20 and CD59 membrane attack complex-inhibitory protein. The expression of CD59 may indicate a possible role of antigen present cell-derived exosomes in complement regulation. As shown above, bead-based isolations can be analysed by flow cytometry to quickly quantify binding achieved using fluorophore conjugated antibodies or the isolates can be denatured and studied by immunoblot (Théry *et al.*, 2006). Exosome attached beads can also be embedded in resin and sectioned for analysis by TEM.

IP has been used to enrich exosomes, derived from the brain, to provide a potential biomarker for neurological disorders to allow for possible detection and treatment (Mustapic *et al.*, 2017). The study first used ExoQuick to precipitate the exosomes followed by IP targeting neuronal surface markers (neural cell adhesion molecules, NCAM and L1CAM) or control CD81 on plasma exosomes. Analysis using immuno-TEM showed IP was specific as the isolated L1CAM exosomes had less CD81 present, whereas the CD81 isolated exosomes had an increase in CD81. The neuronal-derived EVs enriched from plasma contained increased concentrations of signalling components compared to plasma EVs which may provide insight into possible biomarkers or therapeutic treatments. In 2017, 1.9% original research papers used IP for isolation of exosomes (Konoshenko *et al.*, 2018). The disadvantages of IP are the cost, problems eluting the exosomes from the beads whereby the elution can damage the function of exosomes, low yield, only specific exosomes isolated and also the potential of non-specific binding (Konoshenko *et al.*, 2018) (Table 1.2).

1.3.6 Size exclusion chromatography

By 2014 it became apparent that UC, or density gradient UC, isolated contaminating proteins and protein complexes (Yuana *et al.*, 2014). SEC separates molecules according to size using a porous stationary phase (variable pore sizes available). Small molecules such as soluble proteins will spend time passing through the pores, whereas wider molecules such as exosomes will elute first without entering the pores. Sepharose CL-4B or -2B have been used to isolate exosomes from blood plasma (Baranyai *et al.*, 2015), saliva (Ogawa *et al.*, 2008) and urine (Lozano-Ramos *et al.*, 2015). An early study in 2014 suggested that SEC was an effective single-step exosome isolation method, briefly they loaded 1.5 ml of platelet-free supernatant from platelet concentrates on a 10 ml Sepharose CL-2B and collected 0.5 ml fractions (Böing *et al.*, 2014). Their results showed SEC fractions 9-12 had the highest concentration of vesicles bigger than 70 nm (Figure 1.2A) as well as platelet-derived exosomes detected using CD61. They also found these fractions had <5% of high-density lipoprotein (HDL) (Figure 1.2B) and <1% of protein. The majority of HDL was found in fractions 18-20 and proteins in fractions 19-21. An Exo-spin kit is a commercial kit combing precipitation and SEC, in which the SEC bed volume is 500 µl with bead pore sizes of 30 nm and up to 100 µl sample can be loaded. The Exo-spin blood kit was inferior to SEC when analysing the proteins in plasma exosomes using mass spectrometry (de Menezes-Neto *et al.*, 2015). This was due to numerous plasma proteins present in an Exo-spin exosome preparation. Their report also supported the use of SEC as a stand-alone method and using mass spectrometry identified possible markers for plasma exosomes (CD5 antigen-like (CD5L) and galectin-3-binding protein (LGALS3BP)).

Ultrafiltration-SEC isolated more HEK293T cell culture exosomes than using UC, as determined with NTA and western blotting of exosome markers Alix and CD9 (Nordin *et al.*, 2015). The structural integrity and biological activity of exosomes after SEC makes it a good candidate for therapeutic use, plasma exosomes were isolated from 0.5-1.0 ml plasma loaded on a 10 ml Sepharose 2B column and the plasma exosomes from acute myeloid leukaemia cancer patients inhibited NKG2D expression which is important for protecting cells by playing a role in anti-tumour immune responses (Hong *et al.*, 2016). Furthermore, head and neck squamous cell carcinoma plasma exosomes decreased proliferation of T cells which is important for immunity. Hence, SEC allows for functional analysis of plasma exosomes particularly for clinical application.

Sepharose CL-4B and Sephacryl S-400 columns have been shown to isolate plasma exosomes whereby the exosome markers (CD9 and CD81) were present in the peak before plasma proteins

such as albumin eluted (Baranyai *et al.*, 2015). SEC columns are reproducible, relatively inexpensive, remove ~95% of plasma proteins and are quick to use compared to UC. A drawback is that the exosomes are diluted which may require ultrafiltration to concentrate them (Baranyai *et al.*, 2015) (Table 1.2). However, as mentioned above it has been shown that centrifugal filters such as Vivaspin 2 PES 10k, Vivaspin 2 CTA 10k and Vivaspin 2 Hydrosart 10k lead to a 80% loss of exosomes isolated from plasma or urine (Vergauwen *et al.*, 2017). Furthermore, concentrating the plasma SEC exosomes using either Exo-spin precipitant or UC decreases the particle purity by exosome loss (Welton *et al.*, 2015). Another commercial column qEV (Izon) was shown to isolate purer plasma exosomes as compared to those isolated with a density gradient, ExoQuick and Exo-spin with ExoQuick having the least pure exosomes due to low particle purity calculated by particles per µg of protein indicating contaminating proteins present (Lobb *et al.*, 2015). Co-isolation of lipoproteins in the size range around 40 or 75 nm and above when using SEC has been recently reported to be an issue (Sódar *et al.*, 2016, Vergauwen *et al.*, 2017, Karimi *et al.*, 2018). This aspect will be discussed in Chapter 3. Interestingly, Sepharose 2B even though having a larger pore size was found to have greater albumin contamination of SEC isolated plasma exosomes, whereas Sepharose CL-4B or Sephacryl S-400 columns isolated purer plasma exosomes without significant albumin contamination (Baranyai *et al.*, 2015). Upscaling SEC may be challenging as no increase in plasma exosomes was detected when a 120 ml Sephacryl S-400 column was used compared to their 10 ml SEC columns.

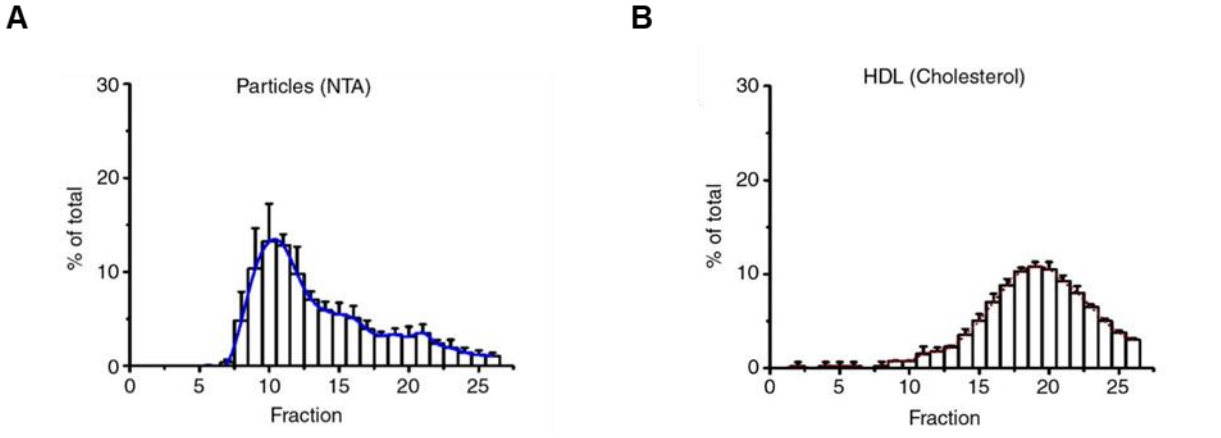

Figure 1.2: Presence of vesicles and HDL lipoproteins per SEC fraction of platelet-free supernatant from platelet concentrates separated on a Sepharose CL-2B column. (A) Vesicles (larger than 70 nm) measured by NTA; (B) HDL cholesterol concentration. Figure modified from (Böing *et al.*, 2014) with permission.

Table 1.2: Advantages and disadvantages of common exosome isolation techniques

Exosome isolation techniques	Advantages	Disadvantages
Ultracentrifugation	No expensive reagents needed, can accommodate large volumes of fluid to isolate exosomes	Expensive equipment needed, long isolation time, protein contamination, high-speed centrifugation could lead to exosome damage
Precipitation	Less time consuming, no expensive equipment needed, simple to use	Not specific to exosome isolation, co-isolation of contaminating proteins, low purity, requires pre- and post-purification steps
Filtration	Decreases protein contamination, simple to use, centrifugal filters can concentrate exosomes	Exosomes can become trapped in the filter, filter clogging, exosomes can shear, increasing filtration steps decreases exosome concentration, unplanned contamination
Density gradients	Purer exosomes as contaminating proteins removed	Low yield of exosomes, long running time, laborious method
Immunoaffinity	Simple, fast, isolates specific exosomes, purer exosomes	Expensive reagents, difficulty eluting the exosomes from the solid phase resulting in low yield or damage, potential of non-specific binding, only subset of exosomes isolated
Size exclusion chromatography	Retains exosomal structural integrity and biological activity, reproducible, relatively inexpensive, minimal protein contamination, quick, simple to use	Exosomes are diluted, co-isolated lipoproteins, difficult to optimise scale up, only one sample processed in one column run

Modified from (Li *et al.*, 2017b).

1.4 Characterising exosomes

As discussed above, all the exosome isolation methods have drawbacks and currently there is no "gold standard method" to isolate pure exosomes. The International Society for Extracellular Vesicles (ISEV) provides researchers with a set of minimal experimental requirements to identify the presence of exosomes to ascertain their specific composition and function (minimal information for studies of extracellular vesicles 2014 (MISEV2014); updated in 2018 (MISEV2018)) (Lötvall *et al.*, 2014, Théry *et al.*, 2018). When reporting a study, the exosome

isolation method used should be described in detail, the characteristics of the exosomes should be clearly displayed and examined. Although exosomes do not have definitive markers they have been found to be enriched in certain biomolecules and together with other techniques their isolation is confirmed based on their biophysical and molecular properties. In 2014, ISEV suggested that a minimum of 2 different characterisation methods be used to identify exosomes (Lötvall *et al.*, 2014). Western blotting, ELISA, flow cytometric analysis, electron microscopy, RT-qPCR, NTA and atomic force microscopy (AFM) are some of the popular techniques used to identify and characterise exosomes. In 2016, the 3 most commonly used exosome characterisation methods were western blotting (74%), particle tracking (72%) and electron microscopy (60%) (Gardiner *et al.*, 2016). About a third of publications report 3 characterisation methods with only 12% of researchers using 5 or more methods. The guidelines for nomenclature, collection and pre-processing of fluids for EV extraction, EV preparation and concentration, EV characterisation, functional studies and reporting were revised and updated which are found in MISEV2018 (Théry *et al.*, 2018). EV-TRACK (http://evtrack.org/) encourages researchers to upload their published and unpublished experiments to assist in standardising EV research.

1.4.1 Electron microscopy

In general, electron microscopy (either transmission or scanning) will reveal the presence, size and morphology of vesicles obtained using various exosome isolation methods. However, electron microscopy is not quantitative due to the variability of vesicles attaching to the grid for visualisation and the numerous and variable steps involved in sample preparation (Turchinovich *et al.*, 2015). Multiple electron micrographs can be taken to measure the average diameter of the exosomes, which should reveal a diameter between 30-100 nm. When using TEM with negative staining the exosomes will have a cup-shaped morphology (Figure 1.3A), opposed to when using cryo-electron microscopy where they are round vesicles (Figure 1.3B) (Conde-Vancells *et al.*, 2008, Banizs *et al.*, 2014). It must be considered that the cup-shaped morphology could be due to an exosome collapsing during TEM preparation (Banizs *et al.*, 2014). Considering the literature on electron microscope analysis of exosomes, it is apparent that results vary in terms of diameter and morphology of exosomes. For example, TEM analyses have revealed that serum-derived exosomes isolated using ExoQuick are spherical and 30-100 nm (Jia *et al.*, 2017), 293T cell-derived exosomes isolated using Exosome Isolation Kit (Invitrogen) are spherical and 40-120 nm, whereby the exosome pellet was fixed in 2.5% glutaraldehyde prior to TEM analysis (Li *et al.*, 2016a) and porcine reproductive and respiratory syndrome infected cell-derived exosomes isolated using PEG precipitation and CD63 IP, are cup-shaped and 30-150 nm (Wang *et al.*,

2018c). Thus, it is challenging to interpret and compare different research studies. It may be accounted by different exosome isolation methods, differing methods to prepare the micrograph grids, and possibly selective imaging and publishing of micrograph grids. One study found differences when they used four different TEM protocols which are commonly used in the exosome field that varied with fixation, absorption and negative staining methods (Rikkert *et al.*, 2019). They found only one method that had similar images (comparable and reproducible) when either the image location was either selected by the operator or was at a predetermined location, this method used 400 mesh carbon coated copper grids, absorption of 2 minutes, blotting for washing and 2% uranyl acetate for <2 min. Hence, standardisation is required for TEM protocols for grid preparation and image selection. For both TEM and AFM, ISEV suggests capturing a wide field image containing numerous EVs and a close-up image of single EVs to allow the analyses of the entirety of the isolate (Lötvall *et al.*, 2014, Théry *et al.*, 2018). A further complication, is if the exosome isolates are not pure, it is difficult to identify the difference between proteins, exosomes, lipoproteins and other EV subtypes using TEM (Simonsen, 2017). A possible alternative method is visualising the EVs using immunogold TEM to reveal the presence of exosome-enriched transmembrane proteins such as CD9 and CD81 (Gurunathan *et al.*, 2019).

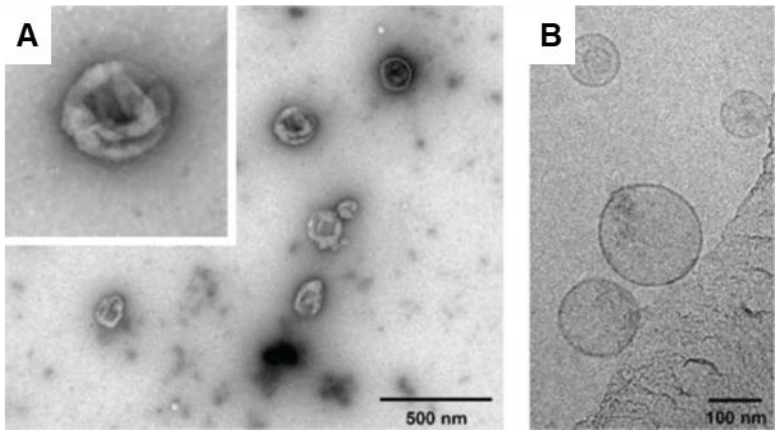

Figure 1.3: TEM analysis of primary endothelial cell-derived exosomes. (A) Classic TEM showing cup-shaped vesicles, inset of a collapsed exosome; (B) Cryo-electron microscopy showing circular membrane bound vesicles. Figure modified from (Banizs *et al.*, 2014) with permission.

1.4.2 Enzyme-linked immunosorbent assay and western blot

Due to exosomes budding off from endosomes they contain integrins and tetraspanins (e.g. CD9, CD63 and CD81), membrane transport and fusion proteins (e.g. annexins, flotillin and Rab GTPases), proteins needed for MVB biogenesis (Alix and TSG101) and heat shock proteins (HSP70 and HSP90) needed for cellular processes (Yu *et al.*, 2014). Moreover, they have lipid-related proteins and raft lipids (e.g. cholesterol, ceramide, phospholipases and sphingolipids). ELISA and western blot are commonly used to identify the presence of enriched proteins in an exosome sample. Most research groups use western blotting with anti-CD63, anti-CD9, anti-CD81 and anti-HSP70 antibodies to confirm exosome isolation where the size of the bands should be about 53, 28, 26 and 53-70 kDa respectively (Lai *et al.*, 2010). There are commercial exosome ELISA kits available to quantify exosomes such as ExoQuant™ Exosome ELISA Kit (BioVision), ExoELISA-ULTRA CD63 (System Biosciences) and ExoAssay™ Human Plasma Overall Exosome ELISA Kit for CD9 (Creative Diagnostics®). One group developed their own sandwich ELISA (Exotest) to quantify exosomes in plasma using CD63 and Rab-5b (Logozzi *et al.*, 2009). Their study showed CD63 positive melanoma-cell derived exosomes were detected in a dose-dependent manner as the exosome concentration increased from 3.1 µg to 50 µg. The Exotest only required a minimum of 3 µg of exosome protein which was more sensitive than the western blot which required 12.5 µg of exosomes. However, there are major differences in exosome protein content using different purification protocols and a high exosome protein yield may indicate contaminants, discussed earlier (Section 1.3).

ISEV recommend a minimum of 3 proteins to be detected and they should come from different categories such as transmembrane proteins (CD9, CD63 and CD81) and cytosolic proteins (TSG101, annexins and Rabs) (Lötvall *et al.*, 2014). ISEV also suggests that the proteins from cell culture-derived exosomes should be compared to the cell's proteins to detect the enrichment of markers after exosome isolation. A negative protein marker control is used to confirm the absence of cellular proteins not found in exosomes, such as calnexin, in exosome samples. However, this is not possible for body fluid-derived exosomes due to the variety of cells secreting exosomes. ISEV suggests the antibody details (company name, catalogue number, dilution), exposure time and SDS-PAGE conditions should be reported (Lötvall *et al.*, 2014). Western blotting or ELISA have issues in representing the actual quantity of exosomes isolated, as any co-isolated exosome proteins will also be detected. Furthermore, they will not differentiate between microvesicles and exosomes (Tauro *et al.*, 2012). This again highlights the need for a specific exosome marker to be discovered.

1.4.3 Flow cytometry

Flow cytometry is a method used to reproducibly analyse the varying physical and chemical characteristics of cells using analysis of the scatter of laser light and concomitant emitted fluorescent light. Ideally flow cytometry relies on the analysis of a single cell at a time but particles less than 300 nm cannot be detected by conventional flow cytometry (van der Pol *et al.*, 2010). The latter necessarily limits the analysis of exosomes and therefore indirect measurement of exosomes captured on microbeads is performed. Exosomes can be captured relatively non-specifically on aldehyde containing beads (Suárez *et al.*, 2017) or through beads coated with exosome markers such as anti-CD9. The beads containing exosomes are then stained with fluorescently labelled detector antibodies (Wiklander *et al.*, 2018). Using a capture antibody approach is inherently more precise but also has the potential for greater bias. Flow cytometry especially with a multiplex approach allows for significant information but the use of beads does introduce variability and can only be semi-quantitative in nature. A major and very recent advance is through the use of imaging flow cytometry which promises to allow for detection of single exosomes across the entire range of sizes (Mastoridis *et al.*, 2018). Though a significant advance, the method requires dedicated specialised equipment and still needs standardisation with regards to issues such as differential forward scattering by exosomes, low intensity fluorescence of single exosomes and for “swarming” to contaminate data (Welsh *et al.*, 2017).

1.4.4 Quantitative PCR

RT-qPCR due to its great sensitivity is the technique of choice for quantifying the miRNA present in exosomes. It is used to monitor the changes in exosomal miRNA levels in patients, animal models and cell culture media. The exosomal cargo does change depending on the parent cell and the environmental condition the cells are in. For example, radiation induced changes in 9 out of 214 plasma exosome proteins and significantly increased the concentration of miR-204-5p, miR-92a-3p and miR-31-5p (Yentrapalli *et al.*, 2017). Numerous miRNAs such as miR-16, miR-24, miR-26a, miR-451 and let7e have been detected in exosomes using RT-qPCR (Schageman *et al.*, 2013). A much-discussed concern with respect to RT-qPCR-based quantification of miRNA in exosomes is the lack of consensus on normalising the PCR output. Presently, the most accepted approaches are complex and involve application of a global mean or identification of stably expressed miRNAs through the use of specialised algorithms (Thorsen *et al.*, 2017).

1.4.5 Nanoparticle tracking analysis

NTA is a method used to determine the size and concentration of exosomes isolated from cell culture media or biological fluids. The measurement is based on the properties of the laser light scattering on particles experiencing random Brownian motion. The exosomes are tracked by recording a video of their movements and their hydrodynamic radius is calculated by their mean squared displacement and the data is shown as a distribution graph (Soo *et al.*, 2012). Specificity and sensitivity of NTA can be improved by either fluorescently labelling the general exosome population with CellMask Orange™ (Carnell-Morris *et al.*, 2017) or using fluorescently labelled antibodies (Oosthuyzen *et al.*, 2013). NTA has detected the size of bone marrow stromal cell and multiple myeloma cell-derived exosomes to range from 50-250 nm (Wang *et al.*, 2014). These diameters were larger than the diameter of the cup-shaped exosomes measured by TEM (50-80 nm). A reason for this could be that NTA has a lower sensitivity for particles between 20-60 nm. Another study using NTA had similar results, also detecting larger diameters (mean 175 nm) for adipose tissue MSC-derived exosomes (Katsuda *et al.*, 2013). In 2016, NTA was the most commonly used particle analyser (80% of researchers) followed by 18% using tunable resistive pulse sensing and 12% using dynamic light scattering (Gardiner *et al.*, 2016). NTA results should also be analysed with caution as a previous study detected the majority of plasma exosomes isolated using a large scale Sephacryl S-400 SEC column appeared in a different fraction using NTA (fraction 4, ±85-105 ml) as compared to their western blot detection of exosome markers CD63 and TSG101 (pooled fraction 1-3, ±40-85 ml), which it was speculated was due to NTA being unable to accurately detect particle diameters less than 70 nm (Baranyai *et al.*, 2015). Another major drawback of non-fluorescent NTA is its inability to distinguish between synthetic nanoparticles, protein aggregates, lipoproteins and EV subtypes including exosomes (Gercel-Taylor *et al.*, 2012). Furthermore, one study showed 1-12% coefficient of variation of sequential NTA readings of the same sample within one day and 2-25% coefficient of variation of day-to-day readings of EVs and artificial vesicles with the same operator and machine (Vestad *et al.*, 2017). They also detected significant variation in NTA results between two instruments from different laboratories using the same software settings. These findings highlight the need for standardising NTA analysis.

1.4.6 Atomic force microscopy

AFM is a quantitative and sensitive nanoscale method used to characterise exosomes. It has only recently begun to be utilised as in 2016 only 9% of researchers used AFM (Gardiner *et al.*, 2016).

This method can characterise the exosomes' shape, size and density. A 3D image is created without using electron dense staining, fixation or extreme temperatures that normal electron microscopes use (Sharma and Gimzewski, 2012). Biological fluid-derived particles from plasma (Yuana *et al.*, 2010) and exosomes from human saliva (Palanisamy *et al.*, 2010) have been analysed using AFM. The saliva-derived exosomes revealed a flattened donut-like shape in a 3D image, and had a diameter of 65 nm and a height of 2.5 nm (Palanisamy *et al.*, 2010), correlating to previously mentioned TEM findings for exosomes. The plasma analysis revealed spherical microparticles with a range of 10 to 475 nm and mean diameter of 67.5 nm ±26.5 (Yuana *et al.*, 2010). After 0.22 µm filtration the mean diameter was 37.2 nm ±11.6. The study did not investigate the proportion of exosomes present in the microparticle population. A drawback of AFM is the slow scan speed and cost. Additionally, image analysis of AFM results is also tedious requiring a standard linear regression subtraction, Labview IMAQ to locate the vesicles and a background subtraction calculation to create a flatter surface (Ashcroft *et al.*, 2012).

1.5 Function of exosomes

The physiological function of exosomes is an undoubtedly complex subject that is constantly evolving as research progresses. The initial hypothesis was that exosomes were involved in waste management allowing for removal of unwanted proteins (Johnstone, 1992). Currently exosomes are known to be involved in paracrine signalling and integral to the communication function is their lipid membrane which protects the signalling cargo (Sahoo and Losordo, 2014). In the last decade, the role of exosomes in cell to cell communication have been studied with respect to influences on physiological and pathological processes, such as immune response, angiogenesis, therapeutic regeneration and pathology.

1.5.1 Immune function

The role of exosomes in immune responses have been explored and been recently and thoroughly reviewed in (Wu *et al.*, 2019b). It is difficult to tell that exosomes are the driving entities of cellular physiology and pathology with the present technology. Exposure to magnetic iron oxide nanoparticles has been shown to cause a dose-dependent increase in exosome release into the alveolar region of BALB/c mice which quickly circulated into the immune system resulting in a maturation of dendritic cells and activation of splenic T cells, implicating exosomes in immune activation (Zhu *et al.*, 2012). It was suggested that the MHC-I, MHC-II and CD80 detected on the

exosomes may have assisted in the immune defence mechanism. Further to the *in vivo*-based study on exosome involvement in immunity discussed above, *in vitro* studies support this immunity involvement. Human breast milk-derived exosomes may play a role in immune modulation, as a functional *in vitro* assay (enzyme-linked immunospot assay) showed they inhibited cytokine production of IL-2, interferon gamma (IFN-γ), and tumour necrosis factor alpha (TNF-α) which was induced by anti-CD3 blocking T cell activation in peripheral blood mononuclear cells (Admyre *et al.*, 2007). Removing both CD81 and MHC-II exosomes decreased the inhibition of IL-2 production showing that the exosomes were contributing to the inhibition; however, they couldn't rule out the possible effect of co-isolated soluble milk proteins. Furthermore, peripheral blood mononuclear cells incubated with 500 μg/ml milk-derived exosomes increased specific T regulatory cells, which may have suppressed the effector T cells to release cytokines. T and B lymphocytes have a key role in cell-mediated immunity, the antigen presenting cells (such as B cells or dendritic cells) present the antigens bound onto MHC-I or MHC-II complexes to the T cells for an immune response (Germain and Margulies, 1993). It has been shown that human and mouse B-cell derived exosomes carry these peptide-MHC-II complexes for antigen presentation to CD8+ and CD4+ T cells (Raposo *et al.*, 1996, Segura *et al.*, 2007). Exosomes derived from cancerous and non-cancerous amniotic fluid also have potential immunomodulatory capacities. A study showed the exosomes to be internalised into human monocytic THP-1 cells which activated secretion of inflammatory cytokines IL-1β, TNF-α, and IL-6 (Bretz *et al.*, 2013). Analysis of phosphorylation revealed stimulation of nuclear factor kappa-light-chain-enhancer of activated B cells/signal transducer and activator of transcription 3 (NF-kB/STAT3) mediated cytokine release via a toll like receptor (TLR)-dependent signalling pathway.

1.5.2 Angiogenic function

Angiogenesis is a vital part of healing and reproduction (Otrock *et al.*, 2007). Platelet-derived EVs have been detected at sites of angiogenic sprouts, vessel sprouts composed of endothelial cells which are activated in response to angiogenic stimuli, in mice which underwent hypoxia-induced retinal neovascularisation and may deliver pro-angiogenic components (Rhee *et al.*, 2004). Endothelial progenitor blood cell-derived exosomes have been reported to stimulate angiogenesis *in vivo* (Deregibus *et al.*, 2007). Severe combined immunodeficient (SCID) mice injected subcutaneously with human microvascular endothelial cells (HMEC) (pretreated with 30 μg/ml exosomes for 30 minutes at 37°C) in Matrigel, formed vessels after 7 days whilst untreated HMEC did not. Here horizontal mRNA transfer was the proposed mechanism as RT-qPCR detected mRNA within the exosomes, which is associated with PI3K/Akt signalling pathway that is linked

to the angiogenic response. It should be noted that HMEC treated with exosomes exposed to RNAse also did not form vessels. In light of the present knowledge that the contents of exosomes are protected from RNAses, it is not immediately clear how this abrogation of the angiogenic effect occurred. There is a fairly substantial body of *in vitro* evidence supporting the involvement of exosomes in angiogenesis. Using a real-time cell imaging system, it has been seen that placental MSC-derived exosomes help placental HMEC migrate after a scratch wound assay (Salomon *et al.*, 2013). The exosomes increased the tube formation as the oxygen concentrations decreased (hypoxia). Another experiment also used a cell invasion assay which showed that adipose MSC EVs increased the invasiveness of HMEC and promoted *in vitro* vessel-like structures (Lopatina *et al.*, 2014). It was further found that adipose MSCs stimulated with platelet-derived growth factor-BB (PDGF-BB), but not vascular endothelial growth factor (VEGF) and basic fibroblast growth factor (bFGF) increased exosome release with pro-angiogenic molecules such as stem cell factor which improved their angiogenic response. It has also been shown that cardiosphere-derived cell exosomes induced tube formation in a HUVEC angiogenesis assay, moreover, they stimulated angiogenesis to a greater extent than normal human dermal fibroblast (HdFb) exosomes (Ibrahim *et al.*, 2014). In the same study it was also shown that neonatal rat cardiomyocytes had greater proliferation with cardiosphere-derived cell exosomes as well as decreased apoptosis.

1.5.3 Cardiac function

Myocardial infarction (MI) is a worldwide problem causing death and heart failure. It affected 7.6 million Americans in 2015 (Mozaffarian *et al.*, 2015). Heart attack or MI is most commonly caused by a blood clot and MI refers to the damaged heart muscle. Exosomes have been shown to partake in remote ischemic preconditioning (RIPC), which is phenomenon where brief ischemia events in a remote tissue can protect the target organ from ischemia injury. Exosomes may also decrease cardiac dysfunction and remodelling. The damage caused by a MI (Enoki *et al.*, 2010) or diabetic cardiac disease (Huynh *et al.*, 2010) can be protected by cardiac activation of insulin-like growth factor-1 receptor (IGF-1R). Serum-derived exosomes from rats that underwent RIPC contained a high concentration of IGF-1R protein (Yamaguchi *et al.*, 2015). IGF-1R was also expressed in the remote non-infarcted myocardium and skeletal muscles of the hindlimbs. Their *in vitro* study revealed that hypoxic conditions (which occur during an ischemic event) increased the concentration of IGF-1R in C2C12-derived exosomes and not in the cell lysates. Overall, their results indicate that exosomes may have transferred IGF-1R from the hindlimb into the cardiomyocytes. Plasma exosomes are suggested to be cardioprotective, the study isolated

human plasma exosomes before and after male volunteers underwent RIPC, which involved four cycles of 5 min upper limb ischemia and 5 min reperfusion (Liu *et al.*, 2015). They assessed for *in vitro* cardioprotection whereby rat ventricular cardiomyocytes underwent 2.5 hours of simulated ischemia and 1 hour simulated reperfusion and the plasma exosomes were administered either 30 minutes or 24 hours before hypoxia. Their findings showed that control or RIPC exosomes were able to elicit *in vitro* cardioprotection acutely or after 24 hours. The lack of difference between the control and RIPC exosomes may be due to their varied particle dosage, ~1.06×10^7 control exosomes and 1.80×10^7 RIPC exosomes as equal volumes were used in the experiment. Further literature on the regenerative properties of cell and blood-derived exosomes will be discussed in section 1.6.1 and 1.7.4 respectively.

1.5.4 Pathological function

Not all exosomes have therapeutic benefits as tumour cells appear to release exosomes to assist in tumour growth (Whiteside, 2016). It was reported that mouse melanoma cells secreting tumour-derived exosomes primed a bone marrow environment to transform into a melanoma environment using a MET receptor (Peinado *et al.*, 2012). In addition, tumour-derived exosomes were found to inhibit maturation of dendritic cells and human monocytes *in vitro*, and *in vivo* though tumour-derived exosomes caused less inhibition of bone marrow dendritic cell differentiation in IL-6 knockout mice, suggesting a relationship between tumour exosomes and IL-6 in bone marrow dendritic cell differentiation (Yu *et al.*, 2007). There are studies that suggest that exosomes can alter cellular phenotypes by interacting with surface receptors. Tumour-derived exosomes promoted the metastatic phenotype of primary tumours using the MET-receptor on bone marrow progenitor cells (Peinado *et al.*, 2012). Exosomes also play a role in diseases such as neurodegeneration (prion, Alzheimer's and Parkinson's disease) and harbour neurodegenerative-associated proteins (prion protein, β-amyloid and α-synuclein) (Vella *et al.*, 2016). Microparticles, 100-1000 nm vesicles released from cells undergoing cellular activation and apoptosis, are also suggested to contribute to a variety of disease states, reviewed in (Bebawy *et al.*, 2013). Though pathological in nature, these findings do reinforce the understanding that EVs function as cell-to-cell communication vehicles.

In summary, exosomes derived from cultured cells, blood and other biofluids have various functional properties. It should be noted that above are indirect evidence of physiological and pathological functions. The inability to knockout or overexpress exosomes, or directly modify their contents *in vivo* is a clear limitation in gaining direct evidence for their roles. Understanding the

mechanisms of exosomes also remain challenging as most research relies on a mixed population of exosomes to determine their function. A very recent paper suggested a way forward to overcome some of these issues through the development of an *in vivo* model using zebrafish embryos to track individual exosomes (Verweij *et al.*, 2018). They developed a CD63-pHluorin reporter which is a fluorescent tetraspanin-based pH-sensitive reporter that targets late endosomes, labelling exosomes for detection. Using this reporter, they live tracked individual exosomes and observed a large exosome release from the yolk syncytial layer into the blood stream which was regulated by syntenin as shown through knock-down. Furthermore, they found the exosomes were internalised by macrophages and endothelial cells for lyosomal degradation near the tail using high-speed imaging. This technique could be used to examine more directly exosome function *in vivo* (Verweij *et al.*, 2019).

1.6 Source of therapeutic exosomes

Exosomes have been isolated from many cell types that include dendritic cells, cancer cells, stem cells, endothelial cells, B cells, T cells, tumour cells, mast cells and neurons (Tsao *et al.*, 2014, Huang *et al.*, 2015). They are also isolated from almost all body fluids inclusive of blood, saliva and urine. Though exosome studies have been dominated by cell culture-based approaches due to their potentially more defined nature, there is increasing interest in those from body fluids, mainly due to their promise as biomarkers but also more recently for their possible therapeutic effects. MSCs have been most extensively studied for application in regenerative medicine, thus they were focused on.

1.6.1 Cell culture exosomes

MSCs and their secretome has been extensively reviewed as a possible therapy to treat human diseases (Salgado *et al.*, 2015, Konala *et al.*, 2016, Cunningham *et al.*, 2018). Bone marrow culture was where MSCs were first discovered (Friedenstein *et al.*, 1976). These stem cells can be obtained from various species and tissues (adipose, bone marrow, dental pulp and umbilical cord). They are heterogeneous in shape (spindle shaped to cuboidal), have plastic adherence and express markers such as Sca-1, CD105, CD73, CD29 and CD90 (Konala *et al.*, 2016). MSCs are adult stem cells which are capable of self-renewal and differentiation into various cell types such as adipocytes, chondrocytes and osteoblasts (Pittenger *et al.*, 1999). They can be used in autologous or allogeneic stem cell transplants as they are suggested to be hypoimmunogenic

(Beyth *et al.*, 2005) and have been widely explored in regenerative-based therapeutic strategies. The initial hypothesis was that their ability to differentiate was behind therapeutic effects observed in tissues such as the heart and brain but it has become clear that a paracrine effect is responsible (Fitzsimmons *et al.*, 2018). Human MSC-conditioned media has been found to be effective for MI (Timmers *et al.*, 2008), liver (Van Poll *et al.*, 2008) and kidney injuries (Zarjou *et al.*, 2010). In 2008, conditioned media from human embryonic stem cell-derived MSCs decreased infarct size by 60% in pig and mouse models of myocardial ischemia/reperfusion injury (Timmers *et al.*, 2008). Their fractionation studies identified the cardioprotective component was 50-200 nm in size. In 2010, the cardioprotective component was identified as exosomes determined by TEM and enrichment of exosome markers Alix, CD9 and CD81 (Lai *et al.*, 2010). These MSC-derived exosomes were then shown in mice suffering from an ischemia/reperfusion injury to reduce myocardial injury. A follow up study showed that mice suffering from ischemia/reperfusion injury had decreased levels of misfolded proteins when treated with MSC exosomes indicated a possible mechanism for their cardiac protection (Lai *et al.*, 2012). Exosomes derived from MSCs had proteasome subunits and the 20S proteasome was detected using mass spectrometry. The 20S proteasome may contribute toward the cardiac therapeutic benefit of MSC-derived exosomes as their function is to breakdown oxidatively damaged proteins; which correlated with the fact that misfolded proteins are reduced in mice suffering from a myocardial ischemia/reperfusion injury when injected with MSC-derived exosomes.

There are some studies that investigated the regenerative potential of exosomes derived from cells other than MSCs. It has been demonstrated that cardiomyoctyes that had undergone simulated ischemia and reperfusion when preincubated with 10^8/ml preconditioned HUVEC-derived exosomes, had significantly decreased apoptosis from 88% ±4 to 55% ±3 (Davidson *et al.*, 2018b). Ischemic preconditioning of the HUVECs (hypoxic chamber for 30 minutes) increased exosome concentration three times to control HUVEC-derived exosomes. Cardioprotection needed ERK1/2 MAPK signalling pathway, shown by inhibition using PD98059 and U0126. Dendritic cell-derived exosomes have seen to promote migration of MSCs through a transwell system in a dose dependent manner (10 µg and 50 µg exosomes) and through a 2D chemotaxis chamber (10 µg exosomes) (Silva *et al.*, 2017). However, their analysis revealed dendritic-cell derived exosomes did not influence MSC proliferation or differentiation.

It has been shown that MSCs can secrete more exosomes than other cells (myoblast and human embryonic kidney cell line), as determined with CD81 ELISA to detect the relative exosome concentration secreted after 3 days by various cell lines (Yeo *et al.*, 2013). The MSC-derived

exosomes express adhesion molecules from their MSC parent cell (CD44, CD73 and CD90) as well as the common surface markers (CD9 and CD81) (Ramos *et al.*, 2016). There have been attempts to compare the therapeutic effects of MSC-exosomes to MSCs, such as in a rat MI model (Bian *et al.*, 2014) and mice with brain ischemia (Doeppner *et al.*, 2015), where they show similar regenerative effects. A recent study has indicated that exosomes from different MSC are not identical. Bone marrow- and umbilical cord-derived MSC exosomes inhibited cell proliferation and caused apoptosis of glioblastoma cells *in vitro* whilst adipose tissue-derived MSC exosomes increased cell proliferation and had no effect on cell survival of glioblastoma cells (Del Fattore *et al.*, 2015).

Exosomes also play a role in the niche function of different stem cells. MSC-derived exosomes from multiple myeloma patients increased multiple myeloma cell growth *in vitro* and promoted tumour growth in SCID mice more than those from normal patients (Roccaro *et al.*, 2013). Fluorescent exosome internalisation studies confirmed the multiple myeloma MSC-derived exosomes were secreted and transferred to the multiple myeloma cells. The multiple myeloma MSC-derived exosomes contained a decreased concentration of tumour suppressor miR-15a and an increased concentration of oncogenic cytokines and proteins compared to those from healthy MSC-derived exosomes. It has also been found that healthy limbal stromal (eye) cell-derived exosomes increase wound healing, migration and proliferation of limbal epithelial cells in healthy and diabetic corneas relative to diabetic limbal stromal cell-derived exosomes (Leszczynska *et al.*, 2018). Western blot analysis identified increased Akt phosphorylation in the wounded limbal epithelial cells and organ-cultured corneas treated with the healthy exosomes which may have promoted the wound healing. Next generation sequencing revealed small RNA differences in the diabetic exosomes versus the healthy exosomes which may have brought about the diseased niche.

It should be noted that cell culture conditions are of necessity not optimal as a potential contributor of contamination within cell culture-derived exosomes is foetal bovine serum (FBS), due to its own EVs and lipoproteins. Researchers tend to use FBS that has been ultracentrifuged for 18 hours at 100 000 g to remove the exosomes. However, FBS RNA could still interfere with RNA analysis of exosomes (Wei *et al.*, 2016b). Using serum-free conditions also poses problems as the cells may stop growing and enter apoptosis which could influence exosomes released (Sluijter *et al.*, 2018).

1.6.1.1 Clinical trials with cell-derived exosomes

The move towards therapeutic use of exosomes in clinical trials has grown due to increasing evidence on the benefits of exosomes. Dendritic cell-derived exosomes can induce T cell responses and tumour rejection as the exosomes contain MHC-I and MHC-II (Pitt *et al.*, 2016, Liu *et al.*, 2017a). From 2000 to 2002 the first phase I clinical trial used exosomes derived from autologous dendritic cells. Each of the 15 patients suffering from stage III/IV melanoma received 4 exosome vaccinations intradermally and subcutaneously over one month (Escudier *et al.*, 2005). The exosomes were pulsed with melanoma-associated antigen 3 (MAGE3) peptides, which tumours express, to immunise the patients. Only one patient had a slight response when using the Response Evaluation Criteria In Solid Tumours (RECIST). This phase I trial showed that the exosomes were safe to use as no MAGE3 specific CD4+ and CD8+ T cell immune reaction was detected. Furthermore, autologous dendritic cell-derived exosomes have also been administered to patients with non-small cell, lung cancer (Morse *et al.*, 2005). The dosage was the same where 4 injections were given at weekly intervals. The exosomes were also loaded with tumour antigens MAGE-A3, -A4, -A10 and -3DPO4 peptides. In contrast to Escudier *et al.* the results showed that 1/3 of the patients had a MAGE specific T cell response. Some patients also did not have the cancer spread while undergoing treatment.

Another phase I clinical trial subcutaneously injected autologous ascites-derived exosomes four times at weekly intervals to 40 patients with colorectal cancer (Dai *et al.*, 2008). Granulocyte macrophage colony stimulating factor (GM-CSF) was used as an adjuvant together with the exosomes. Their results showed that the exosomes alone are immunogenic; however, only the exosomes with the GM-CSF promoted an anti-tumour specific cytotoxic T lymphocyte response specific for carcinoembryonic antigen peptide-1 (CAP-1) (20% response exosome alone versus 76.9% exosome plus GM-CSF). Hence, ascites-derived exosomes with GM-CSF adjuvant could be used as a vaccine. This is a potential immunotherapy method to treat colorectal cancer and it is safe and viable.

The market of exosome diagnostics and therapeutics is expected to increase from $16.1 million in 2016 to $111.8 million in 2021 (Tcherpakov, 2016). Moreover, USA grants by National Institutes of Health (NIH) increased by 201% from 2000 to 2016 for research done on exosomes or microvesicles (Roy *et al.*, 2018). Interestingly blood as the source reflects over 93% of the market share (Tcherpakov, 2016) but this most likely reflects the immense amount of research directed towards finding exosome biomarkers for diagnosing diseases such as cancer. A crucial question

now is how to standardise exosome isolations to allow clinical trials to proceed with more defined preparations of exosomes.

1.6.2 Blood

1.6.2.1 Regenerative plasma and platelet-rich plasma

Serum and plasma samples are commonly investigated for biomarking potential as blood is easy to collect and process. Serum and plasma samples are processed differently after blood collection (Liu *et al.*, 2018a). Serum is generated by allowing the blood to clot at room temperature (RT) for about 30-60 minutes and may contain coagulation enhancers. A clots forms which removes the majority of the fibrinogen and platelets which have either activated or attached to the clot (Lundblad, 2005). Plasma blood collection tubes contain materials to prevent coagulation (Liu *et al.*, 2018a). There is also increasing evidence that blood may contain components that have regenerative potential function (Villeda *et al.*, 2014, Wyss-Coray, 2016, Sun *et al.*, 2019). Perhaps one of the more dramatic indications of this is the range of studies that have shown that blood plasma from young mice can reverse cardiac hypertrophy and cognitive dysfunction in aging mice, though it must be emphasised that these benefits were accrued after extensive periods of parabiosis (Pusic and Kraig, 2014). A further broad indication of this potential is the extensive research into the use of platelet-rich plasma (PRP) in regenerative approaches. PRP contains a high concentration of platelets in a small volume of plasma and once these platelets are activated they release a pool of proteins, growth factors, cytokines and exosomes (Anitua *et al.*, 2015). Plasma isolations use higher centrifugations speeds compared to PRP e.g. 1000-2000 g for 1 minutes to remove cells, followed by 2000 g for 15 minutes to remove majority of the platelets. PRP methods vary; however, they all use “soft spins” compared to plasma isolation e.g. 180 g for 10 minutes to centrifuge the blood, followed by 890 g for 10 minutes to centrifuge the plasma and obtain the platelet concentrate i.e. PRP, which is the lower 1/3rd fraction (Etulain *et al.*, 2018). The platelets are enriched in growth factors which are important for wound healing initiation (Marx, 2004).

Human PRP has the potential to treat late stage cerebrorenal syndrome which is associated with acute kidney injury and ischemic stroke. A late stage cerebrorenal syndrome rat model was injected with 80 µl PRP via left common carotid artery and abdominal aorta followed by acute kidney ischemia-reperfusion and acute ischemic stroke (Yip *et al.*, 2019). At day 28, PRP treated rats showed protection in the brain and kidney through inhibition of inflammation as well as

improved neurological function and decreased expression of brain-related DNA, mitochondrial damage and oxidative-stress biomarkers and; improved renal function, increased podocyte components and decreased collagen deposition and fibrosis.

PRP is being studied in clinical trials for various regenerative purposes in therapeutic targets as wide-ranging as ulcer wounds, tendon injuries, cosmetic purposes, scar healing and hair loss (Alves and Grimalt, 2018). One study using freeze-dried PRP together with a gelatin sheet showed an ulcer wound had substantially epithelised (phase 1, randomised controlled single-center trial) (Lin *et al.*, 2019). The gelatin hydrogel allowed for a sustained release of the PRP. Interestingly, PRP (1 ml) has been found to have a more pronounced affect than MSCs (3×10^6 cells in 1 ml) on wound healing suppressed by corticosteroid in rats after 10 days (Aydin *et al.*, 2018).

PRP has been used to treat various musculoskeletal indications, especially for tendon pathologies caused by sport injuries (Kon *et al.*, 2011). A randomised blinded phase 1 clinical study enrolled 36 patients for intraoperative injection of control or PRP for acute Achilles tendon rupture repair (Zou *et al.*, 2016). The PRP patient group had significantly better isokinetic muscle at 3 months and increased Short Form-36 and Leppilahti scores (protocol for evaluating outcome) at 6 and 12 months. At 24 months, PRP patient group had significantly improved ankle range of motion. A level I, meta-analysis of level I studies showed that intra-articular injection of PRP for knee osteoarthritis compared to hyaluronic acid and saline, significantly improved the function and pain relief at 1 year (Dai *et al.*, 2017). The study included 10 randomised control trials (1069 patients). It has recently been found that there was no difference in using PRP compared to platelet-poor plasma (PPP) in a phase 1 trial on patients with chronic plantar fasciitis (Malahias *et al.*, 2019). Both treatments yielded significant improvement after 6 months following PRP or PPP injection, relative to baseline control.

For a cosmetic dermatology application, a clinical trial (phase 1) enrolled 4 healthy patients for assessment of the histological changes induced in human skin by 0.5 ml PRP-fibrin matrix injection into the human deep dermis and immediate subdermis (Sclafani and McCormick, 2012). Histology results revealed collagen deposition, activated fibroblasts by day 7, angiogenesis and adipose tissue formation by day 19. Another application of PRP is for the treatment of scars (Alser and Goutos, 2018). A split-face trial (phase 1) was carried out in 14 Korean patients with acne scars who received ablative CO_2 fractional resurfacing for removal of damaged skin (Lee *et al.*, 2011). One side of the face was injected with PRP and the other side received saline. The PRP

treated side had significantly decreased erythema at day 4 and oedema time (6.1 ±1.1 versus 7.1 ±1.5 days) and crusting (5.9 ±1.1 versus 6.8 ±1.0 days) was also significantly reduced on the PRP treated side. After four months the overall clinical improvement was significantly greater. However, there are discrepancies in clinical trials using PRP for scar treatments. Another phase 1 clinical trial found significant clinical improvement after fractional surfacing; however, there was no difference between the control (no PRP) and PRP topical treated side (Kar and Raj, 2017). They do justify the use of PRP as it significantly reduced the redness, swelling and pain associated with the fractional surfacing.

PRP treatment has also been considered for hair loss such as that occurring in androgenetic alopecia. One clinical trial (phase 1) enrolled 23 male patients with hair loss and injected PRP (0.1 ml/cm^2) to one side of the affected area of the head and placebo control to the other half, one treatment every 30 days for 3 months (Gentile *et al.*, 2015). The PRP treated side had a significant increase of 33.6 in the mean number of hairs and 45.9 hairs/cm^2 increase in mean total hair density, as well a tiny significant increase in angiogenesis around the hair follicles. Although, a recent meta-analysis of pooled results from seven studies with 194 patients revealed no significant increase in hair number or hair thickness between patients administered with PRP (Giordano *et al.*, 2018). The authors suggest this is due to the lack of controlled clinical trials and standardised protocols.

The proposal of using standardised terminology to ascertain how the PRP is derived, may lead to a better understanding of the data. In 2009, four PRP classifications defining the leucocyte and fibrin content was suggested: 1. pure-PRP (no leucocytes and a low concentration of fibrin after activation), 2. leucocyte-PRP (leucocytes are present and a low concentration of fibrin after activation), 3. pure platelet-rich fibrin (PRF) (no leucocytes and a high concentration of fibrin forming an activated gel), 4. leucocyte-and PRF (leucocytes are present and a high concentration of fibrin forming an activated gel) (Dohan Ehrenfest *et al.*, 2009). In 2016, another proposed classification was DEPA (Dose, Efficiency, Purity, Activation) which includes defining the platelet concentration used (Magalon *et al.*, 2016).

The regenerative potential of PRP is considered to be caused by the supra-physiological concentrations of growth factors (Qian *et al.*, 2017). Platelets have also been found to release exosomes (Heijnen *et al.*, 1999, Aatonen *et al.*, 2014, Tan *et al.*, 2016). This raises the possibility of obtaining a more concentrated and defined bioactive component from blood for potential use in regenerative therapies. This will be discussed further in sections 1.7.3 and 1.7.4.

1.6.2.2 Blood-derived exosomes

Blood-derived exosomes are easily accessible which makes them more appealing in clinical applications. Blood-derived exosomes are slightly more complex to study due to the various cells contributing to the exosomes present but it is estimated that roughly two thirds of circulating exosomes in human peripheral blood are derived from platelets (Hunter *et al.*, 2008). Other cells such as erythrocytes, endothelial cells and leukocytes can also secrete exosomes in differing quantities (Gyorgy *et al.*, 2014). One study investigated the cell source of plasma-derived exosomes from normal mice or those suffering from sleep fragmentation (Khalyfa *et al.*, 2016). The cell source of the exosomes was identified by expression of the various cell markers on the exosomes i.e. CD41 for platelets (absence of CD45 and CD144), CD45 for leukocytes (additionally CD115 for monocytes) and CD144 for endothelial cells (additionally CD34 for progenitor endothelial cells) using flow cytometry. There was a significant increase in the concentration of exosomes from sleep fragmented mice from platelet-derived cells (22 100 versus 13 017), progenitor endothelial-derived cells (7 308 versus 5 300) and monocyte-derived cells (10 832 versus 7 782). However, there was no significant difference in exosome content from other leukocyte-derived cell sources. Exosomes are isolated from both plasma and serum (Vicencio *et al.*, 2015, Chen *et al.*, 2018b) and serum is expected to have more platelet-derived exosomes than plasma (Tao *et al.*, 2017a). There are roughly 3 000 000 exosomes per µl of serum (Vlassov *et al.*, 2012); however, the presence of contaminating lipoproteins could be influencing this number (Sódar *et al.*, 2016). This confounding issue in exosome research will be discussed in Chapter 3.

Exosomes from blood plasma have been isolated using various techniques such as differential centrifugation combined with UC (Kalra *et al.*, 2013), epithelial cell adhesion molecule immunoaffinity pull-down, OptiPrep density gradient separation (Cavallari *et al.*, 2017) and recently SEC (Böing *et al.*, 2014); which can cause variability in data obtained from various exosome research groups. In a comparative study, where out of 213 proteins only 30 common proteins were identified in all three isolation techniques (density gradient, UC and epithelial cell adhesion molecule-based immunoaffinity pull-down) (Kalra *et al.*, 2013). Furthermore, as with MSC exosomes, there is a variability among proteins found within plasma exosomes. Two studies have shown only 59 plasma exosomal proteins being commonly identified during isolation using mass spectroscopy e.g. HSP70, transferrin, transferrin receptor, ubiquitin B, and ubiquitin C (Bastos-Amador *et al.*, 2012, Kalra *et al.*, 2013). Kalra *et al.* had 147 unique proteins compared to 44 proteins for Bastos-Amador *et al.* (Kalra *et al.*, 2013). This variability is likely linked to the

different exosome isolation methods used, Bastos-Amador *et al.* used UC to isolate plasma EVs, whereas Kalra *et al.* used a density gradient as they found UC and epithelial cell adhesion molecule immunoaffinity pull down isolated contaminating plasma proteins.

The miRNA within blood-derived exosomes has gained immense attention in the research field, with human plasma and serum-derived exosomal miRNA having the potential to be biomarkers for diseases such as esophageal squamous cell cancer, cardiovascular disease, breast cancer, lung cancer, prostate cancer and ovarian cancer; discussed earlier in section 1.2.3. It has been shown that the exosome isolation method could influence the miRNA profile of serum exosomes as different clusters of miRNAs were detected with the isolation method significantly affecting miR-92a and miR-486-5p levels, although, the most common miRNAs were still similar between the ExoQuick and UC exosome isolation methods used (Rekker *et al.*, 2014). Again, this highlights the need for optimised exosomes isolation methods particularly for blood-derived sources. Research has also illuminated the fact that blood-derived exosomes have regenerative properties which will be discussed later in section 1.7.4.

1.7 Exosome-based therapeutics

As exosomes, at least in part are designed to deliver effectors to cells, it is not surprising that extensive research is being devoted to determining their potential as therapeutic agents. Due to the paracrine mechanism through which MSC are believed to achieve their therapeutic outcome, the majority of analysis is devoted to their exosomes though exosomes from other cell sources has received attention. Furthermore, recently there has been increasing research into the regenerative capability of blood-derived exosomes. The latter will be discussed in depth at the conclusion of this chapter.

Several authors have reported the regenerative potential of MSC-derived exosomes for MI injuries (Lai *et al.*, 2010, Arslan *et al.*, 2013, Bian *et al.*, 2014, Wang *et al.*, 2018d). An early study found that 0.4 µg (protein) of MSC-derived exosomes administered intravenously to a mouse model of MI/reperfusion injury decreased the infarct size, whereas 3 µg of MSC conditioned media was required to achieve the same effect (Lai *et al.*, 2010). Recently, it has been shown that MSC-derived exosomes can be modified with a peptide CSTSMLKAC to home in on the ischemic myocardium (Wang *et al.*, 2018d). A mouse MI model was used and exosomes (4×10^9 particles/50 µg of protein) were intravenously administered via the tail vein. There were

significantly more modified exosomes in the ischemic heart region compared to control exosomes, detected using a near-infrared fluorescence tracer. The modified MSC-derived exosomes also decreased inflammation and cardiomyocyte apoptosis, increased angiogenesis, reduced infarct size and ameliorated cardiac function. Tumour angiogenesis has been seen to decrease after treatment with mice MSC-derived exosomes (Lee *et al.*, 2013). The exosomes decreased the VEGF expression *in vitro* and *in vivo*. It was also detected that the exosomal cargo had a high content of miR-16 which could have caused the anti-angiogenesis effect. Other cell-derived exosomes apart from MSCs have also shown regenerative potential for MI injuries. Immunodeficient mice with acute MI treated with cardiosphere-derived cell exosomes were shown to have improved heart function, decreased scar size and increased infarcted wall thickness compared to treatment with serum-free media or normal HdFb exosomes (40 µl injections at 15 and 30 days) (Ibrahim *et al.*, 2014). Mouse embryonic stem cell-derived exosomes injected into the infarct border zone of a mouse MI model (10 µl injections on each side of the ligation) had increased neovascularisation, cardiomyocyte survival and decreased fibrosis; compared to treatment with mouse embryonic fibroblast-derived exosome and saline (Khan *et al.*, 2015). Furthermore miR-294 from the embryonic stem cell-derived exosomes was linked to the enhanced cardiac progenitor cell survival and proliferation.

Other than MSC-derived exosomes being cardioprotective, they have shown potential to treat other diseases too. MSC exosomes have potential to treat certain types of cancers. A study showed that exosomes from bone marrow MSCs contain miRNA-23b which promotes dormancy in breast cancer cells (Ono *et al.*, 2014).

Human adipose tissue MSC-derived exosomes contain active neprilysin which degrades the β-amyloid peptide that builds up in the brain of those suffering from Alzheimer's disease (Katsuda *et al.*, 2013). It was found that 1 µg of protein from the exosomes had the same neprilysin activity as 0.3 ng of recombinant human neprilysin. The adipose tissue MSC-derived exosomes were able to incorporate into N2a cells and assisted in down regulating the β-amyloid peptides. It was found that bone marrow MSC-derived exosomes were less effective than adipose tissue MSC-derived exosomes.

Another study investigated the effect of exosomes in liver injuries. Carbon tetrachloride-induced mouse liver fibrosis has also been effectively treated with umbilical cord MSC-derived exosomes (250 µg in 330 µl PBS) (Li *et al.*, 2013). After 2 weeks, the exosomes reduced hepatocyte apoptosis and hepatic lobule destruction in the injured liver and after 3 weeks liver injury was

significantly reduced. The exosomes reduced liver injury by inactivating the transforming growth factor beta 1 (TGF-β1)/Smad pathway and decreased epithelial-to-mesenchymal transition (believed to play a central role in liver fibrosis). In agreement, Tan *et al.* showed that MSC-derived exosomes administered to mice with carbon tetrachloride-induced liver fibrosis had an increase in liver cell proliferation and a higher cell viability than the mice treated with the PBS control (Tan *et al.*, 2014). Immunoblotting showed that the markers for hepatic proliferation (NF-κB, cyclin D1 and cyclin E) increased in mice treated with the exosomes relative to PBS control.

MiR-133b improves functional recovery in spinal cord injury shown in adult zebra fish (Yu *et al.*, 2011) and regulates the function of midbrain dopaminergic neurons (Kim *et al.*, 2007) and the proposed mechanism has recently been explored (Xin *et al.*, 2012). Upregulation of miR-133b was detected when neurons and astrocytes were treated with exosomes derived from MSCs treated with an ischemic brain extract from rats subjected to middle cerebral artery occlusion (stroke) (Xin *et al.*, 2012). The proposed therapeutic mechanism is that the MSC-secreted exosomes transferred the miR-133b to the neurons and astrocytes which increased neurite outgrowth. Even though numerous exosomes have seen to have therapeutic effects in diseases such as Alzheimer's, liver injuries and tumour angiogenesis, their therapeutic potential might be significantly increased by using them as a delivery vehicle for therapeutic agents.

1.7.1 Exosomes used as delivery vehicles

Due to exosomes being nano-sized vesicles that naturally transport RNA, mRNA and miRNA around the body, they are potentially an optimised delivery vehicle for exogenous bioactive reagents (Valadi *et al.*, 2007). These types of agents can be packaged into exosomes via engineering the cells to self-incorporate proteins and mRNA (You *et al.*, 2018). For investigation into a cell-free vaccine for hepatocellular carcinoma, mouse dendritic cells were transfected with α-fetoprotein and the secreted α-fetoprotein-enriched exosomes isolated (Lu *et al.*, 2017). Foetal liver protein, α-fetoprotein, is utilised as a tumour antigen due to its high concentration in hepatocellular carcinoma patients. The engineered exosomes were administered intravenously into mice with hepatocellular carcinoma (40 or 150 μg/mouse/week for three weeks). The engineered exosomes enhanced antigen-specific anti-tumour-immune responses as shown by increased IFN-γ-expressing CD8+ T lymphocytes, higher concentration of IFN-γ and IL-2, less CD25+Foxp3+ regulatory T cells, lower concentration of IL-10 and TGF-β in the tumour microenvironment and induced a significant tumour suppression. Cell transfection can be used to load mRNA or miRNA into exosomes. Exosomes (50 μg protein in 5 μl) isolated from marrow

stromal cells transfected with a miR-146b expression plasmid significantly decreased glioma xenograft growth in rat brain tumour model compared to the miRNA-67 loaded-exosomes or PBS control (Katakowski *et al.*, 2013). The exosomes were able to deliver miR-146b which assists in decreasing glioma cell invasion, migration and viability.

Exosomes may be particularly desirable for delivering short interfering RNA (siRNA) as they can prevent siRNA degradation, prevent immune responses and help the siRNA cross the cell membrane (El-Andaloussi *et al.*, 2012). Exosomes are most commonly directly transfected with siRNA using electroporation which uses an electric field to create pores in the exosome lipid membrane to assist the cargo to enter the exosomes but other means such as liposomal delivery are also used. An early study showed that HeLa and HT1080 human fibrosarcoma cell-derived exosomes transfected with siRNAs against targets for cancer cells, RAD1 and RAD52, either by liposomal or electrophoretic delivery to the exosome caused specific gene silencing which both led to similar levels of cancer cell death *in vitro* (Shtam *et al.*, 2013). Blood-derived exosomes have also been explored as delivery vehicles, due in part to the more ready availability. Human plasma exosomes electroporated with mitogen-activated protein kinase-1 (MAPK1) siRNA have been shown to deliver effectively to monocytes and lymphocytes (Wahlgren *et al.*, 2012). By isolating exosomes after electroporation, they showed that the siRNA was contained in the isolated exosomes. Their gene silencing was effective as MAPK1 was down-regulated in monocytes and lymphocytes as confirmed by western blotting. Furthermore, confocal microscopy and flow cytometry have also been used to confirm that siRNA is successfully transfected into exosomes by fluorescently labelling the siRNA. Caution should be taken when using electroporation as it has been reported using NTA and confocal microscopy that siRNA can aggregate thereby overestimating the amount of siRNA loaded into exosomes (Kooijmans *et al.*, 2013). The addition of EDTA or using an acidic citrate electroporation buffer can reduce siRNA aggregates; however, these methods are not considered effective enough. The use of liposomes to transfect exosomes is complicated by the similarities in size and composition of the two components.

Loading of agents through simple incubation with exosomes is another route. Curcumin was loaded into tumour cell-derived exosomes through incubation at 22°C for 5-15 minutes and the curcumin loaded exosomes were seen to reduce brain inflammation in GL26 brain tumour mice models treated intranasally (Zhuang *et al.*, 2011). In a follow up study by another group, curcumin was loaded into embryonic stem cell-derived exosomes with the aim of combining the regenerative potential of embryonic stem cells (Khan *et al.*, 2015) with the anti-inflammatory

activity of curcumin. The curcumin loaded embryonic stem cell-derived exosomes were shown to restore neurovascular units after an ischemia-reperfusion injury in mice (Kalani *et al.*, 2016) but it should be noted that only the combination was tested.

Loading DNA into exosomes is more sterically challenging than loading siRNA. Linear DNA smaller than 1000 bp will transfect easier into exosomes than using larger DNA or plasmid DNA as exosomes have a small inner volume (Lamichhane *et al.*, 2015). Larger microvesicles have a higher capacity for DNA loading than exosomes. It has been shown that exosomes can deliver transfected DNA into recipient cells; however, no functional gene activity was detected (Lamichhane *et al.*, 2015). Their data supports the idea that microvesicles are more efficient for DNA delivery as exosomes reach saturation. To overcome the small size of exosomes for DNA delivery, one study modified HEK293FT-cell derived exosomes to encapsulate plasmids (Lin *et al.*, 2018). They created hybrid exosomes by incubating liposomes, exosomes and pEGFP-C1 plasmids for 12 hours at 37°C. Moreover, they showed MSCs internalised the hybrid exosomes to express the genes of a CRISPR/Cas9 expression vector which liposomes alone could not do.

A significant problem in delivering cargo loaded exosomes is directing the exosomes toward a specific site if they are injected systemically. Modifying exosomes to allow for targeted delivery is being explored. For example, autologous dendritic cell-derived exosomes were used to deliver glyceraldehyde-3-phosphate dehydrogenase (GAPDH) siRNA (electroporated) to mice brains (Alvarez-Erviti *et al.*, 2011). Dendritic cells were engineered to express lysosome-associated membrane protein 2B (Lamp2b) with neuron-specific rabies virus glycoprotein (RVG) peptide 3 to achieve specific targeting of the released exosomes. The peptide (derived from the rabies virus) was expected to facilitate crossing blood-brain barrier to occur. There was significant gene silencing of GAPDH in many brain regions (neurons, microglia and oligodendrocytes) intravenously injected with the siRNA loaded exosomes. Their study also tested a therapeutic benefit where exosomes loaded with a gene target against Alzheimer's disease (beta-secretase 1 (BACE1)) caused a knockdown of BACE1 mRNA (60%) and protein (62%). The research into exosomes as specific cargo delivery vehicles holds great promise. The stability of exosomes will necessarily both here and generally impact on their translation to the clinic.

1.7.1.1 Stability of exosomes

Pharmaceutical companies have an obligation to prevent loss of therapeutic properties during delivery of drugs. Hence, a temperature-controlled environment is required for certain therapeutic

products. It is good practice for drug products to be tested for stability (Ammann, 2011). A guideline is given by the World Health Organization Technical Report Series, No. 953, 2009, Annex 2 (Organization, 2009). Due to exosomes having a potential to be used for therapeutic purposes, it is important to determine the temperature stability of the exosomes to be suitable delivery vehicles or potential biomarkers for diseases. Cancer LIM 1863 cell-derived exosomes stored in plasma have been shown to be stable over 3 months when stored at 4, -20 and -80°C as detected by TEM and exosome marker TSG101 (Kalra *et al.*, 2013). They also stored plasma for 30 days at 37°C and exosomes were stable to an extent as TSG101 was detected. It was also reported that protease inhibitors had no effect on the stability of plasma exosomes. Furthermore, it was reported that the exosomes recovered from plasma, stored for 30 days at -20°C, were still functional as they were uptaken by LIM 1215 colorectal cancer cells. However, another study revealed that cell-derived exosomes from HEK 293T cells, endothelial colony forming cells and MSCs decreased in size when stored at 4°C and 37°C over 8 days as detected by NTA suggesting structural change and deterioration (Sokolova *et al.*, 2011). The exosome size was stable after multiple freeze-thaws at -20°C. This indicates the need for further studies in this area with well-defined isolation methods and characterisation. Bioactivity studies need to be carried out to determine the functional stability of stored exosomes.

1.7.2 Exosomes embedded in hydrogels

1.7.2.1 Hydrogels for regenerative treatment

Hydrogels are a type of biomaterial which is defined as a synthetic substance used as an implanted medical device. Hydrogels are three-dimensional polymer networks that swell in size as they can absorb up to thousands of times their dry weight in water; hence, mimicking properties of tissues suitable for an extracellular matrix (ECM) (Hoffman, 2002). A desirable property of hydrogels in tissue regeneration is that it should allow for synchronicity between its degradation and replacement by tissue (Otrock *et al.*, 2007). Certainly, no toxic by-products should form. Hydrogels are suitable for tissue engineering as their pores are either broad enough for cells to enter or they can be designed to allow ingress through dissolving or enzymatic degradation. Hydrogels can be formed either physically or chemically. Chemical gels involve using a cross-linker and physical gels rely on hydrophobic interactions. Handling hydrogels poses a challenge as they can have very low mechanical strength (Hoffman, 2002). An advantage is that they be able to gel *in vivo* at body temperature when injected as a liquid.

Hydrogels are suitable as a localised delivery vehicle and have been used in various therapeutic applications such as cardiac illness, ocular pain, cancer and wound healing (Li and Mooney, 2016, Narayanaswamy and Torchilin, 2019). Some of the desirable characteristics of hydrogels include the high concentration of water which makes them compatible with the aqueous tissue environment (Li and Mooney, 2016). Their porosity allows for a sustained release of the loaded therapeutic agent either through control of their mesh size or through swelling, mechanical deformation (such as ultrasound) or the use of covalent linkages (either stable or cleavable). Hydrogel stiffness can be adjusted (0.5 kPa-5 MPa) to be compatible with the tissue where they are to be administered (Arakaki *et al.*, 2010, Li and Mooney, 2016).

1.7.2.2 Fibrin hydrogel

A fibrin gel is formed when fibrinogen is activated by thrombin in the presence of Ca^{2+}. Fibrin gels do not require invasive surgery as they can be injected into the target site (Jeon *et al.*, 2005). VEGF promote angiogenesis; however, with direct delivery there is low efficacy due to rapid clearance from the intended delivery site. A study modified VEGF to incorporate matrix-binding to fibrin to prevent the rapid clearance of native VEGF mixed into fibrin (Ehrbar *et al.*, 2004). The modified VEGF was released from the fibrin implant by cell-associated enzymatic activity. Their engineered VEGF significantly induced vessel formation more than native VEGF, in embryonic chicken chorioallantoic membrane and in adult mice. Moreover, those vessels were structurally intact and permeability data showed they did not leak. Another study examined the effects of varying the concentration of fibrinogen, thrombin and heparin on the kinetics of bFGF release (Jeon *et al.*, 2005). bFGF has been known to induce the regeneration of various tissues. Their studies revealed that incorporation of heparin and increasing the concentration of fibrinogen decreased the release rate of bFGF. The fibrin gel stabilised the bioactivity of bFGF, compared to a free form of bFGF, and there were more microvessels present in mice ischemic limbs injected with bFGF-loaded fibrin gels than those with no treatment. Infarcted rat myocardium has been previously treated with bone marrow mononuclear cells implanted within a fibrin matrix (Ryu *et al.*, 2005). The results showed more tissue regeneration, more extensive neovascularisation and significantly higher microvessel density when the cells were implanted with the matrix than without it. The drawback of using fibrin is its quick degradation time, gel shrinkage and a low mechanical stiffness (Ahmed *et al.*, 2008). A study showed a fibrin hydrogel (3.5 mg/ml) mixed with human myofibroblasts degraded in 2 days when incubated in cell culture medium without aprotinin, examined with light microscopy using haematoxylin and eosin (H&E) staining (Ye *et al.*, 2000).

Overall fibrin is a flexible scaffold for use in delivering therapeutic agents for regenerative medicine.

1.7.2.3 Exosomes delivered in hydrogels

Very recently, hydrogels have been investigated for their ability to deliver exosomes for therapeutic purposes in wound healing (Tao *et al.*, 2017c), MI (Chen *et al.*, 2018a), hindlimb ischemia (Zhang *et al.*, 2018) and enzyme prodrug therapy (Fuhrmann *et al.*, 2018) (prodrugs are converted into an active drug at a targeted location with the introduction of artificial enzymes). The hydrogels are used in part to potentially localise and sustain the delivery of the exosomes as for example numerous studies have shown bone marrow stem cells injected into the myocardium to be washed out (Sheikh *et al.*, 2012, van den Akker *et al.*, 2017) and it is expected that exosomes will behave similarly. Endothelial progenitor cell-derived exosomes, delivered via an injectable hyaluronic acid hydrogel, improved the peri-infarct angiogenesis and function of the heart after MI in rats (Chen *et al.*, 2018a). Chitosan hydrogels have been used to deliver exosomes for various regenerative purposes. One study compared chitosan/silk hydrogel sponges, embedded with either the polysaccharide rhizomes of curcuma zedoaria (ZWP-is an Asian remedy used to treat inflammation, pain, wounds and skin problems) or PRP-derived exosomes (100 µg protein) (Xu *et al.*, 2018). The combined treatment showed the best wound closure in diabetic rats as the ulcer reduced in size and the epidermis thickened. Sustained delivery of miR-126-3p-overexpressing synovium MSCs exosomes, from a chitosan hydrogel, also promoted angiogenesis in a diabetic rat wound healing model (Tao *et al.*, 2017c). Another study tested gingival MSC-derived exosomes (50 µg protein) loaded in a 1 x 1 cm chitosan/silk hydrogel sponge to treat 10-mm diameter full-thickness wounds in diabetic rats (Shi *et al.*, 2017). The exosome loaded hydrogel promoted wound healing via neuronal ingrowth, increased angiogenesis and deposition and remodelling of collagen with the exosome loaded hydrogel having the highest microvessel density and nerve density. Furthermore, tissue regeneration in a murine hindlimb ischemia model has been shown using MSC-derived exosomes delivered in a chitosan hydrogel (Zhang *et al.*, 2018). The hydrogel also enhanced the exosomes therapeutic function.

A sodium alginate hydrogel loaded with PRP-derived exosomes (1% (v/v)) has also been reported to promote skin wound closure in diabetic rats (Guo *et al.*, 2017). The PRP exosomes caused significantly improved wound healing at days 7 and 14 compared to the untreated control wound groups, although wound healing with PRP exosomes was not significantly different to PRP treated wounds. There was significantly increased blood vessel area and blood vessel number with the

PRP exosomes compared to the control groups and PRP. *In vitro*, the PRP exosomes significantly increased cell proliferation and migration of fibroblasts through yes-associated protein (YAP) activation, increasing collagen synthesis suggesting a mechanism for the improved wound healing. MSC exosomes have been investigated for enzyme prodrug therapy, where they carried and delivered β-glucuronidase (loaded by permeabilising the exosomes using saponin treatment), which reacted to release curcumin, an anti-inflammatory product (Fuhrmann *et al.*, 2018). A poly(vinyl alcohol) hydrogel assisted in the precise delivery. A photoinduced imine, crosslinking hydrogel glue, has been tested to deliver human induced pluripotent MSC exosomes to a cartilage defect site (Liu *et al.*, 2017b). The hydrogel patch was able to integrate *in vivo* and there was promotion of cartilage repair due to positive cell regulation. A silk fibroin hydrogel has been used to deliver miR-675 loaded human umbilical cord MSC-derived exosomes (50 µl at 11 mg/ml) to repair ischemic hindlimb injury in an aging mouse model (Han *et al.*, 2019). MiR-675 was delivered at it inhibits the aging process by preventing the TGF-β1/p21 signalling pathway. The silk fibroin hydrogel enhanced the retention of the miR-675 loaded MSC-derived exosomes and significantly increased blood perfusion compared to mi675 loaded MSC-derived exosomes alone. Overall, various hydrogels have provided a scaffold for the sustained delivery of exosomes for diverse regenerative purposes. No prior studies have examined delivery of serum exosomes using a fibrin hydrogel which could be a suitable candidate.

1.7.3 Blood-derived exosomes use in disease

As mentioned previously, blood-derived exosomes are predominantly researched for biomarkers. However, plasma and serum exosomes also seem to have a biological purpose as detected by various researchers as mentioned briefly in the function of exosomes (Section 1.5). A study showed removing exosomes from FBS altered the gene and miRNA expression in muscle cells and decreased their proliferation and differentiation (Aswad *et al.*, 2016). Bovine serum exosomes may also assist in proliferation and migration of human cardiac progenitor cells as depleting the exosomes decreased the cardiosphere size, concentration and ECM production; however, this may have been caused by the depletion of other factors (Angelini *et al.*, 2016). FBS exosomes can also cause significant migration of lung cancer epithelial cells (A549 cells) in a dose-dependent manner (0.03-100 µg/ml) (Shelke *et al.*, 2014). Overall, this highlights the potential of blood-derived exosomes to be useful in either treating or detecting diseases.

The amount of serum-derived exosome mitochondrial DNA and proteins is significantly increased in children with autism spectrum disorder (Tsilioni and Theoharides, 2018). The exosomes from

the autism spectrum disorder serum increased secretion of pro-inflammatory cytokine IL-1β from human microglia *in vitro* compared to the control serum exosomes. Hence, a possible explanation of the inflammation in the brain in children with autism spectrum disorder. Further research on a brain disease, an Alzheimer's disease mouse model has shown that peripheral plasma exosomes can diffuse from the dentate gyrus hippocampus to the cortex and by day 20 most of the exosomes were in the cortex (Zheng *et al.*, 2017). The study showed that exosomes mainly targeted microglia and were still internalised by day 20; however, Alzheimer's disease mice had less exosomal uptake in the astrocytes and neurons. The clustering of plasma exosomes around amyloid-β plaques and exosomes taken up by activated microglia, suggests a role in Alzheimer's disease pathogenesis.

The role of blood exosomes in pregnancy has also been investigated. Plasma exosome concentration in pregnant women (n=20 for each trimester) was 50 times more than non-pregnant women (n=9) (Salomon *et al.*, 2014). The plasma exosome protein significantly increased with gestational age and was 0.94 mg/ml ±0.41 (second trimester) and 1.40 mg/ml ±0.11 (third trimester). Exosomes from the first and second trimester (100 µg/ml) significantly increased HUVEC migration compared to exosomes from non-pregnant woman. The contribution of placental exosomes decreased in the third trimester. Furthermore, the increase in placental-derived exosomes correlated with the increase in total plasma exosome concentration during the first and second trimester, albeit there was a reduction during the third trimester. This could have been caused by a decrease in secretion of placental-derived exosomes, enhanced secretion from non-placental sources or both. Their data may provide clinical value to detect placental problems if the exosome profile changes during pregnancy; however, the role of placental-derived exosomes requires further investigation. Multiple sclerosis relapses decrease during pregnancy and studies have seen that serum exosomes (20 µg/ml), from pregnant and non-pregnant controls, suppress T cell activation (which normally target and destroy myelin antigens during the active disease) (Williams *et al.*, 2013). Also shown in another study, pregnancy serum-derived exosomes (10 µg) elicited significantly more T cell suppression, as well as being at a higher concentration and having a larger diameter (Gatson *et al.*, 2011). Furthermore, pregnant serum exosomes also assist in migration of oligodendrocyte precursor cells into the central nervous system lesions and interestingly both pregnant and non-pregnant-derived serum exosomes contribute to the reduction of experimental autoimmune encephalomyelitis induced by pregnancy, shown in mice (Williams *et al.*, 2013). Hence, serum exosomes may play an important role in neuroprotection and immune regulation during pregnancy.

Intriguingly there is a connection between plasmodium infection and tumour angiogenesis. Intra-tumoural injection of mice plasma exosomes isolated using either UC or ExoQuick-TC precipitation (50 µg exosome protein) from malaria infected hosts decrease tumour angiogenesis (Yang *et al.*, 2017). *In vitro* studies confirmed that these exosomes inhibit VEGF receptor 2 (VEGFR2) expression and tube formation in endothelial cells.

1.7.4 Regenerative properties of blood-derived exosomes

The above looked at instances that have revealed potential physiological and pathological functions of blood-derived exosomes. There are also an increasing number of studies that have investigated their delivery for therapeutic purpose.

1.7.4.1 Myocardial injuries

Intravenous administration of rat plasma-derived exosomes (isolated using UC) via the tail vein 15 minutes before induction of an ischemic reperfusion injury in the recipient rats heart resulted in a decrease in infarct size (Vicencio *et al.*, 2015). They also used a Langendorff-perfused rat heart, in which the heart is removed from the rat and the perfusate is pumped through the aorta into the coronary vessels towards the heart. This removes the complications of the live animal and the influence of blood. The exosomes were administered during perfusion (15 minutes) prior to the rat hearts undergoing 35 minutes of ischemia and 2 hours of reperfusion and here too the exosomes significantly decreased the infarct size. Furthermore, they performed *in vitro* studies where they administered exosomes to cardiomyocytes that underwent hypoxia-reoxygenation (simulating ischemia-reperfusion). Cell death was reduced indicating that the exosomes were cardioprotective via direct interactions with the cardiomyocytes. It was revealed that HSP70 on the surface of exosomes communicated with TLR4 in cardiomyocytes which lead to a signalling pathway involving various kinases which activated cardioprotective HSP27. It has also been found that serum exosomes activate an ERK1/2 and HSP27 signalling pathway to prevent apoptosis of H9C2 cardiomyocytes treated with hydrogen peroxide (Bei *et al.*, 2017, Li *et al.*, 2018c) suggestive of another potential therapeutic mechanism for myocardial injuries. One of those studies compared the difference in serum exosomes (isolated using ExoQuick precipitation) between exercised (swimming) and non-exercised mice (Bei *et al.*, 2017). Both the exercised and non-exercised serum exosomes significantly enhanced the protective effect of mice with acute ischemia/reperfusion injury when injected with equal quantities (10 µg diluted in 25 µl PBS). However, the concentration of exercised serum exosomes was 1.85X more which significantly increased the protective effect when injected as an equal volume, thus exercise stress causes

secretion of exercise-induced exosomes that enhance the therapeutic function of endogenous exosomes against myocardial injury. Another mechanism is that the serum exosomes (isolated using ExoQuick precipitation) are regulating miR-17-3p/TIMP3 to increase the proliferation of cardiomyocyte H9C2 cells (Liu *et al.*, 2018b).

Thus, though there are relatively few studies at present, it appears that plasma or serum exosomes can induce cardioprotective effects through a range of mechanisms.

1.7.4.2 Peripheral ischemia

Angiogenesis is vital for repair and regeneration after ischemia; hence, the importance in isolating bioactive agents that induce angiogenesis. It has been shown that coronary serum exosomes (isolated using UC) from myocardial ischemia patients improved HUVEC proliferation, migration and tube formation better than control exosomes from healthy patients (Li *et al.*, 2018b). Both the ischemic and control exosomes increased the migration of HUVECs in transwell and scratch wound assays, with the ischemic exosomes showing the most pronounced effect. The ischemic exosomes also enhanced blood flow recovery and neovascularisation in a mouse hindlimb ischemia model better than the control exosomes after 21 days post-injection and it was believed that cardiomyocytes are the potential cells releasing the bioactive exosomes in response to ischemic stress. Furthermore, they found that the ischemic exosomes had reduced miR-939-5p levels, which improved angiogenesis by regulating the nitric oxide signalling pathway.

To determine the pro-angiogenic activity within 18 different serum exosome samples (healthy blood bank donors in Italy and exosomes isolated using an OptiPrep density gradient), it was found that 14 out of 18 were able to elicit 50% or more of the increase that the potent angiogenic VEGF was able to produce in HMEC proliferation and tube formation (Cavallari *et al.*, 2017). Using gene ontology (GO) functional analysis, they identified enriched genes linked to TGF-β1 signalling pathway associated with the treatment with active exosomes and not with inactive exosomes and it was speculated that this cascade could be driving the angiogenic response. The findings *in vitro* were found to correlate with those *in vivo* when the active and inactive serum exosomes were subcutaneously injected ($2x10^{10}$) into SCID mice with induced hindlimb ischemia ($1x10^{10}$ injected immediately, $0.5x10^{10}$ on day one and day two). Only the active exosomes increased vessel number and hindlimb perfusion, preventing muscle damage after hindlimb ischemia in mice. This indicates that exosome from serum may need to be screened for angiogenic potential before use in the clinic. Further research is required to identify the mechanism of angiogenesis caused by

plasma and serum exosomes and investigated in large animal ischemic models, to enable clinical trials to move forward.

1.7.4.3 Other diseases

The use of blood-derived exosomes in various other diseases have also been explored recently. Human serum exosomes have the potential to treat dysferlinopathy, which is a muscle disease noted by the atrophy and weakness of the muscles. Exosomes have been found to contain the dysferlin protein which is deficient in dysferlinopathic patient serum exosomes (isolated using UC and sucrose density gradient) relative to normal controls (Dong *et al.*, 2018). The serum exosomes (100 µg/ml) assisted the repair of human dysferlin-/- myotube membranes after laser injury, *in vitro* for 48 hours. Therefore, exosomes can be used as a possible treatment method and also for diagnosis.

Serum exosomes have also been investigated for the potential treatment of hepatic fibrosis. Serum exosomes from healthy mice (isolated using UC or targeted filtration using PureExo® kits), but not fibrotic mice, were able to repress liver injury in mice (induced by carbon tetrachloride or thioacetic acid) (Chen *et al.*, 2018b). The exosomes had anti-fibrogenic properties, identified by a decrease in hepatocyte death, circulating aspartate transaminase/alanine aminotransferase levels and pro-inflammatory cytokines. *In vitro*, the exosomes reduced proliferation and fibrosis-associated molecule expression, as well as repressing the anti-proliferation effects of carbon tetrachloride or ethanol on hepatocytes. Specific miRNAs (-34c, -151-3p, -483-5p, -532-5p and -687), identified in the serum exosomes, caused the above therapeutic actions in hepatic stellate cells (principal cell type in liver fibrosis) or injured hepatocytes (symptom of liver injury).

An *in vitro* study has shown that both serum and PRP (10% (v/v)) from umbilical cord blood significantly increase proliferation of fibroblasts and MSCs more than the serum-free control (Hashemi and Rafati, 2016). Furthermore, exosomes derived from PRP or serum have shown to promote wound healing *in vivo* (Nakamura *et al.*, 2016, Guo *et al.*, 2017). A recent study investigated PRP-derived exosomes (isolated using UC and sucrose cushion) for the use in stimulating neovascularisation (Guo *et al.*, 2017). They showed that the PRP exosomes encapsulated growth factors PDGF-BB, TGF-β, bFGF and VEGF. PRP exosomes stimulated important cellular responses such as assisting proliferation and promoting migration of HMEC-1 and fibroblast cells. PRP exosomes also promoted angiogenesis of HMEC-1 cells as seen by formation of elongated vessels. They overlaid an ECM gel with HMEC-1 cells treated with or without the PRP exosomes. *In vivo*, PRP exosomes embedded in a sodium alginate hydrogel

promoted cutaneous healing of chronic wounds in a diabetic rat model. Mouse serum-derived exosomes (isolated using ExoQuick precipitation) have been shown to increase the healing of full-thickness wounds (10 mm) in mice (Nakamura *et al.*, 2016). The diameter of the wound was significantly smaller with exosome treatment than without (daily treatment), at day 4, 6 and 8. Wound healing was suggested to occur through collagen expression as the mRNA levels of COL1A1 and COL1A2 were increased in the tissues of the exosome-treated wound though not significantly relative to the control without treatment. Furthermore, the concentration of exosomes decreased in human serum from systemic sclerosis patients compared to healthy controls. Systemic sclerosis patients are prone to skin ulcers and pitting scars due to a decrease in collagen. The study proposed that the reduction in serum exosomes, could be the reason of slow wound healing in patients. Contrary to their results, another study found that the serum exosome (isolated using ExoQuick precipitation) particle concentration was higher in systemic sclerosis patients compared to normal control (Wermuth *et al.*, 2017). The differences could be accounted for by the different detection methods used, CD63 ELISA (Nakamura *et al.*, 2016) versus NTA (Wermuth *et al.*, 2017). This further highlights the difficulties of interpreting and comparing data whilst analysis methods are not fully established. The latter also found that the systemic sclerosis serum exosomes were enriched for a few miRNAs anticipated to induce profibrotic genes and decreased for antifibrotic genes, alluding to a possible mechanism for elevated fibrotic tissue in systemic sclerosis patients (Wermuth *et al.*, 2017).

Further research has shown blood-derived exosomes to accelerate wound healing. Mouse skin wounds (12 mm) treated with human umbilical cord blood plasma-derived exosomes (200 µg/100 µl PBS) enhanced wound healing compared to PBS control; as detected by enhanced re-epithelialisation, decreased scar width and increased angiogenesis over 8 days (exosomes isolated using UC and ultrafiltration) (Hu *et al.*, 2018). Their *in vitro* studies revealed a possible mechanism as the exosomes were enriched for miR-21-3p, and inhibition of miR-21-3p resulted in decreased angiogenesis and migration of endothelial cells and fibroblasts. Another research group found that maternal serum-derived exosomes (isolated using ExoQuick precipitation) caused significantly enhanced migration of HUVECs compared to umbilical cord serum-derived exosomes, *in vitro* (Jia *et al.*, 2018). This may be explained by the miRNA differential expression; 11 miRNAs were up-regulated and 15 were down-regulated in maternal serum-derived exosomes compared to umbilical cord serum-derived exosomes. Albeit, both maternal and umbilical cord blood-derived exosomes significantly increased HUVEC proliferation, migration and tube formation compared to the control of no exosomes added.

The role of serum-derived exosomes in preventing an allergic reaction has also been investigated. Serum-derived exosomes (isolated using UC) were isolated from ovalbumin (antigen) fed mice and injected intraperitoneally (exosomes from 1 ml serum in 1 ml PBS) into a mouse allergic asthma model and analysed for the potential transfer of tolerogenic exosomes (antigen-specific tolerance) into the mice exposed to the antigen (Almqvist *et al.*, 2008). Day 0 mice received exosomes, day 7 and 17 mice were sensitized with ovalbumin (intraperitoneal 10 µg), day 25, 26 and 27 mice were exposed to ovalbumin (intranasal 100 µg) and 24 hours later samples were processed. The antigen-fed serum-derived exosomes inhibited allergic sensitization/inflammation in the airway of the recipient mice, as shown by decreased concentration of total and ovalbumin-specific IgE in serum and significant increase of CD4+ CD25+ regulatory T cells.

Intranasal administration of young rat serum-derived exosomes (isolated using ExoQuick precipitation) (100 µg in 50 µl) to aged rats, have been found to significantly enhance myelin in the motor cortex after 3 days, quantified by FluoroMyelin staining and western blotting (Pusic and Kraig, 2014). The *in vitro* studies revealed that both young and environmentally enriched rat serum-derived exosomes contained miR219, and inhibiting exosomal miR-219 prevented myelination in a slide culture. MiR-219 increases the differentiation of oligodendrocyte precursor cells into myelin-producing cells by decreasing the expression of inhibitory regulators of differentiation. Multiple sclerosis lesions contain no miR-219 (Junker *et al.*, 2009). Hence, serum-derived exosomes could be a possible therapy for remyelination for diseases such as multiple sclerosis (Pusic and Kraig, 2014) .

Although research has highlighted the benefits of serum exosomes in various diseases as well as in pregnancy, they are inconsistent with the use of different exosome isolation methods. Furthermore, there are major differences in the concentration of exosomes administered between different research groups e.g. cardiomyocytes treated with 10^8/ml (0.1 µg) rat or human plasma exosomes isolated using UC (Davidson *et al.*, 2018a) versus 10 µg/ml mice serum exosomes isolated using ExoQuick (Bei *et al.*, 2017). This could impact the results reported as any contamination may obscure the data. A new approach is therefore needed to standardise exosome isolation methods, to enable comparison of research studies and identifying the true function of blood-derived exosomes.

1.8 Summary and aims

Although EV isolation techniques are limited in separating the different types of EVs, they are often termed exosomes, EVs or microparticles (Lötvall *et al.*, 2014). In this thesis, we will refer to the isolated EVs as exosomes. Certain components in blood are regenerative and studies have indicated that exosomes are one of these. Exosomes are multifunctional for use in: biomarking diseases, delivery vehicle for drugs and regenerative purposes. Due to blood containing a high concentration of exosomes released by platelets and various other cells (Davidson and Yellon, 2018, Sluijter *et al.*, 2018), numerous studies have investigated and shown that plasma/serum exosomes have regenerative potential in injuries such as myocardial injury (Liu *et al.*, 2015, Vicencio *et al.*, 2015), hindlimb ischemia (Li *et al.*, 2018b) and hepatic fibrosis (Chen *et al.*, 2018b).

Aim 1: Though regenerative potential has been found for blood-derived exosomes, these have almost exclusively been isolated using methods that have been shown to result in high protein contamination levels (UC and precipitation). Thus, it was considered necessary to assess the regenerative potential of exosomes purified from human serum by a low protein contamination method, namely SEC.

Objectives

1. Determine protein purity of SEC isolated exosomes relative to those isolated by UC and precipitation.
2. Assess the uptake of serum SEC-derived exosomes and their effect on cell proliferation and HUVEC spheroid sprouting.
3. Determine their stability.
4. Ascertain the suitability of fibrin as a delivery vehicle for exosomes.

Aim 2: Develop a multi-step purification method for removing lipoproteins from SEC isolated exosomes.

Objectives

1. Optimise a density gradient for removal of lower density lipoproteins prior to SEC.
2. Assess the purified exosomes regenerative potential *in vitro* and *in vivo*.
3. Comparatively characterise the proteomes obtained from the single-step and multi-step isolation methods.

CHAPTER 2: FUNCTION OF SERUM-DERIVED EXOSOMES ISOLATED BY SIZE EXCLUSION CHROMATOGRAPHY

2.1 Introduction

Numerous methods for isolating and characterising exosomes have emerged over the last decade. Purifying exosomes can include UC, precipitation, ultrafiltration, density gradients, immunoaffinity purification or SEC (Section 1.3). Immunoblotting, flow cytometry, mass spectrometry and imaging methods help to identify isolated exosomes (Section 1.4) (Sahoo and Losordo, 2014). The isolation method used depends on the downstream application and the aim of the study. If very pure exosomes are required, then the isolation method must have minimal co-isolation of proteins and, recently discovered, the co-isolation of lipoproteins (Tkach *et al.*, 2017). This latter aspect will be further discussed in Chapter 3. Other studies may require a large yield of exosomes which come at the cost of a reduction in purity. Exosomes have major potential for therapeutic use as they contain miRNA, have regenerative properties as well as being a potential delivery vehicle for drug therapy. However, to completely understand their mechanism suitable isolation techniques need to be employed. As discussed, current isolation techniques have their own advantages and disadvantages, summarised in Table 1.2 (Section 1.3). Blood-derived exosomes isolated from plasma or serum have shown to have regenerative properties for a range of ailments such as myocardial injury, hindlimb ischemia, dysferlinopathy, hepatic fibrosis, skin wounds and allergies; discussed in depth in section 1.7.4 and summarised in Table 2.1. The exosome isolations for these regenerative studies included UC, ExoQuick and density gradients. Most of these serum/plasma-derived exosomes were isolated using UC (Table 2.1). UC is not an optimal exosome method as there are numerous disadvantages discussed earlier in section 1.3.1 and Table 1.2, i.e. protein contamination particularly from blood-derived sources, expensive equipment required, long isolation time and high-speed centrifugation could lead to exosome damage. In 2014, SEC was suggested to be a successful single-step EV isolation method (Böing *et al.*, 2014), discussed earlier in section 1.3.6. The SEC method was found to be a quick and simple method to use, briefly, 1.5 ml of platelet-free supernatant from platelet concentrates was loaded onto the top of the 10 ml Sepharose CL-2B column and multiple 0.5 ml fractions of the eluates were collected. The EVs were detected in SEC fractions 9-12 using NTA and western blotting for platelet marker CD61. Furthermore, SEC was found to have minimal protein

contamination <1%. Thus, it was considered useful to examine the functionality of serum SEC-derived exosomes. Due to exosomes showing potential for delivering specific cargo for therapeutic use, discussed earlier in section 1.7.1, the stability of exosomes (Section 1.7.1.1) require investigation for translation to the clinic as drug products require stability testing (Ammann, 2011). Hence, the stability of the serum SEC-derived exosomes was also examined.

Table 2.1: Regenerative properties of blood-derived exosomes and their isolation method

Blood-derived source	**Function**	***in vitro* or *in vivo***	**Exosome isolation method**	**Reference**
Rat plasma	Myocardial injury: decreased infarct size	*in vivo*	UC	(Vicencio *et al.*, 2015)
Mice serum	Ischemia/reperfusion injury: enhanced protective effect	*in vivo*	ExoQuick precipitation	(Bei *et al.*, 2017)
Human coronary serum	Hindlimb ischemia model: enhanced blood flow recovery and neovascularisation	*in vivo*	UC	(Li *et al.*, 2018b)
Human serum	Hindlimb ischemia: increased vessel number and hindlimb perfusion	*in vivo*	Density gradient	(Cavallari *et al.*, 2017)
Human serum	Dysferlinopathy: assisted the repair of human dysferlin-/- myotube membranes after laser injury	*in vitro*	UC and density gradient	(Dong *et al.*, 2018)
Mice serum	Hepatic fibrosis: repress liver injury	*in vivo*	UC	(Chen *et al.*, 2018b)
Human PRP	Chronic wound: cutaneous healing	*in vivo*	UC and sucrose cushion	(Guo *et al.*, 2017)
Mouse serum	Full-thickness wound: increased healing	*in vivo*	ExoQuick	(Nakamura *et al.*, 2016)
Human umbilical cord blood plasma	Full-thickness wound: enhanced wound healing	*in vivo*	UC and ultrafiltration	(Hu *et al.*, 2018)
Mice serum	Allergies: exosomes inhibited allergic sensitization/inflammation in the airway	*in vivo*	UC	(Almqvist *et al.*, 2008)

2.2 Results and Discussion

2.2.1 Assessment of the size exclusion chromatography exosome isolation method

At the start of this study SEC was found to be a promising alternative for exosome isolation when compared to UC, due to its cost effectiveness and lack of need for large/expensive equipment. Most importantly, SEC was a suitable single-step protocol to isolate a purer population of exosomes without damaging the vesicles (Böing *et al.*, 2014, Muller *et al.*, 2014, de Menezes-Neto *et al.*, 2015). SEC was found to be superior to UC with respect to purity as there was minimal albumin contamination (Baranyai *et al.*, 2015).

Pooled human serum from two individuals was fractionated using SEC on a Sepharose CL-4B column (Figure 2.1A). Exosomes are expected to elute first as they will travel within the void volume of Sepharose CL-4B. A small peak (max A280 at SEC fraction 9) was observed (inset in Figure 2.1B) prior to a large peak which contained the majority of serum proteins (Figure 2.1A). TEM showed particles of dimensions expected of exosomes in SEC fractions 8-10 (Figure 2.1D-F) with average diameters correlating to those of exosomes; 55.3 nm ±21.4, 44.5 nm ±14.5, 38.5 nm ±12.4 respectively (Figure 2.1I). Similar results were obtained using fresh fasted serum (Figure A1, Appendix 1). The spherical properties of the vesicles suggest that they were isolated without being lysed by the isolation process or TEM preparation. No vesicles were visible in SEC fraction 7 (Figure 2.1C) which correlated with the absence of a A280 reading (Figure 2.1B). SEC fraction 11 and 12 had a high background possibly due to the elution of serum proteins (Figure 2.1G and H). The average diameter decreased in size across the SEC fraction 8-10, as expected, as larger vesicles would elute first. The size range of the vesicles in SEC fraction 8 (18.7-125.5 nm) and SEC fraction 9 (15.3-117.5 nm) (Figure 2.1I), correlated with the reported exosome sizes of 20-100 nm (Caradec *et al.*, 2014, Vicencio *et al.*, 2015). The exosome enriched SEC fraction will be referred to as SEC exosomes. Fraction 10 was seen to have exosomes as well as vesicles smaller than exosomes (≤ 20 nm) (Figure 2.1F), with a size range of 10.4-86.8 nm (Figure 2.1I).

It is to be considered that these exosome diameters determined by TEM are an underestimation of their size due to dehydration and shrinkage. It is estimated that the shrinkage is about 0-21% of the real EV diameter as examined by cryo-electron microscopy or resistive pulse sensing (Bachurski *et al.*, 2019, Kotrbova *et al.*, 2019). In addition, NTA is seen to overestimate the size of serum and L-540 Hodgkin cell-derived EVs compared to TEM due to the inability to detect

vesicles below 60 nm; observed with both the NanoSight NS300 and ZetaView (Bachurski *et al.*, 2019).

It has been shown that SEC can be used as a stand-alone exosome isolation method from plasma (de Menezes-Neto *et al.*, 2015). The vesicles isolated from human serum by SEC fraction 8 and 9 appeared very similar to that reported by others with vesicles observed in a size range of 20-100 nm (Caradec *et al.*, 2014, Vicencio *et al.*, 2015, Ibrahim and Marbán, 2016). This suggested SEC fraction 8 and 9 may contain exosomes. The presence of smaller vesicles that was more prominent on the shoulder of the exosome peak has been reported previously and these particles were identified as HDL (Böing *et al.*, 2014).

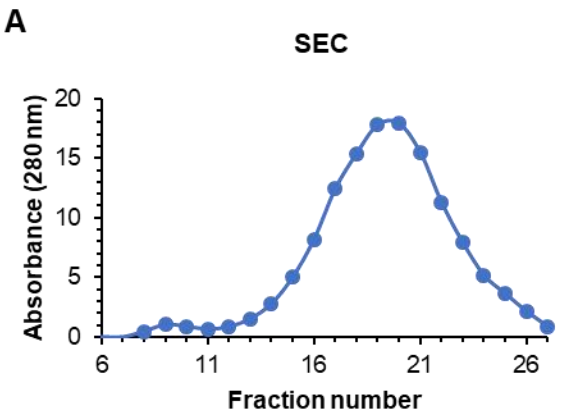

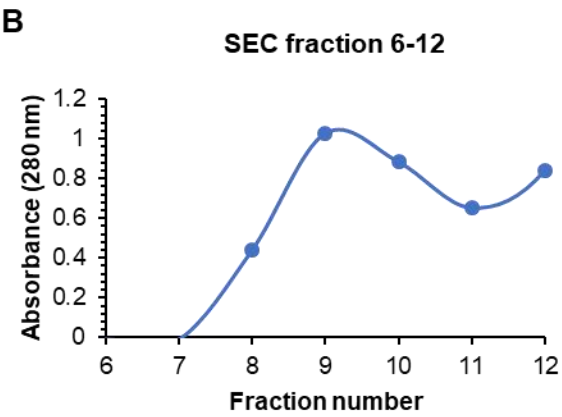

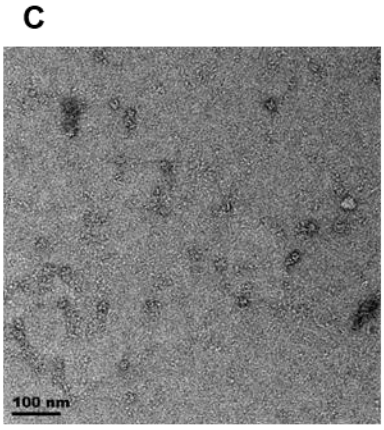

SEC fraction 7

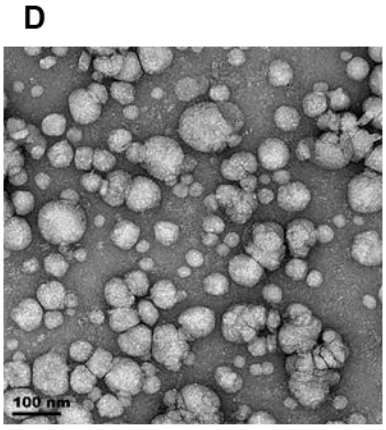

SEC fraction 8

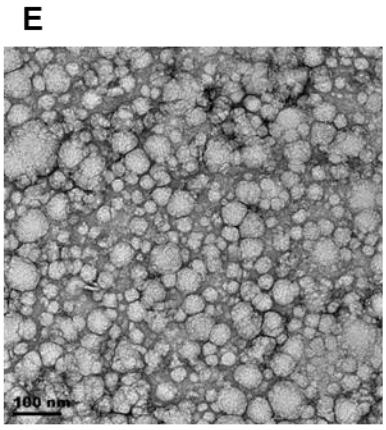

SEC fraction 9

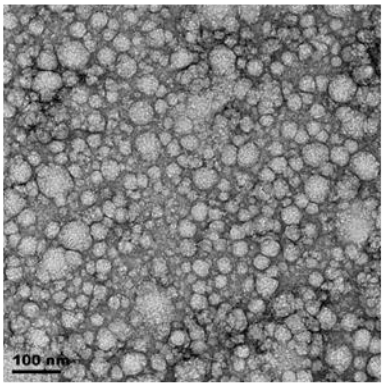

SEC fraction 10

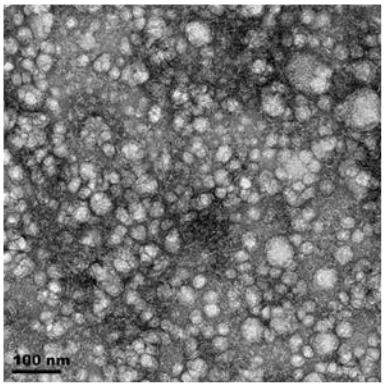

SEC fraction 11

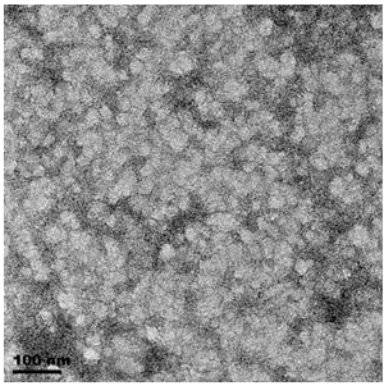

SEC fraction 12

I

	Average vesicle size (nm)	Min vesicle size (nm)	Max vesicle size (nm)
SEC fraction 8	55.3 ±21.4	18.7	125.5
SEC fraction 9	44.5 ±14.5	15.3	117.5
SEC fraction 10	38.5 ±12.4	10.4	86.8

Figure 2.1: SEC of pooled human serum performed on a Sepharose CL-4B column to isolate exosomes. (A) Absorbance profile of 1 ml human serum separated using SEC; (B) Absorbance profile of SEC fractions 6-12 to reveal the exosome enriched peak. Three independent experiments were performed; (C-H) TEM micrograph of SEC fractions 7-12 purified from pooled human serum. Scale bar = 100 nm; (I) TEM image analysis of vesicles present in SEC-derived exosome fractions 8-10. Five technical repeats and standard deviation (SD) shown.

2.2.2 Evaluating the purity of human serum exosomes isolated by three different methods

2.2.2.1 TEM analysis

SEC was then compared to two other popular exosome isolation methods (UC and ExoQuick precipitation). As mentioned in the introduction, PEG is used to precipitate particles by decreasing its solubility in a specific environment (salt concentration and 4°C) thereby forcing the particles together by excluding space, termed 'crowding reagents' (McNamara *et al.*, 2018a). ExoQuick is based on PEG precipitation and many researchers have used this technique to isolate exosomes from human serum/plasma (Yang *et al.*, 2017, Ye *et al.*, 2017, Li *et al.*, 2018c). UC was originally seen as the 'gold' standard to isolate exosomes and in 2016, UC was still being used by 81% of researchers (Gardiner *et al.*, 2016). Multiple centrifugation steps are used to separate particles according to their buoyant density and a final UC step is then used to isolate exosomes at (100 000 - 200 000 g) for 1-3 hours (Contreras-Naranjo *et al.*, 2017, Konoshenko *et al.*, 2018). The identity of the vesicles derived from human serum using three different exosome isolation methods (UC, ExoQuick and SEC) were evaluated using TEM imaging (Figure 2.2).

The negative staining revealed numerous exosome like particles with spherical morphology and diameter size ranging from 20-100 nm for all three exosome isolation methods (Figure 2.2). The UC-derived exosomes (Figure 2.2A) had a higher background compared to SEC-derived exosomes. However, the ExoQuick-derived (Figure 2.2B) exosomes required a 3X dilution to image the vesicles, whereas UC and SEC-derived exosomes (Figure 2.2A and C) required no dilution.

The dilution required to image the vesicles for the ExoQuick isolate suggested a high protein contamination, even when considering the starting amount of human serum and final exosome volume was 6 ml serum and 1.5 ml exosome isolate for UC, 0.5 ml serum and 0.2 ml exosome isolate for ExoQuick and 1 ml serum and 0.5 ml exosome isolate for SEC. One limitation of the ExoQuick study was that ExoQuick-TC was used due to its availability, which is aimed at isolating

exosomes from cell culture media although all ExoQuick products are PEG-based. However, there are widely reported issues with using ExoQuick as a stand-alone method to isolate pure exosomes. A study reported that commercial kits (ExoQuick and Total Exosome Isolation reagent) had the highest yield of serum vesicles detected using NTA; however, they had a lower protein purity and were less enriched for exosome markers (CD9, CD63 and TSG101) compared to UC (Tang *et al.*, 2017). They suggested the UC damaged the vesicles leading to a decrease in particle yield and that ExoQuick was unable to separate exosomes from aggregated high-density serum proteins thereby increasing contaminated proteins. In accordance with another report, ExoQuick and Total Exosome Isolation reagent precipitation had decreased serum-derived exosome purity; however, in this investigation they compared the isolation with Exo-spin which combines precipitation and SEC (Soares Martins *et al.*, 2018). The Exo-spin-derived exosomes had increased particle number and decreased protein concentration. It has been previously shown that commercial qEV SEC columns isolated exosomes of higher purity albeit with low exosome recovery from human plasma exosomes compared to ExoQuick and Exo-spin (Lobb *et al.*, 2015). They also found Exo-spin achieved significantly higher purification than ExoQuick with respect to protein; however, both these techniques had high contamination detected in TEM images and the presence of albumin contamination, which was not present in the qEV SEC exosomes. Furthermore, exosome marker flotillin-1 was only detected in the SEC exosomes.

ExoQuick was not specific to isolating only exosomes as SEC performed after ExoQuick revealed the presence of a substantial peak eluting after the exosome peak (Figure A2, Appendix 2). This confirmed that ExoQuick alone precipitates out contaminating proteins together with exosomes. This agrees with another study stating that ExoQuick requires a further isolation step such as UC and filtration to remove contaminating proteins when they showed that UC and ExoQuick yield the most the exosomes from bovine milk in a rapid amount of time (Yamada *et al.*, 2012). The major problem of protein contamination was considered to outweigh the advantages of ExoQuick such as the need for only a small sample volume (250 µl serum), no UC required, and its rapidity.

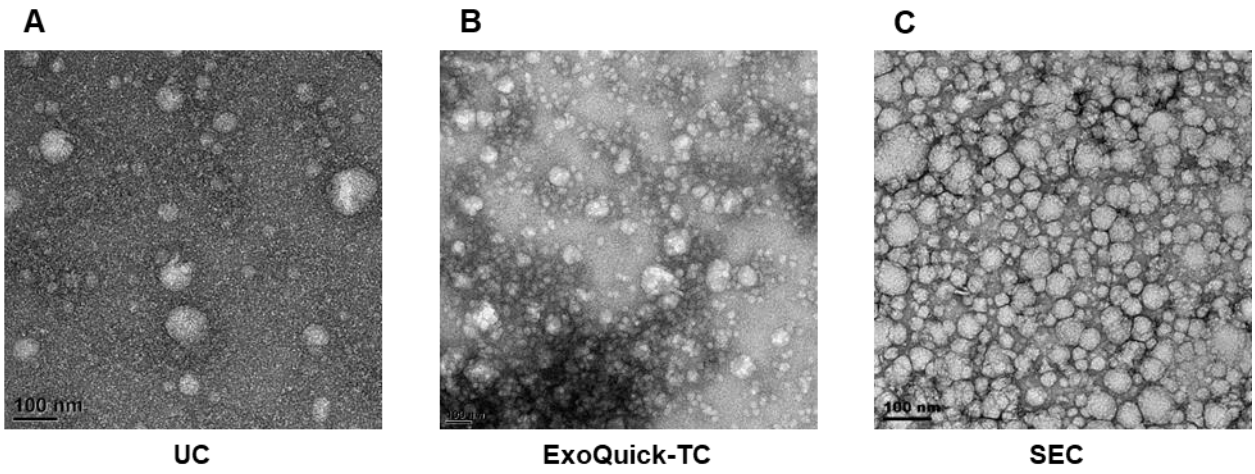

Figure 2.2: TEM micrograph of human serum exosomes isolated using three different isolation techniques. (A) UC (120 000 g for 2 hours); (B) ExoQuick-TC; (C) SEC**.** Scale bar = 100 nm.

2.2.2.2 Protein concentration

To validate the inference that the 'dirty' TEM images of UC and ExoQuick isolates from human serum were due to contaminating proteins, the protein concentrations of human serum exosomes isolated using the different techniques (UC (based on using centrifugal force), ExoQuick-TC (precipitation) and SEC (size separation)) were assessed using a Bradford assay (Table 2.2).

ExoQuick-TC exhibited the highest resultant protein concentration (38.7 µg/µl ±1.2, 200 µl), whereas SEC displayed the lowest (0.2 µg/µl ±0.03, 500 µl). It must be noted that the protein concentration for SEC-derived exosomes was at the limit of assay detection suggesting a very low level of protein which is likely due in part to the efficacy of the isolation method but may also reflect the dilution that occurs during SEC. Attempts were made to try and concentrate the SEC-derived exosome proteins using either Amicon Ultra 0.5 ml 100 kDa centrifugal filters or trichloroacetic acid precipitation (data not shown); however, with lack of success as no evidence of an increase in concentration was observed. This suggests that losses during the concentration process negated the concomitant concentration achieved.

Plasma SEC fractions have been concentrated previously using an Amicon® Ultra-4 10 kDa device (Lobb *et al.*, 2015). It is possible that an Amicon 10 kDa with regenerated cellulose membrane may have improved exosome concentrations rather than 100 kDa, as recent findings showed an Amicon 10 kDa filter concentrated and recovered the highest particle and protein yield

from human plasma SEC-derived exosomes (Vergauwen *et al.*, 2017). Amicon 100 kDa had reduced particle recovery but it was not significantly less. However, other centrifugal filters (Vivaspin 10kDa with either hydrosart, polyethersulfone or cellulose triacetate membranes) had significant particle loss. It has become apparent that accurately quantifying exosome protein is challenging. Previous research investigated the protein concentration of MCF-7 Rab27b-GFP-derived exosomes using four calorimetric assay (DC Protein, BCA, MicroBCA, Bradford) and three fluorometric assays (Qubit, NanoOrange, FluoroProfile) (Vergauwen *et al.*, 2017). The six different protein kits had high variability for the exosome protein concentrations, but showed less variability with known BSA standards (200-400 µg/ml). They found the Qubit fluorometric assay to have the least variance between different experiments and detected 1.5 and 2 times more protein than MicroBCA and Bradford. The Bradford assay may underestimate the protein concentration of samples containing a membrane (Kirazov *et al.*, 1993). Unfortunately, a Qubit assay requires use of a Qubit fluorimeter which is presently not available on our campus. The above findings further highlight the type of methodological issues that still plague the exosome field (Tkach *et al.*, 2017).

There are caveats at this point due to dilutions and concentration issues and lack of appropriate exosome quantification methods. It was challenging to directly compare the exosome protein concentration from the three different isolations. Assuming ExoQuick and UC pellet exosomes highly efficiently their use here would have respectively concentrated exosomes at least 2.5 and 3 times more than SEC. It is challenging to determine the SEC dilution. Furthermore, SEC exosome protein concentration was below an accurate reading and outside the quantitative range of the Bradford assay. NTA was not available at this stage of the investigation in South Africa; hence, particle numbers couldn't be determined or compared.

Even with concerns related to relative dilutions and concentrations, ExoQuick-TC showed minimal purification (38.7 µg/µl ±1.2) as total serum protein content is 60-80 µg/µl (Merrell *et al.*, 2004). Furthermore, in support of our results, Gamez-Velero *et al.* made use of both protein analysis and cryo-electron microscopy to show that SEC was able to remove a large proportion of plasma proteins, which PEG and PRotein Organic Solvent Precipitation (PROSPR) could not achieve (Gamez-Valero *et al.*, 2016). Another study contrasted with the general consensus as they found that UC retained 23% of serum proteins compared to 7.3% using the ExoQuick method (Caradec *et al.*, 2014). Tang *et al.*, showed that ExoQuick was found to have higher protein contaminations and lower exosome purity when compared to UC when used to isolate exosomes from both serum and cell culture media (Tang *et al.*, 2017). The differences could be due to different UC protocols

implemented; Caradec *et al.* used a very small serum volume of 330 µl and with a 30% sucrose cushion with one UC step at 100 000 g for 70 min, whereas Tang *et al.* had a larger serum volume (W32Ti rotor which holds 38.5 ml) and they used two UC spins at 110 000 g for 70 min to wash the exosome pellet. Precipitation-based isolation methods also co-isolate vesicle-free miRNAs, which obscures analysing miRNA cargo of plasma-derived EVs (Karttunen *et al.*, 2018).

The results do confirm that SEC isolates a protein-poor vesicle enriched fraction from human serum, reducing the contribution of plasma proteins towards subsequent functional studies. The high background detected in the TEM images of exosomes isolated by UC or ExoQuick (Figure 2.2) probably reflects the high protein content (Table 2.2); which was further investigated.

Table 2.2: Protein concentration of human serum exosomes isolated using three different isolation techniques

Isolation methods	Protein (µg/µl)	Basis of technique
UC	2.8 ±0.04	Centrifugal force
ExoQuick-TC	38.7 ±1.2	Precipitation
SEC	0.2 ±0.03	Size separation

2.2.2.3 SDS-PAGE analysis

Due to the high presence of contaminating protein in the ExoQuick isolates, ExoQuick was not further examined. To examine the nature of the SEC and UC isolates more closely equal volumes of each preparation were analysed on reducing SDS-PAGE (Figure 2.3).

This was considered reasonable and appropriate as qualitatively there was not a major difference in vesicle number as observed qualitatively by TEM (Figure 2.2). It can be seen that minimal protein banding is present in the SEC lane. Only traces of high molecular weight bands are visible with the most prominent band above 250 kDa. The UC isolate had a wide range of proteins at different molecular weights present. Most prominent was a band at 66 kDa which most likely reflects the preponderance of serum albumin (66.5 kDa, represents 57-71% of serum protein) in serum (Merrell *et al.*, 2004). There are also prominent bands at around 50 and 25 kDa which are probably IgG class γ heavy chains and light chains respectively, thus indicating IgG is at a high concentration in the UC isolate. The higher molecular weight bands in SEC are mirrored in the

UC lane and it is notable that the serum albumin and IgG bands are absent in the SEC isolate. Coomassie blue has detection limits but there appeared to be approximately 18X less protein in SEC compared to UC, in relation to the protein amount loaded in the SDS-PAGE (3.8 µg SEC-derived exosomes and 68.1 µg UC-derived exosomes).

In light of this finding the high background in the TEM image of UC-derived exosomes (Figure 2.2) probably reflects high protein content. This is in agreement with previous findings, as plasma vesicles are detected in UC isolates after 1 hour or 3 hours; however, they are obscured by a high background material which increases after 6 hour and 14 hours UC as detected by TEM (Baranyai *et al.*, 2015). The SDS-PAGE revealed significant albumin impurity in the UC isolate which is in line with previous studies detecting albumin using western blotting (Baranyai *et al.*, 2015) or mass spectrometry (Kalra *et al.*, 2013) in rat or human plasma UC-derived isolates. Further to this, various UC conditions (1 hour UC at 4°C, 10-fold dilution, 1 hour UC at 37°C, 3 hour, 6 hour and 14 hour UC) still result in albumin contamination (Baranyai *et al.*, 2015).

The SDS-PAGE revealed no detectable presence of albumin in the serum SEC-derived exosomes as per Baranyai *et al.* using Sepharose CL-4B or Sephacryl S-400 columns (Baranyai *et al.*, 2015). Due to the abundance of the major soluble plasma protein albumin in UC isolates, UC cannot be used to isolate pure exosomes which is important for identifying the composition and function of exosomes and for *in vivo* studies. Overall isolating human serum exosomes using SEC removed the majority of contaminating serum proteins.

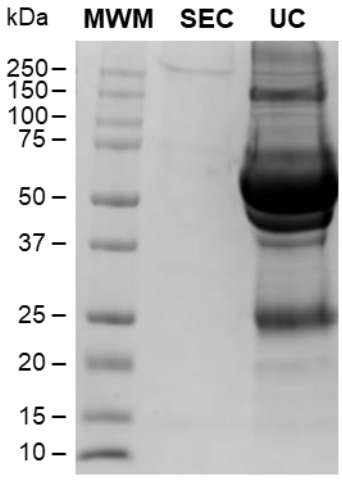

Figure 2.3: SDS-PAGE (12%) of proteins present in the exosome samples isolated from human serum using SEC or UC. Molecular weight marker (MWM). Equal volume loading of SEC and UC-derived isolates (24 µl) that contain 3.8 µg and 68.1 µg of protein respectively. n=2 (technical repeats).

These results so far demonstrate that the Sepharose CL-4B column efficiently isolated human serum vesicles within the exosome size range (20-100 nm) with very low levels of contaminating serum proteins. This correlates with a study where researchers compared different SEC columns and found that blood plasma exosomes had no significant albumin present when using Sepharose CL-4B or Sephacryl S-400 columns (Baranyai *et al.*, 2015). However, these researchers also found Sepharose 2B columns to be inferior due to co-elution of exosomes with albumin suggesting that this matrix is less suitable for purifying exosomes. Though the authors noted this finding as interesting, they did not speculate to why this contamination might occur. It may be possible that in Sepharose CL-4B, all variants of exosomes would elute in the void volume and not enter the matrix due to the 30 nm Sepharose pores, whilst in the CL-2B with 75 nm pores, smaller exosomes would enter the stationary phase and this might result in greater possibility of a peak crossover with the large albumin peak. Other studies have assessed Sepharose CL-2B and found it to be efficient but have not been focussed on albumin contamination. One study used Sepharose 2B SEC prior to UC to remove contaminating plasma proteins from plasma exosomes (Muller *et al.*, 2014). The SEC prior to UC was found to isolate plasma or serum exosomes as determined by significantly decreased total protein concentrations and improved 'clearer' TEM images, an observation that correlates with that seen in Figure 2.2. SEC was determined to be suitable as a stand-alone isolation method where a Sepharose CL-2B column was shown to isolate vesicles larger than 70 nm from platelet-depleted plasma with less than 1% of protein present (Böing *et al.*, 2014). The differences in studies could be due to column volume, volume of sample loaded, type of SEC column and sample size collected, and these parameters are not routinely supplied in the literature. Many studies such as that reported by Böing *et al.* use short columns (diameter of 1.6 cm, height of 6.2 cm and 10 ml of Sepharose CL-2B). Increasing column length improves the resolution of SEC as resolution is proportional to column length$^{1/2}$ according to the resolution equation and a large proportion of SEC columns have a 30 cm length for optimal resolution (Hong *et al.*, 2012). It has been demonstrated that a longer column length of 30 cm with a smaller diameter (~0.5 cm) compared to 10 ml syringes (such as Exo-spin Midi Columns or qEV columns) filled with about 12 ml Sepharose CL-2B, has improved resolution and marginal better separation of plasma vesicles and albumin (Welton *et al.*, 2016). Here we used diameter of 1 cm, height of 12.7 cm and 10 mL of Sepharose CL-4B for SEC. The main advantages of SEC are that it is more likely to preserve the biological activity of the exosomes due to is gentle nature, is relatively inexpensive, results in minimal protein contamination, and is quick and simple to use. However, an important disadvantage to consider is that the exosomes are diluted. UC could be used to enrich exosomes from a larger volume of plasma with the combination of SEC to remove

the contaminating plasma proteins; as Koh *et al.* showed that 10 ml plasma can be concentrated after 2 hours at 100 000 g and the resuspended 500 µl pellet purified on qEV SEC columns, with increased concentration of particles and the detection of exosome markers CD63, flotillin-1 and TSG101 (Koh *et al.*, 2018).

2.2.3 Western blot characterisation of exosomes

To further determine whether human serum exosomes were isolated using SEC, western blotting was used to confirm the presence of proteins enriched in exosomes (Figure 2.4). ISEV recommends a minimum of 3 proteins to be detected and they should come from different categories (Lötvall *et al.*, 2014), thus transmembrane proteins tetraspanins CD9 (23 kDa) and CD81 (26 kDa), as well as cytosolic protein TSG101 (50 kDa) were tested for in the SEC exosome enriched fraction. A negative protein marker could not be employed as serum exosomes are secreted by a variety of cells such as platelets, erythrocytes, endothelial cells and leukocytes (Hunter *et al.*, 2008, Gyorgy *et al.*, 2014).

CD9 and TSG101 were more readily detected after concentration of SEC fraction 9 using Amicon® Ultra-0.5 100 kDa device (Figure 2.4A) indicating achievement of some concentration even though no increase in absorbance at 280 nm was not seen (data not shown). A larger volume of exosome enriched SEC fraction was required for detection of CD81 and it is likely that this caused the spreading of the band. To assess the purity of the SEC fractions, equal protein loadings were analysed by western blots for exosomal markers (Figure 2.4B). TSG101 was found in fractions 8 and 9, whereas CD9 was only found in fraction 9. This confirms that human serum SEC fraction 8 and 9 contained exosomes. However, it can be seen that TSG101 was also detected from fraction 12-15 increasing in concentration.

The human serum SEC exosomes contained exosomal markers from different categories (transmembrane proteins (CD9, CD81) and cytosolic protein (TSG101)); further confirming the presence of an exosome enriched fraction. The abundance of TSG101 in later SEC fractions has been demonstrated previously as well as for CD63 of serum exosome isolations separated using SEC using equal volume loading as well as equal protein. Various studies where SEC-based isolation of exosomes from blood has been performed have shown this (Sepharose 2B, Sepharose CL-4B, Sephacryl S400, qEV size exclusion columns) (Baranyai *et al.*, 2015, Koh *et al.*, 2018). However, this phenomenon is not commented on besides Baranyai *et al.*, who suggested that the separation efficiency of CD63 and TSG101 from albumin was below 1% as they were detected in SEC fractions 6-9 (1 ml fractions) when loading equal volumes (Baranyai

et al., 2015). This may indicate SEC has a low separation efficiency due to overloading the SEC columns as non-exosome associated TSG101 and CD63 are present in serum which increases in concentration in later fractions throughout the isolation. CD9 appears to be more specific for exosomes than TSG101 as it was not detected in later SEC fractions. Although there are markers that are in high abundance in exosomes such as the transmembrane proteins (CD9, CD63, CD81) and cytosolic proteins (TSG101), they only suggest the vesicles are likely exosomes but it is not specific enough to characterise them from EVs of different intracellular origins such as microvesicles (Kowal *et al.*, 2016, Doyle and Wang, 2019). Again, highlighting the lack of specific markers to distinguish exosomes from other vesicles.

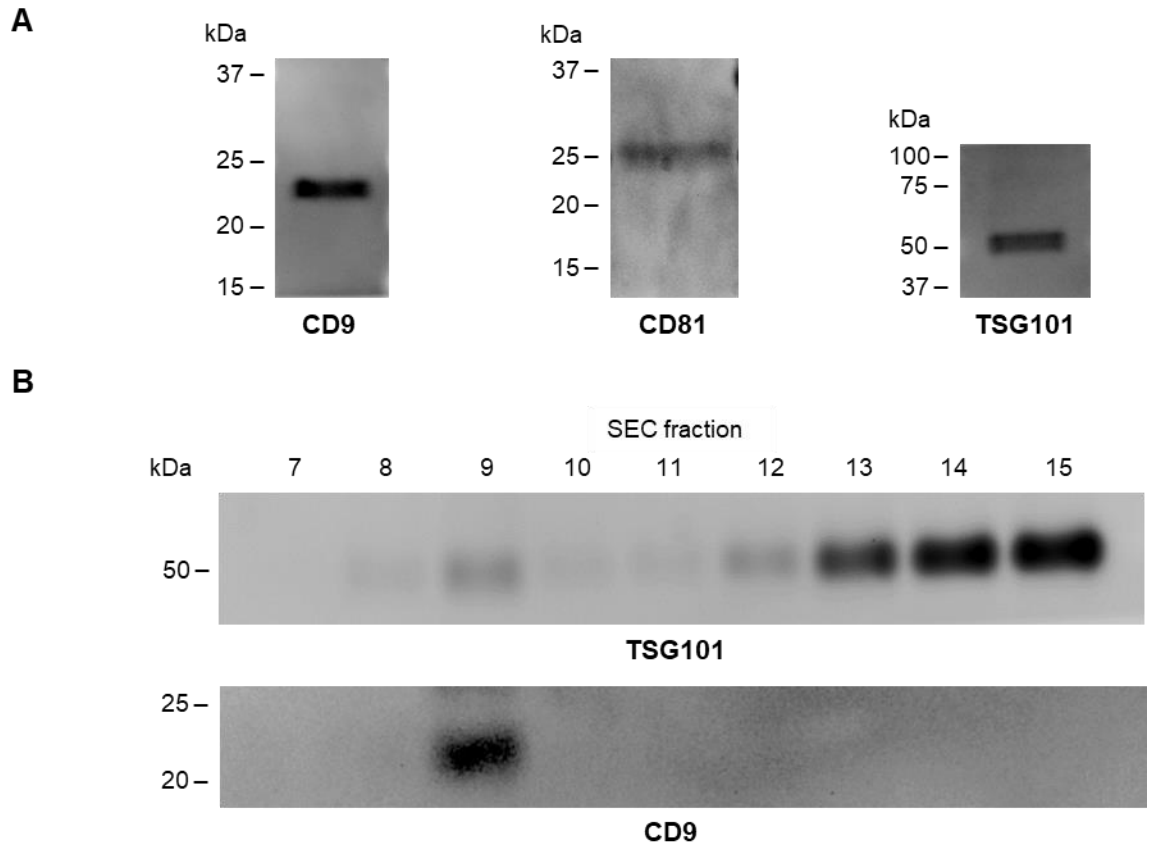

Figure 2.4: Western blot to confirm presence of human serum exosomes isolated using SEC. (A) Presence of the exosome markers CD9, CD81 and TSG101 was determined in SEC fraction 9 (6 µl loaded except for CD81 which was 24 µl). n=3-4 (technical repeats); (B) Presence of exosomal markers (CD9 and TSG101) was determined in the human serum SEC fractions 7-15 (0.27 µg/fraction). n=2-3 (technical repeats).

2.2.4 Functional assessment of exosomes

2.2.4.1 Exosome uptake into cells

A further characterisation and functionality study is to test for exosome uptake into cells where they release their contents into a recipient cell and uptake is often employed to indicate presence of exosomes (Feng *et al.*, 2010). A common technique used to test for exosome uptake into cells is to label the exosomes with fluorescent dyes. These include lipophilic membrane dyes PKH26 (Feng *et al.*, 2010), BODIPY™ TR Ceramide (Cianciaruso *et al.*, 2016), PKH67 (Nakata *et al.*, 2017) and DiD or DiO (Beit-Yannai *et al.*, 2018); cell-permeant nucleic acid stain SYTO™ RNASelect™ green fluorescent cell stain (Singh *et al.*, 2015) and a dye that labels EV proteins green ExoGlow™-protein EV labelling kit (green) (Gutkin *et al.*, 2016). In this exosome uptake experiment a variety of stains were examined (nucleic acid stain (SYTO RNASelect), membrane stain (BODIPY TR Ceramide), dual staining of the membrane and nucleic dye and a dye that labels EV proteins green (ExoGlow)). The cytoskeleton of the cells was stained red or green with Phalloidin to examine the location of the labelled exosomes and the cells nuclei were stained blue with DAPI.

To ensure that the excess fluorescent stain was removed, specialised columns (exosome spin column) were used to remove the unbound dye from the exosome sample. Another study used this column to remove free dye from ceramide-conjugated red fluorescent dye which labels the membrane, to show 293T cell-derived EVs entered U87 cells and not due to free stain labelled the cells (Balaj *et al.*, 2015). This is in alignment with our results in which we showed that exosome spin column removed the free fluorescent dye (Figure 2.5).

When no column was used for the SYTO RNASelect stain, the RNA stain labelled the HT1080 cellular RNA as seen by the green fluorescence within the cells (Figure 2.5A). The exosome spin columns removed the excess SYTO RNASelect stain as no green fluorescence was detected; hence, there was no labelling of the cellular RNA (Figure 2.5B). The level of fluorescence after use of the exosome spin columns was the same as that observed for the PBS control (Figure 2.5C).

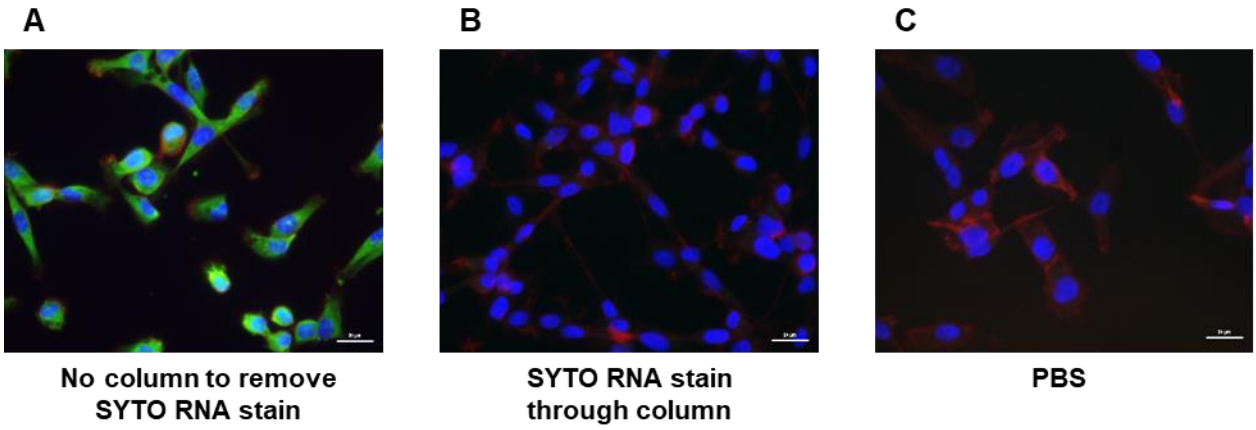

Figure 2.5: Exosome spin column removes unbound SYTO RNASelect as no cellular HT1080 RNA fluoresces. (A) Dye-only sample SYTO RNASelect (green); (B) PBS mixed with SYTO RNASelect and centrifuged through the exosome spin column to remove unbound SYTO RNASelect dye; (C) PBS control. HT1080 cells were cultured for 3 hours with the treatments. After treatment fluorescent images were obtained using a fluorescent microscope (Nikon Eclipse 90i DS-Ri1). Nuclei stained with DAPI (blue) and cytoskeleton stained with Alexa Fluor® 594 Phalloidin (red). Scale bar = 20 µm. n=2 (technical repeats, 5 random fields of view per n).

Various volumes of human serum SEC-derived exosomes labelled with SYTO RNASelect (green) were incubated with HT1080 cells to test the dosage effect on the amount of transfection (Figure 2.6).

Both 25% (v/v) SEC exosomes (Figure 2.6D) and 12.5% (v/v) (Figure 2.6C) gave 100% labelling of the cells with a drop in intensity observed at 12.5% and 6.25% (v/v) (Figure 2.6B) did not label all cells. Therefore, 12.5% (v/v) human serum SEC-derived exosomes was the concentration used to further test a variety of stains for exosome uptake.

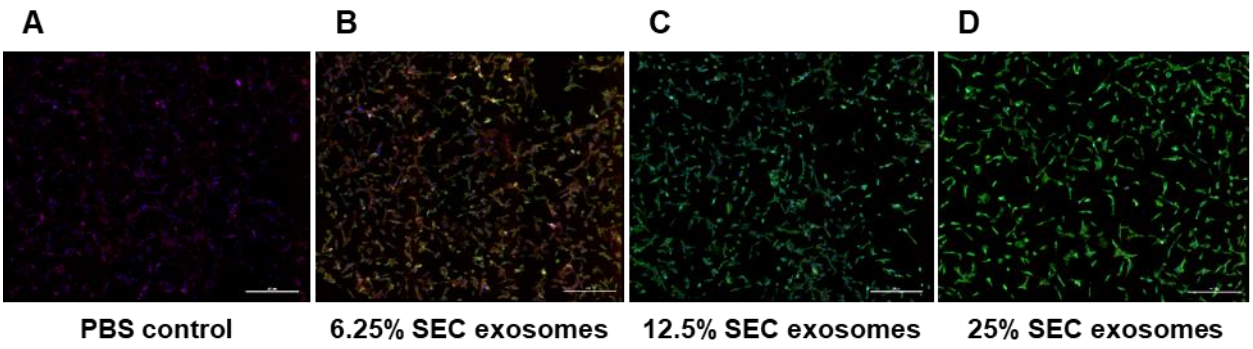

Figure 2.6: Dosage effect of exosome uptake of fluorescently labelled SEC-derived exosomes by HT1080 cells *in vitro*. (A) PBS control; (B-D) Uptake of exosome sample labelled with SYTO RNASelect (green) at various dosages (6.25, 12.5, 25% (v/v)). HT1080 cells were cultured for 3 hours with the treatments. After treatment fluorescent images were obtained using a fluorescent microscope (Nikon Eclipse 90i DS-Ri1). Nuclei stained with DAPI (blue) and cytoskeleton stained with Alexa Fluor® 594 Phalloidin (red). Scale bar = 250 µm. n=2 (technical repeats).

The SEC exosomes were labelled with nucleic acid stain (SYTO RNASelect) which labelled the RNA within the exosomes (green) (Figure 2.7B-C), membrane stain (BODIPY TR Ceramide) which labelled the lipid membrane of the exosomes (red) (Figure 2.7E-F), dual staining of the membrane and nucleic dye (red and green) (Figure 2.7H-I) and a dye that labels EV proteins green (ExoGlow) (Figure 2.7K-L).

It was shown using all dyes that after incubation with HT1080 cells, SEC exosomes entered the cells (Figure 2.7). The PBS controls showed no auto fluorescence of the HT1080 cells labelled with DAPI or Phalloidin (Figure 2.7A and D). Zoomed in images of SEC exosome uptake determined localisation of the exosomes into HT1080 cells using the various stains (Figure 2.7C, F, I and L). The SYTO RNASelect labelled exosomes were detected by green diffuse fluorescence throughout the cell (Figure 2.7C), BODIPY TR Ceramide labelled exosomes were detected by red fluorescence around the cells nuclei (Figure 2.7F), the double staining revealed red punctuation around the cells nuclei and parts of the cytosol and green diffuse labelling throughout the cytoplasm (Figure 2.7I) and ExoGlow labelled exosomes were detected by green punctate fluorescence which accumulated along the cell membranes and there was cytoplasm labelling. All of which indicated exosome uptake into the cells and the release of exosome contents within the cytoplasm (Figure 2.7C, F, I and L).

Reports on exosome uptake efficiency are variable as they range from 1 hour to 24 hours. These experiments showed SEC exosomes entered HT1080 cells after 3 hours, using a variety of stains.

A previous study showed that EVs derived from human embryonic kidney cells 293 were internalised by Uppsala 87 malignant glioma cells after 60 minutes of incubation (Balaj *et al.*, 2015). Numerous studies have used SYTO RNASelect or BODIPY TR Ceramide to test for exosomal uptake into cells (Harp *et al.*, 2016), such as SYTO RNASelect labelled adipose stem cell-derived exosomes were taken up by neuron cells after 3 hours (Ching *et al.*, 2018). ExoGlow has also been used for investigating exosomal uptake into cells (Mead and Tomarev, 2017, Sun *et al.*, 2017), such as human menstrual blood-derived stem cell exosomes labelled with ExoGlow are taken up by AML12 cells after 24 hours (Chen *et al.*, 2017).

All three stains which as indicated above work on very different basis: nucleic acid stain, lipid membrane stain and a dye that labels EV proteins green. The labelled exosomes were found located within the cytoplasm which is in agreement with the literature (Mutschelknaus *et al.*, 2016, Rosenberger *et al.*, 2019). The internalisation of the exosomes suggests that the exosomes break apart to release their contents into the recipient cell, which was seen previously by membrane-labelled cancer cell-derived exosomes gathering along the cell membrane after 3 hours and after 24 hours the exosomes had been taken up by the cells causing cytoplasm labelling (Mutschelknaus *et al.*, 2016). Exosome uptake was dose dependent, as there was as a brighter green fluorescence with increasing exosome concentration (6.25%, 12% and 25% (v/v)). Another study also showed this effect, SW780 cell-derived exosomes were taken up by bladder cancer cells within 4 hours and fluorescent intensity increased with a dose-dependent increase in exosomes (64, 320, 640, $1280x10^6$ exosomes) (Franzen *et al.*, 2014). It has also been found that exosome uptake can be time-dependent, menstrual MSC-derived exosomes were taken up by HUVEC and HMEC in increasing quantities over 4, 8 and 16 hours detected via FACS (Rosenberger *et al.*, 2019). They further confirmed the labelled MSC-derived exosomes were localised in the cytoplasm by confocal microscopy. The incubation time for exosome uptake can be cell-dependent, head and neck cancer cell-derived exosomes were taken up by dendritic cells within 30 minutes, whereas T cells required 24 hours to internalise the exosomes as detected by confocal microscopy (Ludwig *et al.*, 2018). The HT1080 cells readily internalised the human serum SEC-derived exosomes. This is of course functionally important as it shows the exosomes can readily deliver their therapeutic benefit or be a delivery vehicle to cells. However, caution must be taken in interpreting exosome uptake studies. Research had shown that serum and pure protein samples stained with lipophilic dyes (CellMask, PKH67, DiD) transfer the dye into cells (Takov *et al.*, 2017). Hence, a slight contamination of proteins in the exosome preparation can skew the result of the study. This aspect will be discussed further in Chapter 3.

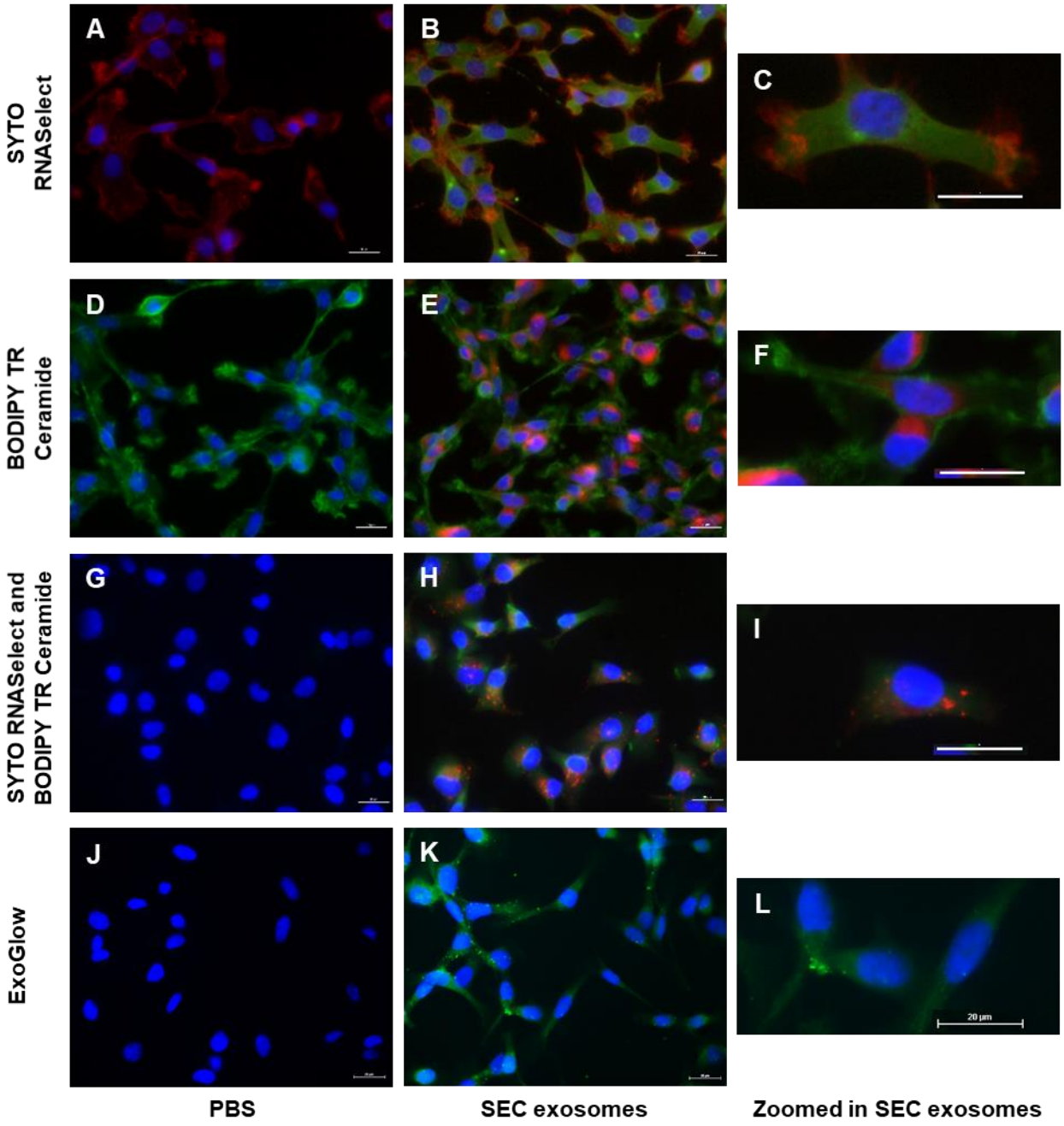

Figure 2.7: Uptake of fluorescently labelled human serum SEC-derived exosomes by HT1080 cells *in vitro*. (B-C) Exosome samples labelled with SYTO RNASelect (green), 12.5% (v/v); (E-F) Exosome samples labelled with BODIPY TR Ceramide (red), 12.5% (v/v); (H-I) Exosome samples double labelled with BODIPY TR Ceramide (red) and SYTO RNASelect (green), 12.5% (v/v); (K, L) Exosome samples labelled with ExoGlow (green), 25% (v/v); (A, D, G, J) PBS control; (C, F, I, L) Zoomed in image of SEC exosome uptake. HT1080 cells were cultured for 3 hours with the treatments. After treatment fluorescent images were obtained using a fluorescent microscope. Nuclei stained with DAPI (blue) and cytoskeleton stained with Alexa Fluor® 594 Phalloidin (red) (A-C) or Alexa Fluor® 488 Phalloidin (green) (D-F). Scale bar = 20 µm. n=3 (technical repeats).

2.2.4.2 The effect of exosomes on fibroblast growth

Serum exosomes have functional properties as removing exosomes from FBS using UC decreases muscle cell proliferation and differentiation (Aswad *et al.*, 2016). Furthermore, human serum exosome isolated using UC and density gradient have been shown to increase HMEC proliferation and tube formation (Cavallari *et al.*, 2017) and coronary serum exosomes from myocardial ischemia patients isolated using UC improved HUVEC proliferation, migration and tube formation (Li *et al.*, 2018b). Most of the functional studies testing the therapeutic effects of serum exosomes use UC isolations which contain non-exosome contaminants that could cause the biological effects detected (Takov *et al.*, 2017, Menard *et al.*, 2018). There are limited studies that investigate the function of serum/plasma-derived exosomes isolated using SEC (Takov *et al.*, 2019). The following experiment was done to determine the optimal storage conditions for assaying the functional effects of serum-derived exosome enriched SEC fraction with low protein content (Figure 2.8). Favourable storage conditions for exosomes have been reported to be below -70°C to preserve isolated exosomes for clinical application and scientific research (Lee *et al.*, 2016). Here various storage conditions of SEC-derived exosome were tested: SEC exosomes used immediately after isolation, stored at -80°C for 2 hours or snap frozen in liquid nitrogen and subsequently stored at -80°C for 2 hours. Due to exosomes having a potential to be used for therapeutic purposes, it is important to determine the stability of the exosomes after freezing.

To determine the effects of exosome enriched fraction on HdFb proliferation, fibroblasts were incubated with SEC exosomes for 72 hours (Figure 2.8). As 12.5% (v/v) were internalised by all cells in the uptake experiment (Figure 2.6), 10% (v/v) of the exosome enriched SEC fraction (SEC exosomes) was considered sufficient for the cell proliferation assay. Treatment with 10% (v/v) SEC-derived exosomes had a significant increase in cell proliferation ($p < 0.05$) compared to fibroblasts treated with PBS control containing no serum. There was no significant difference in proliferation induced by SEC-derived exosome used immediately after isolation, stored at -80°C for 2 hours or snap frozen in liquid nitrogen and subsequently stored at -80°C for 2 hours. Although 10% exosomes significantly promoted the proliferation of HdFb cells, proliferation was significantly more with 5% human serum (set at 100%). This indicates that exosomes play a role in cell proliferation; however, there are other components in serum that can also promote cell proliferation.

The majority of serum exosomes have been found to be derived from platelets (Brisson *et al.*, 2017). Blood is suggested to contain components that have regenerative potential function (Villeda *et al.*, 2014, Wyss-Coray, 2016, Sun *et al.*, 2019). A further broad indication of this

potential is the extensive research into the use of PRP in regenerative approaches in ulcer wounds, tendon injuries, cosmetic purposes, scar healing and hair loss, discussed in section 1.6.2.1 (Alves and Grimalt, 2018). PRP has a higher concentration of platelets than in plasma and once the platelets are activated they release a pool of bioactive agents including proteins, growth factors, cytokines and exosomes (Anitua *et al.*, 2015). Studies have shown that PRP exosomes promote cutaneous healing of chronic wounds in a diabetic rat model (Guo *et al.*, 2017) and plasma/serum exosomes are cardioprotective (Vicencio *et al.*, 2015, Bei *et al.*, 2017). Hence, PRP exosomes could be beneficial for regenerative purposes. It should be noted that at this early stage in this field of research, there are no studies comparing the difference in angiogenic potential of PRP exosomes to serum exosomes. The data suggests that serum exosomes isolated using SEC have bioactivity, as shown by previous researchers. One study found that 14 out of 18 serum-derived exosome samples caused proliferation of HMEC (averaging $5x10^4$ exosomes/target cell) (Cavallari *et al.*, 2017). Further research has shown that human umbilical cord blood-derived exosomes accelerate wound healing by transfer of miR-21-3p into HdFbs and HMEC (Hu *et al.*, 2018). Plasma exosomes have been shown to be cardioprotective and potential mechanisms include HSP70 present on the surface of exosomes communicate with TLR4 resulting in a signalling pathway in cardiomyocytes which activated cardioprotective HSP27 (Vicencio *et al.*, 2015), serum exosomes activate an ERK1/2 and HSP27 signalling cascade to prevent apoptosis of H9C2 cardiomyocytes (Bei *et al.*, 2017, Li *et al.*, 2018c) or serum exosomes are regulating miR-17-3p/TIMP3 to increase the proliferation of H9C2 cardiomyocytes (Liu *et al.*, 2018b). However, three of these reports used ExoQuick to isolate the serum exosomes (Bei *et al.*, 2017, Li *et al.*, 2018c, Liu *et al.*, 2018b). This isolation method is potentially compromised due to the high serum protein contamination as previously discussed which may mislead the conclusion of how the plasma exosomes are cardioprotective. The lack of plasma proteins, especially albumin, in the SEC exosome result in better quality exosomes. The fact that these low protein SEC exosomes significantly increase cell proliferation of fibroblasts suggests that serum exosomes do play a role in cell proliferation.

It was further demonstrated that exosomes are suitable for cryopreservation. In support of this, previous studies have shown that exosomes derived from fresh and frozen plasma cause equal immune suppression by the down-regulation of CD69 expression on activated human CD4+ T cells (Muller *et al.*, 2014). Though few studies testing the functionality of serum-derived exosomes isolated using SEC are available, our results are consistent with a study by Takov *et al.*, who found that plasma-derived EVs isolated using SEC are bioactive as they found they stimulated migration of HUVEC (Takov *et al.*, 2019). Serum provides an accessible and promising source of

exosomes for therapeutic applications. However, further research into exosome stability is required.

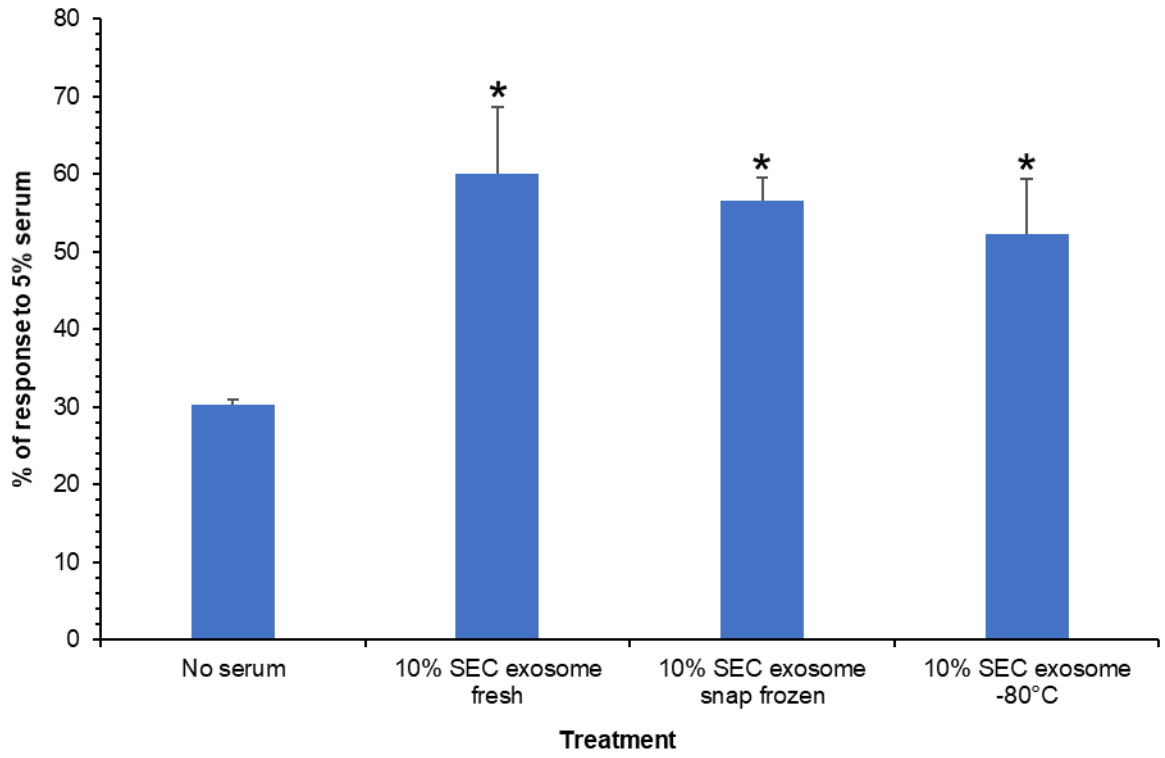

Figure 2.8: *In vitro* effects of human serum SEC-derived exosomes on HdFb proliferation. Human fibroblasts were grown in MCDB media for 72 hours with various treatments shown. Data was normalised to cells cultured in 5% human serum. Proliferation was detected with the XTT assay. Combination of four independent experiments with four technical repeats. * $p < 0.05$ compared to no serum.

2.2.4.3 The effect of exosomes on endothelial cell-derived spheroid sprouting

Most exosome functionality studies test for cellular uptake, proliferation and migration (tube formation assay or transwell assay) (Guo *et al.*, 2017, Tao *et al.*, 2017b, Chen *et al.*, 2018b). The spheroid sprouting assay designed in 1999 (Korff and Augustin, 1999), allows for studying the therapeutic effect of biological components on sprouting angiogenesis in a 3D *in vitro* model (Heiss *et al.*, 2015). The 3D spheroid assay represents *in vivo* angiogenesis better than 2D angiogenesis assays (tube formation on Matrigel) as it illuminates the communication between endothelial cells under various treatments (Nowak-Sliwinska *et al.*, 2018). Angiogenic potential is

analysed by sprout number and length. The minority of exosome functionality studies that do use the spheroid assay, investigate the therapeutic effect of exosomes against cancer growth (Khalyfa *et al.*, 2016, Murgoci *et al.*, 2018, Wang *et al.*, 2018a). Hepatic stellate cell-derived exosomes (5 µg) have been previously shown to deliver miR-335 (tumour suppressor) to cancer spheroids, inhibiting cancer cell invasion *in vitro* which correlated with their inhibition of tumour growth *in vivo* (Wang *et al.*, 2018a). Microglia cell-derived exosomes (isolated from LPS stimulated cells) have shown to inhibit tumour invasion by 50% over 6 days using 3D glioma cell culture spheroids (Murgoci *et al.*, 2018). To test for potential angiogenic properties of human serum SEC exosomes (30% (v/v)), exosomes were incubated with HUVEC spheroids embedded in a fibrin hydrogel (3.25 mg/ml) for 48 hours (Figure 2.9).

Phase contrast images of the spheroids showed more sprout activity when treated with SEC exosomes compared to the PBS control after 48 hours (Figure 2.9A). The sprout number was analysed after 48 hours (Figure 2.9B). The serum SEC exosomes significantly increased the HUVEC sprout number (23 ±0.3) ($p < 0.05$) compared to the PBS control (16 ±2.1). There was no difference in sprout length (data not shown).

Endothelial cell proliferation is located within the stalk cells during sprout elongation and the onset of angiogenesis is tip cell activation and loosening of cell to cell contact for migration (Ausprunk and Folkman, 1977, Gerhardt, 2008). Depending on the microenvironment, pro-angiogenic paracrine signals will initiate endothelial cell sprouting. The spheroid assay is a useful *in vitro* technique to test for migration in a 3D setting. There are limited studies that investigate the effect of exosomes on spheroids. Our data is novel in identifying serum SEC exosomes cause an increase in endothelial sprout number. Other studies have found that conditioned media from MSCs induced significantly longer HUVEC sprout length after 16 hours (Gong *et al.*, 2017). They went on to investigate whether the paracrine mechanism was involved, and they showed exosomes derived from MSCs mediated the transfer of miRs from MSCs to HUVECs and promoted angiogenesis. Their results suggested the exosomes delivered pro-angiogenic miRNAs; albeit they did not directly investigate the effect of MSC exosomes on spheroid sprouting. We did not see an increase in sprout length, but our source of exosomes was from serum and not MSCs. Plasma-derived exosomes, isolated using precipitating Total Exosome Isolation reagent, from patients with sleep apnea stimulate proliferation and migration of lung cancer cells (Khalyfa *et al.*, 2016). However, the plasma-derived exosomes from patients with sleep apnea caused no significant difference in invasion using a 3D spheroid assay with lung cells. As described above, spheroid assays have also been used to test for the role of cancer-

derived exosomes. A study showed that exosomes (100 µg/ml) derived from cancer cell lines (LNCaP and DU145) caused prostate epithelial cell line (RWPE-1) spheroids to disseminate after 48 hours (Hosseini-Beheshti *et al.*, 2016). Two cell types are within the bud of the sprout, tip cells (migration) and stalk cells (elongation) (Irvin *et al.*, 2014) that may provide a reason for the spheroid observations. It is possible the serum SEC exosomes activate the tip cells for migration leading to an increase in sprout number, but they don't activate the stalk cells; hence, no increase in sprout length. As the serum SEC exosomes showed bioactivity through cellular uptake, enhancing fibroblast proliferation and increasing spheroid sprout numbers *in vitro*; the stability of the SEC exosomes stored at 37°C for 3 weeks was further investigated.

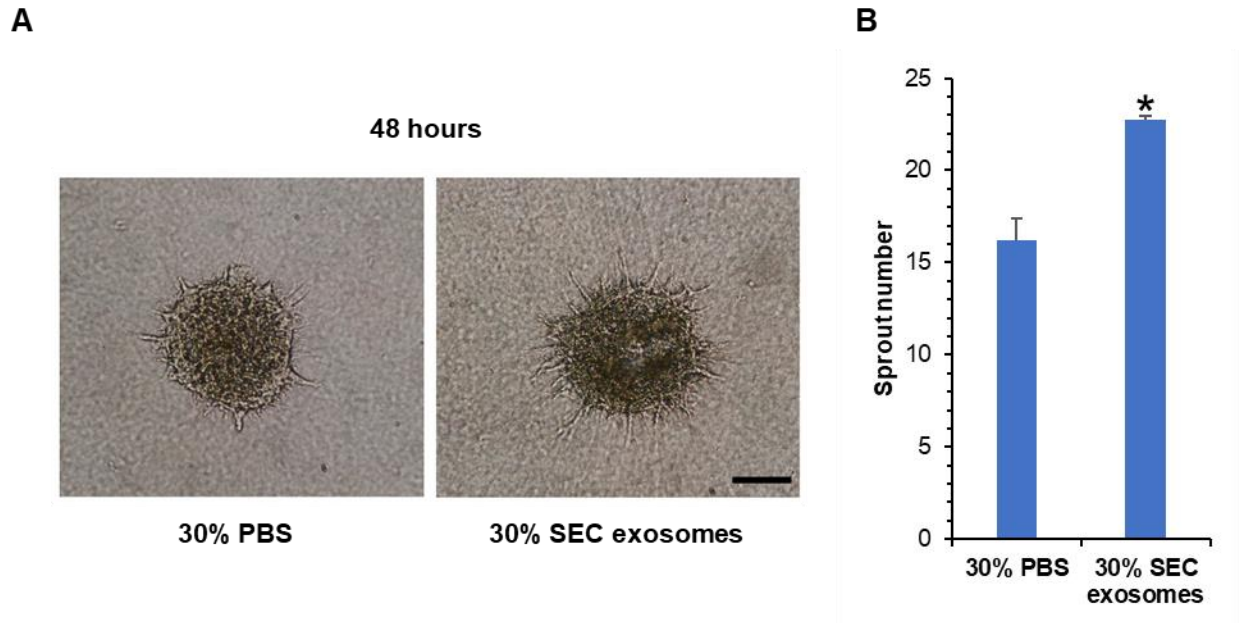

Figure 2.9: *In vitro* effects of human serum SEC-derived exosomes on sprouting of HUVEC spheroids in fibrin hydrogels. (A) Fibrin hydrogels were treated with either 30% PBS or 30% serum SEC-derived exosomes in 2% FBS MCDB media and sprouting was imaged using a phase-contrast microscope at 48 hours. Scale bar = 100 µm; (B) Analysis of sprout number (30% PBS and 30% serum SEC-derived exosomes) after 48 hours. Combination of three independent experiments with four technical repeats. * $p < 0.05$ compared to 30% PBS control.

2.2.5 Stability of exosomes

Pharmaceutical companies have an obligation to prevent loss of therapeutic properties during delivery of drugs. Hence, a temperature-controlled environment is required by certain therapeutic

products. It is good practice for drug products to be tested for stability (Ammann, 2011). Due to exosomes having a potential to be used for therapeutic purposes, it is important to determine the temperature stability of the exosomes. These experiments tested the bioactivity of human serum SEC exosomes that were stored at either -80°C or 37°C. Even though UC-derived exosomes were shown to have high protein contamination, their stability was also tested. The SEC and UC-derived exosomes morphological stability was determined by TEM and their functionality stability by their retention of their ability to stimulate cell proliferation and be taken up by cells.

2.2.5.1 TEM analysis

To determine the stability of the SEC and UC-derived exosomes, they were stored at 37°C for 3 weeks with gentle agitation and their physical properties assessed by TEM (Figure 2.10).

The TEM revealed that SEC-derived exosomes retained their spherical shape and diameter size ranging between 20-100 nm when stored at 37°C for 3 weeks compared to the -80°C storage (Figure 2.10A). The average diameter of SEC exosomes stored at -80°C (41.2 nm ±16.4) decreased in size when stored at 37°C for 3 weeks (36.1 nm ±15.2), which is a 12.4% decrease in average vesicle diameter (Figure 2.10B). The size range of the vesicles in SEC exosomes stored at -80°C (21.0-128.2 nm) and stored at 37°C for 3 weeks (15.5-155.1 nm) (Figure 2.10B), were not significantly different. The TEM revealed that vesicles were isolated using UC as could be seen by the presence of spherical or cup-shaped particles (Figure 2.10A). The average vesicle diameters were difficult to accurately quantify for the UC-derived exosomes due to the high background present on the TEM grid, whereas the SEC-derived exosomes had a cleaner TEM background. The TEM background is higher on the UC-derived exosomes stored at 37°C for 3 weeks compared to being stored at -80°C, likely due to contaminating proteins aggregating. This high background confirms the previous result that UC isolated contaminating proteins which interfere with TEM visualisation (Figure 2.3).

A

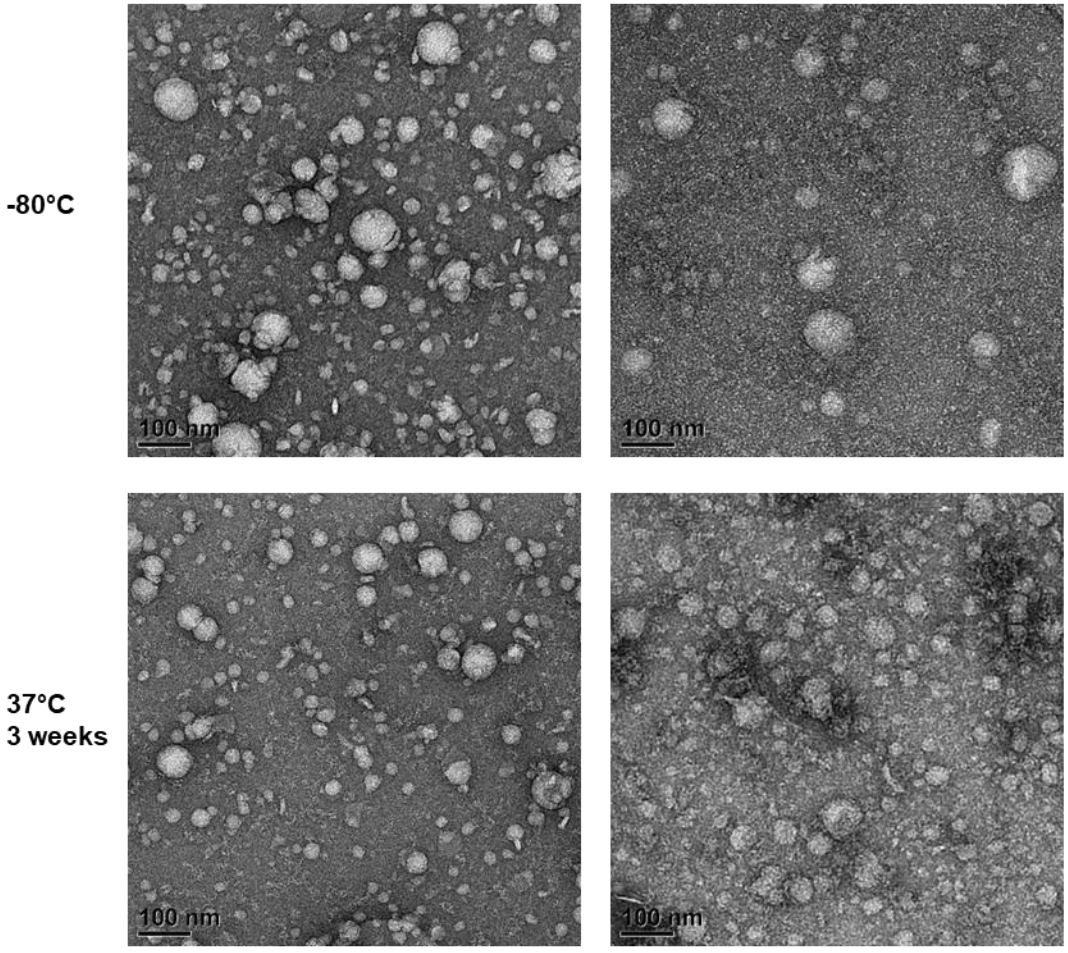

B

	Average vesicle size (nm)	Min vesicle size (nm)	Max vesicle size (nm)
SEC exosome -80°C	41.2 ±16.4	21.0	128.2
SEC exosome 37°C	36.1 ±15.2	15.5	155.1

Figure 2.10: TEM micrograph of human serum exosomes isolated using SEC or UC and stored at either -80°C or 37°C for 3 weeks. (A) TEM micrographs. Scale bar = 100 nm; (B) TEM image analysis of vesicles present in SEC-derived exosome and stored at either -80°C or 37°C for 3 weeks. Five technical repeats and SD shown.

2.2.5.2 Uptake analysis

The stability of the exosomes after storage at 37°C for 3 weeks was then further assessed with respect to both their uptake by cells and their efficacy in stimulating cellular proliferation.

To examine exosome uptake, the exosomes were labelled green with SYTO RNASelect which labelled RNA contained within the exosomes (Figure 2.11). The PBS controls showed no auto fluorescence of the HT1080 cells stained with DAPI and ActinRed™ ReadyProbes® (Figure 2.11A and D). Exosome uptake occurred for the SEC-derived and UC-derived exosomes that were stored at -80°C (Figure 2.11B and E). Both the SEC-derived and UC-derived exosomes retained their functionality as they were taken up by HT1080 cells after being stored at 37°C for 3 weeks as detected by green fluorescence with all cells showing the presence of RNA within their cytoplasmic regions (Figure 2.11C and F). Therefore, the exosomes were still functional and able to enter the HT1080 cells.

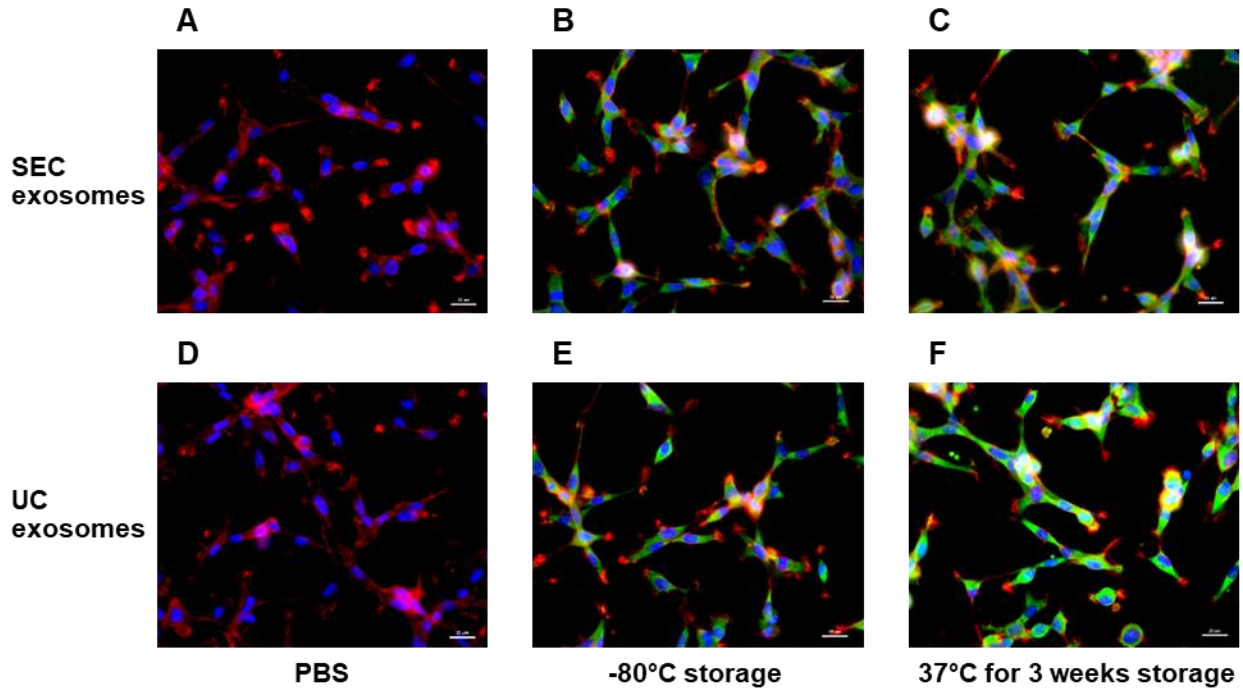

Figure 2.11: Functional stability of human serum SEC or UC-derived exosomes stored at either -80°C or 37°C for 3 weeks. Uptake of SYTO RNASelect (green) labelled exosomes by HT1080 cells *in vitro*. (A) PBS control for SEC-derived exosomes; (B) SEC-derived exosomes stored at -80°C, 12.5% (v/v); (C) SEC-derived exosomes stored at 37°C for 3 weeks, 12.5% (v/v); (D) PBS control for UC-derived exosomes; (E) UC-derived exosomes stored at -80°C, 4.18% (v/v); (F) UC-derived exosomes stored at 37°C for 3 weeks, 4.18% (v/v). HT1080 cells were cultured for 3 hours with the treatments. After treatment fluorescent images were obtained using a fluorescent microscope. Nuclei stained with DAPI (blue) and cytoskeleton stained with ActinRed™ ReadyProbes® (red). Scale bar = 20 µm. Two independent experiments with three technical repeats.

2.2.5.3 Proliferation analysis

To study whether human serum exosomes retained their biological activity after being stored at 37°C for 3 weeks, fibroblasts were incubated with SEC or UC-derived exosomes for 72 hours before analysing cell proliferation (Figure 2.12). It was calculated that 3.33% of UC exosomes was roughly equivalent to 10% SEC exosomes isolated, as determined from initial serum volumes and final isolate volumes. UC was concentrated 3.6X from 5.4 ml human serum and SEC had a final isolate volume of 0.5 ml from 1 ml human serum; hence, it was estimated that there were 3X more EVs in UC-derived than SEC-derived exosomes.

Treatment with 10% SEC-derived exosomes showed a significant increase in cell proliferation ($p < 0.05$) compared to fibroblasts treated with no serum. There was no statistical difference between SEC-derived exosomes stored at -80°C and 37°C for 3 weeks (Figure 2.12A). Treatment with 3.33% UC-derived exosomes stored at -80°C and 37°C trended towards increased cell proliferation; however, it was not statistically significant compared to fibroblasts treated with no serum (Figure 2.12B).

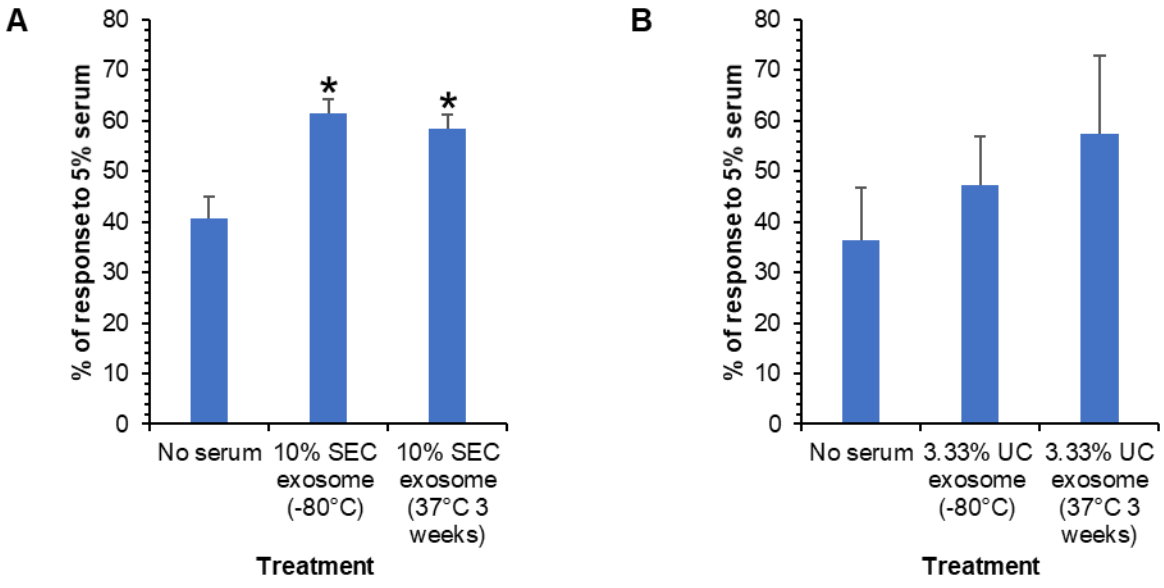

Figure 2.12: *In vitro* effects of human serum SEC or UC-derived exosomes stored at either -80°C or 37°C for 3 weeks on HdFb cell proliferation. (A) Serum SEC-derived exosomes; (B) Serum UC-derived exosomes. Human fibroblasts were grown in MCDB media for 72 hours with various treatments shown. Data was normalised to cells cultured in 5% human serum. Proliferation was detected with the XTT assay. Combination of four independent experiments with four technical repeats. * $p < 0.05$ compared to no serum.

In this study UC was also used to isolate exosomes from human serum as this is still the most common exosome isolation technique (Gardiner *et al.*, 2016). Exosomes were seemingly confirmed to be isolated as determined by electron microscopy that showed vesicles ranging between the sizes of 20-100 nm. It was not possible to detect the exosome markers in the UC exosomes using western blotting (data not shown) as there were prominent bands at around 50 and 25 kDa. These are probably IgG class y heavy chains and light chains as prominent bands could be observed in the SDS-PAGE gel (Figure 2.3). It was shown that UC was a less optimal isolation method as large levels of contaminating proteins were isolated as seen by the electron micrograph and SDS-PAGE (Figure 2.3). As discussed in section 2.2.2, UC isolations have been shown by us and others (Kalra *et al.*, 2013, Baranyai *et al.*, 2015) to be contaminated with albumin and other proteins such as IgG.

Human serum exosomes in PBS isolated using SEC or UC and stored at 37°C for 3 weeks with gentle agitation were shown to retain their morphological characteristics. Their spherical shape was still intact as evident on the electron micrographs (Figure 2.10). A previous study stored plasma exosomes spiked with LIM 1863 exosomes for 30 days at 37°C and suggested some stability as they detected undamaged TSG101 on a western blot; however, they suggested high levels of protein disrupted the microscopic analysis due to isolation with UC (Kalra *et al.*, 2013). This is in agreement with the observation of a substantial precipitate with exosomes isolated by UC (Figure 2.10). The SEC-derived exosome size decreased by 12.4% when stored at 37°C for 3 weeks compared to storage at -80°C. In another study the exosome size was found to decrease by 60% when stored at 37°C for 2 days as determined by NTA (Sokolova *et al.*, 2011). This difference could arise from their differing characterisation method or the use of exosomes from human embryonic kidney 293 cells, endothelial colony forming cells and MSCs and not human serum exosomes. This potential difference between tissue culture and serum-derived exosomes will need further investigation. In another study, superparamagnetic nanoparticles (SPMNs) were anchored onto exosomes and isolated the reticulocyte-derived exosome-based superparamagnetic nanoparticle cluster (SMNC-Exos) from mice serum using magnetic separation (Qi *et al.*, 2016). The stability of the SMNC-Exos at 4°C in PBS buffer and 37°C in serum was assessed by changes in exosome diameter using dynamic light scattering at various time intervals. The SMNC-Exos did not aggregate in PBS buffer at 4°C and 37°C after 7 days once magnetically separated and redispersed. This indicates the exosomes were stable which agrees with our results for SEC exosomes. A shorter storage of 18 hours at 37°C, as well as at 4°C, 27°C, 42°C and changes in pH (6.6, 7.1 and 7.4) have been reported for cardiac myocyte exosomes in PBS isolated using ultrafiltration and UC and they retained HSP60 (membrane

bound) as well as GAPDH (cytosol) indicating exosome stability (Malik *et al.*, 2013). Urine has been stored at 37°C for 24 hours and the exosomes remained stable in size (Lv *et al.*, 2013). Thus, several studies indicate morphological stability.

The SEC-derived exosomes and UC-derived exosomes stored at -80°C and 37°C for 3 weeks were internalised by HT1080 cells indicating exosome functionality. A similar type of study stored 35 µg of LIM 1863 exosomes spiked into 1 ml plasma at -20°C for 30 days and the reisolated exosomes were taken up by LIM 1215 colorectal cancer cells revealing functionality (Kalra *et al.*, 2013). Furthermore, the SEC-derived exosomes stored at -80°C and 37°C for 3 weeks both similarly and significantly increased cellular proliferation of HdFb compared to no serum. Human serum SEC-derived exosomes stored at 37°C are functionally stable as there was no statistical difference between -80°C and 37°C stored exosomes. The 12.4% decrease in SEC exosome diameter size stored at 37°C for 3 weeks size had no apparent influence on their bioactivity. The UC-derived exosomes trended towards increasing cellular proliferation; however, they did not significantly increase proliferation of HdFb when stored at either -80°C or 37°C. The results had a high degree of variability, and this could have been caused by the contamination of serum proteins and aggregation which was evident on the TEM micrographs which co-isolated with the exosomes. Though in this study dose from equivalent starting volumes were used, it is possible a higher dose of UC exosomes might have induced a significant proliferation effect. However, it is also perhaps likely that the variability observed may have worsened by the greater absolute levels of contaminating protein. It has been previously shown that human induced pluripotent stem cell-derived MSC exosomes substantially increased the proliferation of HUVEC and fibroblasts in a dose-dependent manner over a period of 5 days (Zhang *et al.*, 2015) but as of yet this type of functional assay has not been used to assess stability of exosomes stored at 37°C.

These experiments showed that human serum SEC-derived exosomes in PBS are stable and functional when stored at 37°C for 3 weeks. However, the presence of smaller vesicles that was more prominent on the shoulder of the exosome peak has been reported previously and these vesicles were identified as HDL (Böing *et al.*, 2014). The isolation of pure exosome preparations is still a challenging area that requires intensive investigation (Baranyai *et al.*, 2015), which will be discussed and investigated in the following chapter. Long term survival of exosomes is an advantage for further pharmaceutical therapeutic applications using exosomes. From these results it could be assumed that exosomes are stable at RT for up to 3 weeks perhaps due to their membrane stability which is advantageous for transporting and storing exosomes for

potential clinical use. The stability of the exosomes could assist in their exploitation for drug or RNA delivery.

2.2.6 Exosomes embedded in hydrogels

Hydrogels have a similar structure to that of the ECM, making them suitable for delivery to a variety of tissues. Hydrogels can be designed such that their release rate can be controlled by environmental conditions such as pH and cellular degradation (Hoffman, 2002, Zisch *et al.*, 2003, Wang *et al.*, 2012). They are suitable for the controlled localised release of various bioactive factors such as stem cells, plasmid DNA and growth factors to promote regeneration in damaged tissue (Lei *et al.*, 2010, Farhat *et al.*, 2018). For example, it has been shown that adipose stem cells delivered in a chitosan/gelatin hydrogel significantly increased capillary density in a mice wound healing model compared to hydrogel or stem cell only treatment (Cheng *et al.*, 2017). Another study showed that a multiarmed PEG and heparin hydrogel increased cell proliferation in an acute mice kidney injury when loaded with bFGF or murine EGF (Tsurkan *et al.*, 2013).

The delivery of bioactive molecules from hydrogels has been widely studied over the last decade due to their ability to localise and sustain the delivery of the factors. It is reasonable to predict that these characteristics of delivery may be desirable for exosome delivery. The use of hydrogels for exosome delivery has very recently begun to be reported on in recent years. Hydrogels tested for exosome delivery include chitosan (Xu *et al.*, 2018), chitosan/silk (Shi *et al.*, 2017), hyaluronic acid (Chen *et al.*, 2018a), hydroxyapatite/chitosan (Li *et al.*, 2016b), poly(vinyl alcohol) (Fuhrmann *et al.*, 2018), silk fibroin (Han *et al.*, 2019) and sodium alginate (Guo *et al.*, 2017). As detailed in section 1.7.2.3, a range of pathologies have begun to be targeted with exosomes encapsulated in hydrogels. Hydrogels have been investigated for their ability to deliver exosomes for therapeutic purposes such as in wound healing (Guo *et al.*, 2017, Tao *et al.*, 2017c, Xu *et al.*, 2018), MI (Chen *et al.*, 2018a) and hindlimb ischemia (Zhang *et al.*, 2018, Han *et al.*, 2019). PRP-derived exosomes embedded in a sodium alginate hydrogel promoted cutaneous healing of chronic wounds in a diabetic rat model (Guo *et al.*, 2017). In another example silk fibroin hydrogel improved the retention of miR-675 loaded MSC-derived exosomes and significantly enhanced blood perfusion (Han *et al.*, 2019). Due to the therapeutic potential of sustained delivery of exosomes from hydrogels, serum SEC-derived exosomes were investigated for their delivery from a naturally derived fibrin hydrogel.

2.2.6.1 Exosomes embedded in a fibrin hydrogel

A fibrin hydrogel is a naturally derived gel which functions as a haemostatic plug and a matrix for cell migration and wound healing. Fibrin glue has been used instead of sutures or staples to enhance healing and minimise scarring (Janmey *et al.*, 2009) and is FDA approved. Fibrin has also been shown to be directly protective after injection into an infarcted heart (Christman and Lee, 2006) as well as to deliver bioactive components such as bone marrow mononuclear cells resulting in increased tissue regeneration and significantly higher microvessel density (Ryu *et al.*, 2005). Fibrin hydrogels are suitable as a delivery mechanism as they gel *in situ*, degrade naturally in the body and show controlled release. Currently there are no studies that we are aware of that have tested the use of serum exosomes in a fibrin hydrogel.

2.2.6.1.1 Distribution

To assess the distribution of the exosomes within the fibrin hydrogel, BODIPY TR Ceramide labelled SEC-derived exosomes were entrapped at a 30% (v/v) in a 3 mg/ml fibrin hydrogel. The exosomes were seen to be entrapped and distributed throughout the depth of hydrogel with confocal microscopy. A maximum intensity projection Z-stacked confocal image is shown (Figure 2.13). The release rate was then investigated.

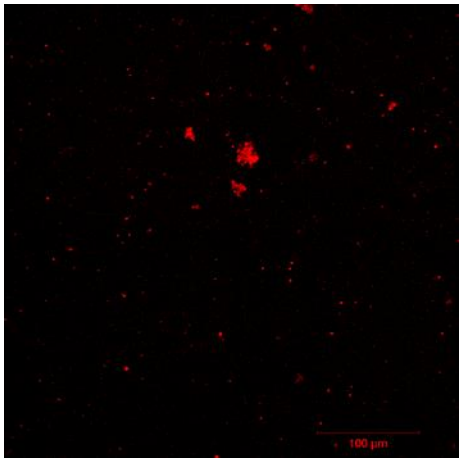

Figure 2.13: Distribution of human serum SEC-derived exosomes in a fibrin hydrogel. Maximum intensity projection of BODIPY TR Ceramide (red) labelled SEC-derived exosomes suspended within a fibrin hydrogel (3 mg/ml). Compressed Z-stack image using a confocal microscope. Scale bar = 100 µm.

2.2.6.1.2 Release rate

A standard dilution curve was obtained for BODIPY TR Ceramide labelled SEC-derived exosomes (Figure 2.14A) to establish a means of quantifying released exosomes from a fibrin hydrogel (Figure 2.14B). The exosomes were diluted with PBS and the exosome concentrations ranged from 0.8 µl to 10 µl/100 µl. A cumulative percentage release of BODIPY TR Ceramide labelled exosomes from a 3 mg/ml fibrin hydrogel over 96 hours is shown (Figure 2.14B). There was a burst release of approximately half of the label in the first 24 hours followed by a sustained release until completion at 96 hours.

A release study on PRP-derived exosomes from sodium alginate hydrogels, detected with CD63-based ELISA, saw complete release by 12 hours which suggests that fibrin may have more favourable release characteristics with sustained release over 96 hours. This release rate presumably reflects steric hindrance of the diffusion of the exosomes out of the hydrogel and/or the degradation of the hydrogel. It was observed that the fluorometer signal was found to increase over the 24 hours prior to stabilising (Figure A3, Appendix 3). It is not clear why this increase in signal occurred but the linearity of the standard curve indicated that delaying fluorescent measurements for 24 hours was suitable.

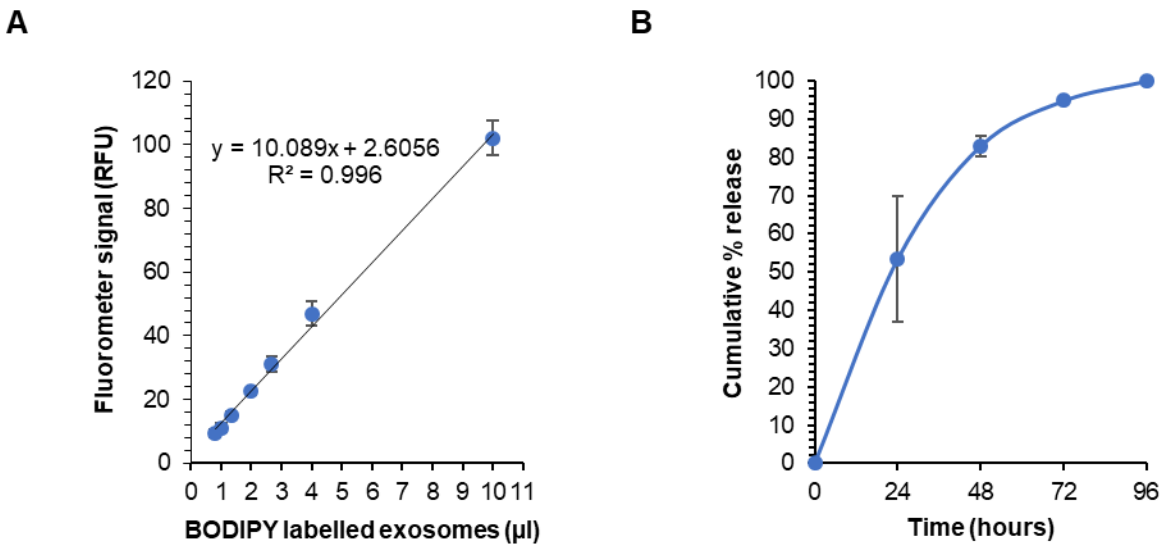

Figure 2.14: Release rate of exosomes from a fibrin hydrogel. (A) Standard curve generated from dilutions of BODIPY TR Ceramide labelled SEC-derived exosomes. Four technical repeats; (B) Cumulative percentage release of BODIPY TR Ceramide labelled SEC-derived exosomes from a 3 mg/ml fibrin hydrogel over 96 hours. Four technical repeats.

2.2.6.1.3 Uptake of exosomes embedded in a fibrin hydrogel

The transwell migration assay, also known as the Boyden chamber assay, was developed in 1962 to analyse cell migration in response to a chemotactic agent (Boyden, 1962). The assay uses a cell culture insert with a porous membrane to separate the upper and bottom compartment. Cells are seeded on the upper layer of the insert and the chemotactic agent is placed in the bottom compartment. To test for invasion, the membrane is coated with a gel comprised of ECM. After the chamber is incubated (3-18 hours), the cells that have migrated through the membrane are fixed and stained. The cells on the bottom compartment are counted to quantify migration induced by chemotactic agents (Marshall, 2011). Transwell assays have also been used to test exosomes for chemoattractant properties; however, there is variation in the concentration of exosomes required for a response. MSC-derived exosomes promote migration of cardiac stem cells in a dose-dependent manner (100, 200, 400 and 800 µg/ml) with significance from 400 µg/ml (Zhang *et al.*, 2016). Whereas, a lower concentration of PRP-derived exosomes (5 and 50 µg/ml) have been shown to significantly increase migration of fibroblasts and HMEC compared to control and supernatant of activated PRP (Guo *et al.*, 2017). Differences could be attributed to the different source of exosomes, exosome isolation method or cell types tested.

A novel modified transwell assay was used to assay for uptake of SEC-derived exosomes embedded in a fibrin hydrogel by invading HT1080 cells that migrated down through the hydrogel to the bottom of the transwell insert (Figure 2.15). HT1080 cells (20 000) were seeded on top of a 50 µl 3 mg/ml fibrin hydrogel polymerised in the insert. The hydrogel contained 63.6% SYTO RNASelect labelled SEC-derived exosomes (Figure 2.15A). The chemoattractant consisted of 10% FBS and 10 ng/ml bFGF in MCDB media. The cells were left for 24 hours to allow for migration through the fibrin gel and for uptake of the RNA labelled exosomes (Figure 2.15B). The cells potentially containing the green RNA labelled exosomes migrated to the bottom of the polycarbonate insert membrane (Figure 2.15C). The bottom of the insert was cut out, fixed and imaged (Figure 2.15D).

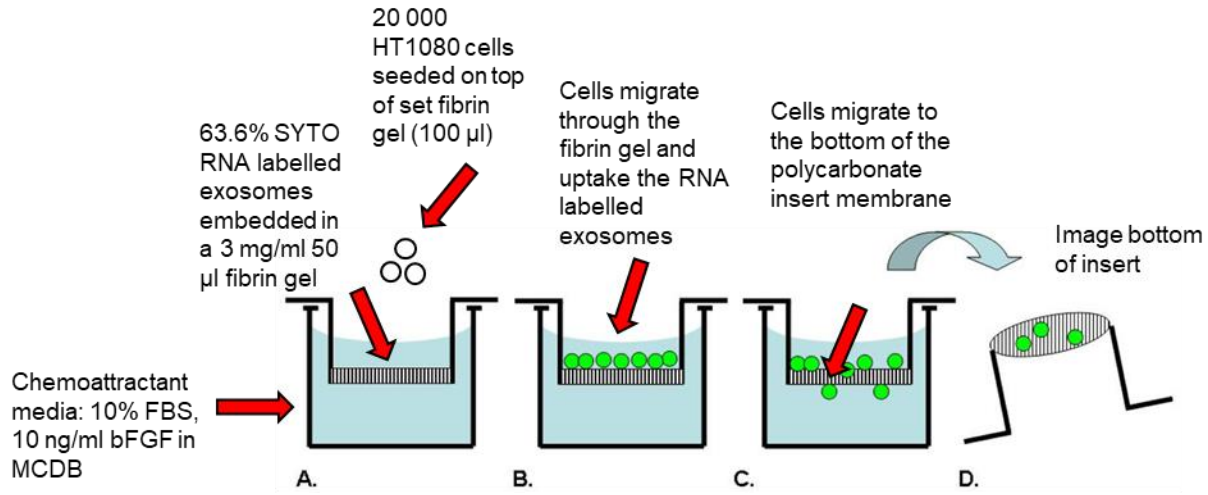

Figure 2.15: Transwell assay using SYTO RNASelect labelled human serum SEC-derived exosomes embedded in a fibrin hydrogel. Diagram showing the modified transwell experiment to test for uptake of exosomes when HT1080 cells migrate through a fibrin hydrogel. (A) HT1080 cells seeded on top of fibrin hydrogel (3 mg/ml) containing SYTO RNASelect labelled serum SEC exosomes (green) (63.6%); (B) Cells allowed to migrate for 24 hours; (C) Cells migrated through the fibrin hydrogel to the bottom of the polycarbonate insert membrane; (D) Bottom of the insert is cut out, fixed and imaged using a fluorescent microscope.

After 5.5 hours HT1080 cells did not migrate through the fibrin gel as no cells were detected at the bottom of the polycarbonated transwell cell culture inserts (Figure 2.16A). This control also indicated that any cells that remained above the cell culture insert membrane were completely removed. Hence, only the cells that would have migrated through the fibrin gel and the polycarbonated pores would be detected. After 24 hours HT1080 cell migrated through the 3 mg/ml fibrin hydrogel; with the majority of cells fluorescing green indicating effective ingress of the exosomes as the HT1080 cells invaded and moved through the hydrogel (Figure 2.16A).

To investigate the stability of exosomes over time, the fibrin hydrogels containing exosomes were incubated in excess media (36X hydrogel volume) for various time periods prior to cells being added. HT1080 cells were again seen to be transfected effectively by exosomes embedded in the fibrin hydrogel (3 mg/ml) for 1 day as well as for 3 days as detected by green fluorescence though there was a not unexpected reduction in intensity at day 3 (Figure 2.16B). Exosomal uptake was not detected when the exosomes were previously embedded in the fibrin hydrogel (3 mg/ml) for 7 days as no green fluorescence was detected. This correlates with the release profile (Figure 2.14B) as by day 4 all exosomes are released from a 3 mg/ml fibrin hydrogel. It was considered that a 10 mg/ml fibrin hydrogel might reduce the release rate due to increased steric

hinderance. There was substantial transfection when cells were allowed to migrate through an exosome loaded 10 mg/ml fibrin hydrogel that had been preincubated for 7 days.

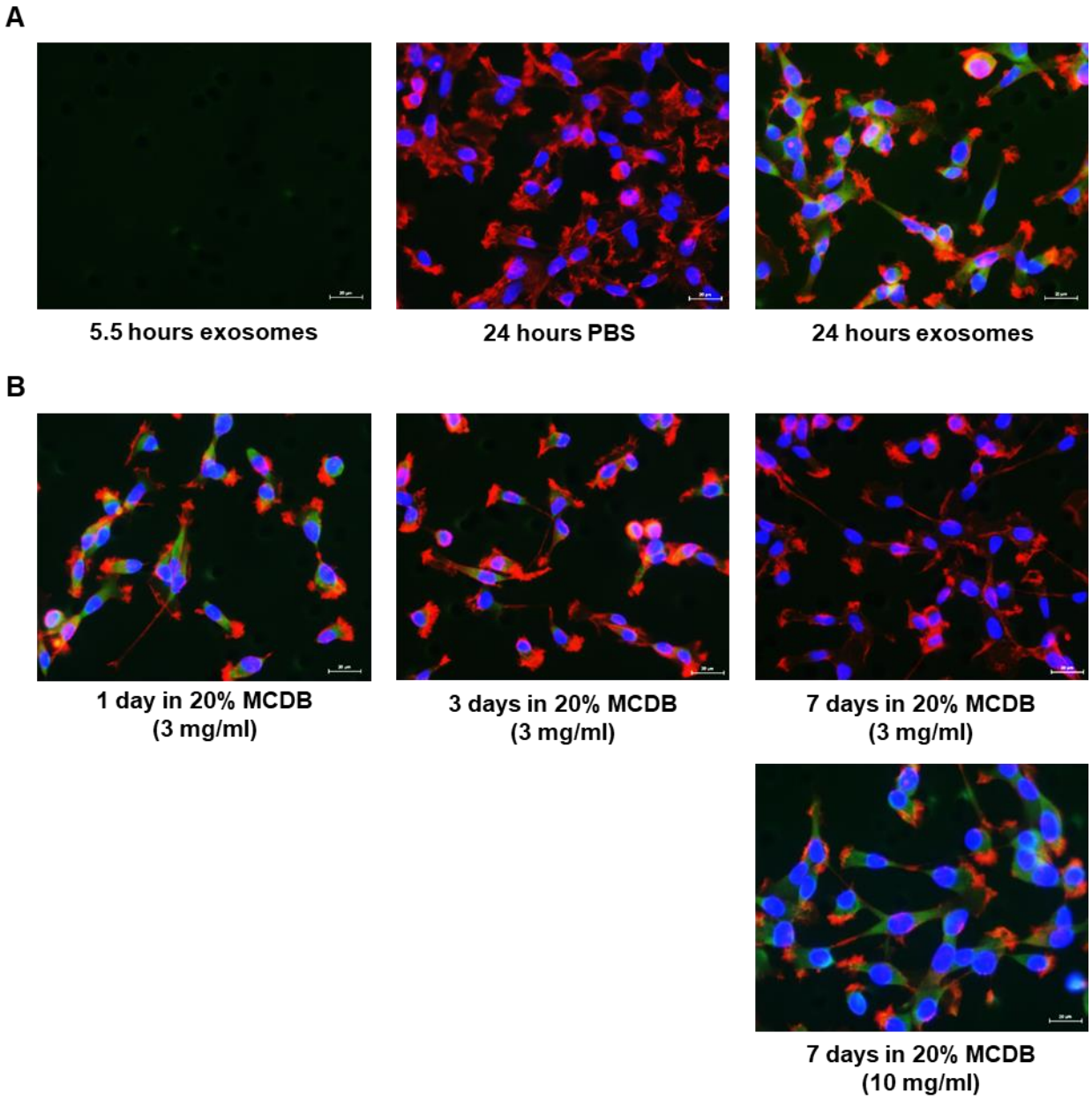

Figure 2.16: HT1080 uptake of human serum SEC-derived exosomes embedded in fibrin hydrogels using transwell cell culture inserts. (A) Treatments: 5.5 hours of migration through fibrin hydrogel with 63.6% SYTO RNASelect labelled exosomes (green), 24 hours of migration through fibrin hydrogel PBS control, 24 hours of migration through fibrin hydrogel with 63.6% green exosomes; (B) HT1080 uptake of exosomes embedded in a 3 or 10 mg/ml fibrin hydrogel over 1, 3 or 7 days in 20% FBS MCDB media. After migration the transwells were processed for fluorescent imaging. Nuclei stained with DAPI (blue) and cytoskeleton stained with ActinRed™ ReadyProbes® (red). Scale bar = 20 µm. Three independent assays with two technical repeats.

A concern was that dye from disrupted exosomes might persist in the fibrin and label cells in an artefactual manner. To reduce the concern that such artefactual dye transfer was occurring, RNA labelled SEC-derived exosomes were sonicated and tested for dye transfer in the 2D transfection assay (Figure 2.17A). If free SYTO RNASelect was present after sonication of exosomes, cells would be expected to be labelled.

Examination with TEM indicated that sonication of the SEC-exosomes severely disrupted their morphology (Figure 2.17B). There was a marked decrease in fluorescent intensity in cells incubated with sonicated exosomes (Figure 2.17A). This indicates that it is unlikely that dye released from vesicles that might have decayed within the fibrin would have generated the cell labelling observed.

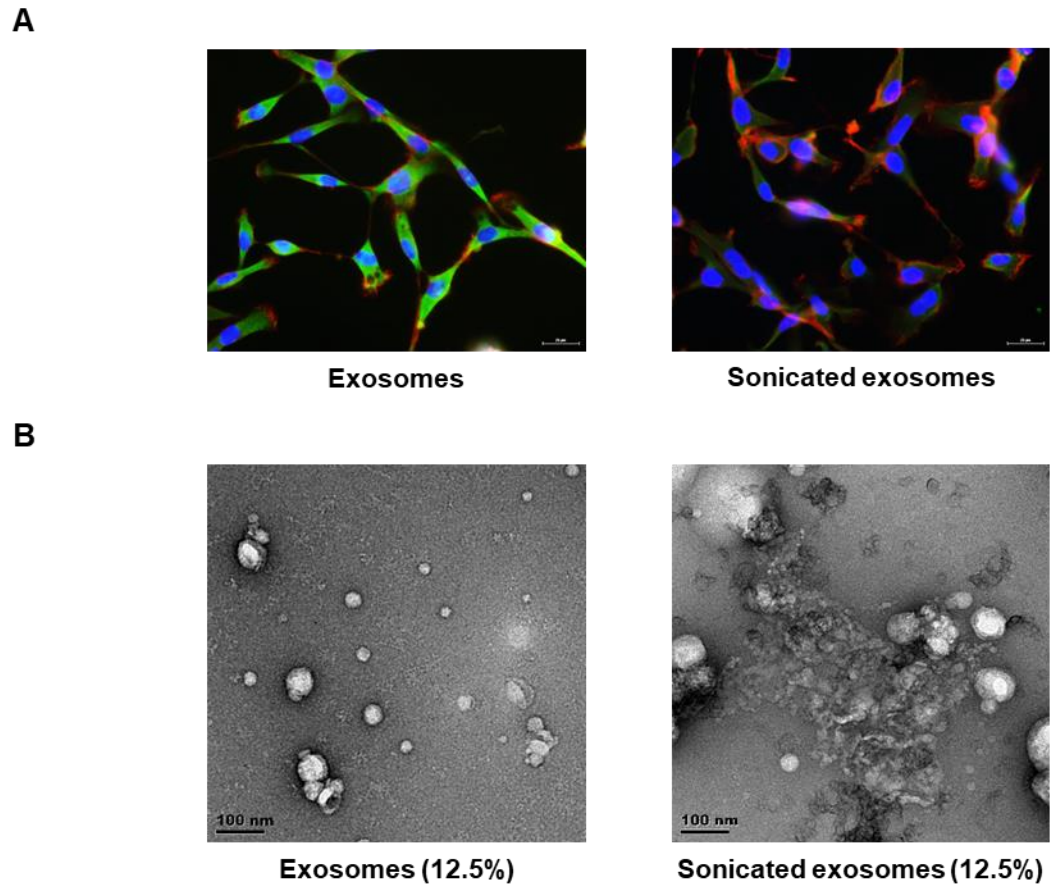

Figure 2.17: Controls to ensure the transwell experiment was not an artefact of released fluorescent dye. (A) Uptake experiment to test if sonicated fluorescently labelled (SYTO RNASelect dye) exosomes affected their uptake into cells. Nuclei stained with DAPI (blue) and cytoskeleton with Alexa Fluor® 594 Phalloidin (red). Scale bar = 20 µm. Two independent experiments with four technical repeats; (B) TEM image of 12.5% exosomes and of 12.5% sonicated exosomes to ensure sonication worked. Scale bar = 100 nm.

The morphological stability of the encapsulated vesicles was then assessed by digesting the hydrogels with proteinase K to allow for their release. The physical effect of proteinase K on exosomes and exosomes in the fibrin hydrogel was assessed first using TEM (Figure 2.18). Exosomes incubated with proteinase K at 500 µg/ml (Figure 2.18A) were visible and had a circular shape. A control fibrin hydrogel without exosomes was digested with proteinase K (500 µg/ml) showed minimal background (Figure 2.18B). Exosomes were detected and retained their circular shape when digested from the fibrin hydrogel (50 µl) with proteinase K at 500 µg/ml (Figure 2.18C) and when incubated for 1 day at 37°C prior to being digested with proteinase K (Figure 2.18D).

Overall, the SEC-derived exosomes seemed to retain their physical properties when embedded in a fibrin hydrogel. This result and that after sonication indicate that uptake observed for HT1080 cells was a result of uptake of vesicle encapsulated dye. Serum SEC-derived exosomes retained their shape within a fibrin hydrogel and if any of the exosomes had lysed it would have led to a decrease in exosome uptake. Together, these results show that fibrin hydrogels are a good candidate to deliver exosomes for targeted and sustained release.

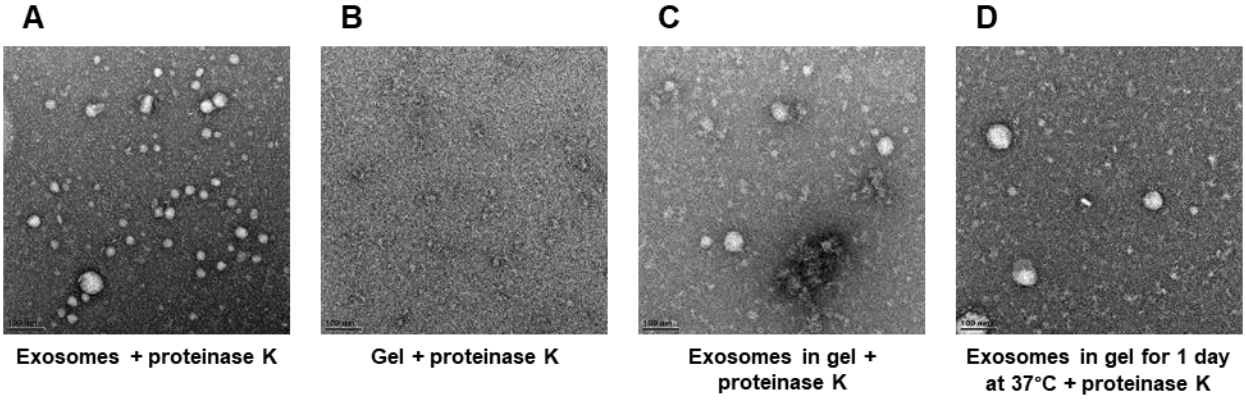

Figure 2.18: TEM micrograph of fibrin hydrogels and fibrin hydrogels containing SEC-derived exosomes digested with proteinase K. (A) SEC exosomes digested with proteinase K (500 µg/ml); (B) 50 µl fibrin gel (10 mg/ml) digested with proteinase K (500 µg/ml); (C) 50 µl fibrin gel (10 mg/ml) containing 31.8 µl SEC exosomes digested with proteinase K (500 µg/ml); (D) 50 µl fibrin gel (10 mg/ml) containing 31.8 µl SEC exosomes incubated for 1 day at 37°C prior to being digested with proteinase K (500 µg/ml). Scale bar = 100 nm.

2.3 Summary

Blood is another source of exosomes and it is advantageous over cell culture sources due to its simple collection and processing. Furthermore, there is growing research that blood may contain bioactive biomolecules that have regenerative potential (Villeda *et al.*, 2014, Wyss-Coray, 2016, Sun *et al.*, 2019). PRP has been shown to be a potential therapy for ulcer wounds, tendon injuries, cosmetic purposes, scar healing and hair loss (Alves and Grimalt, 2018) and once the platelets in PRP are activated they release bioactive components (Anitua *et al.*, 2015), discussed in section 1.6.2.1. Indeed, exosomes from PRP have been found to have regenerative potential as in stimulating neovascularisation (Guo *et al.*, 2017). Furthermore, over the recent years the interest in understanding the function of serum or plasma exosomes has grown. They have potential to be biomarkers for diseases such as cancer (Krafft *et al.*, 2017), cardiovascular problems (Wu *et al.*, 2018) and liver disease (Suehiro *et al.*, 2018). Serum or plasma exosomes have also been determined to have anti-fibrotic properties (Chen *et al.*, 2018b), be cardioprotective (Vicencio *et al.*, 2015) and improve blood flow recovery and neovascularisation in a mouse hindlimb ischemia model (Li *et al.*, 2018b) (Section 1.7.4).

However, there are issues in standardising exosome isolations with a variety of methods being utilised that include UC, precipitation, ultrafiltration, density gradients, immunoaffinity purification or SEC (Section 1.3). The choice of exosome isolation method largely depends on the application of the exosomes such as analysing the proteome of exosomes requires minimal co-isolation of contaminating proteins. As shown in these experiments ExoQuick precipitation and UC isolate human serum exosomes with contaminating proteins; verified with SDS-PAGE, TEM and protein concentration. This has been found to be a major issue in the exosome field, where other researchers confirmed that ExoQuick as well as UC isolate contaminating serum proteins (Baranyai *et al.*, 2015, Lobb *et al.*, 2015, Tang *et al.*, 2017). In recent years SEC has provided a simple, and efficient method to isolate exosomes with minimal protein contamination (Böing *et al.*, 2014, Baranyai *et al.*, 2015). Hence, the present study was carried out to determine the presence of protein-based contaminants in isolated human serum exosomes using Sepharose CL-4B chromatography, assess their function and additionally assess the efficacy of exosome-releasing fibrin hydrogels.

The outcome of the present study verified that SEC using Sepharose CL-4B isolated a fraction enriched with 20-100 nm vesicles and exosomal markers CD9, CD81 and TSG101 and was able to label HT1080 cells with a range of fluorescent labels targeting different aspects of exosome-

based uptake. Furthermore, they were devoid of significant contaminating serum proteins particularly albumin. This correlates with previous findings that Sepharose CL-4B isolates plasma exosomes without significant albumin content and they further found that Sepharose CL-2B columns isolated exosomes with albumin contamination (Baranyai *et al.*, 2015).

Our studies further showed that SEC exosomes promoted proliferation of fibroblasts and increased HUVEC sprout numbers. Currently there are no prior studies that have used serum SEC-derived exosomes and shown them causing cell proliferation of fibroblasts and initiating HUVEC sprouting *in vitro*. However, plasma exosomes (20 µg) derived from qEV SEC columns have shown to be enriched for pro-angiogenic factor endothelin-1 and promoted migration of HUVECs (Takov *et al.*, 2019). Another study found that maternal and umbilical cord serum-derived exosomes increased HUVEC proliferation and migration, with maternal exosomes showing greater migration (Jia *et al.*, 2018). However, they isolated their exosomes using ExoQuick which isolates contaminating proteins potentially clouding the finding (Lobb *et al.*, 2015). Another group isolated PRP-derived exosomes (5 and 50 µg/ml) using UC, and found them to increase proliferation and migration of fibroblasts and HMEC-1 and increased tubule formation of HMEC-1 (Guo *et al.*, 2017). Overall, the literature and this data suggest that serum exosomes do have regenerative properties to treat various ailments.

To use exosomes in a clinical setting, knowledge of their stability is important. These experiments showed that human serum SEC exosomes in PBS are stable and retain function when stored at 37°C for 3 weeks. Long term survival of exosomes is an advantage for further pharmaceutical therapeutic applications using exosomes. From these results it would be reasonable to extrapolate that exosomes are stable at RT for up to 3 weeks, which is advantageous for transportation of exosomes for potential clinical use. Furthermore our findings in conjunctions with others, with observation of preservation of the internal exosomal marker TSG101 after 30 days in plasma (Kalra *et al.*, 2013) and maintenance of size in serum (Qi *et al.*, 2016) for 7 days at 37°C, suggest that exosomes would endure in the circulation and tissue increasing their potential as therapeutic delivery vehicles.

Controlled release of exosomes will likely become increasingly utilised as has occurred in the past for the delivery of other bioactive reagents such as growth factors (Ehrbar *et al.*, 2004) and MSCs (Ciuffreda *et al.*, 2018). We showed that the FDA approved fibrin hydrogel could control the release of exosomes over 96 hours. Further, using a novel modified transwell assay, with human serum exosomes encapsulated in a fibrin hydrogel showed uptake of label by HT1080 cells migrating and invading through the gel. There was no uptake when a 3 mg/ml fibrin hydrogel

containing labelled exosomes was preincubated for 7 days prior to cellular invasion. A 10 mg/ml fibrin hydrogel appeared to retain exosomes better than 3 mg/ml as labelling still occurred when cells invaded the higher concentration hydrogel after it had been preincubated for 7 days. To our knowledge, this is a novel means of showing exosomal bioactivity in 3D. One limitation could be that the exosomes have burst open allowing the RNA dye to be released staining the RNA within the HT1080 cells. Thus, further control experiments were performed to indicate that this artefactual outcome was unlikely. It is important to highlight the fact that exosomes can be used as a delivery mechanism as they are readily engulfed by cells even when embedded in a hydrogel simulating a 3D environment. The human serum SEC exosomes seem to be functional when entrapped in hydrogel which will also be useful for therapeutic effect for a local and prolonged exposure. In correlation, literature has also seen regenerative results when exosomes are delivered in hydrogels. One study showed that PRP exosomes loaded in a sodium alginate hydrogel promoted chronic wounds in diabetic rats to heal faster with improved angiogenesis and re-epithelialisation (Guo *et al.*, 2017). They promoted the proliferation and migration of endothelial cells and fibroblasts.

Overall, the human serum SEC fraction 8 and 9 contained vesicles within the exosome size range, had very minimal serum protein contamination, contained exosomal markers, was able to transport lipid and RNA stains and vesicle entrapped dyes into cells collectively suggesting that SEC fraction 8 and 9 contained exosomes. Furthermore, the SEC exosomes had functional properties including increasing fibroblast proliferation and promoting HUVEC sprouting. The exosomes appeared stable which is beneficial for therapeutic application. They appear to be functional when entrapped in a fibrin hydrogel which is valuable for a local and prolonged therapeutic effect.

A possible limitation with the above findings is the recently acquired knowledge that there is a potential problem with lipoprotein contamination when isolating exosomes from bodily fluids such as serum or plasma (Yuana *et al.*, 2014, Sódar *et al.*, 2016, Karimi *et al.*, 2018). At the start of this investigation there was no significant concern about lipoprotein contamination as it was considered that apolipoprotein B (ApoB) present in isolates was thought to be a component of exosomes (Looze *et al.*, 2009, Liang *et al.*, 2013, Welton *et al.*, 2016). However, in 2016 it was suggested that low-density lipoprotein (LDL) co-isolated with plasma EVs (Sódar *et al.*, 2016). Lipoprotein content can affect lipophilic dye staining experiments (Takov *et al.*, 2017). Due to this potential limitation, it remains unclear whether lipoproteins could also be contributing to the uptake into cells. It has been suggested a 2-step purification involving a density gradient UC and SEC

should be used (Simonsen, 2017). Apolipoprotein B100 (ApoB100) (very low-density lipoprotein (VLDL), intermediate-density lipoprotein (IDL), LDL) and apolipoprotein A1 (ApoA1) (HDL) lipoproteins may be removed from human serum exosomes respectively. The next Chapter 3 looks at characterisation/evaluation of lipoprotein content in the serum SEC exosomes.

CHAPTER 3: ANALYSIS OF LIPOPROTEINS IN SERUM-DERIVED EXOSOMES ISOLATED BY SIZE EXCLUSION CHROMATOGRAPHY

3.1 Introduction

3.1.1 Lipoproteins co-isolate with exosomes

An example of the state of flux in the exosome field (Bhome *et al.*, 2018) is that the presence of ApoB in exosome containing fractions was postulated to derive from the exosomes themselves (Looze *et al.*, 2009, Liang *et al.*, 2013, Welton *et al.*, 2016). Reports in the literature where exosomes have been isolated from serum, blood and plasma with SEC, UC etc. are still frequently published (Bei *et al.*, 2017, Cavallari *et al.*, 2017, Li *et al.*, 2018b, Ghai *et al.*, 2019). However, it has recently become apparent that density gradient, PEG precipitation, SEC and UC of human serum or plasma co-isolates lipoproteins with the exosomes (Deregibus *et al.*, 2016, Sódar *et al.*, 2016, Grigor'eva *et al.*, 2017, Foers *et al.*, 2018, Karimi *et al.*, 2018, Takov *et al.*, 2019).

Several publications in 2014-2015 indicated that SEC purification of blood-derived exosomes was optimal (Böing *et al.*, 2014, Baranyai *et al.*, 2015, de Menezes-Neto *et al.*, 2015). More recently (Sódar *et al.*, 2016) showed that lipoproteins are found co-isolating with EVs isolated from platelet concentrates using qEV SEC columns as well as in plasma EVs isolated using an OptiPrep density gradient. These findings were confirmed by other researchers as plasma and serum SEC-derived exosomes were seen to be contaminated with ApoB lipoproteins, as detected using mass spectrometry (Karimi *et al.*, 2018) and an immunoassay (Takov *et al.*, 2019), after isolation using Sepharose CL-2B and qEV SEC columns respectively. The co-isolated ApoB lipoproteins would be expected to be VLDL and IDL due to their larger size, whereas the smaller sized LDL would elute in later SEC fractions (Takov *et al.*, 2017). It should be emphasised that other methods of isolation such as UC were also found to be contaminated (Deregibus *et al.*, 2016). Particularly contamination of HDL still occurs when using UC and density gradient, which was seen when isolating exosomes from human synovial fluid and plasma (Yuana *et al.*, 2014, Foers *et al.*, 2018). There are roughly 10^7-10^9 exosomes/ml plasma, whereas lipoproteins are in abundance at 10^{16} (Simonsen, 2017) and thus co-isolation of only a very small proportion of the lipoproteins present

can result in significant contamination. This makes it difficult to interpret data as lipoproteins can attach non-specifically to antibodies as well as transfer lyophilic fluorescent dyes into cells which are used to test for exosomal uptake (Takov *et al.*, 2017, van der Pol *et al.*, 2018). It is difficult to determine what is transporting miRNA when there is co-isolation of lipoproteins and exosomes, discussed below (Vickers *et al.*, 2011, Yuana *et al.*, 2014). It is important that researchers understand the limitations and issues in exosome research to avoid drawing incorrect conclusions.

3.1.1.1 Lipoproteins

Lipoproteins are also nanoparticles which transport cholesterol, triacylglycerols and phospholipids. After consuming fat-containing meals chylomicrons (75-1200 nm) are generated. They travel through the blood plasma to deliver lipids and cholesterol to the liver (German *et al.*, 2006). Lipoproteins are divided into classes according to their ratio of triglycerides, cholesterol and apolipoproteins. The fat in chylomicrons is converted by the liver into VLDL (30-80 nm) followed by conversion into lipoproteins of smaller diameter. These include IDL (25-35 nm), LDL (21-27 nm) and HDL (7-13 nm); which also transport lipids and cholesterol to surrounding tissues. There are various apolipoprotein markers for different lipoproteins. ApoA1 is predominantly associated with HDL, ApoB100 is associated with IDL, LDL and VLDL and apolipoprotein B48 (ApoB48) is affiliated with chylomicrons (Ramasamy, 2014).

Lipoproteins may have functions beyond the transport of lipids as recent papers have shown that they also carry miRNA. Vickers *et al.* showed that HDL contained miRNA, the most abundant being miR-223 followed by miR-105 and miR-106a and their concentration increased with humans having atherosclerosis (Vickers *et al.*, 2011). The HDL miRNA was shown to be transferred to recipient hepatocyte cells. Furthermore, they detected LDL to contain miRNA. However, a density gradient was used to isolate HDL which contained about 1% of EVs. Due to EVs having a larger diameter than HDL (100 nm versus 10 nm), the EVs will have greater volume for miRNA cargo; hence, potentially influencing HDL studies too (Yuana *et al.*, 2014).

3.1.1.2 Co-isolation of lipoproteins and exosomes

There is potential for co-isolation of lipoproteins and exosomes apart from the extreme mismatch in number of particles as they overlap in size and density (Figure 3.1). Chylomicrons, IDL and VLDL overlap in size with exosomes, whereas HDL overlaps in density. Another issue is that LDL may attach to exosomes which would make it difficult to separate them using current isolation

techniques (Sódar *et al.*, 2016). TEM has also identified contaminating particles such as IDL (25-35 nm), LDL (21-27 nm) and VLDL (30-80 nm) in exosome preparations from plasma, urine and conditioned cell culture media (10% depleted serum) when using UC (Grigor'eva *et al.*, 2017). VLDL can interfere with determining the concentration of exosomes using NTA (Jamaly *et al.*, 2018) and IDL are also likely to be an issue due to their size. One bio distributive difference is that exosomes are circulated quickly away from the point of an injection and accumulate in the liver, lungs and spleen, whereas VLDL and HDL can remain for hours and LDL for 4 days before being metabolised in the liver or adipose tissue (Choi and Lee, 2016, Menard *et al.*, 2018).

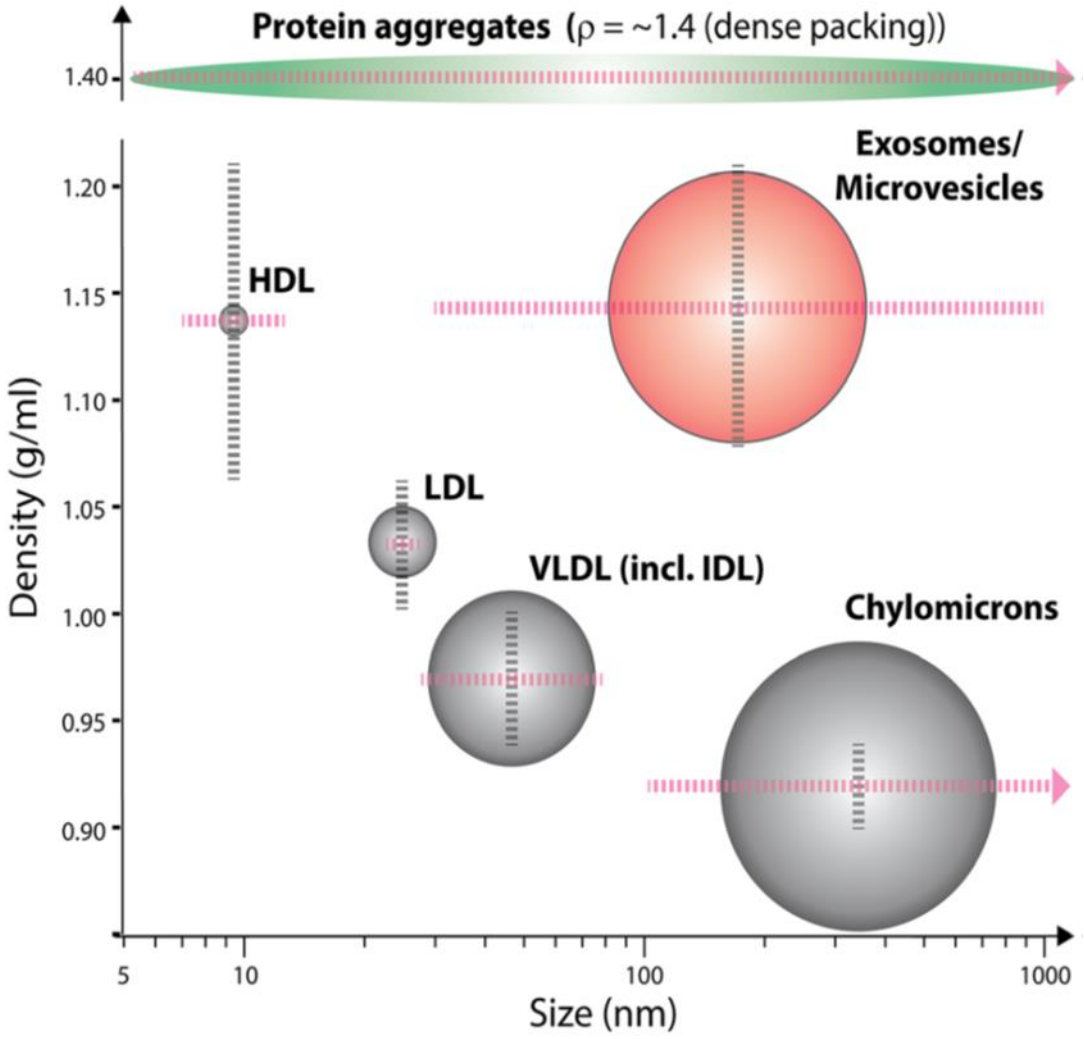

Figure 3.1 Outline of the overlap of size and density of exosomes/microvesicles and lipoproteins. High-density lipoproteins (HDL) overlap in density, whereas low-density lipoproteins (LDL), intermediate-density lipoproteins (IDL), very low-density lipoproteins (VLDL) and chylomicrons overlap with the size of exosomes. Figure from (Simonsen, 2017) with permission.

There are still a substantial number of blood-derived exosome publications that do not acknowledge the potential for interference from lipoproteins, but awareness is increasing. For example, when looking for biomarkers for metastatic breast cancer through isolating exosomes from plasma, 2 possible biomarkers were identified (Tucker and Pedro, 2018). However, they noted the limitation that lipoproteins were precipitated using their UC method and that their NTA results (12.3-298.4 nm) also corresponded with some of the sizes of lipoproteins. In this chapter, the purity of exosomes isolated with Sepharose CL-4B in Chapter 2 with respect to lipoproteins was determined and characterised with a lipoprofiling method, western blotting and ELISA. Furthermore, the potential for interference of lipoproteins with fluorophore staining used for uptake studies was determined.

3.2 Results and discussion

3.2.1 Assessment of lipoprotein contamination

As a consequence of the reported lipoprotein, described above, it was considered necessary to assay their presence in our SEC isolates.

3.2.1.1 SDS-PAGE, ELISA and western blot analysis

An initial estimate of the quantity of lipoprotein contamination in the human serum SEC fractions (Figure 3.2) was carried out on SDS-PAGE. An equal volume of SEC fractions 7-14 was loaded on a 4-15% SDS-polyacrylamide gradient gel to separate out high molecular weight proteins (Figure 3.2A). A band corresponding to the molecular weight of ApoB100 lipoproteins (512 kDa) was detected in SEC fraction 8 and increased in intensity to SEC fraction 12, thereafter a slight decrease in intensity in SEC fraction 13-14. As previously observed (Section 2.2.2), minimal overall protein was detected in SEC fractions 8-9 corresponding to the exosome fraction. However, the most prominent band above 250 kDa can now be seen to correlate with the ApoB100 lipoproteins.

The above was then confirmed and quantified with an ApoB ELISA. SEC exosome fraction 8 and 9 contained ApoB lipoprotein at 6.12 µg/ml and 15.03 µg/ml respectively (Figure 3.2B). The ApoB lipoprotein concentration continued to increase across SEC fraction 10-14 (21.59-155.74 µg/ml). The gradient of the increase was larger between SEC fraction 11-14 than 7-10 suggestive of a shoulder prior to a major peak for ApoB. ELISA analysis of ApoB content of the starting human serum gave a concentration of 968.67 µg/ml ±17.7. This falls within values reported for normal plasma and serum (Ridker *et al.*, 2005, Holme *et al.*, 2009, Patel *et al.*, 2017) of 650-1500 µg/ml. This indicates that less than 1% of ApoB loaded is contained in peaks 8 and 9 combined. As there was an indication of a shoulder, an analysis of the proportions of the various LDL classes (VLDL, IDL and LDL) was carried out (see below).

Western blot analysis of the HDL marker, ApoA1 lipoprotein was performed. ApoA1 was not detected in exosome SEC fraction 8-10 (Figure 3.2C). ApoA1 was detected at 25 kDa in SEC fraction 12 and increased in intensity to SEC fraction 20. Thereafter intensity dropped in SEC fraction 22 and SEC fraction 24 contained minimal ApoA1 protein.

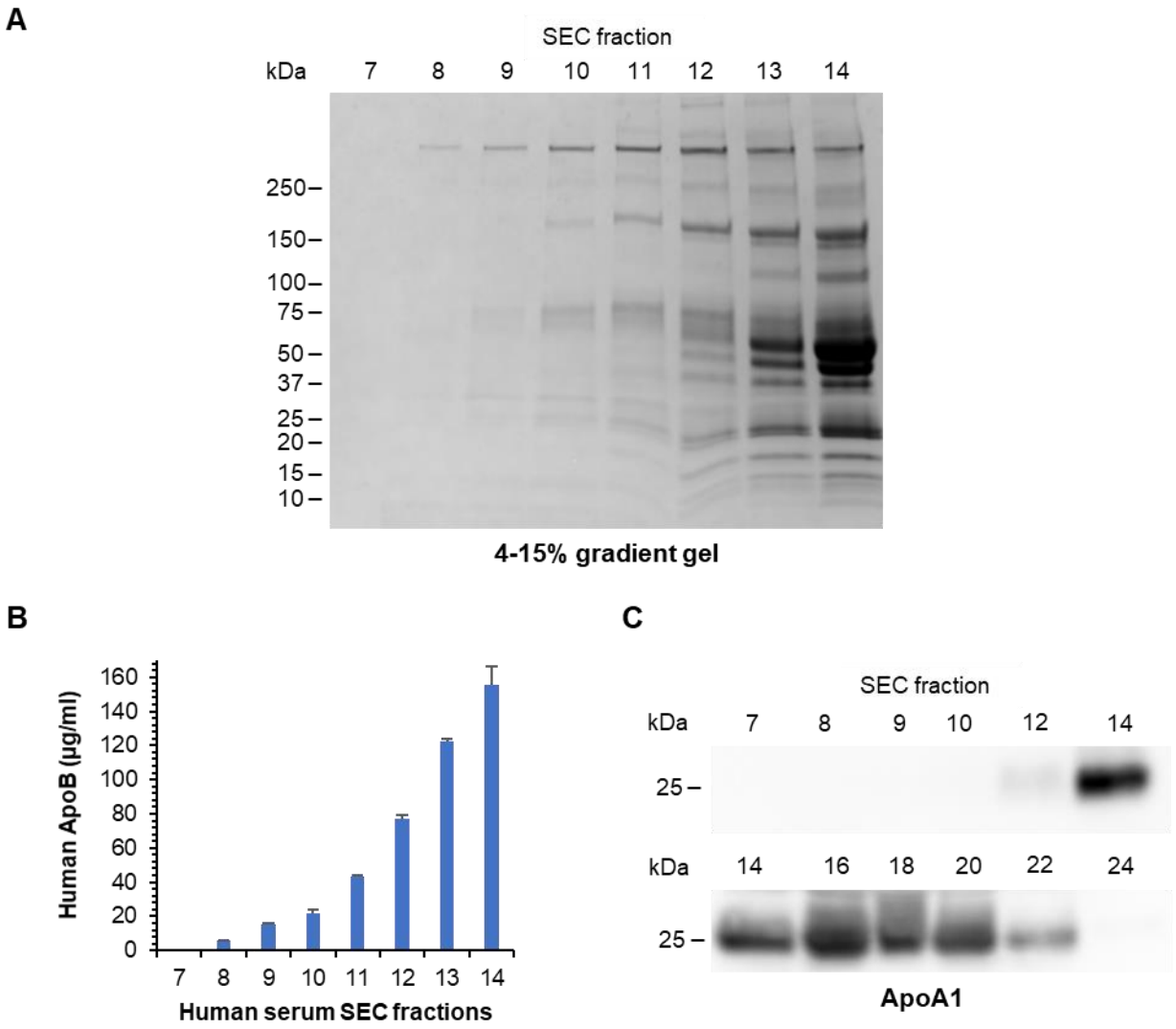

Figure 3.2: Assessment of lipoprotein contamination in human serum exosomes isolated using SEC. One ml of serum was loaded onto 10 ml Sepharose CL-4B columns and fractions of 500 µl were collected. (A) 4-15% SDS-polyacrylamide gradient gel of SEC fractions 7-14 stained with Coomassie Brilliant Blue R-250 (15 µl sample loaded). n=2 (technical repeats); (B) ELISA to quantify ApoB lipoprotein content in SEC fractions 7-14. n=2 (technical repeats); (C) Western blot to identity HDL marker ApoA1 in SEC fractions 7-10, 12, 14, 16, 18, 20, 22, 24 (10 µl loaded). n=2 (technical repeats). Figure 3.2A (gradient gel) and Figure 3.2C (ApoA1) were from the same SEC isolate as Figure 2.4B (EV markers). The exosome markers for other repeated SEC isolates always had EV markers in fraction 9 and sometimes in fraction 8 or 10.

3.2.1.2 Lipoprint analysis

The Lipoprint® System, is a commercial polyacrylamide gel tube electrophoresis system used to resolve subfractions of either HDL or LDL (Hoefner *et al.*, 2001). Minimal sample volume is required (25 µl) and analysis time is only 3 hours. A densitometric scanning system is used to quantify the relative distributions of HDL subclasses (large, intermediate and small) or LDL subclasses (VLDL, IDL (Mid) and small LDL) after electrophoretic separation. The Lipoprint® HDL System and Lipoprint® LDL System were used to assess the distribution of the lipoprotein subclasses in the serum SEC exosome enriched fractions 8 and 9.

Lipoprint gels (Figure 3.3A) were quantified to identify HDL subclass profiles in the Liposure control, serum and serum SEC exosome fraction 8 and 9 (Figure 3.3B-E). The Liposure control was used for quality control to monitor the performance in terms of accuracy and precision of the Lipoprint. Albumin was present in the Liposure control and serum detected by the wide peak (Figure 3.3B and C). As the Lipoprint® System expects to detect albumin in serum samples and SEC exosome fractions had been shown above to have no detectable albumin (Figure 2.3), an artificial line had to be inserted for the serum SEC exosome fractions 8 and 9 (Figure 3.3D and E), which was an approximation based on the leading front of the Liposure loading control containing an albumin peak but this does not influence the quantification. The Liposure control contained 69% large HDL, 29% intermediate HDL and 1% small HDL (Figure 3.3F). The HDL subclass distribution was slightly different for the serum, with less large HDL (26%) and more intermediate HDL (52%) and small HDL (23%). There was no detectable distribution of HDL subclasses for the serum SEC exosome fractions 8 and 9 (Figure 3.3F).

The Liposure control verified that the Lipoprint® System was working; therefore, relative ratios of HDL could be analysed for the remaining samples. The lack of detectable HDL subclasses in the serum SEC exosomes agrees with the western blot results that also didn't detect HDL marker, ApoA1 (Figure 3.2). The detection limit of the HDL Lipoprint® System is around 7.5% of normal levels in human serum. Western blots using the detection system used here can detect a minimum of 0.05 ng of protein (Diagnostics, 2011). This of course is highly antibody dependent but suggests that there is at least less than 0.5% of ApoA1 in serum present (1100-1500 µg/ml in normal plasma) (Ridker *et al.*, 2005, Holme *et al.*, 2009). Both methods confirm the lack of detectable HDL in serum SEC exosome fractions 8 and 9.

A

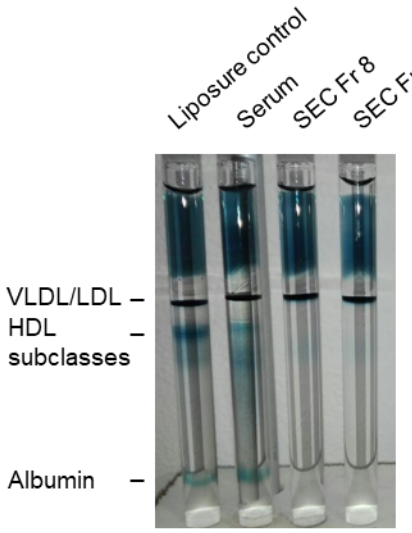

B

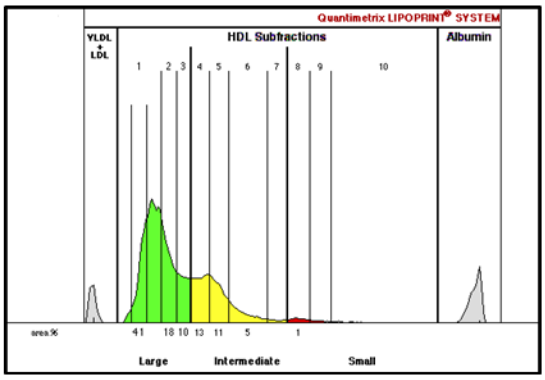

Liposure control

C

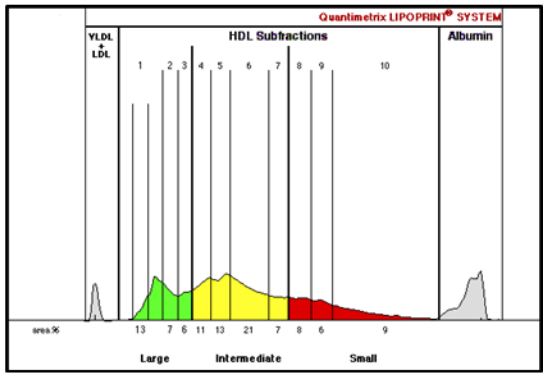

Serum

D

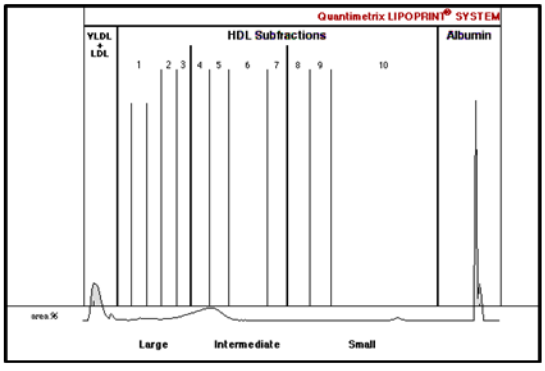

SEC fraction 8

E

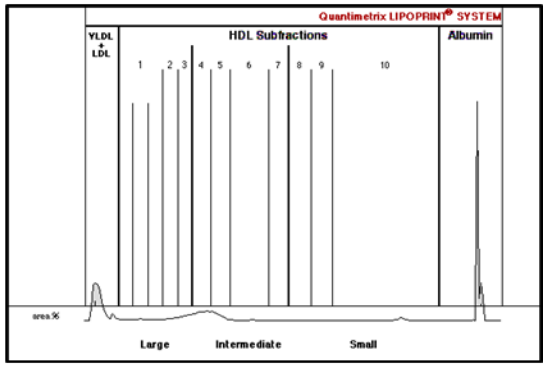

SEC fraction 9

F

HDL Subclass (%)	Liposure control	Serum	SEC fraction 8	SEC fraction 9
Large	69	26	0	0
Intermediate	29	52	0	0
Small	1	23	0	0

Figure 3.3: Distribution of HDL subclasses in human serum SEC exosome fraction 8 and 9. The fractions were analysed using a Lipoprint® System and Lipoware software. (A) Representative Lipoprint gels; (B) Scan result of Liposure control showing the HDL subclasses; (C) Scan result of serum; (D-E) Scan results of serum SEC exosome fraction 8 and 9; (F) Table of percentages of large, intermediate and small HDL subclasses.

A Lipoprint® System was then used to detect distribution of VLDL, IDL and LDL subclasses in serum SEC exosome fractions 8 and 9 (Figure 3.4). Lipoprint gels (Figure 3.4A) were quantified to identify any LDL subclass profiles (Figure 3.4B-E). HDL was present in the Liposure control and serum as detected by the wide green peak (Figure 3.4B and C). Again, as the Lipoprint® System expects to detect HDL in serum samples and these were absent as expected in the serum SEC exosome fractions 8 and 9, an artificial HDL line had to be inserted (Figure 3.4D and E) in reference to the Liposure loading control which contains a HDL peak. The Liposure control contained 19% large VLDL, 21.6% IDL and 34.8% small LDL (Figure 3.4F). The serum contained similar ratios of LDL subclasses to the Liposure control, 19.1% large VLDL, 25% IDL and 36.4% small LDL (Figure 3.4F). The serum SEC exosome fractions 8 and 9 contained increased VLDL (41.5% and 27.8%) compared to serum (19.1%), as well as increased IDL (Mid) (58.1% and 67.5%) compared to serum (25%). Serum SEC exosome fraction 8 contained more VLDL (41.5%) compared to fraction 9 (27.8%) (Figure 3.4F). The IDL profile was slightly higher in fraction 9 (67.5%) compared to in fraction 8 (58.1%). There was no detectable distribution of LDL subclass for the serum SEC exosome fractions 8 and 9 (Figure 3.4F).

Compared to serum, the SEC exosomes were enriched for the VLDL and IDL (Mid) subclasses with relatively increased percentages. This might be predicted due to the isolation method, SEC, used as the void volume for Sepharose CL-4B should contain particles greater in size than 30 nm and thus should preferably contain VLDL (30-80 nm) and IDL (25-35 nm) rather than LDL (21-27 nm) together with the exosomes present (German *et al.*, 2006). As VLDL (30-80 nm) are larger than IDL (25-35 nm) they might be expected to be at the front of the void volume fractions as seen by the relatively higher distribution of VLDL in SEC fraction 8 compared to fraction 9. The detection limit of the Lipoprint® System for LDL-cholesterol (LDL-C) is ≥ 8.30 mg/dL (Quantimetrix, 2005).

This indicates that the minimal amount of LDL present in fraction 9 is less than 5% of the LDL-C loaded (150 mg/dL LDL-C in normal human plasma (Ridker *et al.*, 2005)). This also suggests the majority of the ApoB present in fractions 8 and 9 is contained in VLDL and IDL particles.

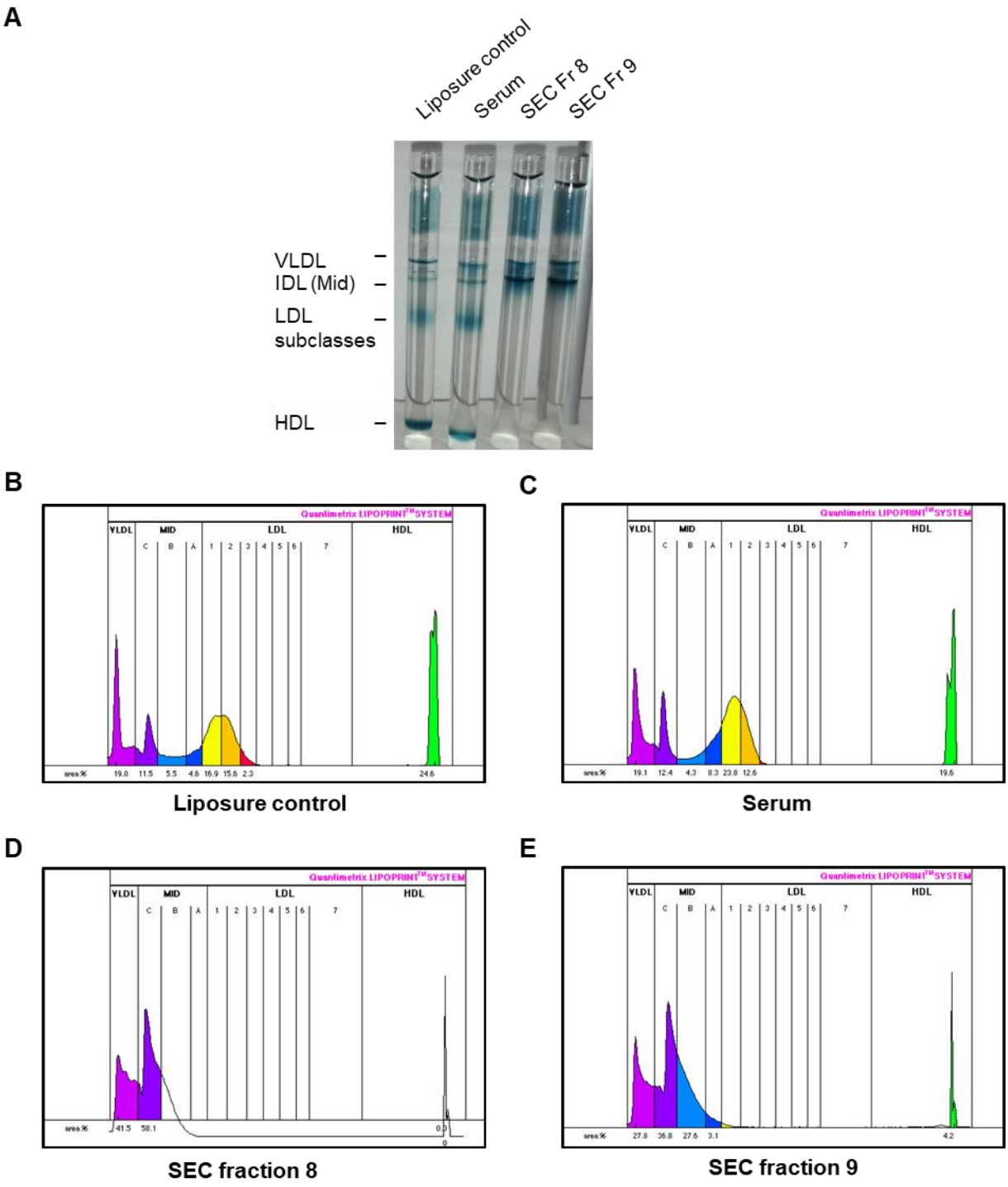

F

LDL Subclass (%)	Liposure control	Serum	SEC fraction 8	SEC fraction 9
VLDL	19	19.1	41.5	27.8
Mid	21.6	25	58.1	67.5
LDL	34.8	36.4	0	0

Figure 3.4: Distribution of LDL subclasses in human serum SEC exosome fraction 8 and 9. The fractions were analysed using a Lipoprint® System and Lipoware software. (A) Representative Lipoprint gels; (B) Scan result of Liposure control showing the LDL subclasses; (C) Scan result of serum; (D-E) Scan results of serum SEC exosome fraction 8 and 9; (F) Table of percentages of VLDL, Mid and LDL subclasses.

Using an ELISA, Lipoprint® System and SDS-PAGE the results show that ApoB containing lipoproteins do contaminate SEC-derived exosome containing fractions. This agrees with recent literature (Sódar *et al.*, 2016, Karimi *et al.*, 2018, Takov *et al.*, 2019). One study isolated plasma EVs from 1 ml of plasma loaded on a qEV SEC column and detected ApoB within the exosome fractions enriched for CD81 and HSP70 (SEC fraction 5.5 ml) (Takov *et al.*, 2019). Furthermore, their ApoB concentration increased to SEC fraction 6 ml, equivalent to our fraction 12, and thereafter decreasing. Whereas our results show a continuous increase up to fraction 14. This difference could be due to the different SEC columns used. Increasing column length improves the resolution of separating molecules (Ricker and Sandoval, 1996); Takov *et al.* separated 1 ml of rat plasma on commercial qEV columns where these columns are shorter, wider (3.2 cm bed volume height and 2 cm column width) and contain Sepharose CL-2B as compared to the longer Sepharose CL-4B column used here (12.7 cm bed volume height and 1 cm column width). Their shorter column and different Sepharose may have resulted in less efficient separation of ApoB (see section 2.2.2). The ApoB concentrations reported here are quantitative, whereas Takov *et al.* reported arbitrary units derived from a dissociation-enhanced lanthanide fluorescence immunoassay (DELFIA). The DELFIA assay is designed to capture samples and detect the presence of a compound which was ApoB lipoproteins in this case using lanthanide chelate labelled reagents (Takov *et al.*, 2019). Takov *et al.* used 1 µg/ml of biotin-conjugated goat anti-rabbit IgG for ApoB to measure the relative degree of ApoB contamination in SEC fractions; however, their ApoB was represented as arbitrary fluorescent units and not exact ApoB concentrations. It is also not clear what the detection limit for their modified DELFIA assay. The commercial ELISA used in this study has a limit of 39.1 ng/ml.

Reports also predominantly detected plasma protein ApoB in human plasma SEC fractions 8 and 9 (1 ml plasma separated on 10 ml Sepharose CL-2B) (Karimi *et al.*, 2018) and in human serum SEC fraction 8 (0.5 ml diluted serum separated on qEV columns) (An *et al.*, 2018) using mass spectrometry; however, they also detected ApoA1. This conflicts with these results that SEC removes HDL from exosomal fraction 8 and 9 but could reflect a greater sensitivity of mass spectrometry than the immunoblotting used here. Though again, this might reflect the longer and narrower column filled with Sepharose CL-4B in this study, whereas they used shorter and wider in house-made columns with Sepharose CL-2B or qEV commercial columns. Our findings are in line with those of (Böing *et al.*, 2014, Baranyai *et al.*, 2015). Böing *et al.* used a 10 ml Sepharose CL-2B with a column diameter of 1.6 cm and height of 6.2 cm and found that SEC removes more than 95% of HDL in SEC exosome containing fractions 9-12 of platelet-derived exosomes (from supernatant of platelet concentrates) (Böing *et al.*, 2014). The total recovered HDL cholesterol was 4.8% in SEC fractions 9-11 using the colorimetric reagent HDL-Cholesterol Plus third generation (Roche Diagnostics) on a Cobas C8000 analyser (Roche). However, the ApoA1 protein marker for HDL was below the detection limit (0.01 g/L) measured on an Architect. Fractions 9-12 contained the majority of vesicles and additionally contained 4.8% ±1 of total recovered HDL cholesterol, whereas HDL ApoA1 was below the detection limit (0.01 g/L) in those fractions. Karimi *et al.* based their Sepharose SEC column on Böing *et al.* method; however, they detected ApoA1 in SEC fractions in human plasma 7-12 using a more sensitive method (western blotting). This likely represents the 5% of HDL that the SEC column couldn't resolve. Again our longer column might be expected to elute the HDL in later fractions and the Sepharose pore size may have also had an influence (30 nm for Sepharose CL-4B and 75 nm for Sepharose CL-2B) due to the small diameter (7-13 nm) of HDL (German *et al.*, 2006). Our Sepharose CL-4B matrix may have allowed for better separation of HDL than Sepharose CL-2B as was observed for serum albumin (Baranyai *et al.*, 2015).

Others have predicted that the lipoprotein contamination would be expected to be VLDL and IDL due to their size (Simonsen, 2017) but we are the first to our knowledge to show this directly. Whereas, another study suggested them to originate from LDL copurifying with plasma derived-EVs and microvesicles (Sódar *et al.*, 2016). They showed using flow cytometry and western blotting, plasma or platelet concentrate-derived microvesicles or exosomes isolated using either UC, OptiPrep density gradient or SEC contain contaminating ApoB, even when isolated from donors under fasting conditions. Mass spectrometry and western blot analysis identified ApoB100 to be the most abundant protein. Sódar *et al.* hypothesised that the ApoB100 represented LDL, as ApoB100 in blood plasma is mainly found on LDL compared to less than 10% for IDL and

VLDL. To investigate this hypothesis further, they mixed commercial LDL with cell-derived exosomes and microvesicles and found the LDL to bind to the EVs as determined by TEM. TRPS analysis revealed the commercial LDL average diameter to be 110 nm indicating aggregation as LDL are 21-27 nm. However, it must be emphasised that the suggestion that the ApoB100 was derived from LDL was speculative and not supported by direct evidence. Furthermore, they used a short commercial qEV column (5 cm height, 2 cm width, 10 ml volume, 70 nm beads, Sepharose CL-2B) for their SEC isolation, which as indicated above is not ideal for isolation of exosomes.

Though this present study focuses on serum-derived exosomes, it should be noted that caution also needs to be taken when using exosome depleted serum for isolating cell culture exosomes. ApoB was detected in both peaks when isolating EVs from HEK293 cell culture conditioned media using anion exchange chromatography (Heath *et al.*, 2018). They used a step gradient of 335 mM NaCl and 890 mM NaCl over 10 column volumes each to isolate EVs from 1 litre of HEK293T-conditioned media using a flow rate of 10 ml/minute. The cell-derived exosomes were enriched in peak 2 as determined by NTA and western blotting confirmed the presence of exosomal markers CD63, CD81 and Alix and cryo-electron microscopy showed vesicles. Western blotting revealed ApoB in the conditioned media and in equal concentrations in peak 1 and 2 after the anion exchange. As in this study, ApoA1 was undetectable in peak 1 and peak 2. To eliminate lipoprotein contamination, one may have to use serum-free cell culture media with the downside of altering cellular function. For example, N2a neuroblastoma cells grown in serum-free media for 48 hours had increased EV release and were enriched for specific proteins such as G-proteins, small GTPases and kinases, compared to cells cultured in serum-containing media (Li *et al.*, 2015).

Identifying the contribution of each bioactive component in serum is vital to understand the mechanisms of regeneration that has been observed after delivery of exosomes. Lipoproteins also have potential regenerative roles and the co-isolation of lipoproteins is therefore not desirable when trying to determine the functional aspects of blood-derived exosomes nor when assessing their cargo. HDL transports miRNA such as miRNA-223 to recipient cells. Endothelial cells incubated with HDL have been found to have increased mature miR-223 which resulted in decreased adhesion molecule expression (Tabet *et al.*, 2014). They demonstrated that HDL transferred miR-223 to the endothelial cells and was not a result of miR-223 being transcribed within the cell. The presence of miR-233 also contributed to the anti-inflammatory properties of HDL. *In vivo* anti-inflammatory effects of HDL has also been shown, increasing ApoA1 levels using human ApoA1 transgenic mice (lacking mouse ApoA1) demonstrated atheroprotective

properties such as a decrease in plaque size compared to the mice expressing normal amounts of mouse ApoA1 or mice lacking mouse ApoA1 (Valenta *et al.*, 2006). Furthermore HDL has antithrombotic properties shown by inhibition of thrombin induced platelet aggregation caused by thrombin and fibrinogen binding (Nofer *et al.*, 1998). The function of HDL has been previously reviewed in (Murphy, 2013). There is evidence that LDL can inhibit, promote or have no effect on endothelial cells; however, it also depends on the whether the LDL is oxidised (harmful cholesterol) or native. One study showed that 100 µg/ml of oxidised LDL decreased bFGF expression by 40-50% within 24-48 hours; hence, inhibiting bovine aortic endothelial cell proliferation (Chen *et al.*, 2000). Whereas, native LDL and mildly oxidised LDL had no effect on bFGF expression. In contrast Zhang *et al.* showed that 50 µg/ml of oxidised LDL significantly increased proliferation of human aortic endothelial cells after 24 hours compared to untreated cells; native LDL (50 µg/ml) also significantly increased endothelial cell proliferation albeit not as effective as oxidised LDL (Zhang *et al.*, 2017). Exosomal miRNA appears to more closely resemble LDL miRNA than HDL miRNA, as the miRNA signature of LDL have a closer alignment with human plasma exosomes isolated using UC and fast protein liquid chromatography (FPLC) (correlation = 0.72) compared to HDL-miRNA signature (correlation = 0.54) (Vickers *et al.*, 2011). Furthermore, there was no correlation with the HDL-miRNA profile compared to the exosome-miRNA profile from the same plasma, due to differences in miRNA signature, concentration and the top-ranked miRNA. Due to FPLC being used, the possibility of VLDL co-isolating with the exosomes in the above study may have influenced their exosome-miRNA profile.

3.2.2 Lipoproteins a confounding factor for exosome uptake studies

As described in detail above (Section 2.2.4.1), fluorescent label uptake studies are widely used to identify exosome containing samples (Feng *et al.*, 2010, Nakata *et al.*, 2017) and to highlight or indicate their cell delivery function (Tian *et al.*, 2014, Hu *et al.*, 2018). As lipoprotein contamination had been identified in our SEC purified exosome isolates, their potential interference with the fluorescent label uptake studies with the isolates (Figure 2.7) was assessed with the canonical lipoprotein LDL (Figure 3.5). Though significant contamination with this lipoprotein was not identified above, it was thought reasonable that its behaviour would be similar to that of the higher molecular weight variants and we had access to purified LDL from the Lipidology Unit, University of Cape Town. The purified LDL was isolated from human plasma using a potassium bromide (KBr) gradient (0.5 g/ml) centrifuged at 100 000 g for 17 hours, after which the LDL was removed and dialysed to remove the KBr. TEM confirmed the LDL were

uniform in size 21.7 nm ±2.5 (Table A4, Appendix 4). The aim was to examine whether LDL can transport fluorescent dyes commonly used in exosome uptake studies into recipient cells.

The uptake assays with BODIPY TR Ceramide, SYTO RNASelect and ExoGlow-protein label (as discussed in section 2.2.4.1) were repeated with LDL (Figure 3.5A). There was no cytoskeleton stain for BODIPY TR Ceramide and ExoGlow. As can be seen the concentration of LDL particles used was substantially higher than those previously seen in the exosome containing isolate uptake studies as determined by TEM (Figure 3.5B). It was felt that this was appropriate so as to identify any potential for interference. The LDL were readily taken up by HT1080 cells as all labels utilised were present within cells with a particularly bright signal for the SYTO RNASelect dye (Figure 3.5A). The transfer of BODIPY TR Ceramide label when using LDL might have been expected as it is a lipid dye. The SYTO RNASelect dye appears to have bound to the RNA present in LDL (Vickers *et al.*, 2011, Tabet *et al.*, 2014) and upon entry into the cells allowed them to intensely fluoresce green. There are previous findings that show that lipoproteins such as VLDL (Hussain *et al.*, 1991), LDL (Sawamura *et al.*, 1997) and HDL (Ahmed *et al.*, 2003) may be labelled by lipophilic dyes, e.g. Dil-labelled oxidised HDL and DiO-labelled oxidised LDL (25 µg protein/ml) were internalised into THP-1 machrophages after 2 hours at 37°C (Ahmed *et al.*, 2003). Though as detailed, others have seen evidence of transfer by LDL of the lipophilic “exosome labels”, we have not seen previous evidence that this can also occur with RNA label and ExoGlow-protein label. The ExoGlow-protein label should be more specific as it relies on an enzymatic conversion of the native, non-fluorescent dye to an activated fluorescent moiety when taken up by EVs and this might not be expected to occur in lipoproteins. This is either not the case or there is non-specific transport of the dye into the cell that then allows for labelling of intracellular proteins. Functional studies testing for exosome uptake require special evaluation for contamination with LDL as LDL is clearly capable of transporting a wide range of fluorescent dyes into cells.

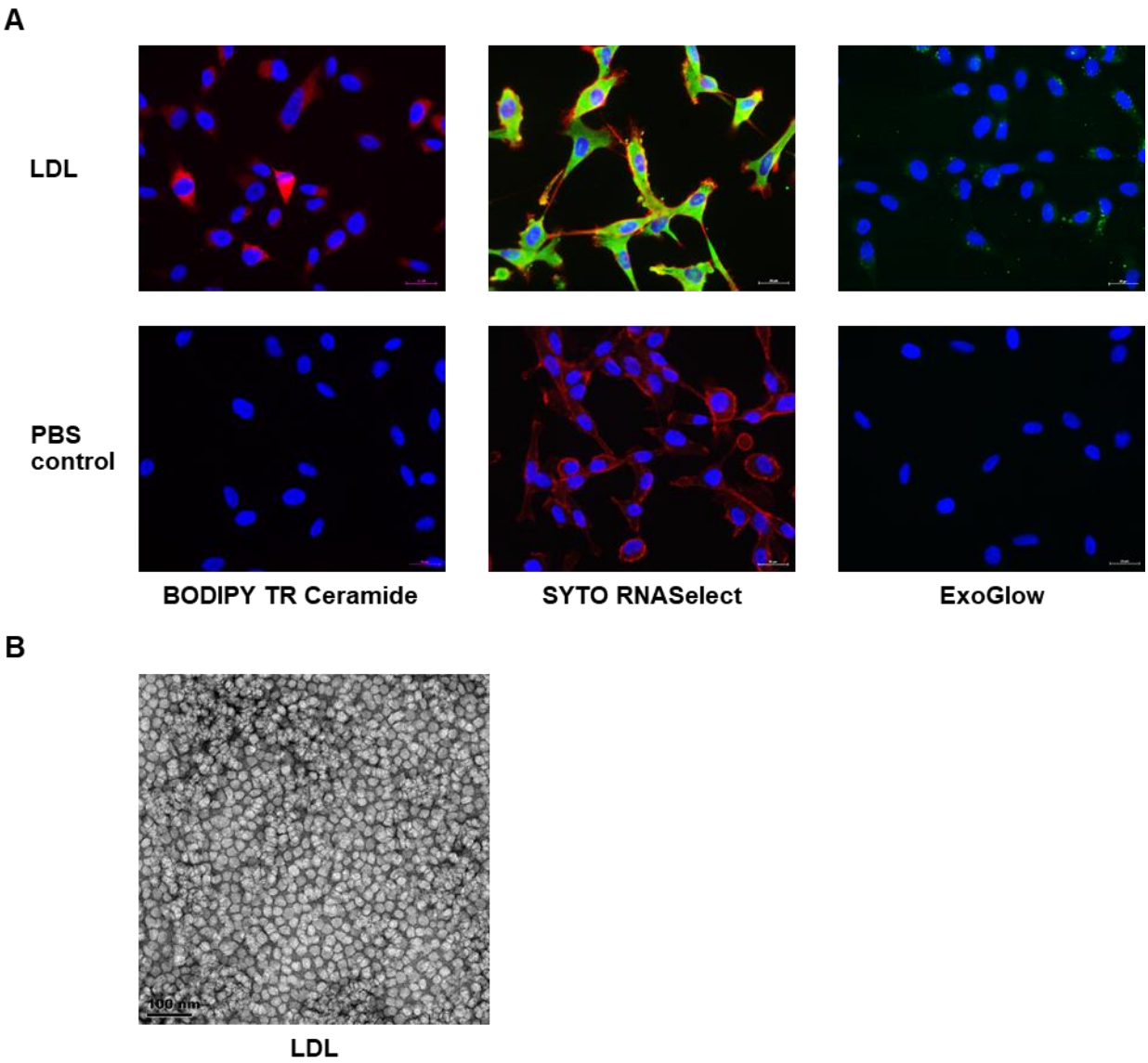

Figure 3.5: Uptake of lipophilic, RNA and protease dye-labelled LDL, a confounding factor for exosome uptake studies. (A) LDL were labelled red with BODIPY TR Ceramide, green with SYTO RNASelect and green with ExoGlow. HT1080 cells were cultured with either fluorescently labelled LDL (12.5% (v/v) LDL diluted to the same concentration as SEC exosomes) or PBS (control) for 3 hours. After treatment fluorescent images were obtained using a fluorescent microscope. Nuclei stained with DAPI (blue) and cytoskeleton stained with Alexa Fluor® 594 Phalloidin (red) for SYTO RNASelect dye treatment. Scale bar = 20 µm. n=2 (technical repeats); (B) TEM micrograph of LDL. Scale bar = 100 nm.

3.2.3 Attempt to isolate platelet exosomes from PRP with calcium activation

Platelets are considered to be the major contributor of mitogenic activity in serum. Further investigation revealed that platelets contained various growth factors including PDGF-BB (Kaplan *et al.*, 1979), TGF-β (Assoian *et al.*, 1983), IGF-1 (Karey and Sirbasku, 1989), bFGF (Brunner *et al.*, 1993) and VEGF (Banks *et al.*, 1998), located in the platelet alpha granules. Protein synthesis by platelets has also been discovered (Schwertz *et al.*, 2012). In the 1980s and 1990s PRP started being administered in a clinical setting for its regenerative potential in a range of acute and chronic conditions, as discussed previously in section 1.6.2.1. Recently exosomes have also been found to be derived from platelets (Aatonen *et al.*, 2014, Tan *et al.*, 2016). This raises the possibility of obtaining a more concentrated and defined bioactive component from plasma for potential use in regenerative therapies. Torreggiani *et al.* showed that platelet-derived exosomes significantly promoted bone marrow stromal cell growth, migration and osteogenesis (Torreggiani *et al.*, 2014). Furthermore, the exosomes were enriched for bFGF, VEGF, PDGF-BB and TGF-β1 and non-coding RNA as compared to platelet lysate. In further validation for platelets as a source for regenerative exosomes, PRP-derived exosomes improved proliferation and migration of endothelial cells and fibroblasts similar to PRP suggesting exosomes are the functional cause (Guo *et al.*, 2017).

In light of the lipoprotein contamination identified above, it was considered whether lipoprotein contamination could be reduced by isolating exosomes directly from platelets. The aim was to isolate platelets from PRP followed by exosome isolation and assess for lipoprotein contamination.

3.2.3.1 Scanning electron microscope, TEM and western blot analysis

Platelet exosome isolation was based on carefully pelleting platelets from PRP using a low centrifugation (900 g) (Tan *et al.*, 2016) and activating the platelets with 1 mM $CaCl_2$ (Goetzl *et al.*, 2016), instead of thrombin to avoid clot formation potentially trapping released exosomes. ExoQuick-TC was used to precipitate the exosomes after the platelets were activated (Goetzl *et al.*, 2016) (Figure 3.6). Goetzl *et al.* further showed that $CaCl_2$ activated platelets further activated with 30 nm thrombin or 0.3 µm collagen did not influence the concentration of secreted exosomes.

The shape of the isolated platelets needed to be assessed to ensure that the platelets remained inactivated, to prevent platelet releasate being lost through washes, prior to the activation step. To assess the level of activation of the platelets, scanning electron microscope (SEM) analysis

was performed on platelets before and after activation (Figure 3.6A). The majority of the platelets before activation were round and not activated. However, there were some single pseudopods indicating early activation prior to the chemical activation was initiated. This may be an issue as the platelets could have started activating before the pellet was spun down which might have result in loss of exosomes. Once the platelet pellet was resuspended this caused more activation as platelet aggregation was detected and more pseudopods were detected and spheroid stage platelets. The platelets were extensively activated after incubation with $CaCl_2$. The platelets were in late stage activation as seen by their spheroid shape and aggregation. The SEM images of the activated platelets agreed with previous studies that the platelets after activation had a spheroid shape with aggregation (Hantgan *et al.*, 1985, Pleines *et al.*, 2010).

Platelet exosome isolation was proceeded using ExoQuick-TC (Goetzl *et al.*, 2016). Vesicles with a diameter range of 18.5-52.1 nm and average diameter of 29.5 nm were detected using TEM (Figure 3.6B). The sample had to be diluted 50X to image the vesicles, which could mean that ExoQuick-TC isolated contaminating proteins, lipoproteins or there were many vesicles present. Exosome like vesicles were present as the markers CD9 (24 kDa) and TSG101 (50 kDa) were detected using western blotting (Figure 3.6C) and there were vesicles that had diameters of 52.1 nm, that of exosomes.

A major concern was the co-isolation of lipoproteins as spherical white vesicles with diameters comparable to that of IDL (25-35 nm) were detected on the TEM micrograph. Analysis for lipoprotein contamination in the platelet-derived exosomes was further performed.

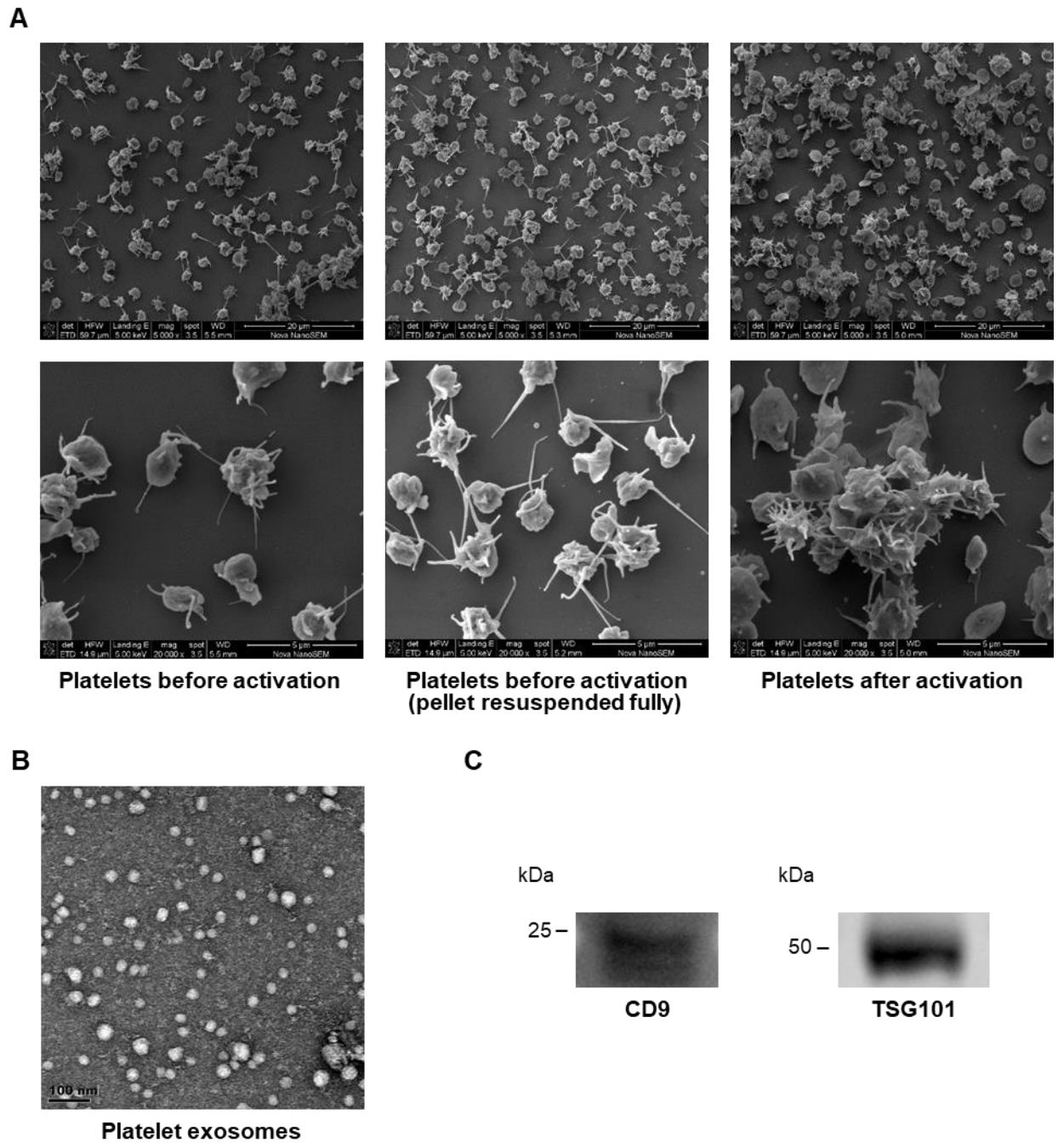

Figure 3.6: Isolation of human platelets and platelet exosomes using calcium activation of the platelets and exosomes isolated using ExoQuick-TC. (A) SEM of platelets before activation immobilised on 3-aminopropyltriethoxysilane (APES) coated coverslips, platelets after the platelet pellet was completely resuspended and platelets after activation with 1 mM $CaCl_2$. Observations made using Nova NanoSEM 230. Scale bar indicated on each figure. n=2 (technical repeats); (B) TEM micrograph of platelet exosomes from activated platelets using ExoQuick-TC (50X diluted). Scale bar = 100 nm; (C) Western blot of CD9 and TSG101 to confirm exosome markers are present in the platelet exosome isolation (6 µl platelet exosomes loaded). n=2 (technical repeats).

3.2.3.2 Lipoprint analysis

The Lipoprint® HDL System and Lipoprint® LDL System was used to assess for any distribution of the lipoprotein subclasses in the platelet exosomes isolated using calcium activation of the platelets.

A Lipoprint® System was used to detect any distribution of large, intermediate and small HDL subclasses in platelet exosomes isolate using calcium activation of platelets (Figure 3.7). Lipoprint gels (Figure 3.7A) were quantified to identify any HDL subclass profiles in the Liposure control, plasma and platelet exosomes (Figure 3.7B-D). The Liposure control contained 67% large HDL, 30% intermediate HDL and 1% small HDL (Figure 3.7E). The plasma control contained 32% large HDL, 56% intermediate HDL and 12% small HDL, a slightly different profile to the Liposure control. However, these data indicated the lipoprotein system was working. Surprisingly the platelet exosomes co-isolated 70% large HDL, 31% intermediate HDL and 0% small HDL (Figure 3.7E). This agrees with the TEM image as small round white vesicles were detected (Figure 3.6), correlating to HDL. However, the minimum diameter of vesicles from the platelet exosome isolation was 18.7 nm and HDL are 7-13 nm. The HDL may have been obscured from vision in the TEM image due to high background (Figure 3.6B).

The relative ratios of HDL could be analysed for the plasma and platelet exosomes due to the Liposure control working. The platelet exosomes were contaminated with HDL, and they had a higher percentage of large HDL and less intermediate HDL compared to the plasma control. There was no detectable presence of small HDL in the platelet exosomes which may be attributed to the sensitivity limit of the Lipoprint HDL analysis which is ≥ 3.65 mg/dL (Quantimetrix, 2005). However, the Lipoprint did reveal the impurity of other subtypes of HDL in the platelet exosomes.

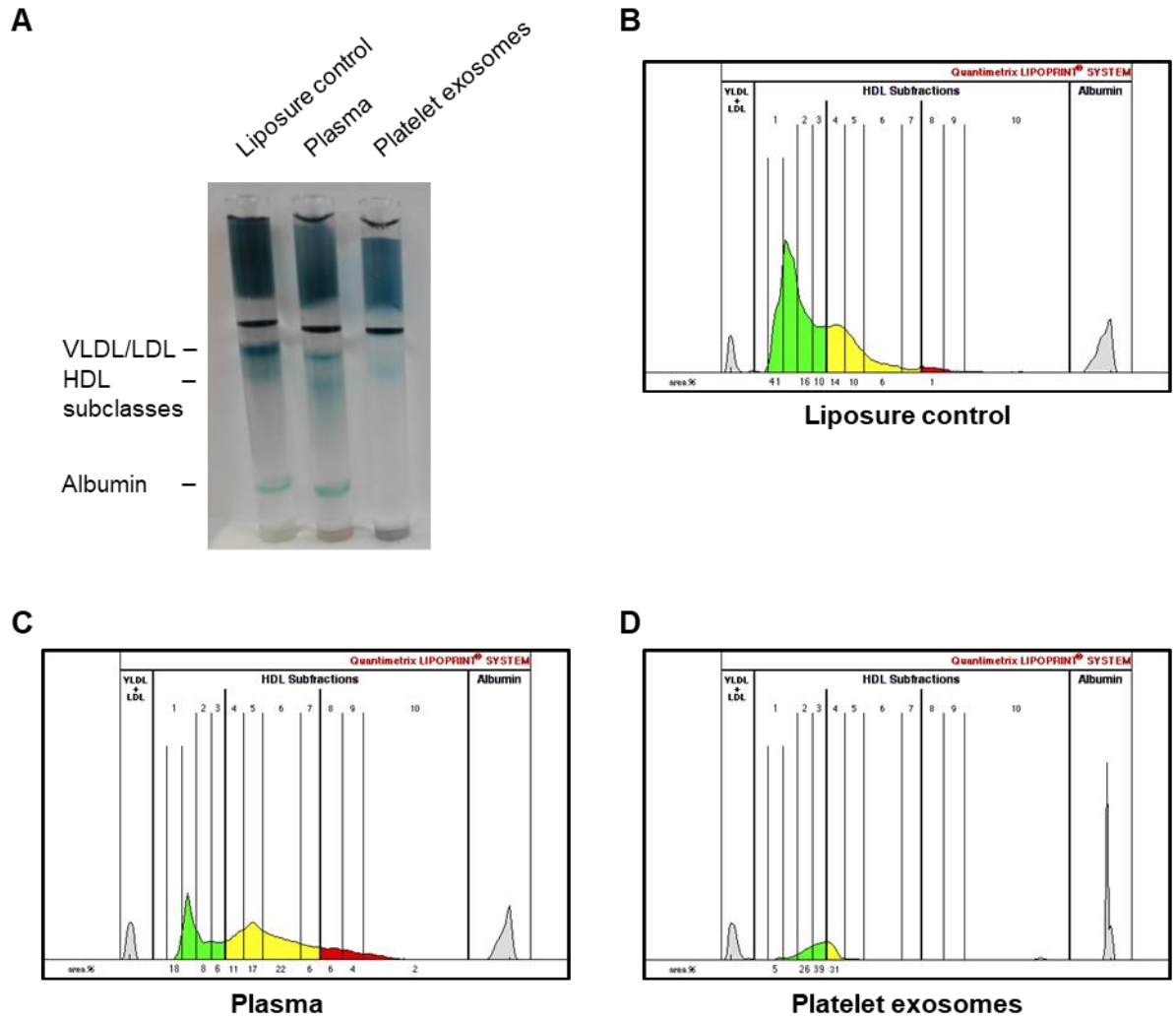

E

HDL Subclass (%)	Liposure control	Plasma	Platelet exosomes
Large	67	32	70
Intermediate	30	56	31
Small	1	12	0

Figure 3.7: Distribution of HDL subclasses in platelet exosomes isolated using calcium activation of the platelets. The fractions were analysed using a Lipoprint® System and Lipoware software. (A) Representative Lipoprint gels; (B) Scan result of Liposure control showing the HDL subclasses; (C) Scan result of plasma; (D) Scan result of platelet exosomes; (E) Table of percentages of large, intermediate and small HDL subclasses.

A Lipoprint® System was also used to detect presence of VLDL, IDL (Mid) and small LDL subclasses in platelet exosomes isolated using calcium activation of the platelets (Figure 3.8). Lipoprint gels (Figure 3.8A) were quantified to identify any LDL subclass profiles in the Liposure control, plasma and platelet exosomes (Figure 3.8B-D). The Liposure control contained 16.7% large VLDL, 25.7% IDL and 35.8% small LDL (Figure 3.8E). The plasma control contained similar ratios, 21.8% large VLDL, 36.7% IDL and 21.2% small LDL. The platelet exosomes also contained LDL lipoproteins. The platelet exosomes contained 18% large VLDL, 65.3% IDL and 12.3% small LDL. This agrees with the TEM image as round white vesicles were detected, comparable to lipoproteins. The platelet exosomes were enriched for the IDL and contained 3.8% less VLDL and 8.9% less small LDL compared to the plasma control.

The Lipoprint® LDL System confirmed the suspicion that IDL was present in the platelet exosomes as observed from the TEM analysis (Figure 3.6B). The platelet exosomes were enriched for IDL (25-35 nm) which correlates with the observed diameters of the vesicles present in the platelet exosomes isolation 18.5-52.1 nm and average diameter of 29.5 nm.

The $CaCl_2$ activation method seemed promising and the platelet exosome isolation contained exosome markers (CD9 and TSG101) as previously reported (Tan *et al.*, 2016). The morphology of the platelet exosomes were slightly smaller in diameter compared to another study where they had a range from 30-150 nm (Tan *et al.*, 2016). However, the same research group published another paper in which their TEM image resembled ours having a high background with small rounded white vesicles (Li *et al.*, 2017a). They did not test for lipoprotein contamination. The white rounded appearance of the vesicles was concerning, and the data showed that the platelet-derived exosomes co-isolated HDL, VLDL, IDL and LDL. It was considered that the contamination observed precluded progress to further purification with SEC. A protocol was then developed to isolate a purer population of exosomes from human serum.

A

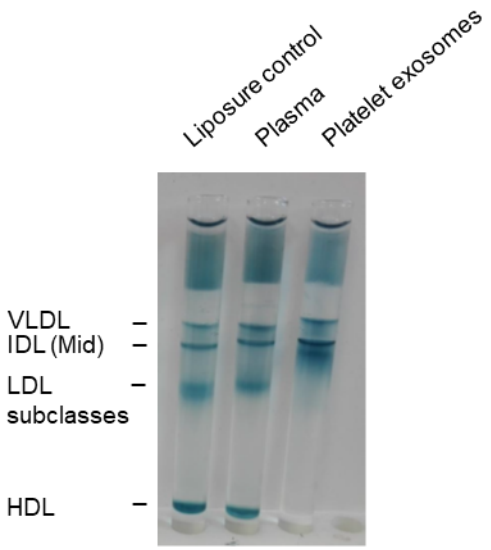

B

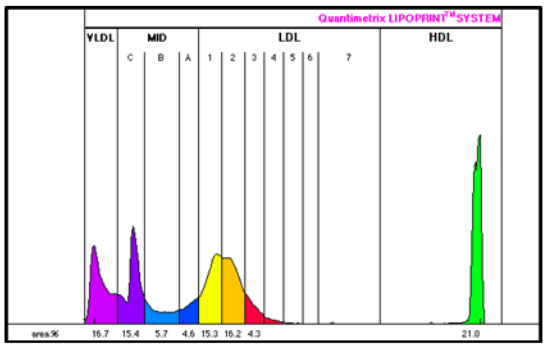

Liposure control

C

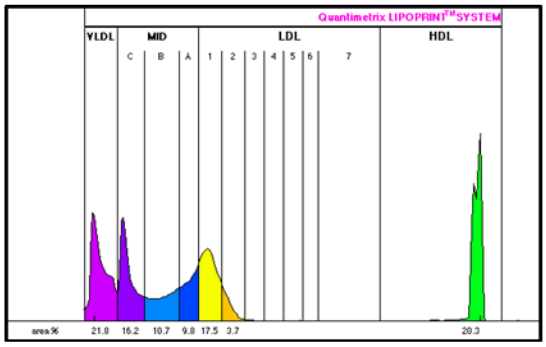

Plasma

D

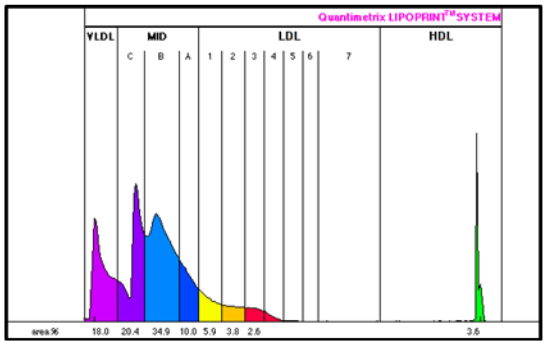

Platelet exosomes

E

LDL Subclass (%)	Liposure control	Plasma	Platelet exosomes
VLDL	16.7	21.8	18
Mid	25.7	36.7	65.3
LDL	35.8	21.2	12.3

Figure 3.8: Distribution of LDL subclasses in platelet exosomes isolated using calcium activation of the platelets. The fractions were analysed using a Lipoprint® System and Lipoware software. (A) Representative Lipoprint gels; (B) Scan result of Liposure control showing the LDL subclasses; (C) Scan result of plasma; (D) Scan result of platelet exosomes; (E) Table of percentages of VLDL, Mid and LDL subclasses.

3.3 Summary

As shown with ELISA, the Lipoprint® System and gradient SDS-PAGE, SEC using Sepharose CL-4B isolates contaminating ApoB lipoproteins with human serum-derived exosomes. This purification issue has recently become a concern in the exosome research field (Sódar *et al.*, 2016, Karimi *et al.*, 2018, Takov *et al.*, 2019). Here we went further to show that the ApoB lipoprotein contaminants were almost exclusively VLDL and IDL. As these are lipoproteins that have equivalent sizes to the exosomes, their predominance might be expected. The platelet exosome isolation method seemed promising as the isolate contained exosome markers (CD9 and TSG101) as previously reported (Tan *et al.*, 2016). The initial approach used was to target a more defined population of exosomes from blood, namely platelet-derived exosomes to discern whether lipoprotein contamination could be avoided. However, there were also contaminating lipoproteins present. Further highlighting the immense challenge of isolating EVs from blood including platelets.

Exosome activity is often tested by detecting uptake of exosomes into recipient cells. Various fluorescent dyes which stain lyophilic membranes, RNA or proteins are employed to label the exosomes for uptake experiments (Singh *et al.*, 2015, Cianciaruso *et al.*, 2016, Gutkin *et al.*, 2016). Proteins and lipoproteins have also been seen to transfer membrane dyes (CellMask, PKH67, DiD) to recipient cells (Takov *et al.*, 2017) in agreement with our finding that LDL carried the lipophilic dye BODIPY TR Ceramide into the HT1080 cells. The issue in exosome uptake studies are that the contaminating lipoproteins are directly competing with and can overrepresent the effect of the exosomes present or the lipid dye forming dye aggregates (Simonsen, 2019). More surprisingly there was substantial uptake of SYTO RNASelect (RNA dye) which might have been due to nonspecific transfer of the dye by LDL or perhaps more likely due to staining of LDL RNA. Literature has shown LDL can transport and deliver miRNA to cells (Vickers *et al.*, 2011). Further studies also show that lipoproteins may contribute towards exosome uptake studies, fasted rats had less lipophilic dye transfer with the exosome enriched plasma SEC fractions 4.5 ml and 5 ml (Takov *et al.*, 2017).

The ExoGlow-protein EV labelling kit is understood to label internal exosome proteins green to allow detection of uptake into cells, through the use of carboxyfluorescein succinimidyl diacetate ester (CFSE) chemistry (Parish, 1999). Esterases within exosomes would hydrolyse the CFSE which activates to fluoresce green once bound to the amino ends of proteins (Konadu *et al.*, 2016, McNamara *et al.*, 2018b). ExoGlow-protein label is indicated to be specific for exosome proteins;

however, LDL incubated with the ExoGlow stain resulted in some unexpected green fluorescence within cells. It is perhaps most likely that LDL non-specifically transported the stain into the cell whereby cellular esterases then labelled intracellular proteins; however, the punctate pattern is curious. This study together with other literature highlights the importance of interpreting cellular uptake of exosomes from biological fluid as co-isolated lipoproteins could obscure the findings. There is an issue with lipophilic dyes (Takov *et al.*, 2017) and as discovered here also with RNA and exosome protein fluorescent dyes.

A major caveat for many of these studies is the absolute purity of exosomes utilised (Simonsen, 2017, Tkach *et al.*, 2017). The numerous exosome isolation methods were discussed in section 1.3 and the issue of purity is highlighted here in Chapter 3. Therefore, there is a major need for an optimised exosome isolation technique from both cell culture and biofluids and standardised exosome analyses. It was considered optimal to further purify blood-derived exosomes in a manner so as to avoid lipoproteins skewing the results observed.

CHAPTER 4: PURIFICATION OF SERUM-DERIVED EXOSOMES TO REMOVE CONTAMINATING LIPOPROTEINS

4.1 Introduction

4.1.1 Removing the contaminating lipoproteins

As the significant issue of contamination of exosome isolations with lipoproteins, which is more pronounced but not limited to blood-derived exosomes (due to the huge preponderance of lipoproteins) has become more apparent, increasing effort has been devoted to improved isolation methods. Overall, the literature highlights the issue of contaminating ApoB and ApoA1 lipoproteins. UC isolates contaminating ApoB as seen for plasma-derived EVs (Sódar *et al.*, 2016) and urine-derived EVs (Andreu *et al.*, 2017). Other single-step isolations such as PEG precipitation and SEC of human serum or plasma also co-isolate lipoproteins with the exosomes (Deregibus *et al.*, 2016, Sódar *et al.*, 2016, Grigor'eva *et al.*, 2017, Foers *et al.*, 2018, Karimi *et al.*, 2018, Takov *et al.*, 2019). However, density gradients have been used to separate ApoB from serum exosomes, one study used this method to prove that serum exosomes had a strong procoagulant activity devoid of ApoB lipoproteins (Verbree-Willemsen *et al.*, 2018, Wang *et al.*, 2018b). It should be noted that in addition to identifying transmembrane or GPI-anchored proteins and cytosolic proteins recovered in EVs, the current minimal information for studies of EVs as detailed (MISEV2018) now advises that non-EV contaminants such as lipoproteins, protein and protein/nucleic acid aggregates must be determined to assess purity of the EVs (Théry *et al.*, 2018).

As SEC has become increasingly popular as an isolation technique due to ease of use; low protein contamination and preservation of exosomal morphology, researchers have begun to investigate the lipoprotein content in SEC-derived exosomes. As described above, Chapter 3, plasma and serum SEC-derived exosomes co-isolate with ApoB lipoproteins (Karimi *et al.*, 2018, Takov *et al.*, 2019). Our results were in agreement and showed that SEC using Sepharose CL-4B isolates contaminating ApoB lipoproteins with human serum-derived exosomes, with increasing ApoB concentrations in later SEC fractions as detected using an ApoB ELISA (Chapter 3). The co-isolated ApoB lipoproteins were the larger lipoproteins namely VLDL and IDL. It has been

predicted that LDL would elute later in the SEC fractions due to its smaller size (Takov *et al.*, 2017), in agreement with the results shown in Chapter 3. Researchers using cell culture-derived exosomes should also take caution as trace amounts of ApoB have seen to be present in exosome isolations using anion exchange chromatography of cell culture media (Heath *et al.*, 2018). A solution to ensure no lipoprotein contamination, is to grow the cells in serum-free media; however, this comes at the cost of altering the cells properties.

Due to exosomes having a similar size and density to lipoproteins (Figure 3.1), recently it was suggested to combine density gradient with SEC to remove the lipoproteins from the exosomes (Simonsen, 2017). OptiPrep™, a density gradient medium used for the isolation of cells, cell organelles, virus particles and lipoproteins, is a 60% (w/v) solution of iodixanol in water with a density of 1.32 g/ml. It has been found that OptiPrep purification of HIV-1 virion preserved the shape of the virus compared to sucrose purification which may have caused damage due to the high osmotic pressure of sucrose, whereas OptiPrep is iso-osmotic (Kol *et al.*, 2010). OptiPrep has been used as a discontinuous gradient for the isolation of exosomes (Greening *et al.*, 2015, Sung *et al.*, 2015). As VLDL, IDL, LDL and chylomicrons (<1.06 g/ml) have a lower density than exosomes (>1.10 g/ml), a density gradient can be used to separate these lipoproteins from exosomes. SEC can remove HDL as their diameter (7-13 nm) is smaller than the Sepharose pores (35 nm for Sepharose CL-4B and 75 nm for Sepharose CL-2B) (Section 3.2.1.1). Therefore, we and others (Karimi *et al.*, 2018, Onódi *et al.*, 2018) have begun to investigate this approach.

In this following chapter, various density gradients in combination with SEC were assessed for purifying and separating lipoproteins from serum exosomes.

4.2 Results and discussion

4.2.1 Determining optimal density gradient conditions

The aim here was to develop a simple OptiPrep step gradient that would function as a flotation gradient for lower density lipoprotein particles (chylomicrons, VLDL, IDL and LDL) and would also allow for the sedimentation of exosomes. The layering of density gradients is relatively technically difficult and thus for reproducibility, simplicity is advantageous. The density gradient isolates were then to be further purified with a Sepharose CL-4B SEC column to remove HDL and plasma proteins.

The initial approach was to assess the efficacy of a minimal 2-step gradient that consisted of a 40% iodixanol high-density cushion overlayed with serum that was adjusted to 18% iodixanol. Density was assessed by weighing precise volumes (Table 4.1), it would be predicted that the lower density lipoprotein particles would float to the top of the 18% step and the exosomes would sediment towards the bottom. The cushion is there to potentially reduce loss due to sticking of exosomes via non-specific adsorption to the tube polymer. The 18% OptiPrep diluted in human serum had a density of 1.069 g/ml. This should allow sedimentation of the exosomes and HDL as they have a higher density. Technically the chylomicrons, VLDL, IDL and LDL would move above this layer of 18% OptiPrep and serum, due to them having a lower density. Though this is a desirably simple gradient, concern was that separation would be insufficient and a 3-step gradient was also considered where a low-density overlay onto the 18% iodixanol:serum step was incorporated. It was believed that a 4% or 6% overlay would allow for greater separation as they both have a higher density than chylomicrons, VLDL and IDL. Proportion of LDL would be expected to remain in the 4% or 6% density layer as their density goes as high as 1.063 g/ml (Vance and Vance, 2008). Therefore, both 4% and 6% OptiPrep was investigated to find the most suitable top density layer. The aim was to create a simple density gradient with only 2-3 layers to remove low-density lipoprotein particles.

Table 4.1: Densities of gradient components, lipoproteins and exosomes

	Density (g/ml)	Reference
40% OptiPrep and sucrose buffer	1.164	Our analysis (Section 7.9.1)
18% OptiPrep in serum	1.069	"
4% OptiPrep and sucrose buffer	1.023	"
6% OptiPrep and sucrose buffer	1.029	"
Chylomicrons	<0.95	(Vance and Vance, 2008)
VLDL	0.95-1.006	"
IDL	1.006-1.019	"
LDL	1.019-1.063	"
HDL	1.063-1.21	"
Exosomes	1.08-1.21	(Colombo *et al.*, 2014)

4.2.2 Determining the efficiency of a simple 2-step gradient

It was determined whether the 2-step gradient (Figure 4.1) could achieve separation with a short centrifugation period as the use of a swing out SW 60 Ti allowed for high centrifugal force. Thus, the gradients were spun at 200 000 g for 3 hours. However, visual examination of the gradients showed no visible evidence of separation such as a layer at the top. Most significantly, there was no evidence of sedimentation of exosomes away from the top of the gradient. TSG101 was found to be present at equal concentration throughout the gradient. Thus, though the simplicity of the approach was technically appealing, it was decided to move to 3-step gradients with longer centrifugation time.

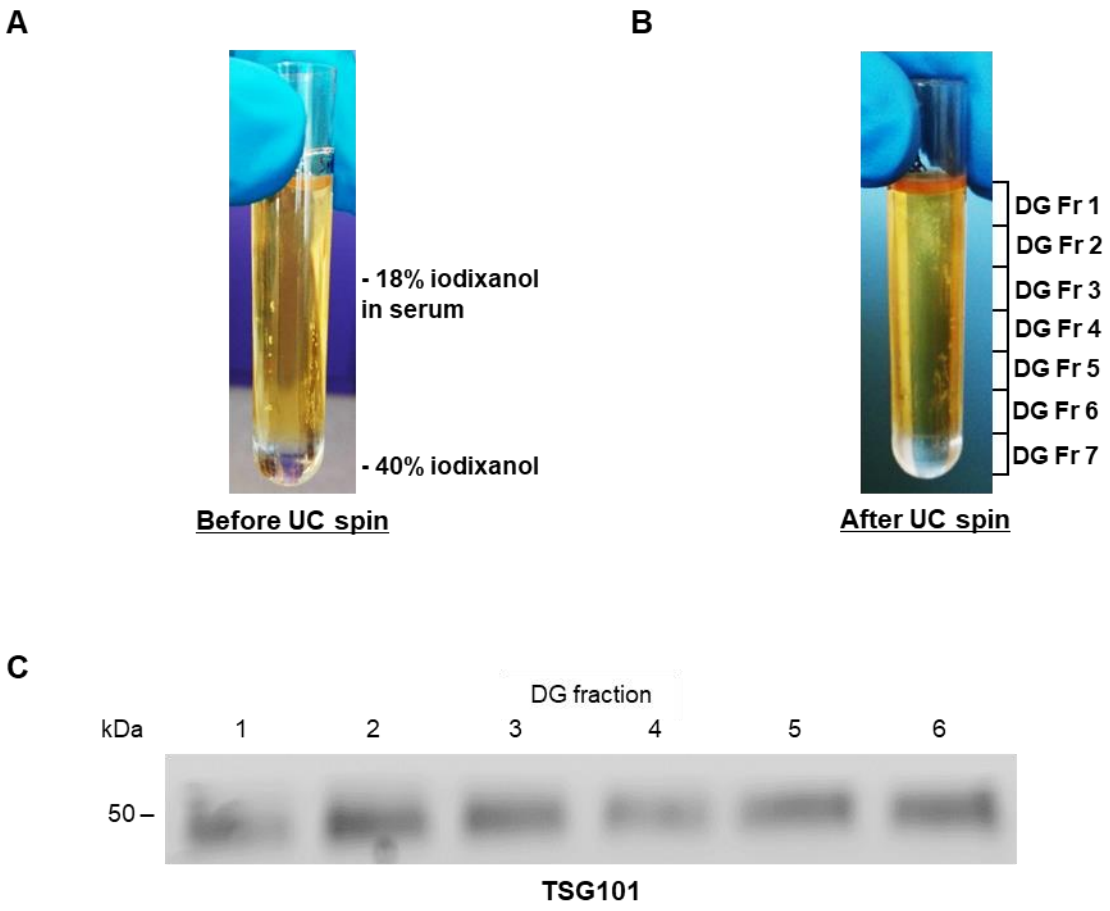

Figure 4.1: Determining the efficiency of the floatation density gradient conditions to separate lipoproteins from exosomes. (A) Gradient consisted of 0.5 ml 40% iodixanol and 3 ml 18% iodixanol in serum. Gradient spun at 200 000 g, 3 hours, 4°C; (B) After centrifuging 0.5 ml fractions were collected from the top of the gradient; (C) Western blot to detect exosome marker TSG101 in DG fractions 1-6 (25 µl) of the gradient.

4.2.3 Determining the efficiency of a 3-step gradient using 4% or 6% iodixanol

The efficiency of the new density gradient was tested when centrifuged for an extended time of 20 hours (Figure 4.2). This gradient consisted of 3 layers, 0.5 ml 40% iodixanol, 1 ml 18% iodixanol in serum and 2 ml 4% or 6% iodixanol (Figure 4.2A). Gradients were spun at 265 000 g for 20 hours at 4°C in a SW 60 Ti rotor.

After 20 hours of centrifugation, a separation was visible as the yellow serum was seen to decrease in height compared to before the centrifugation (Figure 4.2B). The yellow colour in serum is due to beta-carotene present in human LDL and HDL (Knipping *et al.*, 1990). The gradient that had a 6% iodixanol step also had a faint yellow band at the top of the gradient that

was assumed to result from LDL, which was an indication that the 6% iodixanol step might more efficiently float lower density lipoprotein particles than the 4% iodixanol step. The 6% iodixanol with its slightly higher density than 4% iodixanol, would be predicted to drive a higher proportion of LDL upwards due the greater buoyant force generated. The 0.5 ml density gradient fractions were separated on a 4-15% SDS-polyacrylamide gradient gel to assess the ApoB lipoprotein separation (Figure 4.2C and D). Equal volumes (10 µl) were loaded for density gradient fractions 1-4. Serum proteins were likely to be present in in the lower fractions and due to high protein content, 3.3 µl were loaded for fractions 5-7. A band corresponding to the molecular weight of ApoB100 lipoproteins (512 kDa) was detected in density gradient fraction 1-4 (Figure 4.2C) using the 4% iodixanol. Using the 6% iodixanol there was a higher concentration of ApoB100 in density gradient fraction 1-2 as detected by the increased intensity compared to fraction 3-4 (Figure 4.2D). This correlates with the presence of the upper beta-carotene containing band in this gradient.

Thus, the 6% iodixanol step separated the ApoB lipoproteins from serum better than 4% iodixanol and it considered likely that this was due to more efficient flotation of LDL, the most prevalent lower density lipoprotein particle in blood (Feingold and Grunfeld, 2018). Therefore, for future purifications the gradient consisting of 18% iodixanol in serum and 6% iodixanol was chosen. One limitation of this method is the small volumes of the gradient which could lead to a low yield of exosomes isolated. Hence, the volume of the gradient was increased prior to detailed analysis of lipoprotein and exosome markers. As the vast majority of the serum proteins were present in fraction 5-7 and predominately in fraction 6-7, the 40% iodixanol density cushion at the bottom was replaced with 60% iodixanol instead to create a higher density cushion to more effectively prevent the exosomes sedimenting to the bottom of the UC tube so as to reduce any potential loss due to adhesion to the centrifuge tube.

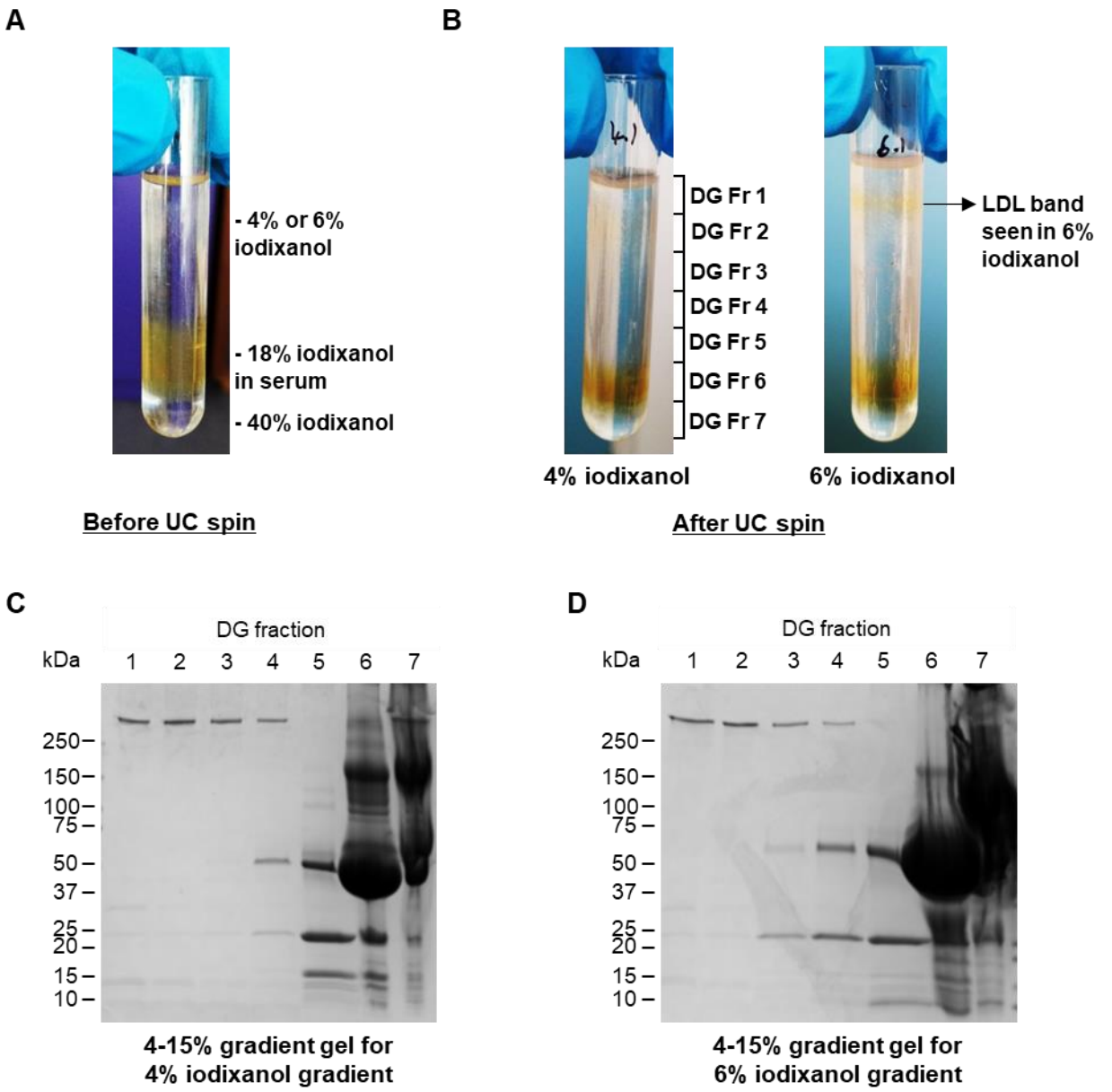

Figure 4.2: Optimising the density gradient conditions to separate lipoproteins from exosomes. (A) Gradients consisted of 0.5 ml 40% iodixanol, 1 ml 18% iodixanol in serum, 2 ml 4% or 6% iodixanol. Gradients were spun at 265 000 g, 20 hours, 4°C; (B) After centrifuging the gradient using 6% iodixanol contained a faint yellow band. 0.5 ml fractions were collected from the top of the gradient; (C and D) 4-15% SDS-polyacrylamide gradient gel of DG fractions 1-7 stained with Coomassie Brilliant Blue R-250 (10 µl sample loaded for fractions 1-4 and 3.3 µl for fractions 5-7); (C) Gradient using 4% iodixanol; (D) Gradient using 6% iodixanol.

4.2.4 Assessment of lipoprotein separation in a larger scale density gradient

The scaled up and refined iodixanol density gradient was assessed for its ability to remove ApoB lipoprotein contamination in serum (Figure 4.3). The gradient consisted of 0.5 ml 60% iodixanol, 6 ml 18% iodixanol in serum and 6.5 ml 6% iodixanol (Figure 4.3A) and the gradient was centrifuged using a SW 40 Ti rotor for 24 hours at 195 000 g at 4°C. The time was increased to partially compensate for the reduced centrifugal force.

After centrifuging for 24 hours, a faint yellow band was again visible at the top of the gradient and an intense yellow band sitting above the 60% iodixanol cushion (Figure 4.3A). The density gradient was fractionated into 2 ml fractions collected from the top, except fraction 6 was 1 ml, adding up to the total volume loaded. The density gradient fractions were separated on a 4-15% SDS-polyacrylamide gradient gel to assess the ApoB lipoprotein separation (Figure 4.3B). Equal volumes (10 µl) were loaded for density gradient fractions 1-4 and again due to high protein content, 3.3 µl were loaded for fractions 5-7. A band corresponding to the molecular weight of ApoB100 lipoproteins (512 kDa) was detected in density gradient fraction 1-4. There was possibly a higher concentration of ApoB100 in density gradient fraction 2 as detected by the increased intensity compared to fraction 1, 3 and 4. The ApoB lipoproteins were distributed in the upper fractions 1-4, whereas the serum proteins started to appear in fraction 4 and had condensed into lower fractions 5-7. Fraction 7 appeared overloaded which might reflect sedimentation of the serum proteins and/or the presence of a higher concentration of iodixanol (Figure 4.3B). An ApoB ELISA was used to quantify the concentration of ApoB in the density gradient fractions 1-7, to assess the efficiency of ApoB lipoprotein separation from serum (Figure 4.3C). The ApoB concentration was the highest in fraction 1 (594.7 µg/ml) and decreased in concentration to fraction 6 (10.4 µg/ml). Fraction 7 (19.8 µg/ml) had a slightly higher ApoB concentration than fraction 6; however, it was lower than fraction 5 (29.6 µg/ml). Thus, the gradient was able to separate 62% of ApoB on the gradient into the top two fractions.

Western blots were used to detect HDL marker ApoA1 in the density gradient fractions 1-7 (Figure 4.3D). A faint trace of ApoA1 was detected in fractions 1-3 with the majority of the ApoA1 found in fraction 4-7. This indicates that the majority of ApoA1 loaded onto the gradient was contained in HDL and not chylomicrons suggesting that the pre-gradient chylomicron removal from unfasted serum was highly effective (13 000 g for 10 min). The exosomal markers CD9 (25 kDa) and TSG101 (50 kDa) were detected in density gradient fractions 5-7 (Figure 4.3E) with the majority

in fraction 7. CD9 was more clearly sedimented into fraction 7 than TSG101, suggestive of different exosome subtypes.

Here it can be seen that the longer centrifugation period had concentrated the exosomes markers towards the bottom of the step gradient with some separation from ApoA1. This is in line with the known density ranges for HDL and exosomes (Table 4.1). Additionally, the two fractions that contained the bulk of the exosome markers (6 and 7) only contained 1.6% of the ApoB on the gradient.

UC was used after the density gradient (DG UC) to concentrate fractions 6 and 7 from four repeats as these fractions contained most of the exosome markers and had the least contaminating ApoB present. The resulting pellet was resuspended in a final volume of 1 ml which resulted in 1.8 µg/ml ApoB lipoprotein being present (Figure 4.3F). Thus, UC resulted in removal of a further 98% of ApoB that was present after the density gradient in agreement with a recent analysis of UC-based removal of ApoB (Takov *et al.*, 2019).

As the step gradient separated the ApoB lipoproteins from the exosome fractions, the exosome samples were then loaded onto an SEC column.

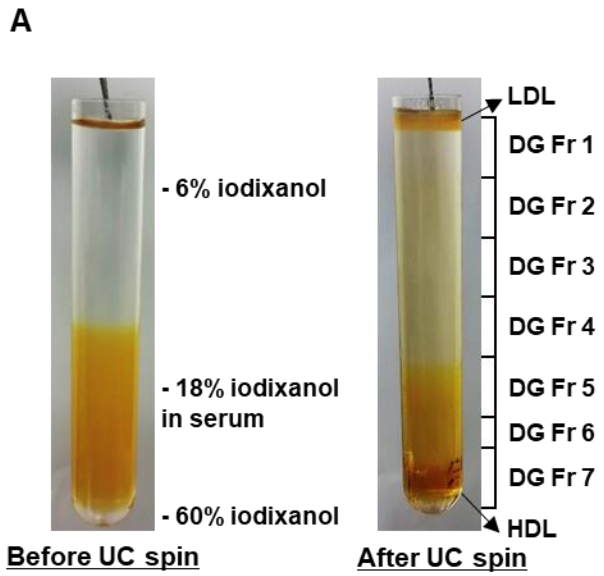
A
- 6% iodixanol
- 18% iodixanol in serum
- 60% iodixanol
Before UC spin
LDL
DG Fr 1
DG Fr 2
DG Fr 3
DG Fr 4
DG Fr 5
DG Fr 6
DG Fr 7
HDL
After UC spin

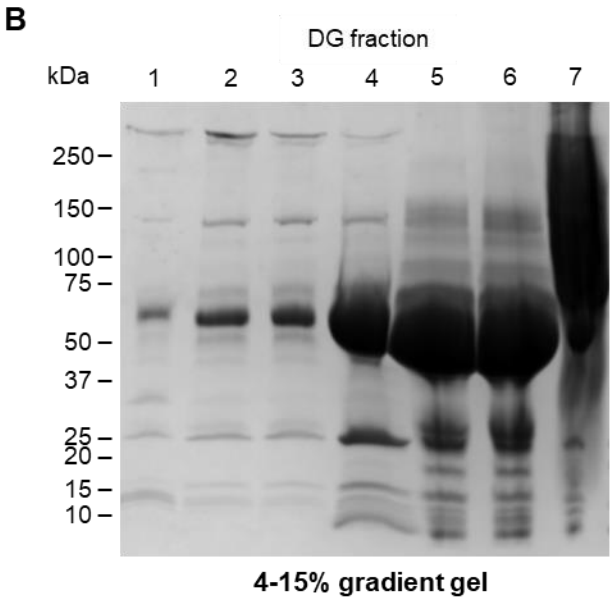
B
DG fraction
kDa
1 2 3 4 5 6 7
250
150
100
75
50
37
25
20
15
10
4-15% gradient gel

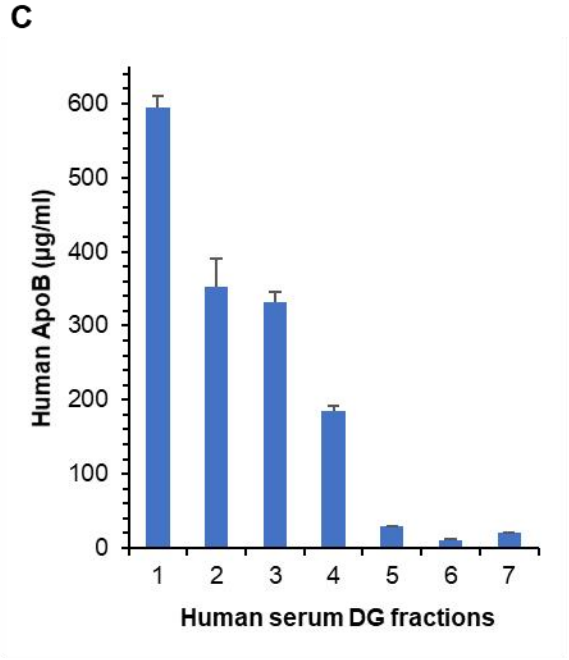
C
Human ApoB (µg/ml)
600
500
400
300
200
100
0
1 2 3 4 5 6 7
Human serum DG fractions

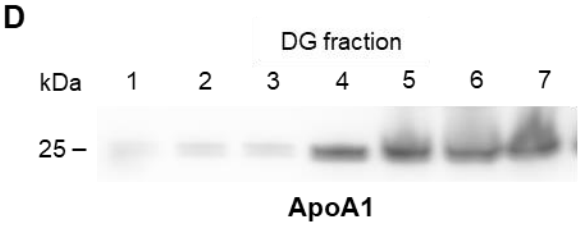
D
DG fraction
kDa
1 2 3 4 5 6 7
25
ApoA1

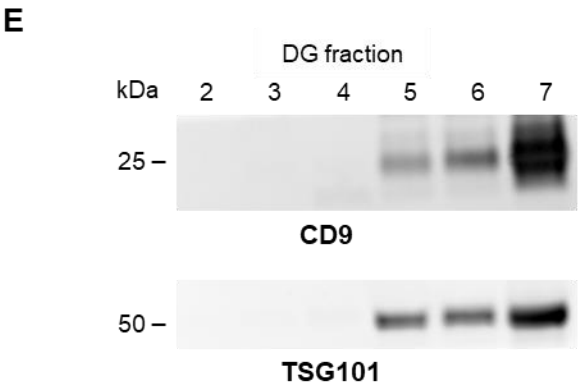
E
DG fraction
kDa
2 3 4 5 6 7
25
CD9
50
TSG101

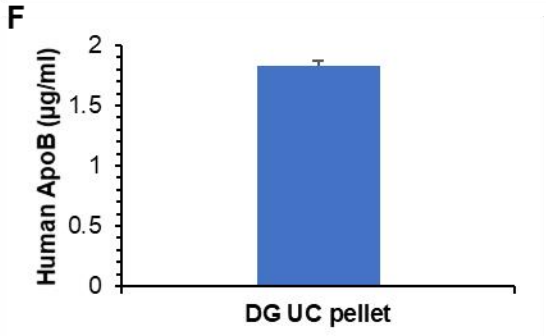
F
Human ApoB (µg/ml)
2
1.5
1
0.5
0
DG UC pellet

Figure 4.3: Assessment of removing ApoB lipoprotein contamination in human serum using an iodixanol density gradient. (A) Gradient consisted of 0.5 ml 60% iodixanol, 6 ml 18% iodixanol in serum and 6.5 ml 6% iodixanol. After centrifuging a faint yellow band is visible at the top and a dense yellow band condensing at the bottom; (B) 4-15% SDS-polyacrylamide gradient gel of DG fractions 1-7 stained with Coomassie Brilliant Blue R-250 (10 µl sample loaded for fractions 1-4 and 3.3 µl for fractions 5-7); (C) ELISA of ApoB lipoproteins in DG fractions 1-7. n=2 (technical repeats); (D) Western blot to identity HDL marker ApoA1 in DG fractions 1-7 (3.3 µl loaded). n=3 (technical repeats); (E) Western blot to detect exosomal markers (CD9 and TSG101) in DG fractions 2-7 (6.7 µl loaded). n=2 (technical repeats); (F) ELISA of ApoB lipoproteins in DG UC pellet (1 ml). n=2 (technical repeats).

4.2.4.1 Assessment of lipoprotein separation after density gradient followed by size exclusion chromatography

Density gradient fraction 6 and 7 from four tubes were concentrated using UC (fractions diluted in PBS and concentrated by centrifuging at 100 000 g for 3 hours at 4°C with a Type 40 Ti rotor). The pellet was resuspended in 1 ml which was subsequently loaded on SEC to further purify the exosomes (Figure 4.4). This method of density gradient followed by SEC will be referred to as DG SEC.

The A280 profile of DG SEC performed on a Sepharose CL-4B column displayed a shoulder peak in fraction 8-10 (Figure 4.4A). Western blot showed that CD9 was present, in two forms 25 kDa and 22 kDa, in DG SEC fraction 10 (Figure 4.4B). TSG101 was present in DG SEC fraction 9-10 at 50 kDa. TSG101 was also detected in DG SEC fraction 13-15 with increasing intensity as had been observed previously for single-step SEC. Electron microscopy revealed exosome like structures in DG SEC fractions 8-10 ranging from 30-100 nm (Figure 4.4C) though the fractions had to be diluted 5X due to a high background. Even accounting for this dilution, there appeared to be a lower number of particles per field than seen in the single-step SEC (Figure 2.1). There was a higher portion of cup-shaped particles than previously observed for SEC (Figure 2.1). This is accepted now as the classical appearance of exosome as viewed in TEM (Sluijter *et al.*, 2017). ApoA1 was detected in DG SEC fractions 12 and 14 at 25 kDa and majority of the HDL was in fraction 14 (Figure 4.4E). An ApoB ELISA was used to quantify the concentration of ApoB in the DG SEC fractions 7-14, to assess ApoB lipoprotein separation from serum exosomes (Figure 4.4F). There was no detectable ApoB lipoproteins in DG SEC fraction 7-11. Hence, less than 39.1 ng/ml of ApoB lipoproteins were present in DG SEC exosome fraction 9-10. ApoB started to appear from DG SEC fraction 12 (0.07 µg/ml) and continued to increase until at least DG SEC fraction 14 (0.16 µg/ml). This indicates that Sepharose CL-4B separates LDL from exosomes as

that is the most likely ApoB particle to elute after to the void volume as the particle size cut off for Sepharose CL-4B is 35 nm. Additionally, LDL was considered the most likely ApoB containing particle to sediment with the exosomes on the density gradient. NTA became available in Cape Town, South Africa, during the time of the establishment of these density gradients. NTA results revealed no clear evidence of peaks across DG SEC fractions 8-15 (Figure 4.4D).

SDS-PAGE gradient gel analysis indicated that density gradient fraction 2 contained the highest ApoB100 concentration; however, density gradient fraction 1 contained the highest overall ApoB lipoprotein as determined by ELISA. Thus, it is possible that chylomicrons also contributed to the ApoB lipoprotein concentration (ELISA detects ApoB100 and ApoB48) as ApoB100 is associated with IDL, LDL and VLDL and ApoB48 with chylomicrons (Ramasamy, 2014). Although exosomes were present in density gradient fraction 5, there was a slightly higher level of ApoB lipoprotein present than in the last two fractions. Thus, only fraction 6 and 7 was used to obtain a purer population of exosomes. After SEC, it appeared most to all of the HDL was removed from the serum exosomes using DG SEC and they were enriched for exosomal markers CD9 and TSG101. Furthermore, the DG SEC exosomes contained no detectable ApoB lipoproteins. The ApoB detected in later DG SEC fraction 12-14 suggests it derives from LDL.

NTA was unable to detect a peak of particles for the DG SEC exosome fraction 9 and 10. As TEM had a high background, perhaps due to aggregation caused by UC of the density gradient fractions prior to SEC, this could have obscured the signal due to the presence of exosomes. Though good separation of exosome markers from ApoB and ApoA1 was achieved by DG SEC, the lack of a clear peak on NTA, the presence of aggregates and the apparent low yield as determined by TEM indicated that the procedure should be further modified. It was considered perhaps more optimal to concentrate exosomes prior to DG and SEC as the sedimentation might be more gentle and reduce adhesion to tube polymer in the presence of an excess of serum proteins and lipoprotein particles.

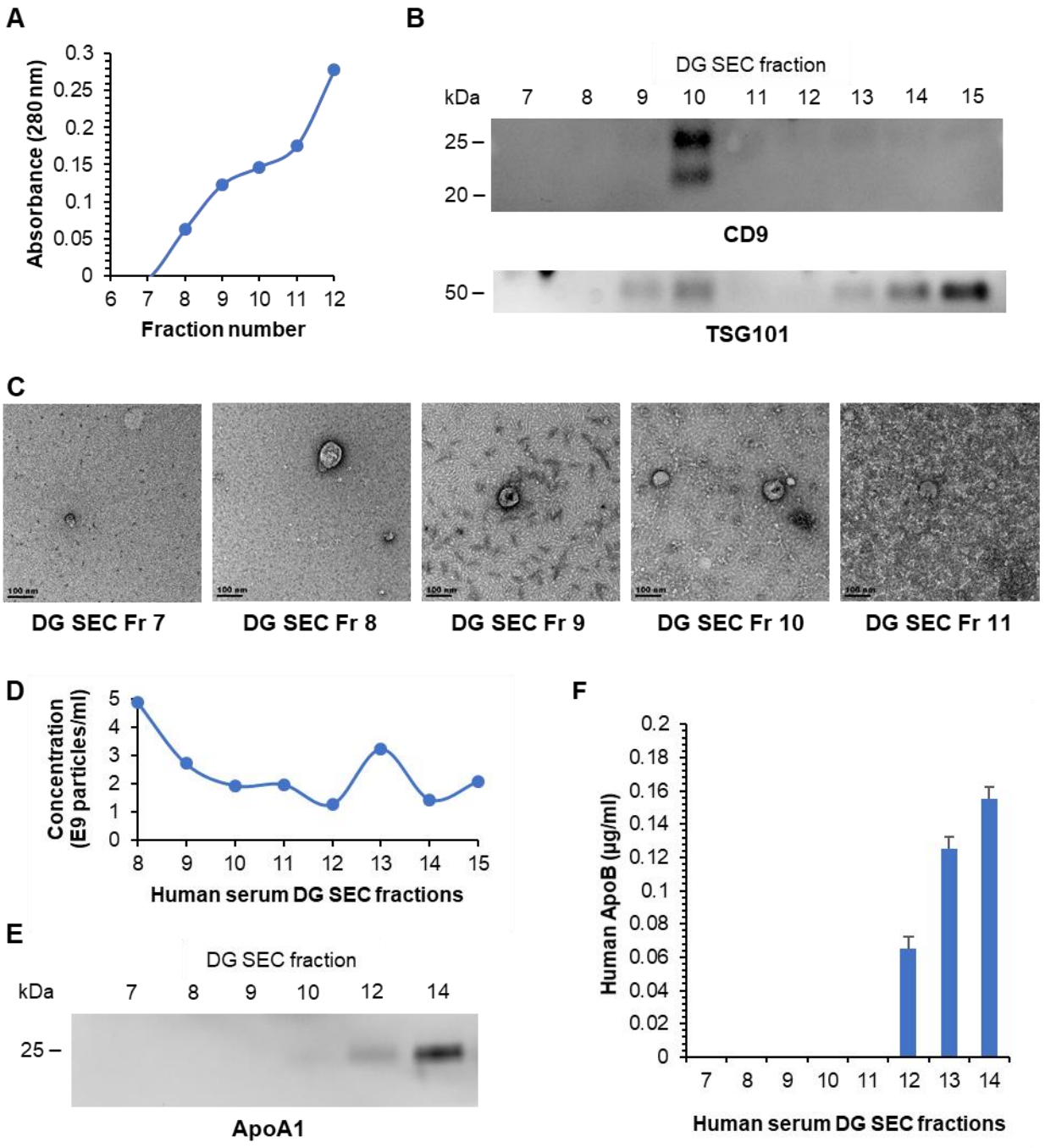

Figure 4.4: Assessment of removing ApoA1 and ApoB lipoprotein contamination in human serum using an iodixanol density gradient followed by SEC. (A) A280 profile of DG SEC performed on a Sepharose CL-4B column. 1 ml of UC concentrated DG fractions 6&7 was loaded onto the column; (B) Western blot to detect exosomal markers (CD9 and TSG101) in DG SEC fractions 7-15 (equal protein loading 0.16 µg). n=3 (technical repeats); (C) TEM micrograph of DG SEC fractions 7-11 (5X diluted). Scale bar = 100 nm; (D) NTA of particles/ml vs the fraction number of human serum DG SEC fractions 8-15; (E) Western blot to identity HDL marker ApoA1 in DG SEC fractions 7-14 (3.3 µl loaded). n=3 (technical repeats); (F) ELISA to identify ApoB lipoproteins in DG SEC fractions 7-14. n=2 (technical repeats).

4.2.5 Assessment of lipoprotein separation by first concentrating exosomes using ultracentrifugation followed by density gradient

Human serum (31 ml) was concentrated using UC thereafter the UC pellet was resuspended in 2 ml 18% iodixanol. The gradient consisted of 0.25 ml 60% iodixanol, 1 ml 18% iodixanol UC pellet (from 15.5 ml serum) and 2.6 ml 6% iodixanol (Figure 4.5A). The gradient was centrifuged in a SW 60 Ti rotor for 24 hours at 195 000 g at 4°C. The UC and density gradient step will be referred to as UC DG.

An ApoB ELISA was used to quantify the concentration of ApoB in the UC pellet (Figure 4.5C). The ApoB concentration was 44.1 µg/ml, showing that 95% of ApoB in serum was removed in this instance. This confirms the finding that was observed for UC after DG (see above) and shows that UC though not removing all ApoB can contribute significantly to purification. After centrifuging the density gradient for 24 hours, even though the concentration of ApoB loaded was significantly reduced relative to on the density gradient of the DG SEC procedure, a faint yellow band was still visible at the top of the gradient and a condensed cloudy yellow band at the bottom (Figure 4.5A). This is suggestive that the main lipoprotein particles present after UC are LDL and HDL. Four fractions were collected from top to bottom (1 ml, 1 ml, 0.5 ml and 1.1 ml). Western blot only detected HDL marker ApoA1 in UC DG fraction 4 (Figure 4.5B). The ApoB concentration was the highest in UC DG fraction 1 (22.7 µg/ml) and decreased in fraction 2 (3.3 µg/ml) and fraction 3 (2.6 µg/ml) (Figure 4.5D). There was a slight increase in fraction 4 (5.3 µg/ml) compared to fraction 2 and 3. This pattern of decreasing ApoB concentration till there is a slight increase in the last fraction of the density gradient is as was observed for the DG SEC approach though with much reduced ApoB on the UC DG gradient due to the prior removal of ApoB by UC. The exosomal markers CD9 (25 kDa) and TSG101 (50 kDa) were only detected in UC DG fraction 4 (Figure 4.5E). Thus, HDL and exosomes co-isolated as expected. This does show that though 83% of ApoB on the gradient was separated away from exosome marker containing fractions, there was a higher proportion present in these fractions than seen in the DG SEC approach at this stage. This perhaps reflects the enrichment of higher density LDL particles by UC.

As the UC and step gradient separated the majority of the ApoB lipoproteins from the exosome fraction, UC DG fraction 4 was further purified using SEC.

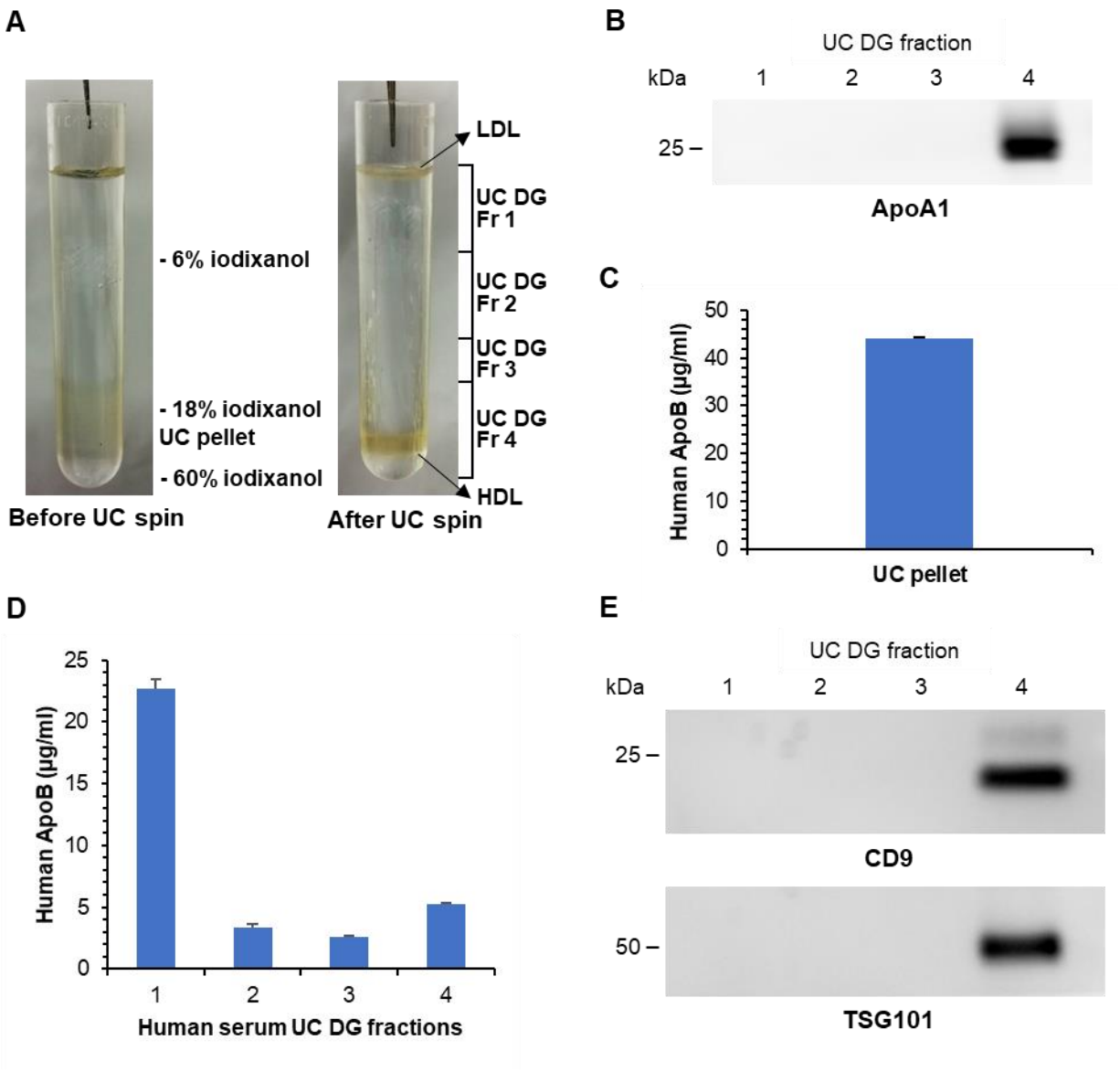

Figure 4.5: Assessment of removing ApoB lipoprotein contamination in human serum using UC followed by an iodixanol density gradient. (A) Gradient consisted of 0.25 ml 60% iodixanol, 1 ml 18% iodixanol UC pellet and 2.6 ml 6% iodixanol. After centrifuging the LDL were visible by a faint yellow band at the top and HDL condensing at the bottom. Isolations were performed on three independent pooled human sera batches with two technical repeats for two of the batches; (B) Western blot to identity HDL marker ApoA1 in UC DG fractions 1-4 (3.3 µl loaded); (C) ELISA to identify ApoB lipoproteins in UC pellet. n=2 (technical repeats); (D) ELISA to identify ApoB lipoproteins in UC DG fractions 1-4. n=2 (technical repeats); (E) Western blot to detect exosomal markers (CD9 and TSG101) in UC DG fractions 1-4 (6.7 µl loaded).

4.2.5.1 Assessment of lipoprotein separation after ultracentrifugation, density gradient followed by size exclusion chromatography

The 1 ml UC density gradient fraction 4 was loaded directly onto the SEC column to isolate the purified human serum exosomes (Figure 4.6). The UC, density gradient followed by SEC method will be referred to as UC DG SEC.

The A280 profile of UC DG SEC performed on a Sepharose CL-4B column displayed a peak in fraction 8-10 (Figure 4.6A) unlike the shoulder observed for DG SEC. Western blot detected CD9 present in UC DG SEC fraction 9 and slightly less in fraction 10 (Figure 4.6B). TSG101 was present in UC DG SEC fraction 9 and was again also detected in UC DG SEC fraction 13-15 increasing in intensity. Thus, UC DG SEC fraction 9 contained majority of the exosomal markers as well as having the highest absorbance reading in the peak. The lowest magnification TEM (0.5 µm scale bar) revealed numerous vesicles (Figure 4.6C). When observed at higher magnifications the vast majority of vesicles are seen to be cup-shaped with a few spherical particles that more resembled lipoprotein particles. TEM showed particles of dimensions expected of exosomes in UC DG SEC fraction 9 with average diameters correlating to those of exosomes (71.7 nm ±22.3). The size range of the vesicles in UC DG SEC fraction 9 (40.3-121.3 nm) correlated with the reported exosome sizes of 30-100 nm (Caradec *et al.*, 2014, Vicencio *et al.*, 2015). The UC DG SEC fraction 9 had a larger average diameter (71.7 nm ±22.3) and larger minimum vesicle size (40.3 nm) compared to SEC fraction 9 (44.5 nm ±14.5 and 15.3 nm respectively, Figure 2.1), further evidence that more exosomes and less lipoproteins were isolated particularly since LDL are 21-27 nm. The marker ApoA1 was mainly detected in UC DG SEC fraction 14 (Figure 4.6D). A faint band of ApoA1 was detected in fraction 12 with a very slight trace in fraction 10. UC DG SEC fraction 9 did not contain a detectable amount of ApoA1. ApoB concentration was detected from UC DG SEC fraction 11 (0.05 µg/ml) and continued to increase after (UC DG SEC fraction 14 (0.535 µg/ml)) (Figure 4.6E). As UC DG fraction 4 contained ApoB (Figure 4.5D) these later UC DG SEC fractions containing ApoB are suggested to be LDL of 21-27 nm as the Sepharose CL-4B have 35 nm pores. There were no detectable ApoB lipoproteins in UC DG SEC fraction 7,8, 9 and 10. Thus, there was no or minimal ApoB lipoproteins in UC DG SEC exosome fraction 9-10.

NTA was then used to compare the particle number in serum SEC-derived fractions and purified UC DG SEC-derived exosome fractions (Figure 4.6F). The NTA results showed an initial rise in particle number in SEC fraction 8 ($7.28x10^{10}$ particles/ml) and a peak in fraction 9 ($1.24x10^{11}$ particles/ml). The particle number continued to decrease from fraction 10 ($7.66x10^{10}$ particles/ml)

through to fraction 12 ($1.10x10^{10}$ particles/ml). The peak particle count in SEC fraction 9 coincides with the A_{280} peak and exosome marker reported previously (Figure 2.1 and 2.4). A clear peak was visible for the UC DG SEC isolation unlike that observed for DG SEC further indicating that the aggregates observed on TEM may have obscured the particle count in DG SEC or that there were less particles present. There was an initial increase in particle number in UC DG SEC fraction 8 ($1.80x10^{9}$ particles/ml) and a shared peak in fraction 9 ($4.47x10^{9}$) and 10 ($4.72x10^{9}$ particles/ml). The particle concentration decreased in fraction 11 ($2.77x10^{9}$ particles/ml) and 12 ($2.05x10^{9}$ particles/ml). The shared peak particle concentration in UC DG SEC fraction 9 and 10 coincided with the A_{280} peak and exosome marker densities (Figure 4.6A and B). The purified UC DG SEC serum fractions contained ~100 times less particles than SEC strongly indicating that lipoproteins like VLDL and IDL contributed the majority of particles observed on TEM for SEC isolations. The representative graph of particles/ml vs particle diameter (nm) from the NTA report, for SEC and UC DG SEC exosome fraction 9, is shown in Appendix 5 (Figure A5).

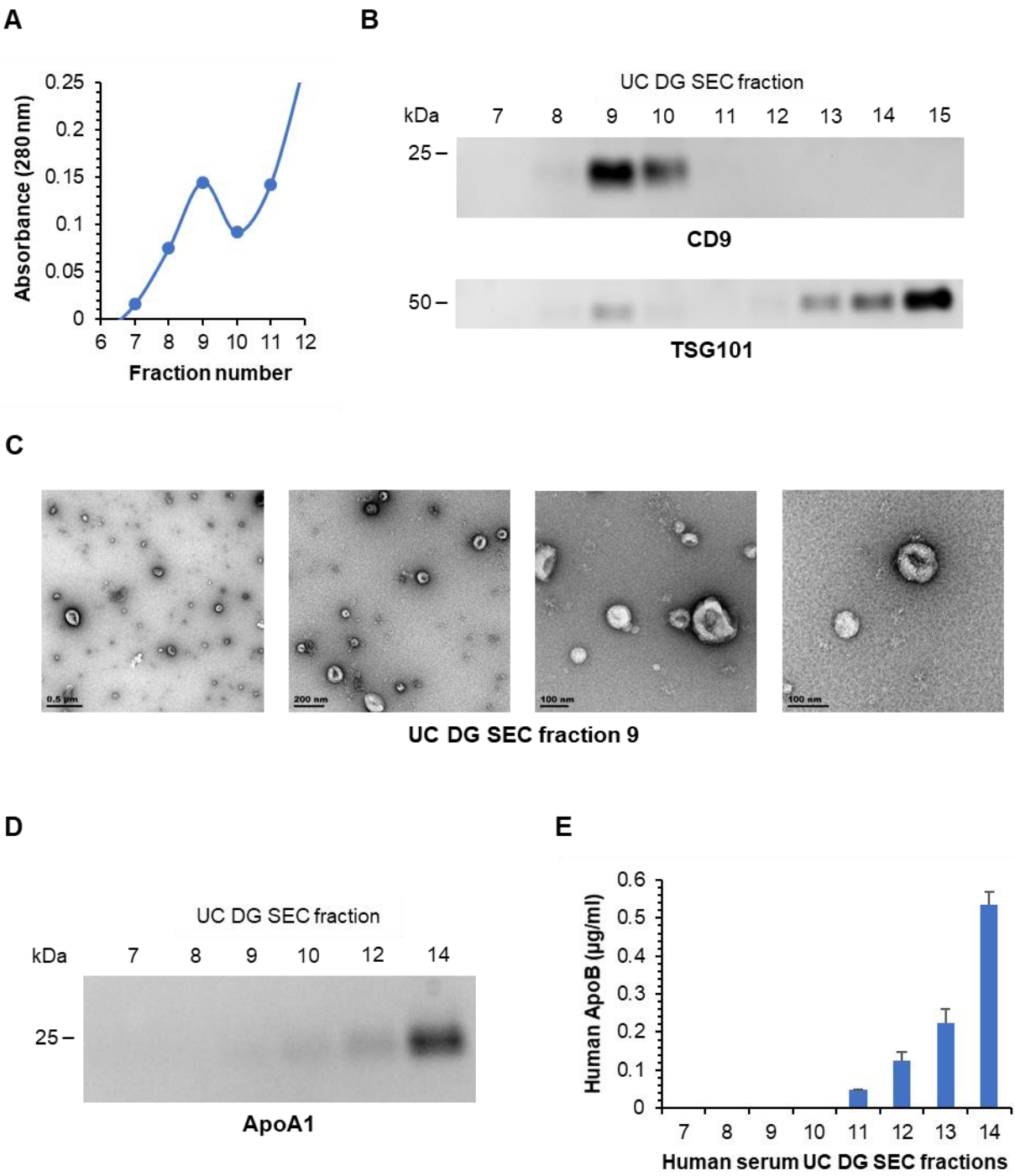
A
Absorbance (280 nm)
0.25
0.2
0.15
0.1
0.05
0
6 7 8 9 10 11 12
Fraction number
B
UC DG SEC fraction
kDa
7 8 9 10 11 12 13 14 15
25 –
CD9
50 –
TSG101
C
0.5 µm
200 nm
100 nm
100 nm
UC DG SEC fraction 9
D
UC DG SEC fraction
kDa
7 8 9 10 12 14
25 –
ApoA1
E
Human ApoB (µg/ml)
0.6
0.5
0.4
0.3
0.2
0.1
0
7 8 9 10 11 12 13 14
Human serum UC DG SEC fractions

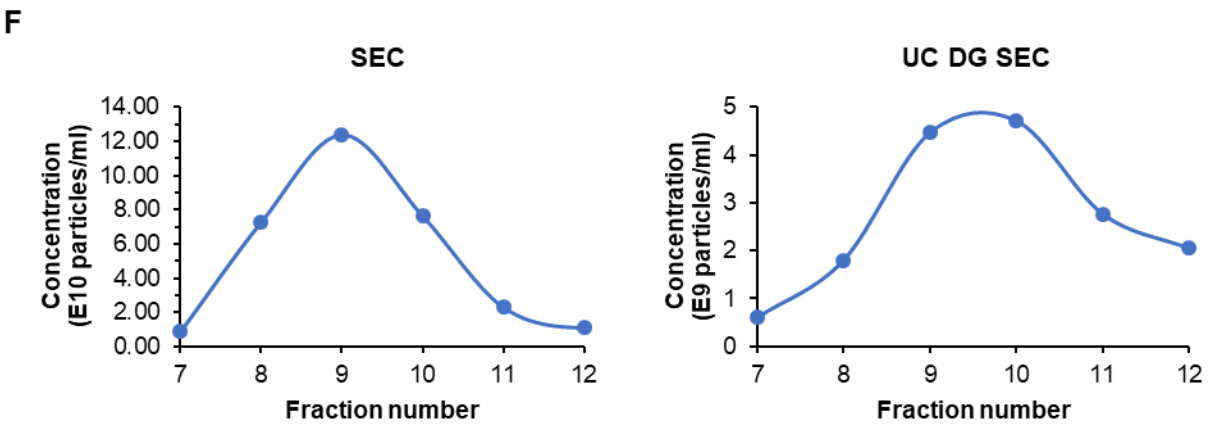

Figure 4.6: Assessment of removing ApoA1 and ApoB lipoprotein contamination in human serum using UC followed by an iodixanol density gradient and SEC. (A) A280 profile of UC DG SEC performed on a Sepharose CL-4B column. 1 ml concentrated UC DG fraction 4 was loaded onto the column; (B) Western blot to detect exosomal markers (CD9 and TSG101) in UC DG SEC fractions 7-15 (equal protein 0.4 µg). n=2 (technical repeats); (C) TEM micrograph of UC DG SEC exosome fraction 9 at different magnifications. Scale bars indicated on figures; (D) Western blot to identity HDL marker ApoA1 in UC DG SEC fractions 7-14 (3.3 µl loaded); (E) ELISA to identify ApoB lipoproteins in UC DG SEC fractions 7-14. n=2 (technical repeats); (F) NTA of particles/ml vs the fraction number of serum exosomes isolated using SEC or UC DG SEC.

As blood is a very complex medium, the co-isolation of lipoproteins and exosomes is an issue when using a single-step purification. In 2017, it was proposed that a combination of density gradient and size exclusion techniques would obtain a purer population of EVs (Simonsen, 2017). This should be expected to reduce incorrect interpretations regarding exosome bioactivity and composition. Even though the issue of co-isolation is more prominent in EV isolations due to the higher concentration of lipoproteins in blood, a minor contamination of EVs in lipoprotein isolations can also significantly influence the protein and RNA composition when detected using mass spectrometry or qPCR respectively (Simonsen, 2017). We are presently aware of only two studies that have explored the utility of density gradient isolation followed by further downstream SEC purification (Karimi *et al.*, 2018, Onódi *et al.*, 2018). Both these studies used identical iodixanol gradients (equal volumes of 10, 30 and 50% iodixanol) overlayed with plasma. In the earlier publication, Karimi *et al.* loaded onto the density gradient 6 ml of human plasma (equal to total density gradient volume) or a 6 ml resuspension of an UC pellet of 40-80 ml plasma (large scale). For the latter, though microvesicles were pelleted at 16 500 g (20 min) and exosomes at 118 000 g (2.5 hour), the two pellets were combined prior to being loaded on the density gradient. Onódi *et al.* modified the approach of Karimi *et al.* in several ways. They loaded 0.5 ml rat plasma (1/8th

total density gradient volume, small scale) or 2 ml (1/4 total density gradient volume, large scale). They also, as we did for serum (UC DG SEC), centrifuged the plasma to remove microvesicles prior to addition to the density gradient. Furthermore, unlike Karimi *et al.* who centrifuged their gradient at 178 000 g for 2 hours, Onódi *et al.* spun their gradients at 120 000 g for 24 hours. Both studies investigated the utility of SEC as a post-purification procedure (Sepharose CL-2B) with Onódi *et al.* additionally examining the efficiency of UC (100 000 g, 3 hours) or bind-elute SEC (Hiscreen Captocore700).

The major differences in our approach to the above are the use of human serum as a source for exosomes, the construction of a technically simpler gradient that only requires three loadings of components rather the four used in both above studies. The separation of lipoprotein particles from exosomes on the density gradients was reliant on sedimentation of exosomes in the above whilst our approach focused more on buoyant force driven flotation of the lipoprotein particles. Furthermore, we used Sepharose CL-4B in a longer column (all SEC columns were 10 ml volume) for post density gradient purification. As detailed above (Chapter 2), we used this matrix as it had been reported to optimally separate exosomal sized vesicles (Baranyai *et al.*, 2015). Analysis of lipoprotein content also differed, our study employed a highly quantitative and sensitive sandwich ELISA to detect ApoB (100 and 48) while Onódi *et al.* used western blotting to relatively quantify ApoB (100 and 48). Interestingly, Karimi *et al.* did not directly assay for ApoB contamination but did assay ApoA1 via western blotting as did we and Onódi *et al.*

From the results, the gradient was efficient at removing majority of the ApoB lipoproteins from the serum exosomes and it was very simple to construct as it only contained three layers. The density layers were underlayed which is much easier than overlaying, especially with the denser 60% cushion (Pandya and N, 2015). Our approach allowed for underlaying the gradient as the serum was within the 18% iodixanol layer.

The majority of ApoB content was present in density gradient fraction 1-4 (DG SEC method) and UC DG fraction 1 (UC DG SEC method) with low levels of ApoB (5-20 µg/ml) present in exosome marker containing fractions. Though difficult to directly compare as their analysis was a relative measure (western blotting), our data is in accordance with Onódi *et al.* who also found ApoB100 and ApoB48 in upper density fractions (1-4 and 1-3 for small and large scale respectively) and exosome markers (Alix, CD81 and TSG101) into denser fraction 5-7, detected by western blotting (Onódi *et al.*, 2018). They had a trail of ApoB100 in density fractions 5-7, coinciding with the exosome markers. This further correlates with the minor detection of ApoB in density fraction 6 and 7 (DG SEC method) and UC DG fraction 4 (UC DG SEC method). Hence, the co-isolation of

the minor LDL using the density gradient was shown to be separated into the later DG SEC and UC DG SEC fractions 12-14. The minimal LDL detected in the lower gradient fractions may have not separated efficiently to the top of the gradient due to their higher density than the other ApoB lipoproteins.

In both our density gradients, ApoA1 was not seen to co-isolate with low-density lipoproteins unlike as observed by Karimi *et al.* They detected the majority of ApoA1 present in a low-density band (<1.025 g/ml). This suggests the possibility of a significant amount of early stage chylomicrons associated with ApoA1 and further that as indicated above, that our pre-gradient removal of chylomicrons was effective. In our UC DG SEC approach, we did not observe any separation of ApoA1 from exosome markers in the density gradient but did see some on the density gradient in the DG SEC study as was observed by both Karimi *et al.* and Onódi *et al.* Though this separation is desirable, it was not considered a serious concern as Sepharose CL-4B SEC effectively separated ApoA1.

Sepharose CL-4B SEC of density fractions from either DG SEC or UC DG SEC resulted in exosome marker (CD9, TSG101) enriched fractions having no detectable ApoB or ApoA1. However, it was noted that in the UC DG SEC approach, ApoB and ApoA1 (very faint trace) were detected one fraction earlier and closer (11 and 10 respectively) to the exosome marker fraction than that seen in DG SEC (12 and 11 respectively). Though indicating a possible reduction in purification for UC DG SEC relative to DG SEC, this needs to be contextualised with the morphological and quantitative analysis of the particles obtained.

Our UC DG SEC exosome fraction 9 did not contain a detectable amount of ApoA1, whereas Karimi *et al.* did detect some ApoA1 contamination in their exosome fraction 8 and 9 using both their small and large scale DG SEC methods. Onódi *et al.* DG SEC method using a commercial column also agreed with our results as they detected ApoB100 in later fractions 12-17. However, they also detected ApoB48 in fractions 9-11 and a slight trail in fractions 12-17. This could be due to that they didn't use a UC step between the DG and SEC, which would have further removed low-density ApoB48 as was shown in these studies in which no detectable ApoB was found in exosome DG SEC fractions or UC DG SEC fractions.

The morphology and concentration of exosomes isolated improved using the UC DG SEC method compared to DG SEC even though the UC DG SEC method used slightly less starting serum (UC DG SEC: 15.5 ml serum; DG SEC: 16.8 ml serum). It must be noted that density gradient fraction 5 containing exosome markers was sacrificed for the DG SEC method due to a relatively higher

level of ApoB. The A280 absorbance was less for the DG SEC fraction 9 exosome shoulder (0.123 AU) compared to UC DG SEC method fraction 9 exosome peak (0.145 AU). Electron micrography showed the particles to be cleaner and containing a high percentage of exosome like particles. It is difficult to compare the NTA data for both preparations as there was not a clear peak for the DG SEC, suggestive of the presence of aggregates that were also detected by TEM. However, even with the assumption of no aggregates, there were 1.6 times more particles present in the UC DG SEC exosome sample. It is possible as indicated above that with concentration by UC at the start, exosomes were protected by the presence of excess particles and other serum components and that less exosomes were lost due to adhesion to the centrifuge tube in UC DG SEC. Sódar *et al.* suggested that commercial LDL attached to 5/4E8 Th1 T hybridoma cell-derived exosomes isolated using differential UC (Sódar *et al.*, 2016). However, we did not see evidence of LDL attaching to the serum UC DG SEC-derived exosomes in our TEM analysis.

We also saw as expected that NTA failed to distinguish between exosomes and lipoproteins, as reported by other authors (Karimi *et al.*, 2018, Takov *et al.*, 2019). The particle number was 100-fold more in SEC-derived exosomes compared to purified UC DG SEC-derived exosomes, even though only 1 ml of serum was used for SEC compared to 15.5 ml for the UC DG SEC method. Karimi *et al.* found 30-100 times more particles in the low-density band as compared to their high-density band isolated off their 4-step density gradient (Karimi *et al.*, 2018). These results highlight the issue of quantification in the exosome field when working with blood-derived components such as serum, as exosomes are alike in shape and size to lipoproteins. Thus, using the UC DG SEC method, provides a more suitable method to estimate particles concentration with NTA.

The repeated detection of TSG101 in western blots of later SEC, DG SEC and UC DG SEC fractions 13-15 suggests the presence of substantial amounts of free TSG101 or that TSG101 may be bound to other much smaller vesicles. As mentioned and discussed previously other researchers using SEC to isolate plasma/serum exosomes observed the same pattern for TSG101 and CD63 (Baranyai *et al.*, 2015, Koh *et al.*, 2018). Karimi *et al.* also observed flotillin-1 and TSG101 in their downstream fractions on SEC (Karimi *et al.*, 2018). This requires further analysis though it should be noted that CD9 in our isolations did not have the same distribution being detected only in the void volume peak. Interestingly, when Karimi *et al.* separated the low-density band from their DG on SEC columns, TSG101 was detected in fractions 10-14 and flotillin-1 in fractions 7-9 suggesting there are particles with a density <1.025 g/cm^3 containing exosome markers. It might also indicate a too brief centrifugation period 2 hours versus 24 hours for Onódi *et al.* (Onódi *et al.*, 2018). When we centrifuged for 3 hours at 200 000 g relative to their 2 hours

at 178 000 g, though at a higher iodixanol density, we observed no sedimentation of exosomal markers.

A few other purification approaches directed towards purifying exosomes away from lipoprotein particles in blood-derived samples have been reported recently.

As mentioned above, Onódi *et al.*, assessed the utility of bind-elute SEC after density gradient isolation. They further purified density gradient fraction 6-8 from the large scale (1.5 ml) using bind-elute SEC using a 4.7 ml CaptoCore 700 column. They did not detect ApoB100 in their DG bind-elute SEC fractions 1-12; however, they had minor levels of ApoB48 in fractions 6-7 coinciding with exosome markers TSG101, CD81 and Alix. It is to be noted they used western blotting to quantify ApoB which may not be as sensitive as the ELISA used here. Furthermore, their Capto Core 700 column was shown to retain a significant amount of exosomal markers which would have reduced their exosome yield.

One study investigated the efficiency of SEC, heparin-Sepharose, lipopolysaccharide-Sepharose, (2-hydroxypropyl)-β-cyclodextrin-Sepharose, and concanavalin A-Sepharose in separating serum EVs and lipoproteins (Wang and Turko, 2018). They found that SEC followed by heparin-Sepharose isolated purer exosomes; however, it still recovered 0.6% ApoA1 and 0.4% ApoB100. It should be noted that our approach of utilising a density gradient followed by SEC reduced ApoB to at least 0.002% of serum levels.

The use of anti-ApoB antibody magnetic beads have also been used to remove contaminating lipoproteins from plasma or cell culture exosomes; however, a substantial loss of exosomes and NTA artefacts were noted as issues (Mørk *et al.*, 2017).

An approach whereby 5 UC steps were used to remove more than 95% of serum proteins and to remove ApoB and ApoA1 lipoprotein contamination from exosome samples with minimal loss in yield is promising in its simplicity (An *et al.*, 2018). There are discrepancies in the literature though, another report suggested two UC steps removes ApoB as determined detected by western blot but the concentration of exosomal marker CD9 dropped 50% with the second UC step (Nielsen *et al.*, 2018). It should be noted with respect to the latter finding that detection of ApoB by western blot is challenging (Sódar *et al.*, 2016).

Acoustofluidic technology has also been suggested to separate exosomes and lipoproteins, with the advantage of a simple, fast (25 min), only 100 µl undiluted human blood required and continuous-flow isolation. Acoustofluidics employs a continuous acoustic streaming, and the

device separated the EVs and lipoproteins according to their acoustic properties. Yet, the UC DG SEC method was superior in removing more lipoproteins as only 70% of VLDL was reduced using the acoustofluidic method (Wu *et al.*, 2019a). A further possibility would be to combine SEC with immunoaffinity. This has been performed previously to isolate tumour-derived exosomes from plasma using SEC and immunoaffinity capture with a unique melanoma cell epitope (Sharma *et al.*, 2018). However, the lack of a specific exosome marker (Théry *et al.*, 2018) limits the potential to isolate all exosomes using immunoaffinity capture.

As our UC DG SEC method isolated exosome like particles, enriched for exosomal markers with non-detectable levels of ApoB and ApoA1, the exosome fraction protein content was assayed by liquid chromatography with tandem mass spectrometry (LC-MS/MS) and compared to the proteomic data gained by Karimi *et al.*

4.2.6 Proteomic analysis of SEC and UC DG SEC isolates

An initial proteomic pilot study was carried out to determine whether mass spectrometry of proteins from the two isolates was feasible. Runs with UC DG SEC isolates satisfied quality control of the LC-MS/MS core facility, which was running a complex reference sample (human neuroblastoma cell line) with the calibration of the mass spectrometer to benchmark the instrument. The samples were initially overloaded, but after dilution these too passed the relevant quality control. The mass spectrometry data was obtained using label-free discovery proteomics which uses a data-dependent Top 10 method that picks the most abundant peptides from the survey scan which does allow for quantification. However, as this was a pilot study several caveats with respect to quantification must be noted. The inherent random nature of complex biological samples means that peptides can appear to be absent in a sample when they are present but at very low amounts. To achieve better quantitative accuracy in label-free proteomics, biological and technical replicates are recommended. Furthermore, it is common practice to quantify total proteins prior to tryptic digest so that the amount of protein in each sample is equal. However, due to the concern that there might be a very low amount of starting material in this exploratory study, it was decided to proceed with tryptic digest without performing protein quantitation. Thus, the amount of total protein in these samples was not normalised. Though comparison of the total ion intensity of these samples, to that of a known reference sample, determined that this method provides sufficient starting material to allow for protein quantitation prior to tryptic digest. This indicates the isolation method will be suitable for follow up studies in replicate.

Bearing the above limitations in mind, the readouts of the LC-MS/MS were further analysed and it was noted that the level of ApoA1, as determined by LFQ intensity, was similar between the two. CD9 was similarly elevated approximately 3-fold for UC DG SEC relative to SEC (Appendix 6) as had been observed with western blotting (Figure 5.1 - Data shown in section 5.2.1). It was thus suggestive that the readouts obtained were probably reasonably representative of the pattern of protein levels in the two isolates. It can be seen that 224 proteins were identified in UC DG SEC exosomes and 135 proteins in SEC exosomes (Figure 4.7 and 4.8) using the MaxQuant search engine, Andromeda. This is perhaps not unexpected as the very high level of lipoproteins might have impeded detection of lower level proteins. If one looks at the top 10 proteins in SEC (LFQ levels in SEC) (Table 4.2), four were lipoproteins with ApoB having the highest LFQ intensity ($2.56x10^{11}$). Thus, the high levels of lipoproteins overwhelmed the mass spectrometry data as was also observed by Karimi *et al.* who found a lower number of proteins identified in their plasma SEC exosomes with the majority being lipoproteins, predominately ApoB with only minimal EV proteins identified.

The Funrich analysis of cellular components, based on their GO identification numbers, indicated that 81% and 85% of GO identified proteins within UC DG SEC and SEC samples, respectively, are exosome associated ($p < 0.001$) (Figure 4.7). This reflects 182 and 115 proteins for UC DG SEC and SEC respectively. When the SEC and UC DG SEC isolated proteins were compared to each other (Figure 4.8) there was an overlap of 117 proteins with the UC DG SEC proteome containing 107 unique proteins whilst SEC had only 18 unique proteins.

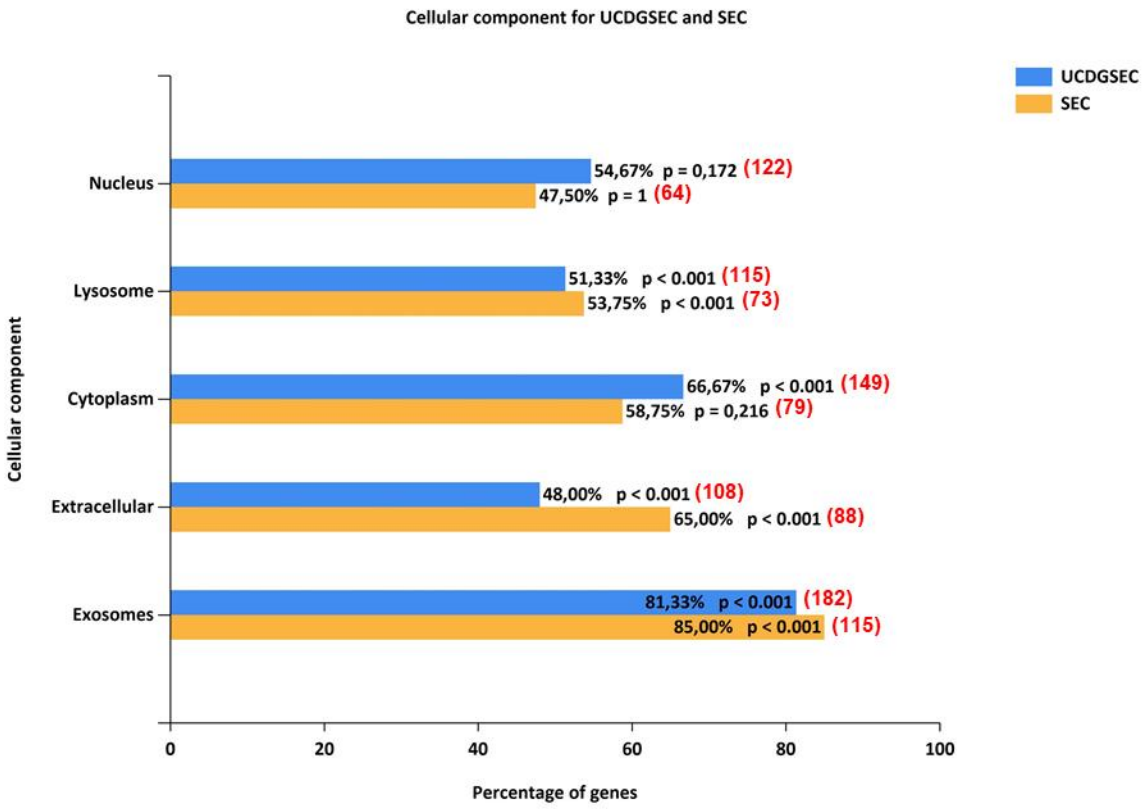

Figure 4.7: Enrichment of cellular components in SEC and UC DG SEC exosomes. LC-MS/MS was performed on the exosomes isolated from fraction 9 using either SEC or UC DG SEC. In total, 224 proteins were identified in UC DG SEC exosomes and 135 proteins in SEC exosomes and were analysed with MaxQuant version 1.3.1.12 followed by Funrich. In brackets, the number of protein hits.

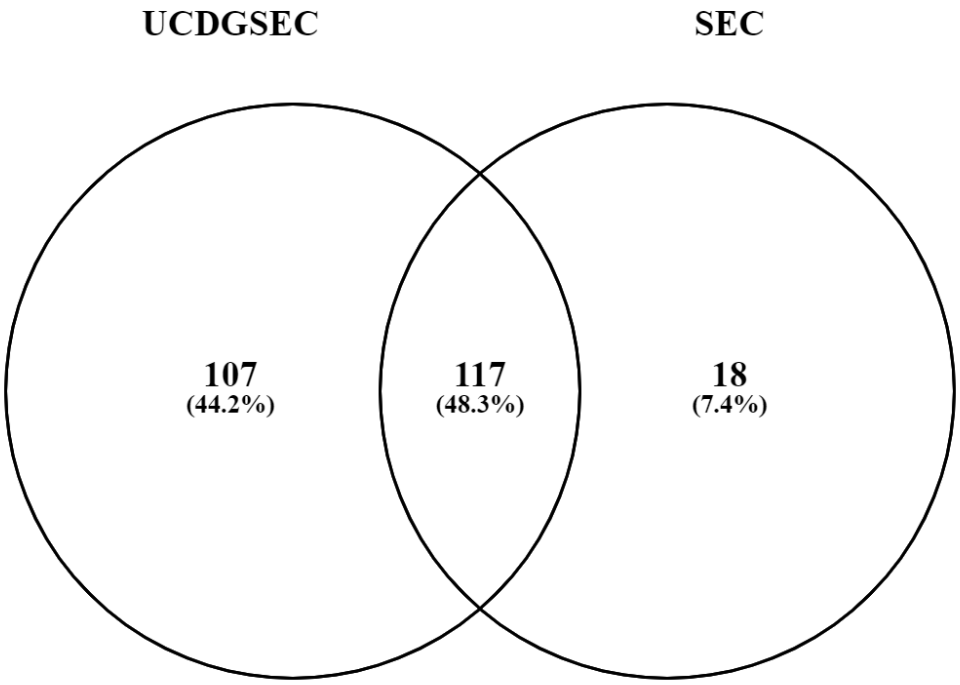

Figure 4.8: Venn diagram comparing the proteins in SEC and UC DG SEC exosome fraction 9.

Table 4.2: Top ten proteins in SEC exosomes

	Protein IDs	Proteins	LFQ intensity
1	P04114	ApoB 100	2.56E+11
2	P01871	Immunoglobulin heavy constant mu	1.26E+11
3	P02649	Apolipoprotein E	7.19E+10
4	P04275	von Willebrand factor	4.09E+10
5	P02656	Apolipoprotein C-III	3.79E+10
6	P02655	APOC4-APOC2 readthrough	3.76E+10
7	P00738	Haptoglobin	3.76E+10
8	P68871	Hemoglobin subunit beta	3.43E+10
9	P01834	Immunoglobulin kappa constant	3.18E+10
10	P04003	C4b-binding protein alpha chain	3.04E+10

Analysis of biological functions showed significant association with the immune response for both SEC and UC DG SEC. Among the top 10 most abundant proteins identified in UC DG SEC exosomes, the amount of immunoglobulin and complement-related proteins were substantially elevated higher (Table 4.3), than in the corresponding SEC exosome proteins. The complement system is part of the innate immune system and has an array of plasma proteins that when activated function to eliminate pathogens through a biological cascade (Sarma and Ward, 2011). It assists the antibodies and phagocytic cells to clear microbes and damaged cells, increase inflammation and attack the pathogen's cell membrane. Numerous publications have reported the association of complement factors and immunoglobulins with exosomes and EV from blood (Radons and Multhoff, 2005, Wei *et al.*, 2016a, Buzás *et al.*, 2018). It has recently been suggested that immunoglobulin associated exosomes may be due to a primary secretion of immunoglobulin packed within B-cell derived exosomes (Huang *et al.*, 2018). Thus, the elevated presence of immune components further indicates the enrichment and purification of exosomes in UC DG SEC.

Alix and flotillin were only present in UC DG SEC exosomes and CD9 LFQ intensity was 3.7-fold higher relative to in SEC exosomes (Appendix 6), again indicating the removal of lipoproteins by UC DG SEC and the probable enrichment of exosomes. Interestingly, the common exosome protein markers TSG101, CD81 and CD63 were absent in the total protein sets even though the former two were positively detected by western blotting in our isolates (Figure 2.4 and Figure 4.6). This probably reflects the nature of mass spectrometry whereby very low-level proteins may not be captured by the detectors. Similarly, Karimi *et al.* did not detect TSG101, with CD81 identified only by the presence of a single peptide and CD63 by two peptides, which does not indicate a very confident identification for either protein by mass spectrometry. Molecular and Cellular Proteomics guidelines discourages the use of identifying proteins by a single unique peptide (Biology, 2019). A peptide-count level assessment of protein quantity is not a suitable quantitative measurement as protein-level inferences based on pure peptide counts cannot be made. Proteins identified on basis of a single unique peptide are discouraged, but if included, the ability to view annotated spectra for these identifications must be made available. It should be noted that proteins were only assigned to our data sets using LFQ which is a stringent way of quantifying proteins based on peptide-level signals that takes intra-sample peptide variation into account, normalises for small technical differences between samples, and its quantitative accuracy is not affected by the size of the protein. Our LC-MS/MS analytical approach was more quantitative in nature than Karimi *et al.*, as it was based on LFQ analysis rather than peptide counting.

There were several UC DG SEC exosome proteins not previously associated with exosomes that were confidently identified in our mass spectrometry dataset. Two of the most prominent were platelet factor 4 variant (released from activated platelets and linked to immune and inflammatory responses, and leukocyte and neutrophil chemotaxis) and properdin (positive regular of complement activation, linked to immune response and neutrophil degranulation). It is noteworthy that these are both immune response linked proteins. Interestingly, at the time of drafting this manuscript, platelet factor 4 itself was identified as a novel exosome marker for human serum exosomes (Nguyen *et al.*, 2019).

Table 4.3: Top ten proteins in UC DG SEC exosomes

	Protein IDs	Proteins	LFQ intensity
1	P68871	Hemoglobin subunit beta	1.99E+11
2	P01871	Immunoglobulin heavy constant mu	1.50E+11
3	P69905	Hemoglobin subunit alpha	1.11E+11
4	P01024	Complement C3	4.79E+10
5	P01834	Immunoglobulin kappa constant	3.97E+10
6	P01857	Immunoglobulin heavy constant gamma 1	3.47E+10
7	P00738	Haptoglobin	2.16E+10
8	P0CG04	Immunoglobulin lambda-like polypeptide 5	1.86E+10
9	P04114	ApoB 100	1.80E+10
10	P01023	Alpha-2-macroglobulin	1.34E+10

Furthermore, as would be predicted of the 10 proteins most reduced in UC DG SEC, relative to in SEC, eight were apolipoproteins (Table 4.4). This again indicates effective removal of apolipoproteins by density gradient isolation. ApoB100 was reduced by 14-fold and was the 11th most reduced proteins in UC DG SEC. However, ELISA indicated, if the assumption is made that ApoB100 levels were around 39.1 ng/ml (minimum detection), that at least 156.5-fold reduction was achieved. As the ELISA recognises both ApoB100 and ApoB48, this might suggest the presence of significant levels of chylomicrons in SEC samples that might have been missed by LC-MS/MS which would require the analysis of specific peptides to allow the levels of the two variants to be determined. This type of analysis was not possible during this pilot. However, no prominent band was observed in SDS-PAGE at ~250 kDa (ApoB48) for SEC but only at ~512

kDa which was most likely ApoB100. Most of the apolipoproteins that were reduced or absent were components of VLDL and IDL (Table 4.4). ApoE, ApoC-II and ApoD which are associated with LDL (according to UniProt) were also reduced in the UC DG SEC sample, highlighting the depletion of LDL in the UC DG SEC exosomes. Perhaps a more likely explanation for the discrepancy noted for ApoB100 removal between ELISA and mass spectrometry is that the intensity of ApoB in the SEC isolate was above the maximum threshold for the detector of the mass spectrometer, which is accurate to about 10^{10}, possibly resulting in an underestimation of ApoB levels in SEC exosomes by mass spectrometry analysis. Additionally, the ELISA results reflect data from two repeats and at present ELISA is considered the more quantitative approach (Cross and Hornshaw, 2016).

Table 4.4: Top ten proteins reduced in UC DG SEC exosomes compared to SEC exosomes

	Protein IDs	Proteins	Fold reduction
1	P55056	Apolipoprotein C-IV	46
2	P02656	Apolipoprotein C-III	39
3	P02649	Apolipoprotein E	33
4	P02654	Apolipoprotein C-I	29
5	O95445	Angiotensinogen	29
6	P08519	Apolipoprotein(a)	26
7	P04275	von Willebrand factor	20
8	P02655	Apolipoprotein C-II	17
9	P05090	Apolipoprotein D	16
10	P35542	SAA2-SAA4 readthrough	14

The 2 proteomes were compared to that of Karimi *et al.* (Figure 4.9). It was decided to exclude all proteins from the Karimi *et al.* data set that were only identified by a single peptide as Molecular and Cellular Proteomics guidelines discourages identifying proteins in this manner (Biology, 2019). About 47% of the proteins identified in UC DG SEC overlapped with those in Karimi *et al.* It is not clear at this stage why the other 53% did not overlap but it probably reflects inherent variability in LC-MS/MS (Øverbye *et al.*, 2015, Parker *et al.*, 2015), variability in the serum source or differences in the isolation technique (e.g. Sepharose CL-4B vs Sepharose CL-2B). ApoB100 was present in their database as the protein with the sixth highest number of peptides present.

Though their LC-MS/MS analytical approach was less quantitative in nature than ours, this does suggest that a density gradient that relies on sedimentation (Karimi *et al.*, 2018) is of the same or less efficiency to the flotation approach used here.

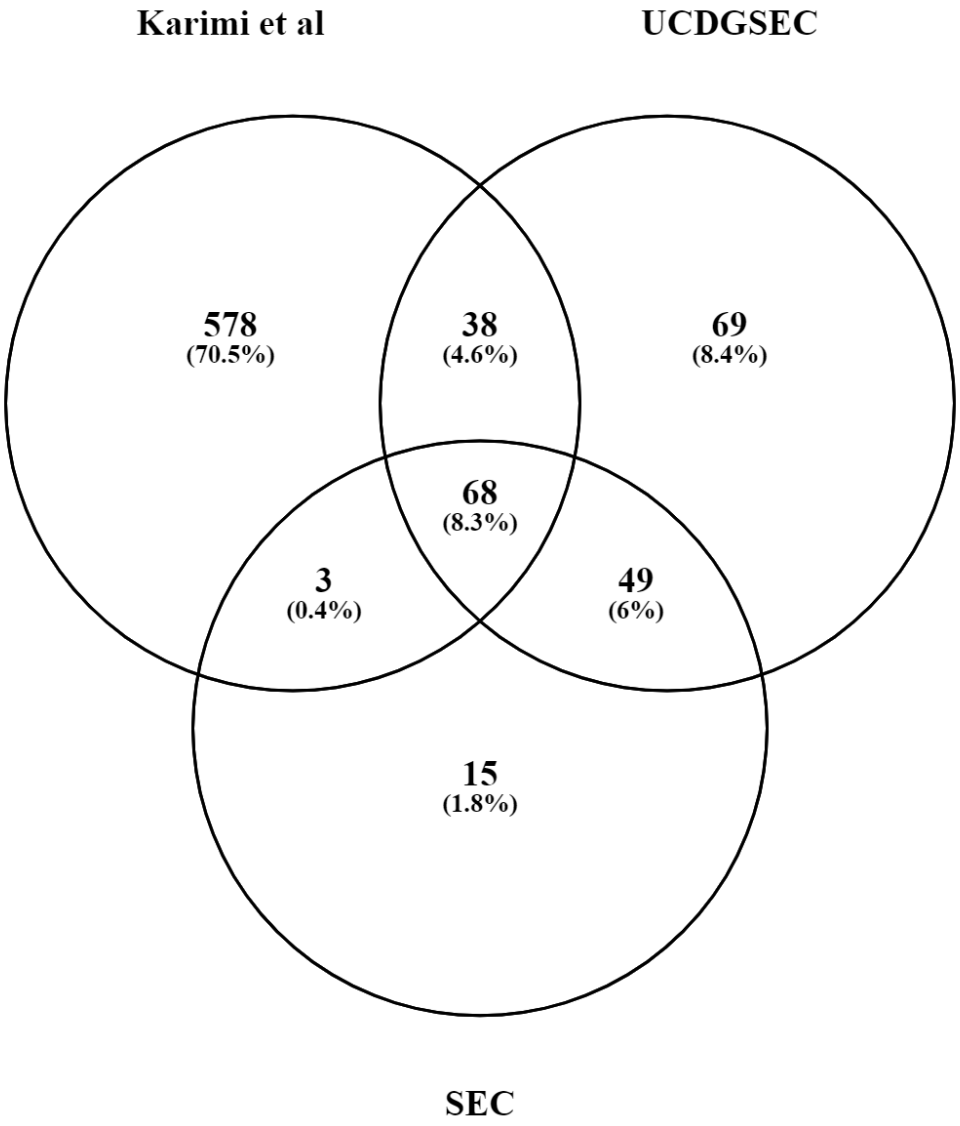

Figure 4.9: Venn diagram comparing the proteins in SEC and UC DG SEC exosome fraction 9, and the previously published proteome of plasma EVs isolated using a similar UC DG SEC method (Karimi *et al.*, 2018).

Our UC DG SEC isolates were enriched for exosomal markers, immunoglobulin and complement related proteins with a reduction in lipoproteins as assayed by LC-MS/MS. Subsequent to that as none of these recent studies investigating the removal of contaminating lipoproteins from exosomes have performed functionality tests on the purified exosomes, cellular and *in vivo* responses were assayed.

4.3 Summary

It is particularly challenging to isolate exosomes from biofluids such as plasma or serum due to their complex composition. This study provides an isolation method that combines a density gradient separation followed by SEC to isolate exosomes from human serum resulting in substantial reduction in lipoprotein contamination. Due to the DG SEC method containing a high precipitant background, low vesicle concentration and variable NTA data, the exosome concentration was increased by first concentrating them from serum using UC followed by a density gradient and SEC. This gradient is an advance over other findings as it is a simpler 3-layer gradient compared to 4 layers (Karimi *et al.*, 2018, Onódi *et al.*, 2018). No ApoB lipoprotein was detectable in UC DG SEC exosome fraction using the ELISA, which though more marked than that seen with LC-MS/MS, indicates removal of more than 99% of lipoprotein. The mass spectrometry data showed a much cleaner preparation with marked reduction in all lipoproteins apart from ApoA1 for the UC DG SEC exosomes as compared to SEC exosomes. Though ApoA1 was present as determined by LC-MS/MS, western blot showed that after the density gradient, SEC successfully removed the vast majority of the HDL from the serum exosomes. This method described here possibly delivered better results than previous studies that had more prominent traces of HDL in their exosome isolation after using a similar DG SEC purification method of plasma exosomes (Karimi *et al.*, 2018). Exosomal markers were increased substantially in the UC DG SEC exosomes. Particularly, exosome marker flotillin was detected in the UC DG SEC exosomes and not SEC exosomes. Furthermore, several novel proteins were identified as exosome components, most particularly platelet factor 4 variant and properdin. Additionally, a strong immune component was identified which is in agreement with findings of others (Radons and Multhoff, 2005, Wei *et al.*, 2016a, Buzás *et al.*, 2018, Huang *et al.*, 2018). A limitation of the present study is the pilot nature of the proteomic study and this must be followed up with an analysis with biological repeats. Also though there is a significant reduction in lipoprotein content, the proteomic analysis indicates that they are still present. However, it should be noted that it is difficult to tell whether those remaining may in part be derived from exosomes (Liang *et al.*, 2013, Van Niel *et al.*, 2015, Welton *et al.*, 2016, Andreu *et al.*, 2017).

As the recent methods investigating the removal of contaminating lipoproteins from exosomes have not as yet tested the functionality of the purified exosomes, cellular and *in vivo* responses were also assayed.

CHAPTER 5: FUNCTIONAL ANALYSIS OF SERUM EXOSOMES PURIFIED BY UC DG SEC

5.1 Introduction

As discussed in the literature review (Section 1.7.4), there are numerous studies on the function of plasma/serum exosomes. Blood-derived exosomes have the regenerative capability to treat various ailments e.g. myocardial injury, hindlimb ischemia, dysferlinopathy, hepatic fibrosis, skin wounds and allergies; summarised in Table 2.1. The exosome isolation methods employed for these *in vivo* functional studies included UC, ExoQuick precipitation and density gradients or a step method using UC combined with a sucrose cushion, density gradient or ultrafiltration (Vicencio *et al.*, 2015, Bei *et al.*, 2017, Guo *et al.*, 2017, Hu *et al.*, 2018, Li *et al.*, 2018b). The majority of the functional *in vivo* studies used UC which as discussed previously (Section 1.3.1) has significant potential issues, predominantly protein contamination especially when using blood-derived sources. SEC seemed to be a promising EV isolation method particularly with the minimal protein contamination (Böing *et al.*, 2014) and our serum SEC exosomes were shown to have bioactivity increasing fibroblast proliferation and enhancing spheroid sprout numbers *in vitro* (Section 2.2.4); consistent with another study showing that plasma-derived EVs isolated using SEC are bioactive as shown by increased migration of HUVECs (Takov *et al.*, 2019). However, as discussed in detail in Chapter 3, plasma/serum lipoproteins co-isolate with exosomes using various isolation methods including UC, PEG precipitation, density gradient, and SEC (Deregibus *et al.*, 2016, Sódar *et al.*, 2016, Grigor'eva *et al.*, 2017, Foers *et al.*, 2018, Karimi *et al.*, 2018, Takov *et al.*, 2019). These contaminating lipoproteins may influence or obscure the biological function of the exosomes, resulting in incorrect conclusions. We and other researchers (Karimi *et al.*, 2018, Onódi *et al.*, 2018) have investigated combining a density gradient with SEC to separate lipoproteins from exosomes. This study showed that combining a density gradient separation and SEC allows for significant separation of isolation of human serum exosomes from lipoproteins. An unsolved question is whether these blood-derived exosomes remain functional after being purified from lipoproteins. The biological function of the 2-step purified exosomes was assessed *in vitro*. This analysis was then followed by an *in vivo* subcutaneous implant study to assess the

influence of the SEC and purified UC DG SEC-derived exosomes on macrophage response and vessel ingrowth.

5.2 Results and discussion

5.2.1 *In vitro* functional analysis of serum exosomes purified by UC DG SEC

The proliferation and spheroid assays (Section 2.2.4.2 and 2.2.4.3) were utilised to determine whether the purified human serum UC DG SEC exosomes retained the regenerative functions observed for the SEC purified exosomes (Figure 5.1).

Human serum UC DG SEC exosomes (30% (v/v)) were incubated with HUVEC spheroids embedded in a fibrin hydrogel (3.25 mg/ml) for 48 hours. Phase contrast images of the spheroids revealed no difference in sprout activity when treated with UC DG SEC exosomes relative to the control (Figure 5.1A). The serum UC DG SEC exosomes had the same HUVEC sprout number (12 ±2.4) relative to the PBS control (12 ±1.3) (Figure 5.1B). To assess the effect of human serum UC DG SEC exosomes on HdFb proliferation, in an initial study fibroblasts were incubated in serum-free media containing 10% UC DG SEC exosomes or 10% PBS for 72 hours. Treatment with 10% UC DG SEC-derived exosomes caused a significant increase in cell proliferation compared to fibroblasts treated with 10% PBS ($p < 0.05$) (Figure 5.1C).

In a follow up study, the effect of human serum SEC exosomes to UC DG SEC exosomes on HdFb proliferation was directly compared, fibroblasts were incubated with SEC and UC DG SEC isolated exosomes for 72 hours. Treatment with 10% SEC-derived exosomes and 10% UC DG SEC-derived exosomes both caused a significant increase in cell proliferation compared to fibroblasts treated with 10% PBS ($p < 0.05$) (Figure 5.1E). The SEC exosomes elicited a greater increase (22% relative to control) in cell proliferation than UC DG SEC exosomes (10% relative to control) though the increase between these two groups was not significant. When the protein concentration of the SEC exosomes was diluted (2.3% SEC exosomes) to the same concentration as UC DG SEC exosomes (according to absorbance at 280 nm), there was no increase in cell proliferation relative to control. This would still correspond to roughly 25 times as many particles (measured by NTA) within the SEC isolate. This is suggestive that the proliferative response is mainly due to exosomes. It could also reflect dilution of another stimulatory component within the SEC isolate such as the presence of lipoproteins. Recently SEC-derived plasma EVs were found to promote migration of endothelial cells (Takov *et al.*, 2019). However, as the migratory response was not proportional to increases in the level of exosome marker CD81, it was suggested that other blood components such as lipoproteins may have played a role.

The purified UC DG SEC exosomes retained their cell proliferative capabilities. Though the stimulatory effect was relatively low (10-17%), it was reproducibly significant across several studies. However, the more purified exosomes were unable to initiate spheroid sprouting which SEC exosomes were previously shown to do. It was observed that the two isolates had differing patterns of the exosome markers CD9 and TSG101 (Figure 5.1D). It is possible this reflects isolation of different subsets of exosomes with differing proliferative potential or another component in the SEC isolate may have played a role in stimulating sprouting. UC DG SEC exosomes were enriched for the 22 kDa form of CD9, whereas the SEC exosomes had increased concentration of the 25 kDa form of CD9. After quantifying the 22 kDa and 25 kDa bands, there was 3X more CD9 present in the UC DG SEC exosome relative to SEC exosomes. SEC exosomes contained 2X more TSG101 compared to UC DG SEC exosomes. It has been shown that different EV types (according to size) are enriched in exclusive proteins or different protein concentrations (Kowal *et al.*, 2016). The EVs were isolated from dendritic cells using UC and an iodixanol gradient. The large EVs (medium >200 nm) were enriched in alpha-actinin-4 (ACTN4), mitochondrial inner membrane mitofilin (IMMT), HSP90B1 and major vault protein (MVP). Whereas, small EVs (<100 nm) were enriched in TSG101, syntenin-1 (SDCBP), a disintegrin and metalloproteinase domain-containing protein 10 (ADAM10) and CD81. Further observations of heterogenous exosomes, Bobrie *et al.* speculated that breast cancer cell-derived exosomes enriched in tetraspanins were found in high-density fractions (1.26 and 1.29 g/ml) compared to exosomes carrying milk fat globule EGF factor 8 (Mfge8) which were enriched in the low-density fraction (1.14 g/ml) (Bobrie *et al.*, 2012).

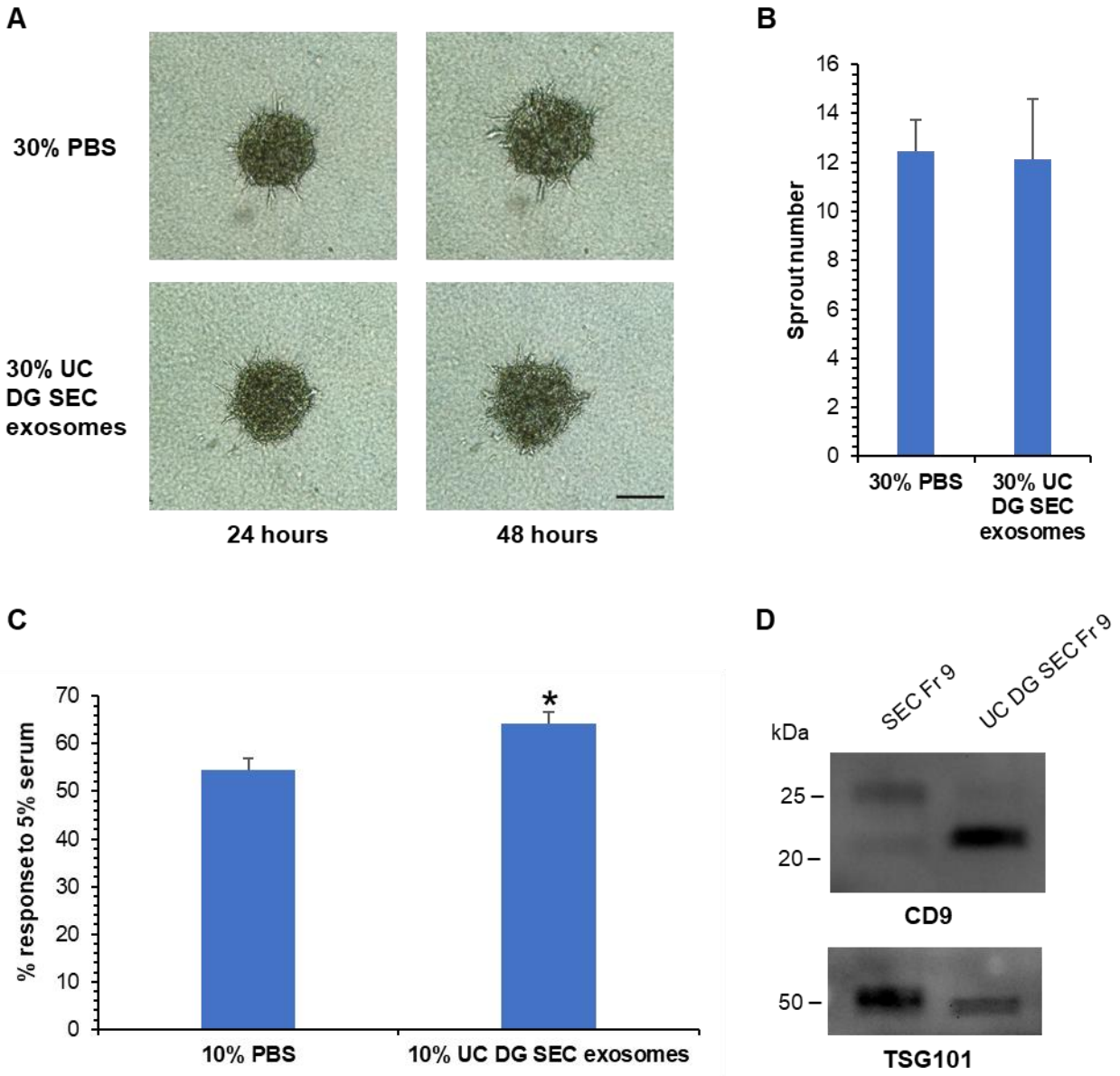
A
30% PBS
30% UC DG SEC exosomes
24 hours
48 hours
B
Sprout number
30% PBS
30% UC DG SEC exosomes
C
% response to 5% serum
10% PBS
10% UC DG SEC exosomes
D
kDa
SEC Fr 9
UC DG SEC Fr 9
25
20
CD9
50
TSG101
E
% response to 5% serum
10% PBS
10% UC DG SEC exosomes
10% SEC exosomes
2.3% SEC exosomes

Figure 5.1: Investigating the functional activity of human serum exosomes isolated using UC DG SEC. (A) Sprouting of HUVEC spheroids in fibrin hydrogels. Each fibrin hydrogel (3.25 mg/ml) contained 8-12 spheroids consisting of 750 cells each. Fibrin hydrogels were treated with either 30% PBS or 30% serum UC DG SEC-derived exosomes in 2% FBS MCDB media. Micrographs taken at 24 and 48 hours. Scale bar = 20 µm; (B) Analysis of sprout number (30% PBS and 30% serum UC DG SEC-derived exosomes) after 48 hours. Combination of three independent experiments with four technical repeats; (C) *In vitro* effects of human serum UC DG SEC-derived exosomes on HdFb cell proliferation. Human fibroblasts were grown in MCDB media for 72 hours with various treatments shown. Proliferation was detected with the XTT assay. Combination of four independent experiments with four technical repeats. * $p < 0.05$ compared to PBS control; (D) Western blot to compare exosomal markers (CD9 and TSG101) in the SEC and UC DG SEC fraction 9 (6 µl loaded of isolates with 0.8 and 0.2 A280 absorbance units/ml respectively); (E) *In vitro* effects of human serum UC DG SEC and SEC-derived exosomes on HdFb cell proliferation over 72 hours. Proliferation was detected with the XTT assay. For the proliferation assays in (C) and (E), 10% UC DG SEC, 10% SEC and 2.3% SEC isolates represent a final A280 of 0.02, 0.08 and 0.02 respectively. Combination of four independent experiments with four technical repeats. * $p < 0.05$ compared to PBS control.

It was thus decided to analyse the influence of ApoB containing lipoproteins on HdFb proliferation whereby the fraction 1 from the top of the step density gradient for the DG SEC isolation was used as the source (Figure 5.2). The isolate from the density gradient from the DG SEC procedure was considered more appropriate as a representation of the lipoproteins in the SEC exosome isolate as none were lost during an UC step. Additionally, as the lipoproteins in fraction 1 were likely to contain the main contaminants identified in the SEC fraction (VLDL and IDL, section 3.2.1.2).

The same concentration of ApoB present in SEC exosome fraction 9 (15 µg/ml) was tested for possible contribution to cell proliferation (Figure 5.2). Density gradient fraction 1 contained 596 µg/ml of ApoB, and was diluted accordingly to 15 µg/ml. For determining potential influence of ApoB lipoproteins on HdFb proliferation, HdFb were incubated with serum-free media containing 1.5 µg ApoB/ml (to mimic the use of 10% (v/v) SEC fraction 9) for 72 hours. Treatment with fraction 1 of the density gradient had no effect on cell proliferation relative to HdFb treated with no serum. This is strongly suggestive that the presence of ApoB lipoproteins in SEC fraction 9 did not contribute to the increase in proliferation observed and that it may be mainly a result of exosomal presence.

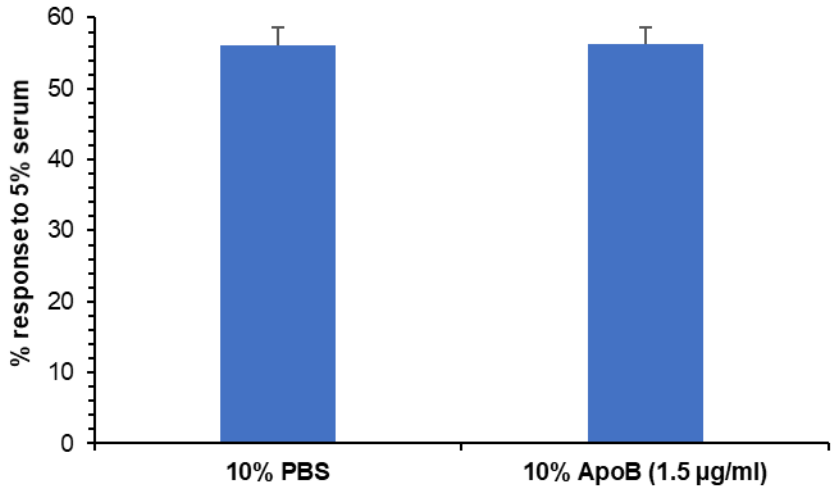

Figure 5.2: Determining the functional activity of ApoB lipoproteins at the same concentration of ApoB present in SEC exosomes. *In vitro* effects of human serum ApoB lipoproteins diluted to the same ApoB concentration (1.5 µg/ml) as serum SEC exosomes on HdFb cell proliferation. 72 Hour reading using the XTT assay. Combination of four independent experiments with four technical repeats.

No studies have investigated the regenerative capabilities of human serum exosomes purified to remove or substantially reduce the lipoprotein content. The human serum UC DG SEC-derived exosomes increased HdFb cell proliferation significantly and that an equal concentration of SEC exosomes did not influence cell proliferation; supporting the theory that the exosomes contributed to HdFb proliferation and not the lipoproteins. However, the UC DG SEC exosomes lost the ability to increase HUVEC spheroid sprout number which human serum SEC-derived exosomes had that capability (Figure 2.9). A possible cause could be a subpopulation of exosomes was lost using the multiple purification method. Interestingly the human serum UC DG SEC-derived exosomes were enriched for the 25 kDa CD9 exosome marker, whereas SEC-derived exosomes were enriched for TSG101. Thus, certain exosome types were enriched using the different purification methods. Another possible reason are the impurities in the SEC-derived exosomes caused the HUVEC sprouts, whereas UC DG SEC-derived exosomes are free from impurities. Thus, losing that function. There is no current literature to compare these functional studies of lipoprotein free purified human serum exosomes to. We then went on to further identify the regenerative capabilities of the purified exosomes and perform a subcutaneous implant in rats to test for an *in vivo* angiogenesis response.

5.2.2 *In vivo* functional analysis of serum exosomes purified by UC DG SEC

As SEC and UC DG SEC exosomes showed functionality *in vitro* (Section 5.2.1), the immune and angiogenic potential of the exosomes were assayed *in vivo* in a rat subcutaneous model. This subcutaneous *in vivo* model is desirable ethically as it is relatively minimally invasive and a number of treatments can be tested simultaneously in one animal.

In the rat subcutaneous model (described in section 7.15), 10 mg/ml fibrin hydrogels (with or without SEC or UC DG SEC exosomes at 72.7% (v/v)) were polymerised within porous polyurethane (PU) discs. These highly porous PU discs have been used many times by our group for angiogenesis studies as they allow for precise delineation of tissue response and vessel ingrowth into the hydrogel polymerised within their pores (Davies *et al.*, 2008, Schmidt *et al.*, 2009, Bezuidenhout *et al.*, 2010, Davies *et al.*, 2011, Goetsch *et al.*, 2015, van Rensburg *et al.*, 2017, Chokoza *et al.*, 2019). The rats were killed after 7 days and the discs explanted.

5.2.2.1 Tissue invasion

Almost full ingrowth of tissue into the porous space was seen for all groups with occasional small patch of undegraded fibrin present in all groups (Figure 5.3). The latter observation indicates that carrier hydrogel was present throughout the implant period and based on the results derived from the release study for 3 mg/ml fibrin gels (see section 2.2.6), it might be expected that there was a sustained release of microparticles throughout the implantation period.

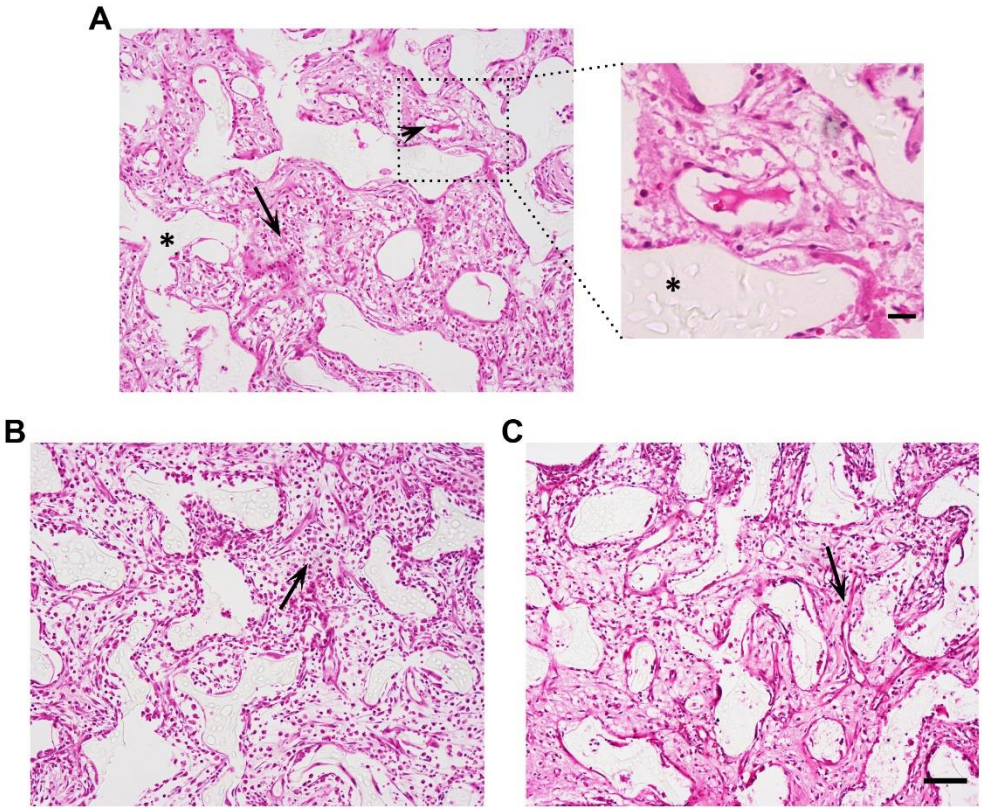

Figure 5.3: Tissue ingrowth into subcutaneous implants. Representative micrographs of haematoxylin and eosin stained cross-sectional areas of explants. Treatments: (A) Fibrin alone; (B) SEC exosomes or (C) UC DG SEC exosomes. Arrowhead indicates pink/purple-stained fibrin hydrogel remnants, and arrows show ingrown tissue with nuclei stained dark purple. Asterisks denote polyurethane struts of the porous disks. The bar represents 100 µm (inset bar 20 µm). n=6 per group.

5.2.2.2 Inflammatory response ED1

As a strong immune component was determined for both isolates in the LC-MS/MS analysis, the influence of the isolates on the inflammatory response to the implants was analysed for CD68 content, a pan-marker for macrophages (Holness and Simmons, 1993). A moderate inflammatory response can be seen in all explants (Figure 5.4A) as is expected for an implant after 7 days. The macrophage response was segmented automatically using the Visiopharm image analysing software. There was no difference between the experimental groups and the fibrin control ($p > 0.8$) (fibrin alone: 3.3% ±2; SEC exosome: 4.9% ±2.6; UC DG SEC exosome: 4.3% ±2.5) (Figure 5.4B). Thus, the presence of complement components and IgG contained in or on exosomes did not influence the inflammatory response.

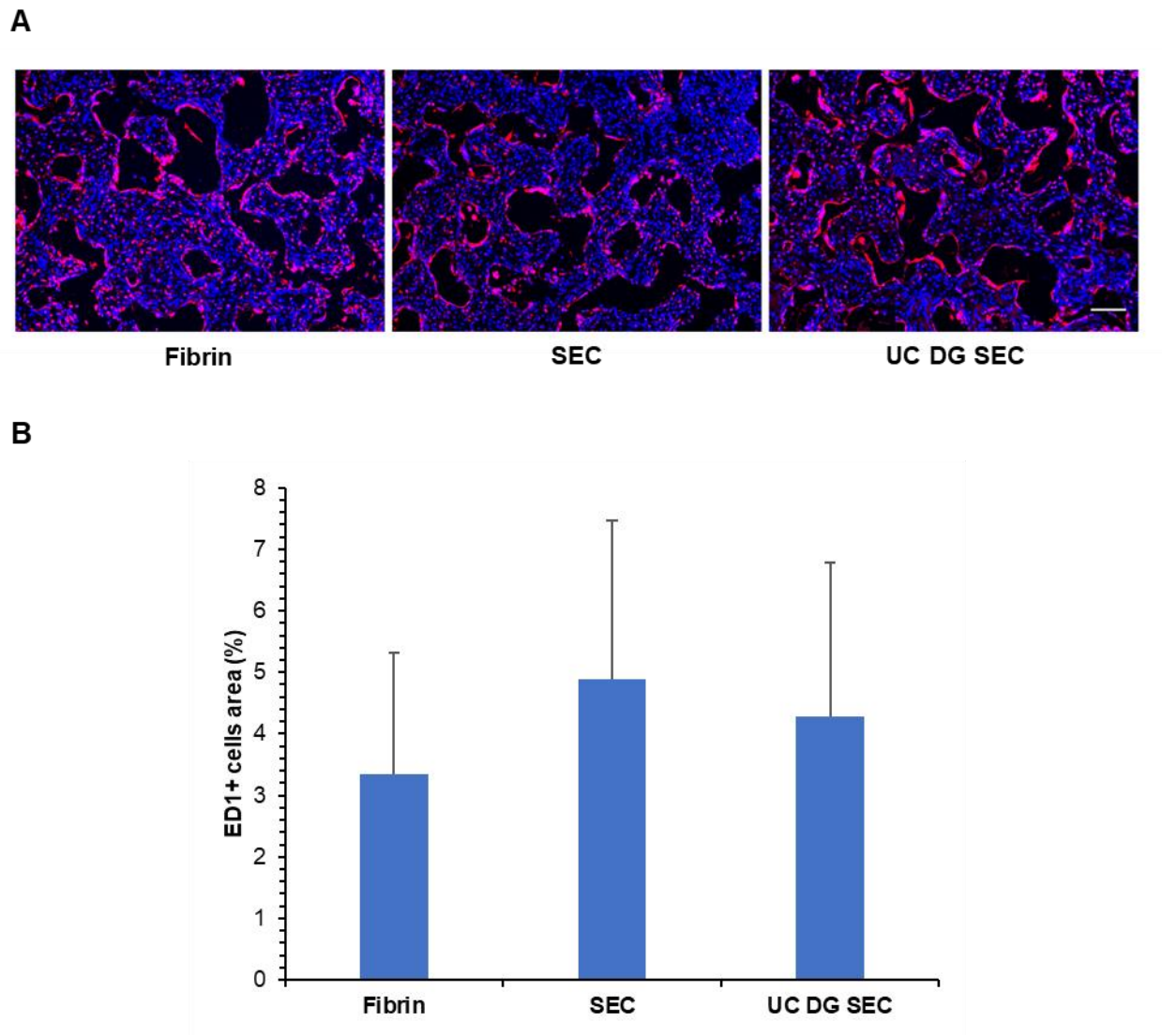

Figure 5.4: Macrophage response. (A) Stitched microscopic images of ED1 (CD68) stained fibrin hydrogel discs. Treatments (from left): Fibrin alone, SEC exosomes or UC DG SEC exosomes. Nuclei (blue), CD68 (red). Scale bar = 100 µm; (B) Area of macrophages relative to total area. n=6 per group.

5.2.2.3 Vessel area

The angiogenic response to the implants was assessed by staining for the mural cell marker smooth muscle actin (SMA) (Figure 5.5A). After automatic segmentation, the cross-sections were further examined by a blinded observer to remove any signal detection that did not correlate with vessels that had a clear vascular morphology and the vessel area as a percentage of total area calculated. Image analysis revealed a 21% increase in vessels for SEC isolates relative to fibrin

control (p=0.75) and a 60% increase for those containing UC DG SEC exosomes (p=0.07) (Figure 5.5B). Thus, there is a suggestion of an increased angiogenic response for the highly purified UC DG SEC exosome isolate. Studies have shown an angiogenic potential of exosomes (Section 1.7.4), such as myocardial ischemia patient coronary serum-derived exosomes increased blood flow recovery and neovascularisation in a hindlimb model after 21 days more than healthy serum-derived exosomes (Li *et al.*, 2018b). Human umbilical cord blood plasma-derived exosomes increased angiogenesis and re-epithelisation in mouse skin wounds compared to PBS control (Hu *et al.*, 2018). Our result is somewhat in line with others; however, the regenerative potential was only observed for the more purified exosomes.

The absence of an *in vitro* angiogenic response as determined in the spheroid model is in contradiction with the finding *in vivo* and this difference may reflect the complexity of the *in vivo* environment. It would be important to follow up these *in vivo* experiments with further investigations utilising more functionally orientated animal models such as the ischemic hindlimb model (Anitua *et al.*, 2015, Cavallari *et al.*, 2017, Zhang *et al.*, 2018) or a MI model (Khan *et al.*, 2015, Wang *et al.*, 2018d) to determine whether the UC DG SEC exosome isolates can elicit a therapeutic response. Potentially the exosome isolates could be concentrated to achieve a more pronounced effect; however, at present most concentrating methods are deficient. With centrifugal filters such as Amicon Ultra-2 10k, Amicon Ultra-2 100k, Vivaspin 2 PES 10k, Vivaspin 2 CTA 10k and Vivaspin 2 Hydrosart 10k having a considerable loss of 80% compared to a 10 kDa regenerated cellulose membrane filter (Amicon 10k RC) (Vergauwen *et al.*, 2017).

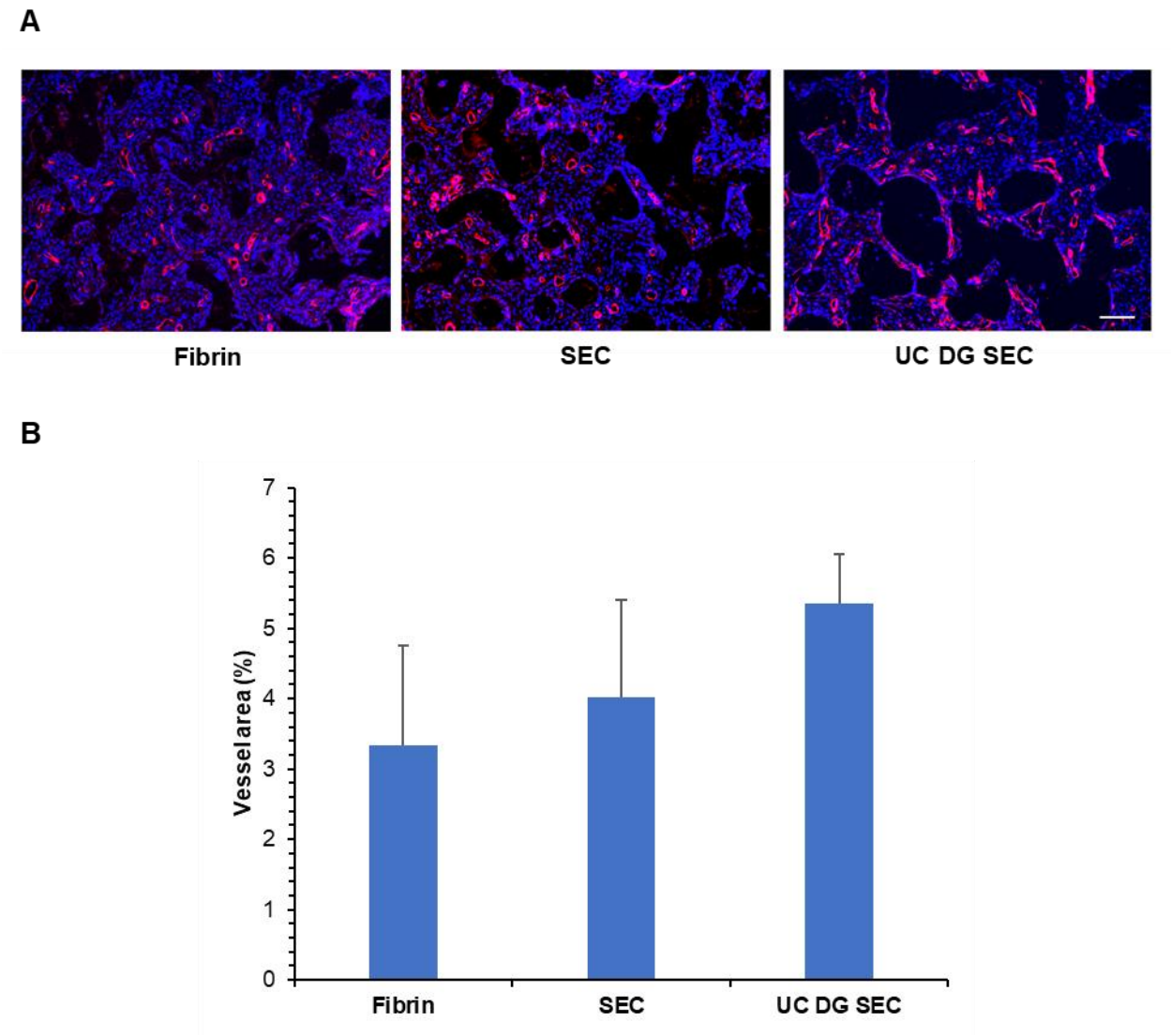

Figure 5.5: Capsule vessel density quantified in fibrin hydrogels mixed with SEC or UC DG SEC exosomes. (A) Stitched microscopic images smooth muscle cell actin stained fibrin hydrogel discs. Treatments (from left): Fibrin alone, SEC exosomes or UC DG SEC exosomes. Nuclei (blue), smooth muscle cells (red). Scale bar = 100 µm; (B) Area of vessels relative to total area. n=6 per group.

5.3 Summary

The purified UC DG SEC exosomes retained an ability to stimulate fibroblast proliferation; however, their enhancement of HUVEC spheroid sprout formation as observed for SEC isolates was not seen with the more purified exosomes. This indicated a possible loss of an exosome population or that another factor present in the less purified exosome preparation contributed to the regeneration. A low-density fraction of ApoB containing lipoproteins from the density gradient did not influence fibroblast proliferation suggesting that if it was a component in the SEC isolate responsible for sprout formation, it was not the lipoproteins. There was also an indication of pro-angiogenic potential for the UC DG SEC isolates in the rat subcutaneous assay. This is the first time functionality has been tested for highly purified serum exosomes isolated using a combined density gradient and SEC approach.

Strict EV isolation methods should be emphasised in order to standardise exosome research, particularly to avoid or substantially reduce confounding effects derived from non-exosome related particles. These results further the knowledge for serum exosome isolation methods and supports the suggested combined use of density gradient and SEC to isolate pure exosomes (Simonsen, 2017). The regenerative aspect seen by the SEC and purified UC DG SEC exosomes is relatively small but is reproducible and thus the findings above do to an extent support those of other researchers who have identified regenerative potential for blood-derived exosomes.

Based on these findings here, it seems unlikely that there is a potent regenerative capacity being transported in the blood within or on exosomes but perhaps more likely indicates gentle capacity for repairing minor injuries/damage. The UC DG SEC method is time consuming and requires a relatively large quantity of starting material to isolate a workable amount. A clear limitation in the above studies is that increased dosages of exosomes were not assessed. Such an approach would possibly allow for a more definitive understanding of their regenerative potential to emerge. This type of undertaking is still a significant challenge in this field. Others who have scaled up the amount of serum processed have found minimal improvement in yield (Karimi *et al.*, 2018, Onódi *et al.*, 2018).

CHAPTER 6: CONCLUSION

6.1 Main conclusions

A range of *in vivo* studies have indicated the presence of regenerative elements in blood (Villeda *et al.*, 2014, Wyss-Coray, 2016, Sun *et al.*, 2019). This is appealing for regenerative medicine approaches as blood is easier to obtain and process than culturing cells and allowing the blood to clot activates the platelets which release a additional pool of proteins, growth factors, cytokines and exosomes (Anitua *et al.*, 2015). Recently, a number of investigators have found that exosomes isolated from blood (plasma or serum) to have regenerative properties in myocardial injuries (Liu *et al.*, 2015, Vicencio *et al.*, 2015), hindlimb ischemia (Cavallari *et al.*, 2017, Li *et al.*, 2018b), dysferlinopathy (Dong *et al.*, 2018), hepatic fibrosis (Chen *et al.*, 2018b) and wound healing (Nakamura *et al.*, 2016).

A potential concern related to the above and other similar studies was that UC was used almost exclusively to purify the exosomes. UC has been shown to co-isolate quite high levels of contaminating proteins (Baranyai *et al.*, 2015) which we also found to be the case. It has been proposed that SEC is a more optimal isolation method to isolate exosomes from human serum (Böing *et al.*, 2014, Baranyai *et al.*, 2015). SEC here was found to isolate a protein poor fraction containing vesicles (30-100 nm detected by TEM) from human serum that was positive for the exosomal markers CD9, CD81 and TSG101. It should be noted that CD9 appeared to be a more precise marker for exosomes than TSG101.

The serum SEC-derived fraction containing exosomes was shown to cause uptake into HT1080 cells of 3 fluorescent dyes that label membrane, RNA and exosome proteins (BODIPY TR Ceramide, SYTO RNASelect and ExoGlow respectively). Importantly the fraction significantly increased both the proliferation of HdFb and promoted a significant increase in sprout number in HUVEC spheroids embedded in a fibrin hydrogel. It must be emphasised that these biological effects were obtained with an isolate that contained at least 400 times less protein than the starting serum. There are presently limited studies that have investigated the biological activity of SEC isolated exosomes. Indeed to our knowledge only one study has done so, showing that plasma EVs isolated using SEC promote migration of endothelial cells (Takov *et al.*, 2019).

The stability of the SEC-derived exosomes stored at 37°C for 3 weeks was then determined. They retained their morphology and ability to enter cells and increase cell proliferation of HdFb. Though this was the most extended period assessed and the only to assess cell proliferation, other studies have seen morphological stability such as storing urine for 24 hours at 37°C does not affect exosome size (Lv *et al.*, 2013). Another study spiked 1 ml plasma with 35 µg of LIM 1863 exosomes -20°C for 30 days and the exosomes still entered LIM 1215 colorectal cancer cells revealing functionality (Kalra *et al.*, 2013).

It must be considered likely that exosomes as a therapeutic will benefit from a controlled and localised delivery. Recently sustained delivery of exosomes from hydrogels have been investigated for therapeutic purposes in wound healing (Tao *et al.*, 2017c), MI (Chen *et al.*, 2018a), hindlimb ischemia (Zhang *et al.*, 2018) and enzyme prodrug therapy (Fuhrmann *et al.*, 2018). A fibrin hydrogel which is created naturally when blood clots and is FDA approved has not been previously considered for this purpose. The particles from the SEC exosome containing fraction were well distributed within the fibrin hydrogel and found to be released over 96 hours from a 3 mg/ml fibrin hydrogel. A novel transwell experiment was developed in which HT1080 cells invaded a 3 or 10 mg/ml fibrin hydrogel and engulfed fluorescently labelled vesicles embedded within the hydrogel. This uptake still occurred when the transwell with the 10 mg/ml fibrin hydrogel containing the SEC exosomes were stored for 7 days in an excess volume of 20% FBS MCDB media, again indicating stability and the potential for sustained release.

The field of exosomal research is a rapidly changing one due in part to its relevant novelty and the difficulties associated with working with particles in the nanometer range. It became apparent during these investigations that there was substantial lipoprotein contamination of isolated exosomes from blood in particular (Sódar *et al.*, 2016, Takov *et al.*, 2019). We also found that the SEC-derived exosomes contained 15 µg/ml ApoB lipoproteins. We also directly showed for the first time that these lipoproteins were primarily VLDL and IDL. The canonical ApoB lipoprotein LDL was shown to be able to transfer BODIPY TR Ceramide, SYTO RNASelect and ExoGlow into HT1080 cells. It is to our knowledge the first time that it has been shown for the latter two dyes that lipoproteins can interfere with exosomal uptake studies. Thus, it was important to develop an isolation method that removed lipoproteins as simply as possible, prior to re-evaluating their regenerative potential. The approach taken here was to utilise a density gradient that exploited the density differences between the ApoB containing lipoproteins and the exosomes followed by SEC to remove remaining LDL and HDL. It was found to be optimal for yield to concentrate exosomes from serum by UC prior to density gradient and SEC rather than after

density gradient and before SEC. The UC DG SEC isolates were found to more closely resemble the expected exosome shape with TEM and to contain non-detectable levels of ApoB as determined by a sandwich ELISA. NTA determined that there were 100 times lower number of particles in UC DG SEC isolates relative to SEC. This highlights the potential of lipoproteins to interfere with exosomal studies. Proteomic analysis with LC-MS/MS found a pronounced reduction of all lipoproteins (apart from ApoA1, a marker for HDL) in UC DG SEC relative to SEC and an increase in proteins identified from 135 in the SEC exosomes to 224 with a pronounced increase in exosomal proteins. We identified several novel exosomal proteins and saw a significant association with immune function for the isolates as determined by FunRich.

We assessed these highly purified exosomes for functionality. They still elicited a significant increase in HdFb proliferation but did not encourage sprout formation from HUVEC spheroids embedded in fibrin. This latter difference from SEC isolated exosomes could be explained by the detection of enriched CD9 in the UC DG SEC-derived exosomes compared to the enrichment of TSG101 in SEC-derived exosomes suggestive of different exosome populations. The proliferative effects seen for both isolates could not be seen with lipoproteins purified away from exosomes suggestive that they are not involved in this function. An *in vivo* subcutaneous analysis showed that even though there was a strong immune component in both exosome isolates, this did not influence the macrophage component of the inflammatory response. There was an indication of a stimulation of neovascularisation for the UC DG SEC exosomes.

Though we are to our knowledge the first to investigate the function of exosomes isolated in this multi-step manner, others have also recently shown a DG SEC approach to effectively remove lipoproteins (Karimi *et al.*, 2018, Onódi *et al.*, 2018). Our density gradient was technically simpler and relied on flotation to remove lipoproteins to remove lipoproteins rather than sedimentation. We also used Sepharose CL-4B which has been shown to be superior to Sepharose CL-2B for exosome purification. The one study that also carried out a proteomic analysis (Karimi *et al.*, 2018) showed a reasonable correlation with our data set with approximately 50% of our proteins identified being the same.

Limitations of our study that we have mentioned above include the lack of a dosage study. This would help clarify the above but significant concentration of exosomes is a challenge. The subcutaneous angiogenesis model does not convey any information on functionality of the vessel bed generated and an ischemic hind limb or MI model should be investigated to reveal the true regenerative potential of these highly purified serum exosomes. The proteomic analysis of the exosomes needs to be replicated with a study that includes biological repeats and the potential

involvement of different exosome populations in the different spheroid outcomes needs to be further explored.

6.2 Overall conclusion

The protein poor serum SEC-derived exosomes co-isolated with ApoB lipoproteins; however, this fraction caused HdFb proliferation and increased sprout number in HUVEC spheroids. By purifying serum exosomes without significant lipoproteins using a novel and simple UC DG SEC method, the exosomes were shown to be bioactive causing HdFb proliferation and potentially causing a regenerative effect *in vivo*.

CHAPTER 7: MATERIALS AND METHODS

7.1 Exosome isolation from human serum

Two units of ± 250 ml of human serum (AB blood group) were obtained from Western Province Blood Transfusion Service (WPBTS). Serum was prepared by WPBTS in the following manner. The blood was collected and allowed to clot overnight at 4°C. The following morning the blood was centrifuged at 4000 rpm for 12 minutes at 4°C. A manual plasma extractor separated the serum. Both serum units were combined, aliquoted and stored at -80°C. Exosome isolations using SEC, DG SEC or UC DG SEC were performed on three batches of pooled human sera.

To obtain fresh fasted serum, peripheral blood was collected from healthy donors (30 and 52 years old, no chronic medications) after overnight-fasting. The blood (50 ml) was collected into falcon tubes and allowed to clot for 30 minutes at RT. Serum was isolated by centrifugation at 2500 g for 10 minutes at RT. The supernatant was carefully removed avoiding disruption of the pelleted blood cells.

7.1.1 Ultracentrifugation

Isolation of exosomes by UC was performed as described previously (Eitan *et al.*, 2015) with minor modifications.

Human serum was thawed at RT in the hood. Human serum (6.5 ml) was diluted with 0.2 µm filtered sterile PBS (NaCl [137 mM], KCl [2.7 mM], KH_2PO_4 [1.4 mM], $Na_2HPO_4.12H_2O$ [8 mM], pH 7.4 (19.5 ml)) and centrifuged at 2000 g for 10 minutes, 4°C. The supernatant was transferred to Beckman UC tubes and centrifuged at 10 000 g for 40 minutes, 4°C (SW 60 Ti Rotor). The resulting supernatant was transferred to a new Beckman UC tube (6 x 3.6 ml) and centrifuged at 120 000 g (34 000 rpm) for 2 hours. Each pellet in the UC tube was resuspended in 250 µl sterile filtered PBS. The resuspended pellets were pooled together, aliquoted into 50 µl and stored at -80°C.

7.1.2 ExoQuick-TC

ExoQuick-TC™ was used to isolate the exosomes from human serum. ExoQuick-TC precipitation was performed according to the manufacturer's instructions. Human serum was centrifuged at

3000 g for 15 minutes, thereafter 500 µl human pooled serum was mixed with 120 µl ExoQuick-TC and incubated for 30 minutes at 4°C. The exosomes were precipitated by centrifuging the sample at 1500 g for 30 minutes, supernatant aspirated followed by a further 5 minutes at 1500 g. The pellet was resuspended in 200 µl PBS.

7.1.3 Size exclusion chromatography

SEC was used to isolate exosomes from human serum. Sepharose CL-4B (10 ml bed volume, 12.7 cm bed volume height and 1 cm column width) was washed with PBS (pH 7.4, 0.22 µm filtered) and the solution was settled for about 30 minutes. The column was washed with 3 column volumes of PBS (10 ml).

Serum was thawed and centrifuged at 6000 g for 10 mins to remove cellular debris and chylomicrons. A yellow and blue tip were used to carefully remove the top layer of chylomicrons, after which the serum was collected from below the top layer of serum. Human serum (1 ml) was loaded on the column, followed by elution with PBS under gravity with maximally a 5 cm head (pH 7.4, 0.22 µm filtered). Fresh fasted serum was also tested. The eluate was collected in 26 sequential fractions of 0.5 ml. For each fraction, A_{280} was read using a NanoDrop microvolume spectrophotometer (protein concentration further determined using the Bradford assay in some instances). The fraction with the maximum A280 in the first eluted peak was aliquoted (50 µl) and stored at -80°C for subsequent studies.

The SEC column was washed with PBS until $A_{280} \sim 0$ and subsequently washed and stored with 0.02% sodium azide at 4°C. When required the Sepharose was cleaned and stripped with 2 column volumes of 0.5 N NaCl in 0.1 N NaOH and washed with 5 column volumes of PBS.

7.1.4 ExoQuick-TC followed by size exclusion chromatography

ExoQuick-TC was used to isolate the exosomes from human serum. ExoQuick-TC precipitation was performed according to the manufacturer's instructions. Human serum was centrifuged at 3000 g for 15 minutes, thereafter 500 µl human pooled serum was mixed with 120 µl ExoQuick-TC and incubated for 30 minutes at 4°C. The exosomes were precipitated by centrifuging the sample twice at 1500 g for 30 minutes and 5 minutes. The pellet was resuspended in 500 µl PBS. The resuspended exosome pellet was loaded on the size exclusion column and the protocol was followed as described for the SEC purification from human serum (Section 7.1.3).

7.2 Protein concentration

The Bradford assay can detect 0.1-1.4 mg/ml of BSA on a linear scale. A standard curve using the Bradford protein assay kit is shown in Figure 7.1. Briefly, 5 µl of sample was added to 95 µl PBS. Bradford reagent (900 µl) was mixed with the sample and incubated for 5 minutes before reading absorbance at 595 nm.

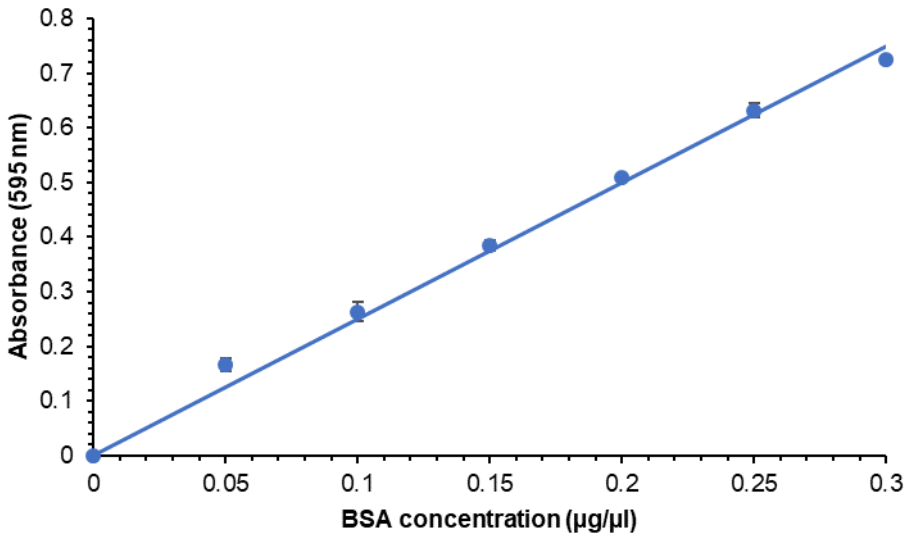

Figure 7.1: Standard curve for the Bradford assay. Bovine serum albumin standards ranging from 0.05 to 0.3 µg/µl were added to the Bradford dye and the resulting absorbance values measured at 595 nm after incubation at RT for 5 min. The equation of the trendline is given by y = 2.5009x with a correlation coefficient of 0.9932. n=4 (technical repeats).

7.3 Gel electrophoresis and western blot analysis

Samples were lysed with 3X reducing sample buffer (62.5 mM Tris-HCl, pH 6.8, 4% SDS, 10% Glycerol, 0.03% Bromophenol Blue and 5% β-mercaptoethanol) and boiled for 5 minutes at 95°C. Equal volumes or concentration of proteins from samples were loaded and resolved by 12% FastCast SDS-PAGE or 4-15% gradient gel. Gels were stained with 1% Coomassie Brilliant Blue R-250 Dye (1 g of dye dissolved in 100 ml dH_2O and stirred for 1 hour at RT and subsequently filtered through Whatman No.1 filter paper) to visualise the proteins.

Western blot analysis of the samples were carried out as described previously (Towbin *et al.*, 1979) with modifications. Exosome samples were approximately 5X concentrated using Amicon ultra 0.5 ml 100 kDa centrifugal filters. A Hela cell lysate control was always used to demonstrate that the western blot was working (data not shown). Samples were lysed with 3X reducing sample buffer (62.5 mM Tris-HCl, pH 6.8, 4% SDS, 10% Glycerol, 0.03% Bromophenol Blue and 5% β-mercaptoethanol) and boiled for 5 minutes at 95°C. The proteins were resolved by 12% FastCast SDS-PAGE and transferred over 45 minutes using a Trans-Blot® SD Semi-Dry Transfer Cell at 10 V onto a nitrocellulose sheet.

The transfers were blocked for 1 hour at RT with 5% (w/v) fat free milk powder in tris buffered saline-tween (TBS-T: 20 mM Tris, 200 mM NaCl, pH 7.4, 0.05% Tween-20). The nitrocellulose membrane was incubated with primary antibody diluted in TBS-T overnight at 4°C. Blot was washed with TBS-T (5 x 8 minutes), followed by incubation with secondary horseradish peroxidase (HRP) conjugated antibody (1 hour, shaking, RT) and washed again with TBS-T (5 x 8 minutes). Protein bands were detected using WesternBright ECL HRP substrate. The following antibody dilutions were used: 1:1000 rabbit anti-human TSG101, 1:500 rabbit anti-human CD9, 1:1000 rabbit anti-human TAPA1 (CD81), 1:20 000 rabbit anti-human ApoA1 and 1:10 000 goat anti-rabbit HRP.

7.4 Transmission electron microscopy

Briefly, 200 mesh carbon coated copper TEM grids were glow discharged and placed on 15 µl droplets of sample and incubated for 10 minutes or 3 µl of sample was directly applied to the grid. Distilled water was used to rinse the grids which were then carefully dabbed on Whatman paper. The grids were incubated on uranyl acetate (2%) to stain the sample. Grids were viewed using a Tecnai G2 TEM. Size analysis of the particles were calculated using ImageJ (1.46r, Wayne Rasband, National Institutes of Health, USA). The number of vesicles counted for size analysis across five TEM grids for the various methods were as follows: SEC fraction 8 (n=399), SEC fraction 9 (n=442), SEC fraction 10 (n=396), SEC exosome 37°C (n=314), SEC exosome -80°C (n=300), LDL (n=92), DG SEC fraction 9 (n=12, sample required 5X dilution) and UC DG SEC fraction 9 (n=23).

7.5 Cell culture conditions

The cells used for *in vitro* experiments were HUVECs, isolated from waste tissue after obstetric procedures and were cultured up to passage 5. HdFbs and fibrosarcoma cell line HT1080 cells were obtained from laboratory stocks. All cell culturing was performed under sterile conditions with the laminar flow hood sterilised by use of UV light exposure for 15 minutes and 70% ethanol. All other items used were sterilised with 70% ethanol. Cells cultured in a humidified incubator at 37°C with 5% CO_2.

Endothelial culture media consisted of MCDB-131, 1.18 g/L $NaHCO_3$, 2 mM L-Glutamine, 1 µg/ml Hydrocortisone, 10 ng/ml EGF and 5 ng/ml bFGF. HT1080 and HdFb culture media consisted of MCDB-131 and 1.18 g/L $NaHCO_3$. Both culture media contained 1% penicillin/streptomycin and 10% FBS.

7.5.1 HUVEC isolation

Ethical approval was attained from the University of Cape Town (Cape Town, South Africa) Human Ethics Committee, in accordance with the Declaration of Helsinki (HREC REF: 407/2017).

The isolation protocol was adapted from (Baudin *et al.*, 2007). Briefly, umbilical cords were collected in Medium 199 (M199) containing 0.2% gentamicin. The umbilical vein was cannulated and the cannula was secured with a suture. The vein was rinsed with a solution of M199 containing 0.2% heparin and 1% gentamicin. The cord was clamped and distended with a solution of M199 containing 0.07% collagenase. The cord was placed in sterile PBS at 37°C and maintained at 37°C for 12 minutes in the incubator. The vein was rinsed with the stop solution (M199 with 20% FBS) into a sterile 50 ml centrifuge tube. The tube was centrifuged (244 g, 5 minutes), supernatant removed, and the cell pellet was resuspended in enriched culture medium and plated into collagen-coated wells. After 24 hours in the incubator at 37°C with 5% CO_2, the cells were rinsed with PBS to remove debris and fresh HUVEC growth medium added. Anti-CD31 flow cytometry confirmed the cells as endothelial cells (Figure A7, Appendix 7).

7.5.2 Fibroblast isolation

HdFbs were isolated by explant culture release. The isolation protocols have been described in depth (Takashima, 1998). Briefly, 3 mm skin biopsies were cultured in a minimal amount of 10% FBS MCDB media until a considerable number of fibroblasts had migrated out of the biopsy. A swirling growth pattern was used to identity the fibroblasts.

7.5.3 Cell passaging

Once cells were about 70-90% confluent they were passaged. The flasks were washed 2X with PBS: 2.5 ml for a 25 cm^2 (T25) flask or 5 ml for a 75 cm^2 (T75) flask. Followed by the addition of 0.25% trypsin-EDTA (volumes as above) for roughly 2-3 minutes in the 37°C, 5% CO_2 incubator. Once the cells had detached, the trypsin was inactivated with an equal volume of 20% FBS MCDB media. The entire solution was pipetted into a 50 ml tube and centrifuged at 400 g for 5 minutes (HUVEC) or 1500 rpm for 3 minutes (HT1080 or HdFb). The cell pellet was resuspended into the required growth medium.

The cells were counted using a haemocytometer. In brief, 20 µl of the cell suspension was mixed with 20 µl of Trypan Blue (0.4% (m/v)). The haemocytometer grid and coverslip were cleaned with 70% ethanol prior to adding 10 µl of the cell suspension under the coverslip. The four corners of the grids were counted, averaged and the number of cells/ml was determined using the following equation:

Average number of cells counted x 2 x 10 000 = *Number of cells per milliliter*

The number of cells required for a particular experiment were then seeded. The remainder of the cell suspension was either divided into a new flask with fresh media or frozen as described below.

7.5.4 Thawing of cells

Cells were removed from the liquid nitrogen tank and thawed in a 37°C water bath. The contents were added to a T25 or T75 flask containing 5 ml or 10 ml 20% FBS media respectively. The flask was placed inside the incubator and after 24 hours to media was changed to 10% media.

7.5.5 Freezing of cells

Stocks of HT1080, HdFbs and HUVECs were cryopreserved. Cells were counted and frozen with roughly 500 000 cells per 600 µl in a 1.5 ml or 2.0 ml cryovial. The cells were diluted with an equal volume of 15% DMSO, to give a final concentration of 7.5% DMSO. Cells were frozen overnight in a polystyrene rack at -65°C and transferred to liquid nitrogen for long term storage. As endothelial cells are sensitive, they were frozen overnight in a Mr. Frosty cell freezing container, which was filled with isopropyl alcohol at RT before being transferred to the -65°C freezer.

7.5.6 Proliferation assay

Cell proliferation was assessed with the XTT cell viability kit according to the manufacturer's protocol. Briefly, 100 µl HdFb cell suspension (passage 4-11) were seeded into 96-well plates at 5000 cells/well. After 12 hours the HdFbs were treated with SEC exosomes (10% (v/v) or 2.3% (v/v)), UC DG SEC exosomes (10% (v/v)), UC exosomes (3.33% (v/v)), ApoB lipoproteins (1.5 ApoB µg/ml (determined by ELISA see section 7.11)), human serum (5% (v/v)) and PBS (10% (v/v)). After 72 hours the media was removed, each well was washed twice with 100 µl MCDB or DMEM media. 100 µl of media was added to each well and 4 wells as background control. After 2 hour incubation with XTT the absorbance was measured at 450 nm, with background correction at 570 nm, using iMark microplate reader. Experiment was independently repeated 4 times and each treatment was carried out with 4 technical repeats.

7.5.7 Uptake of human serum-derived exosomes

Human serum-derived exosomes were fluorescently labelled with either SYTO™ RNASelect™ for RNA staining or BODIPY™ TR Ceramide for membrane staining. One µl of the dye stock solution (1 mM) was mixed with 100 µl exosome sample or 100 µl PBS (control) and incubated at 37°C for 20 minutes in the dark. The excess unincorporated dye from the labelled exosomes were removed using exosome spin columns (MW 3000) according to the manufacturer's protocol.

Human serum SEC-derived exosomes were also labelled with ExoGlow™-protein label. Ten µl of the dye stock solution (10X) was mixed with 100 µl exosome sample or 100 µl PBS (control) and incubated at 37°C for 10 minutes in the dark. ExoQuick-TC (20 µl) was used to stop the reaction at 4°C for 30 minutes. Sample was centrifuged for 3 minutes at 14 000 rpm to pellet the labelled exosomes and resuspended in 100 µl PBS.

A dosage study was performed where cells were treated with 6.25%, 12.5% or 25% (v/v) of SEC-derived exosomes. The stability of exosomes was tested with SEC exosomes stored at -80°C, SEC exosomes stored at 37°C for 3 weeks with gentle agitation (50 rpm), UC exosomes stored at -80°C or UC exosomes stored at 37°C for 3 weeks with gentle agitation. Other samples tested for uptake included LDL (see section 7.7).

CultureWell 16 chambered cover glasses were used for uptake studies. The cover glass was coated with collagen solution from bovine skin (100 µg/ml) diluted in PBS for 2 hours at 37°C. The cover glass was seeded with 15 000 HT1080 cells/well and left overnight. The following morning the labelled exosomes or LDL (12.5% (v/v)) were incubated with the cells for 3 hours at 37°C.

After incubation, the cells were washed with PBS and fixed with 10% formalin for 20 minutes at RT. The cells were washed with PBS (3 x 5 minutes) and permeabilised with 0.1% Triton-X 100 in PBS for 3 minutes. Samples were washed with PBS (2 x 5 minutes) and the cytoskeleton was stained with either Alexa Fluor® 594 Phalloidin stain (1:10 000), ActinRed™ ReadyProbes® Reagent (1 drop per 5 ml PBS which was subsequently diluted 100X) or Alexa Fluor® 488 Phalloidin stain (1:750). Chambered wells were mounted using fluoroshield with DAPI. Cellular uptake was analysed under the fluorescent microscope (Nikon Eclipse 90i DS-Ri1).

7.5.8 Generation of endothelial cell spheroids

HUVEC spheroids were generated as described previously (Korff and Augustin, 1998). In brief, 750 HUVECs (P2-P5) in 150 µl 20% methylcellulose culture media were seeded in non-tissue cultured treated, round bottom 96-well plates. After 24 hours the suspended cells formed a single spheroid in each well.

7.5.8.1 Siliconising 24-well plates

The 24-well plates were siliconised using Sigmacote® to allow the hydrogels to form droplets for use in the spheroid assay. Briefly, Sigmacote® was added to cover each well and left for 30 seconds before being removed and allowed to dry overnight in the laminar flow hood. The wells were rinsed 2X with sterile Nanopure water and allowed to dry. The plates were then sterilised using ethylene oxide.

7.5.8.2 Methylcellulose preparation

For preparation of methylcellulose stock solution, 3.6 g methyl cellulose was autoclaved in a 500 ml Schott bottle with a clean magnetic stirrer bar. The autoclaved methylcellulose was dissolved and mixed on a stirrer for 20 minutes with preheated (60°C) culture medium (150 ml) at RT. Further 150 ml culture medium (RT) was added and mixed on a stirrer overnight at 4°C. The methylcellulose solution was aliquoted and centrifuged at 5000 g for 2 hours at RT and at 3500 g for 40 mins at RT. The cleared supernatant was collected and used for spheroids.

7.5.8.3 Spheroid assay

Roughly 3-6 HUVEC spheroids were embedded into each fibrin hydrogel. The fibrin hydrogels consisted of human fibrinogen (3.25 mg/ml), aprotinin (100 µg/ml) and thrombin (0.625 u/ml). The spheroids, fibrinogen and aprotinin were pipetted into a 48-well Sigmacote treated plate (20 µl containing 3-6 spheroids each). Sigmacote treatment (Section 7.5.8.1) through increasing

hydrophobicity caused the fibrin hydrogel to bead resulting in greater depth within the droplet. Thereafter 20 µl thrombin working solution was added to the spheroid fibrinogen mix. The gels were polymerised at 37°C for 30 minutes. The culture media (150 µl 2% FBS MCDB media) containing either PBS or treatment was pipetted on top of each gel. The gels were incubated in a humidified incubator at 37°C with 5% CO_2. Spheroids were imaged at 24 and 48 hours (X10 objective) with a Nikon Light microscope (Nikon Eclipse Ti-S). Sprout number was assessed with ImageJ 1.46r and 8-12 spheroids per treatment group were analysed. Briefly, a straight line was used to measure all individual sprouts. After all the spheroids' sprouts per treatment were measured, the average sprout number was calculated. Spheroids that were in proximity, touching or near the side of the hydrogel were excluded. Experiment was independently repeated 3 times.

7.6 Exosomes in a fibrin hydrogel

SEC-derived exosomes labelled with BODIPY TR Ceramide (Section 7.5.7) (13.5 µl) were entrapped within a fibrin hydrogel (3 mg/ml), 45 µl gel crosslinked with thrombin (Section 2.2.6.1.1). The distribution of the exosomes was visualised using a confocal microscope (ZEISS LSM510).

7.6.1 Cumulative release of exosomes from a fibrin hydrogel

A dilution curve was obtained for BODIPY TR Ceramide labelled SEC exosomes (Section 2.2.6.1.2). Exosomes (from the same batch as those entrapped in fibrin) were labelled with BODIPY TR Ceramide (Section 7.5.7). The exosomes were serially diluted to prepare dilutions of 1:5, 1:25, 1:50, 1:125 in a final volume of 100 µl. The dilutions were stored in a white plate for 24 hours at 37°C and subsequently the fluorometer signal of the dilutions were read using a Fluorescent spectrophotometer (excitation 594 nm and emission 617 nm). They were stored in a white plate for 24 hours at 37°C as the fluorometer signal was found to increase over the 24 hours prior to stabilising (Figure A3, Appendix 3). Four technical repeats.

To obtain a cumulative exosome release curve 63.6% BODIPY TR Ceramide labelled exosomes were entrapped in a 50 µl 3 mg/ml fibrin hydrogel and incubated with 100 µl of PBS at 37°C with gentle shaking (50 rpm). After 24 hours PBS was removed and stored in a white plate for 24 hours at 37°C and subsequently the fluorometer signal was read. A baseline fluorometer signal was accounted for by collecting supernatant from a fibrin hydrogel with no exosomes. Supernatant was replaced with PBS every 24 hours over 96 hours. Four technical repeats were performed.

7.6.2 Transwell experiment: Cellular uptake of exosomes embedded in a fibrin hydrogel

63.6% of SYTO RNASelect labelled SEC exosomes in a 50 µl 3 mg/ml fibrin hydrogel were gelled inside the 8 µm pore upper inserts of a 6.5 mm transwell insert for 30 minutes at 37°C followed by the seeding of 20 000 HT1080 cells in 100 µl (resuspended in serum-free media) on top of the fibrin hydrogel. The inserts were placed inside 24-well plates containing 600 µl MCDB media (10% FBS, 2% penicillin/streptomycin, 10 ng/ml bFGF) to promote migration of cells through the hydrogel to the bottom of the transwell insert. After 5.5 or 24 hours, the transwells were processed for fluorescent imaging. The inserts were washed with PBS and fixed with 10% formalin for 20 minutes at RT. Cells that remained on the top surface and the fibrin hydrogel inside the insert were removed with cotton swabs. The insert was washed with PBS (3 x 5 minutes) and permeabilised with 0.1% Triton-X 100 in PBS for 3 minutes. They were then washed with PBS (2 x 5 minutes) and the cytoskeleton of the cells were stained with ActinRed™ ReadyProbes® Reagent (1 drop per 5 ml PBS which was subsequently diluted 100X) for 20 minutes at RT and washed with PBS (2 x 5 minutes). The transwell inserts were cut out with a fine scalpel and mounted on a glass slide using fluoroshield with DAPI. Fluorescent micrographs were captured. Three independent experiments with two technical repeats.

To assay the biostability of the exosomes in the fibrin hydrogel, 63.6% (v/v) of SYTO RNASelect labelled exosomes in a 50 µl 3 mg/ml fibrin hydrogel were incubated for 1, 3 or 7 days in 20% FBS MCDB media and a 10 mg/ml fibrin hydrogel containing SEC exosomes were incubated for 7 days in 20% FBS MCDB media. Followed by the seeding of 20 000 HT1080 cells (resuspended in 100 µl serum-free media) on top of the fibrin hydrogel, they were processed as described directly above. Two technical repeats.

7.6.3 Controls to ensure the transwell experiment was not an artefact of released fluorescent dye

SYTO RNASelect labelled SEC-derived exosomes (80 µl) in MCDB media (560 µl) (12.5% exosomes (v/v)) were sonicated (Virsonic 100 probe) with six cycles of 25 Hz at 25 second intervals on ice.

After sonication of the SEC-derived exosomes they were visualised by TEM (Section 7.4) to determine extent of disruption. The uptake of sonicated exosomes was then assayed as described in section 7.5.7.

7.6.4 Physical properties of exosomes embedded in a fibrin hydrogel

SEC exosomes (31.8 µl) were entrapped within a 50 µl fibrin hydrogel (10 mg/ml). The hydrogel was digested with 100 µl proteinase K (500 µg/ml) for 90 minutes at 37°C and overnight at 4°C. Proteinase K was added to exosomes not entrapped in a hydrogel to test if the enzyme had an adverse effect on the exosomes. Fibrin hydrogel without exosomes was also digested to visualise the background of digested hydrogel. Fibrin gel (10 mg/ml) containing SEC exosomes incubated for 1 day at 37°C prior to being digested with proteinase K were also examined. After the digestion of the fibrin hydrogel, the morphology of the exosomes was visualised on a TEM.

7.7 LDL

LDL were supplied by Dr Dee Blackhurst from the Division of Chemical Pathology, University of Cape Town. In brief, the LDL from human plasma were isolated by KBr gradient (0.5 g/ml) centrifuged at 100 000 g for 17 hours, after which the LDL was removed and dialysed to remove the KBr. TEM was used to visualise the structure LDL stored at 4°C. TEM protocol described in section 7.4. The LDL 12.5% (v/v) were tested for uptake into HT1080 cells using the fluorescent dyes (SYTO RNASelect, BODIPY TR Ceramide and ExoGlow-protein label) used for exosome uptake studies. LDL (2.61 µg/µl) were diluted to the same protein concentration as the SEC exosomes (0.24 µg/µl). Uptake protocol described in section 7.5.7.

7.8 Platelet exosome isolation

7.8.1 Platelet exosome isolation with calcium activation

Method modified from (Goetzl *et al.*, 2016, Tan *et al.*, 2016). Blood (25 ml) was collected from fasted healthy donors into a 2 x 50 ml falcon tubes containing 5 mL acid citrate dextrose each. The first 3 ml was discarded. Aliquots of blood (10 ml) were made in 15 ml falcon tubes and centrifuged at 200 g at RT for 12 minutes without brake. PRP was carefully removed with a plastic Pasteur pipette and centrifuged at 900 g at RT for 12 minutes without brake. The platelet pellet was carefully resuspended in 2-4 ml of Tyrode's buffer (137 mM NaCl, 0.3 mM NaH_2PO_4, 3.5 mM Hepes, pH 7.35) and adjusted to 250×10^6 platelets/ml. Platelets were then activated with $CaCl_2$ (1 mM), 30 minutes at 37°C. Platelets and cell debris were removed by centrifugation 4000 g at

RT for 10 minutes. The supernatant was mixed with ExoQuick-TC solution according to their protocol. The exosomes were precipitated at 4°C overnight and centrifuged at 1500 g for 30 minutes at 4°C. The pellet was resuspended in 250 µl PBS.

7.8.2 Scanning electron microscopy of platelets

A sample of platelets (100 µl) were fixed in 2% glutaraldehyde for 30 minutes, and subsequently centrifuged at 300 g (RT, 20 minutes). The platelet pellet was washed in distilled water and centrifuged at 200 g (RT, 10 minutes). Platelet suspension (100 µl) was added on top of a 3-aminopropyltriethoxysilane (APES) coated cover slip and stored at 4°C. The platelets were dehydrated in an ethanol series for 5 minutes each (dH_2O, PBS, 25%, 50%, 60%, 70%, 90%, 100%) and dried by the critical point method (CO_2). The platelet coverslips were mounted on copper stubs and coated with 20 nm gold in a sputter coater. SEM micrographs were taken with a Nova NanoSEM 230.

7.9 Separating lipoproteins from exosomes

7.9.1 Determining the best density gradient conditions to separate lipoproteins from exosomes

Human serum was centrifuged at 13 000 g for 10 minutes to remove chylomicrons and microvesicles (Coumans *et al.*, 2017) (Section 7.1.3). Human serum was then fractionated using an OptiPrep™ density gradient. Briefly, a discontinuous iodixanol gradient was prepared by diluting a stock solution of OptiPrep (60% (w/v)) with 0.25 M sucrose/10 mM Tris, pH 7.5 to generate 40% and 18% (w/v) iodixanol solutions and their densities were assessed. Density was determined by measuring the mass of 1 ml of each iodixanol solution. The 18% iodixanol solution was formed by dilution of stock solution with human serum. With care, the discontinuous iodixanol gradient was generated by underlayering in Beckman centrifuge tubes polyallomer tubes. A 5 ml syringe was used with a long bone marrow needle (bevel removed). The gradient tested consisted of 3 ml 18% iodixanol solution in serum and 0.5 ml 40% iodixanol solution. The gradient was centrifuged using a SW 60 Ti rotor for 3 hours at 200 000 g_{avg} at 4°C. Fractions (7 x 0.5 ml) were collected from the top of the gradient. The density gradient fractions 1-6 were diluted with 3 ml PBS and concentrated at 100 000 g for 1 hour in a SW 60 Ti. The pellet was resuspended in 50 µl PBS.

Gradients as above were also formed with 2 ml 4% or 6% iodixanol solution, 1 ml 18% iodixanol solution in serum and 0.5 ml 40% iodixanol solution (See Figure 4.2). The gradient was centrifuged using a SW 60 Ti rotor for 20 hours at 265 000 g_{avg} at 4°C with no brake. Fractions were collected from the top of the gradient (7 x 0.5 ml).

7.9.2 Density gradient and size exclusion chromatography (DG SEC)

In brief, 0.5 ml 60% and 6 ml 18% in serum were layered underneath 6.5 ml 6% iodixanol OptiPrep in UC tubes. The gradient was centrifuged using a SW 40 Ti rotor for 24 hours at 195 000 g_{avg} at 4°C. Seven fractions were collected from the top of the gradient (2 ml each, except fraction 6 was 1 ml). Fraction 6-7 from 4 tubes were diluted in PBS and concentrated by centrifuging at 100 000 g_{avg} for 3 hours at 4°C with a Type 40 Ti rotor. The resulting pellets were resuspended in a final volume of 1 ml which was separated on the SEC column as described previously (Section 7.1.3).

7.9.3 Ultracentrifugation, density gradient and size exclusion chromatography (UC DG SEC)

UC was used to preconcentrate the exosomes before the density gradient step. Human serum (31 ml) diluted in PBS (31 ml) was centrifuged for 40 minutes at 10 000 g_{avg} at 4°C and the resulting supernatant was centrifuged for 2 hours at 120 000 g_{avg} at 4°C to pellet the exosomes. The resulting pellets were resuspended in final volume of 2 ml of 18% iodixanol which was further purified using an OptiPrep density gradient. In brief, 0.25 ml 60% and 1 ml 18% iodixanol UC pellet (from 15.5 ml serum) was layered underneath 2.6 ml 6% iodixanol OptiPrep in UC tubes. The gradient was centrifuged using a SW 60 Ti rotor for 24 hours at 195 000 g_{avg} at 4°C. Four fractions were collected from the top of the gradient (fraction 1&2 (1 ml), fraction 3 (0.5 ml), fraction 4 (1.1 ml)). Fraction 4 was separated on the SEC column as described previously (Section 7.1.3).

7.10 Determining the functional activity of ApoB lipoproteins at the same concentration of ApoB present in SEC exosomes

ApoB lipoproteins were obtained from density gradient fraction 1 described in section 7.9.2. The concentration of ApoB was determined using an ApoB ELISA (Section 7.11). The ApoB lipoproteins were diluted to 15 µg ApoB/ml, the same ApoB concentration as in SEC-derived exosome fraction 9. The effect of 10% (v/v) ApoB lipoproteins (1.5 µg/ml) on HdFb cell proliferation was assessed using the XTT assay described in section 7.5.6.

7.11 ApoB ELISA

Samples were diluted as follows: DG Fr 1-7 (1:250), UC DG Fr 1 (1:50), UC DG Fr 2-4 (1:25), DG UC pellet (1:50), UC pellet (1:50), SEC Fr 7-10 (1:25), SEC Fr 11-14 (1:100), DG SEC Fr 7-14 (none), UC DG SEC Fr 7-14 (none). Samples (50 µl) were added to a precoated 96-well ApoB immunoplate containing 200 µl assay diluent and incubated for 2 hours at RT on a horizontal orbital shaker. Thereafter the plate was washed three times with PBS and incubated with 200 µl conjugate for 2 hours at RT on a horizontal orbital shaker. The plate was washed three times with PBS and incubated with substrate solution according to the manufacture's instructions and absorbance was measured at 450 nm, with background correction at 570 nm, using an iMark microplate reader. Human ApoB standard solutions were made (39.1-2500 ng/ml) to obtain a 4 parameter logistic curve as the standard curve (Figure 7.2). The ApoB concentrations in SEC, DG SEC and UC DG SEC fractions were calculated using the curve.

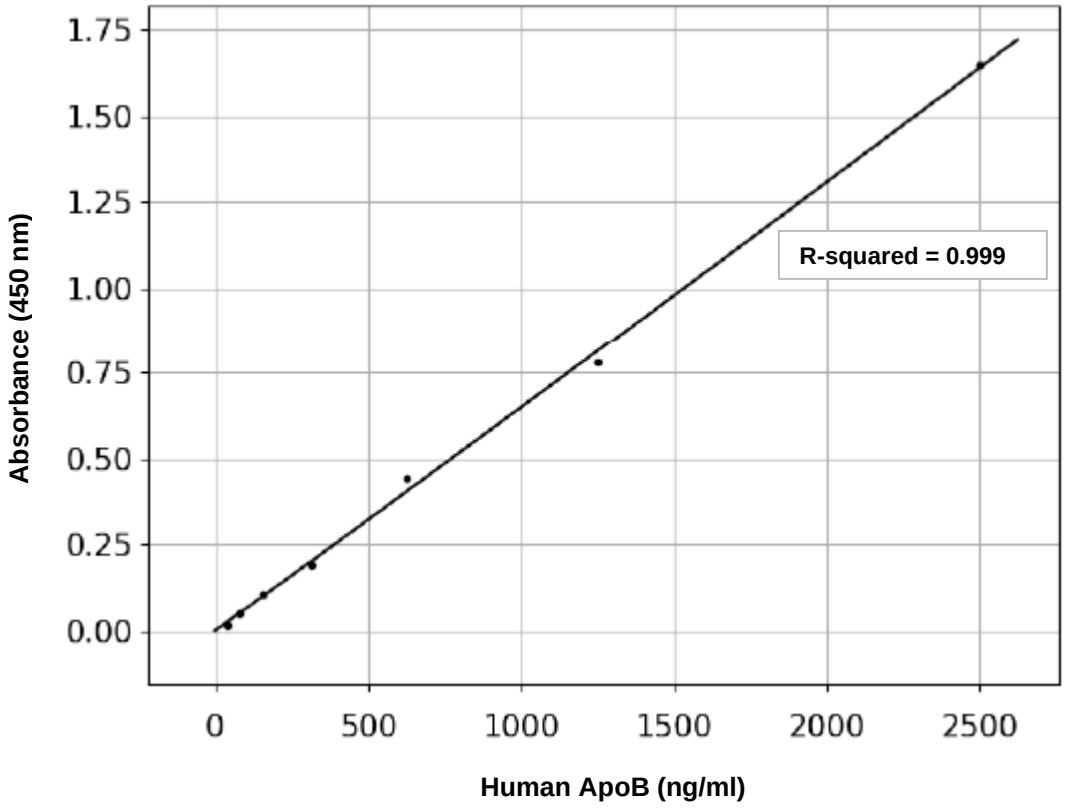

Figure 7.2: Standard curve (4 parameter logistic curve) generated from serial dilution of ApoB (39.1-2500 ng/ml) for calculating ApoB concentrations.

7.12 Quantification of HDL and LDL subclass distribution

The Lipoprint® System (Hoefner *et al.*, 2001) was used from the Hatter Institute for Cardiovascular Research in Africa, University of Cape Town, to assess the HDL and LDL subclass distribution. Serum, SEC fraction 8 and 9 and platelet exosomes from calcium activation of the platelets (25 µl) were mixed with Lipoprint loading gel (300 µl). The Sudan black dye present attaches proportionally to any cholesterol in the sample. The mixed sample was applied to the top of a high resolution 3% polyacrylamide gel. Photopolymerisation of the gels was performed for 30 minutes at RT and electrophoresis for 50 minutes at 3 mA per gel tube. The gel tubes were scanned after 30 minutes and analysed using the Lipoware software. A Lipoprint® HDL and LDL System were performed.

7.13 Nanoparticle tracking analysis

The particle concentration in the SEC, DG SEC and UC DG SEC fractions were analysed with NTA, using the NanoSight LM10. Aliquots from the isolation fractions were diluted 10 to 50-fold in PBS to obtain a suitable particle number per frame. Particle concentration was determined by analysing three x 1-minute videos. All samples were measured using the same instrument settings, camera level was set to 16 and threshold set to 7. In between each reading the frame was completely flushed of the previous sample.

7.14 Mass spectrometry

7.14.1 Exosome lysis, buffer exchange and tryptic digestion

Human serum exosome fraction 9 isolated using either SEC or UC DG SEC (500 µl) were lysed with 167 µl 3X RIPA buffer and vortexed for 1 minute. They were then processed using the filter-aided sample preparation protocol (Wisniewski *et al.*, 2009). The lysed exosome sample was incubated with 0.1 M dithiothreitol at 95°C for 3 minutes to reduce cysteine bonds. The reduced sample solution was transferred to a 30 kDa centrifugal filter unit and centrifuged for 10 minutes at 14 000 g two times to reduce the volume. The sample was denatured and washed with 200 µl 8 M urea in 0.1 M Tris at 14 000 g for 15 minutes two times. The sample was incubated for 20 minutes in the dark with 100 µl of 0.05 M iodoacetamide in urea buffer (for alkylation of cysteine

residues), followed by centrifugation at 14 000 g for 10 minutes. The samples were washed three times with 100 µl 8 M urea in 0.1 M Tris at 14 000 g for 15 minutes. To remove the urea buffer, the sample was washed with 100 µl of 0.05 M ammonium bicarbonate at 14 000 g for 10 minutes three times. The final retentate was ensured to be alkaline pH of roughly pH 9, using pH paper, for trypsin activity to occur. The samples were then digested overnight with 2 µg of Trypsin-ultra™ modified trypsin at 37°C overnight in a wet chamber. The tryptic peptides were eluted through the spin filter by centrifugation at 14 000 g for 10 minutes, in a total volume of 80 µl of 0.05 M ammonium bicarbonate. The samples were acidified with formic acid (0.1%) prior to desalting.

7.14.2 Desalting of tryptic peptides

The samples were desalted using a C18 resin embedded in an in-house produced stage tip. All C18 tips were activated, equilibrated, samples bound, washed and eluted by centrifugation at 4000 rpm for 1 minute. The C18 resin was activated using 100 µl 80% acetonitrile and 0.1% formic acid (four times), followed by equilibration with 100 µl 2% acetonitrile and 0.1% formic acid (three times). Acidified tryptic peptides were bound to the stage tip by centrifugation at 4000 rpm until the entire volume of tryptic digest had passed through the filter. Contaminants were washed out using 100 µl 2% acetonitrile and 0.1% formic acid (four times). The tryptic peptides were eluted out into a glass insert using 50 µl 60% acetonitrile and 0.1% formic acid (four times) at 6000 rpm for 1 minute. The eluted samples were dried in a vacuum centrifuge, and resuspended in 2% acetonitrile and 0.1% formic acid prior to mass spectrometry analysis. The samples were both diluted 1:10 prior to mass spectrometry analysis.

7.14.3 Liquid chromatography with tandem mass spectrometry analysis

LC-MS/MS analysis was carried out in the Institute of Infectious Disease and Molecular Medicine, University of Cape Town core facility. Samples were separated by UHPLC inline on a Thermo Dionex Ultimate 3000 instrument prior to mass spectrometry analysis. The maximum injection volume, as determined by the sample loop (12 µl), of peptides from each sample were loaded onto an in-house packed 2 cm C18 trap (100 µm ID, packed with Phenomenex Luna 100 Å hollow core beads) and washed at a flow rate of 5 µl/min with 2% acetonitrile and 0.1% formic acid. The trap was switched in-line to an in-house packed 30 cm analytical column (75 µm ID, packed with Phenomenex Aeiris peptide C18 3.6 µm solid core beads) and the peptides were separated from 6% solvent B (100% acetonitrile, 0.1% formic acid) in solvent A (100% water, 0.1% formic acid) to 30% solvent B over 30 minutes at a flow rate of 0.4 µl/min. Peptides eluted directly into a Thermo QExactive hybrid orbitrap mass spectrometer.

The QExactive acquired spectra in data-dependent (Top10) mode, with an MS1 resolution of 70 000 and an MS2 resolution of 17 500. MS1 scans were acquired with an AGC target of 3e6 or an IT of 250 ms. MS2 scans were acquired with an AGC target of 1e6 or an IT of 80 ms. Dynamic exclusion was set to 30 seconds, roughly half the average chromatographic peak width.

7.14.4 Data analysis

Raw data were analysed using MaxQuant version 1.3.1.12 with default settings for the QExactive instrument. Match between runs was off and LFQ was used for protein-level label free quantitative comparison. The protein groups output file from MaxQuant was used for functional analysis of the exosomes in Funrich (Pathan *et al.*, 2017).

The quality control used weekly by the mass spectrometry department was running a complex reference sample (human neuroblastoma cell line) with the calibration of the mass spectrometer. This was used to benchmark their instrument.

7.15 *In vivo* study: Subcutaneous implantation

This animal study was approved by the Animal Research Ethics Committee, Faculty of Health Sciences, University of Cape Town (HSF AEC 014/016) and complied with the Principles of Laboratory Care as well as the guidelines within the National Research Council's Guide for the Care and Use of Laboratory Animals (National Institutes of Health, publication no. 86-23).

7.15.1 Preparation of porous polyurethane discs

The various fibrin hydrogels were polymerised within highly porous PU discs. In preparation, porous PU discs were produced by the Polymer Laboratory as previously described by (Bezuidenhout *et al.*, 2002) with a diameter of 5.4 mm, thickness of 2 mm, 82% porosity and 157 µm diameter pores. These highly porous discs allow for a defined tissue ingrowth volume and accurate location of implants when explanted. Discs were sterilised by immersion in 70% ethanol and subsequently sonicated for 20 minutes. The discs were then air dried in the tissue culture laminar flow hood and placed into the wells of a sterile 96-well plate. The unpolymerised fibrin constituents (10 mg/ml fibrinogen, 55 µl total volume) were mixed and aspirated into the PU disc immediately by squeezing the disc at least 3 times with the plunger of a 1 ml syringe to remove all trapped air inside the disc and to efficiently load the hydrogel. For the treatment groups (SEC

exosomes and UC DG SEC exosomes), 40 µl of the exosome solutions were mixed with the fibrin gel components (maintaining 10 mg/ml fibrin) prior to uptake and polymerisation within PU discs (55 µl total).

7.15.2 Subcutaneous implantation

Implants were carried out in male Wistar rats (n=6) as previously described by (Goetsch *et al.*, 2015). Aseptic techniques were used for the surgical procedures. Animals were anaesthetised using isoflourane, shaven and the dorsal skin was disinfected with povidine iodine. Up to six 1.0 cm longitudinal incisions were made subcutaneously on the dorsal midline and a pocket for each disc was secured by gentle blunt dissection (Figure 7.3). The discs were implanted into the pockets, with each rat receiving only one disc of each group (n=6). The incisions were closed with single 4-0 prolene sutures. The study was amalgamated with another study carried out in the laboratory that was examining differently pegylated versions of fibrin. As the control group in this other study consisted of fibrin alone and there were 3 experimental groups, this left 2 free implant positions free per rat. Thus, no extra rats were required to carry out the study described here. The surgeon was blinded to the treatment groups and the implantation was randomised for each animal.

After 7 days of implantation, the animals were euthanised by inhalation of halothane. Discs were explanted with their surrounding capsules, halved into equal semi-cylindrical sections, and fixed in 10% buffered formalin for 24 hours followed by 70% ethanol solution prior to processing.

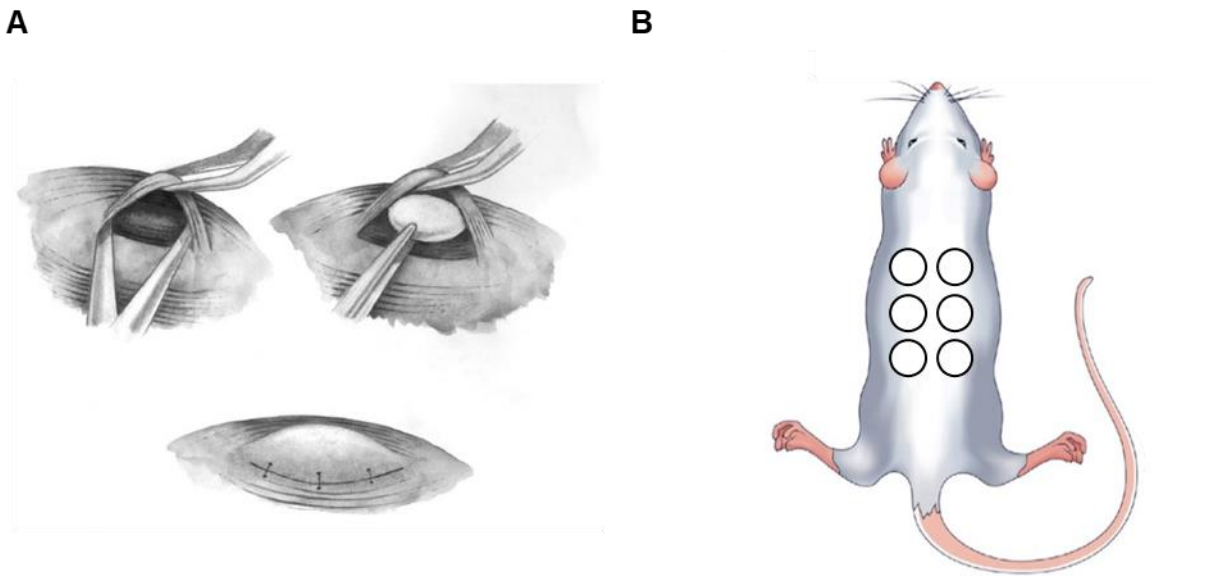

Figure 7.3: Illustration of the subcutaneous implant model in rats. (A) Incision of subcutaneous pockets, disc implantation and sutured closed; (B) Discs placed along the dorsal midline, with 6 randomised discs per rat. Surgical images modified from (Palhares *et al.*, 2009).

7.15.3 Histology

7.15.3.1 Wax processing and embedding

The discs were taken out of the ethanol, inserted into histology cassettes and placed into wire mesh baskets. The samples were immersed in graded alcohol (70% to 90%), for 60 minutes in each. Followed by immersion in 100% alcohol three times for 60 minutes each. The samples then had three changes of iso-octane, three changes of paraffin wax for 60 minutes each at 60°C, with the final change being 120 minutes. The cassettes were opened, and the samples were embedded in paraffin wax using embedding molds. The samples were sectioned from the mid-region of the explanted discs using a microtome.

7.15.3.2 Staining

The cross-sections were mounted on microscope slides and were stained with H&E in order to quantify cellular tissue invasion. The sections were dewaxed using trimethylpentane for 10 minutes, repeated twice. The sections were placed in 100% alcohol three times, then in 96% alcohol two times and in 70% alcohol two times. The slides were then placed in distilled water.

The sections were incubated in haematoxylin and then under running tap water, both for 5 minutes. The slides were then placed in eosin for 30 seconds, dipped in distilled water and dehydrated through the alcohols as mentioned above. The slides were mounted with Canada Balsam and allowed to dry.

The cross-sections were mounted on microscope slides and were stained with ED1 (rat CD68) in order to quantify inflammation. The sections were dewaxed using trimethylpentane for 10 minutes, repeated twice. Cross-sections underwent Proteinase K digestion (diluted to manufacturer's specifications) for 10 minutes at 37°C. Incubated with mouse anti-rat ED1 1:100 dilution in TBS overnight at 4°C. Secondary biotinylated anti-mouse 1:250 dilution for 1 hour at RT. Followed by CY3 labelled streptavidin 1:500 dilution for 1 hour at RT. The slides were mounted in Fluoroshield DAPI.

In order to visualise vascularisation data, sections were incubated in 0.5% triton-100 in TBS for 10 minutes at RT. Then primary mouse anti-human monoclonal SMA diluted (1:100) in TBS overnight at 4°C. Further stained as described above.

7.15.3.3 Microscopic analysis

Samples were viewed and micrographs of entire cross-sections across the mid-region of the explanted disc were captured on a Nikon Eclipse 90i microscope with the stitching algorithm of the Nikon Eclipse software. Micrographs covering the entire disc cross-section were stitched together per explant by a blinded observer using Visiopharm Integrated Systems (VIS) analysis software. For analysis of macrophage content and vascular area, the VIS software was trained to automatically detect CD68 and SMA staining using the decision forest classifier. After segmentation vascularisation analysis cross-sections were then examined by a blinded observer to remove any signal detection that did not correlate with vessels that had a clear vascular morphology. It is to be noted the researcher was blinded to the treatment groups in all analyses.

7.16 Statistical analysis

One-way ANOVA with a block design with Dunnett's post-hoc testing for significance was performed for proliferation assays. This approach was specifically used as it is the most appropriate methodology for repeated cell culture studies (Lew, 2007).

Animal studies were randomised and blinded. One-way ANOVA with Tukey post-hoc testing for significance where appropriate was performed on inflammatory and vascularisation data.

Analyses of all other data were conducted using Student's T-tests (two-sample equal variance (homoscedastic)) in Excel (Microsoft Office). Results are expressed as the mean and error bars are standard error of the mean unless otherwise stated.

7.17 Reagents, equipment and general consumables

Table 7.1: Reagents

Product	Producer/Supplier	Product No.
2-Mercaptoethanol	Sigma-Aldrich, St Louis, MO, USA	M6250
3-Triethoxysilylpropylamine	Sigma-Aldrich, St Louis, MO, USA	A3648
Acid citrate dextrose	Sigma-Aldrich, St Louis, MO, USA	C3821
ActinRed™ ReadyProbes® Reagent	Life Technologies, Carlsbad, CA, USA	R37112
Alexa Fluor™ 488 Phalloidin	Life Technologies (Molecular probes), USA	A12379
Alexa Fluor™ 594 Phalloidin	Life Technologies (Molecular probes), USA	A12381
Aprotinin	Roche, Basel, Switzerland	70257723
BODIPY™ TR Ceramide (red-fluorescent dye)	Thermo Fisher Scientific, Waltham, MA, USA	D7540
Bradford reagent	Sigma-Aldrich, St Louis, MO, USA	B6916
Bromophenol Blue	Sigma-Aldrich, St Louis, MO, USA	B0126
C18 resin	Sigma-Aldrich, St Louis, MO, USA	66883-U
Calcium chloride ($CaCl_{2)}$	Sigma-Aldrich, St Louis, MO, USA	C4901
Collagen type I (bovine skin)	Sigma-Aldrich, St Louis, MO, USA	C4243
Collagenase type II (HUVEC isolation)	Worthington Biochemical Corporation, Lakewood, NJ, USA	LS004174
Coomassie Brilliant Blue R-250	Sigma-Aldrich, St Louis, MO, USA	B0149
Cy3 conjugated strepavidin	Jackson Immuno Research Lab, West Grove, PA, USA	016-160-084
Dimethyl sulfoxide (DMSO)	Sigma-Aldrich, St Louis, MO, USA	D2650
DMEM media	Sigma-Aldrich, St Louis, MO, USA	D5648
Donkey anti-mouse biotin conjugated IgG	Rockland, Limerick, PA, USA	610-706-124
ELISA: Quantikine® ELISA human apolipoprotein B/ApoB immunoassay	R&D Systems, Minneapolis, MN, USA	DAPB00
Ethanol	Servochem (PTY) LTD, Montague Gardens, Cape Town, South Africa	–
ExoGlow™ (protein EV labelling kit, green)	System Biosciences, Palo Alto, CA, USA	EXOG200A-1
ExoQuick-TC™	System Biosciences, Palo Alto, CA, USA	EXOTC10A-1

FastCast SDS-PAGE (12%)	Bio-Rad, Hercules, CA, USA	1610175
Fat free milk powder	LabScientific, Highlands, NJ, USA	M-0841
Fluoroshield with DAPI	Sigma-Aldrich, St Louis, MO, USA	F6057
Foetal bovine serum (FBS) (gamma irradiated)	Gibco® by Life Technologies™, Paisley, UK	10499-044
Gentamicin solution	Sigma-Aldrich, St Louis, MO, USA	G1272
Glycerol	Sigma-Aldrich, St Louis, MO, USA	G5516
Goat anti-rabbit horseradish peroxidase (HRP) conjugated antibody	Abcam, Cambridge, MA, USA	ab97051
Heparin NaCl	Sigma-Aldrich, St Louis, MO, USA	H3393-50KU
Hepes	Sigma-Aldrich, St Louis, MO, USA	H3375
Human epidermal growth factor (EGF)	Peprotech, Rocky Hill, NJ, USA	AF-100-15
Human fibrinogen	Sigma-Aldrich, St Louis, MO, USA	F3879
Human fibroblast growth factor-basic (bFGF)	Peprotech, Rocky Hill, NJ, USA	100-18B
Human serum (Blood group AB)	Western Province Blood Transfusion Service, Cape Town, South Africa	-
Hydrocortisone	Sigma-Aldrich, St Louis, MO, USA	H0396
L-Glutamine	Sigma-Aldrich, St Louis, MO, USA	G-8540
MCDB-131 media	Sigma-Aldrich, St Louis, MO, USA	M8537
Medium 199 growth medium	Sigma-Aldrich, St Louis, MO, USA	M4530
Methyl cellulose: 4000 centipoises	Sigma-Aldrich, St Louis, MO, USA	M0512
Mini-PROTEAN® TGX™ precast protein gels (4-15%)	Bio-Rad, Hercules, CA, USA	4561083
Mouse anti-human monoclonal SMA	Agilent Technologies, Santa Clara, CA, USA	M0851
Mouse anti-rat monoclonal ED1	Bio-Rad, Hercules, CA, USA	MCA341R
OptiPrep™ density gradient medium	Sigma-Aldrich, St Louis, MO, USA	D1556
Penicillin streptomycin (10 000 U penicillin and 10 mg streptomycin/ml)	Sigma-Aldrich, St Louis, MO, USA	P0781
Potassium chloride (KCl)	Sigma-Aldrich, St Louis, MO, USA	P9541
Potassium phosphate monobasic (KH_2PO_4)	Sigma-Aldrich, St Louis, MO, USA	P5655
Prostaglandin E1 (PGE1)	Sigma-Aldrich, St Louis, MO, USA	P5515
Protein G-Agarose	Sigma-Aldrich, St Louis, MO, USA	P7700
Proteinase K	Dako, Glostrup, Denmark	S3020
Proteinase K	Sigma-Aldrich, St Louis, MO, USA	P2308
Rabbit anti-human ApoA1	Abcam, Cambridge, MA, USA	ab52945
Rabbit anti-human CD9	Abcam, Cambridge, MA, USA	ab92726
Rabbit anti-human TAPA1	Abcam, Cambridge, MA, USA	ab109201
Rabbit anti-human TSG101	Abcam, Cambridge, MA, USA	ab30871
RIPA buffer	Sigma-Aldrich, St Louis, MO, USA	R0278
Sepharose CL-4B	GE Healthcare, Chicago, IL, USA	17-0150-01
Sigmacote®	Sigma-Aldrich, St Louis, MO, USA	SL2
Sodium azide	Sigma-Aldrich, St Louis, MO, USA	S2002
Sodium bicarbonate ($NaHCO_3$)	Sigma-Aldrich, St Louis, MO, USA	S5761
Sodium chloride (NaCl)	Sigma-Aldrich, St Louis, MO, USA	S7653
Sodium dihydrogen phosphate (NaH_2PO_4)	Sigma-Aldrich, St Louis, MO, USA	S3139
Sodium dodecyl sulfate (SDS)	Sigma-Aldrich, St Louis, MO, USA	L3771
Sodium hydroxide (NaOH)	Sigma-Aldrich, St Louis, MO, USA	S-5881

Sodium phosphate dibasic dodecahydrate ($Na_2HPO_4.12H_2O$)	Sigma-Aldrich, St Louis, MO, USA	71649
SYTO™ RNASelect™ (green fluorescent cell stain)	Thermo Fisher Scientific, Hillsboro, OR, USA	S32703
Thrombin from bovine plasma	Sigma-Aldrich, St Louis, MO, USA	T4648
Triton-X 100	Sigma-Aldrich, St Louis, MO, USA	T8532
Trizma® hydrochloride (Tris-HCl)	Sigma-Aldrich, St Louis, MO, USA	T3253
Trypan Blue	Sigma-Aldrich, St Louis, MO, USA	T8154
Trypsin-EDTA (10X)	Sigma-Aldrich, St Louis, MO, USA	59427C
Trypsin-ultra™ mass spectrometry grade modified trypsin	New England BioLabs, Ipswich, MA, USA	P8101S
Tween® 20	Sigma-Aldrich, St Louis, MO, USA	P1379
WesternBright ECL HRP substrate	Advansta, Menlo Park, CA, USA	K-12045-D50
XTT cell viability kit	Cell Signaling Technology, Danvers, MA, USA	9095S

Table 7.2: Equipment

Product	Producer/Supplier
-65 °C freezer	Snijders Scientific, Tilburg, Netherlands
Centrifuge: 5415R (for microcentrifuge tubes)	Eppendorf, Hamburg, Germany
Centrifuge: 5810R	Eppendorf, Hamburg, Germany
Centrifuge: J2-21 with a JA20 rotor (for centrifuging methylcellulose)	Beckman Coulter Life Sciences, Indianapolis, IN, USA
Centrifuge: Megafuge 1.0R	Heraeus, Hanau, Germany
Dionex Ultimate 3000 instrument	Thermo Fisher Scientific, Waltham, MA, USA
Fluorescent spectrophotometer: Cary Eclipse serial no. e101124662	Agilent Technologies, Santa Clara, CA, USA
Haemocytometer	Improved Neubauer, Baxter Scientific, Deerfield, IL, USA
HERA cell incubator (for all 37 °C cell culture)	Heraeus, Hanau, Germany
iMark plate reader	Bio-Rad, Hercules, CA, USA
Lipoprint® System	Quantimetrix, Redondo Beach, CA, USA
Liquid chromatography columns: C4169	Sigma-Aldrich, St Louis, MO, USA
Mass spectrometer: QExactive hybrid orbitrap	Thermo Fisher Scientific, Waltham, MA, USA
Microscope: Nikon fluorescent microscope (Nikon Eclipse 90i DS-Ri1)	Nikon, Tokyo, Japan
Microscope: Nikon light microscope (Nikon Eclipse Ti-S)	Nikon, Tokyo, Japan
Microscope: ZEISS LSM510 Confocal microscope with MaiTai two photon laser	Carl Zeiss Microscopy GmbH, Göttingen, Germany
NanoDrop: NanoDrop 2000	Thermo Fisher Scientific, Waltham, MA, USA
NTA: NanoSight LM10	Malvern Instruments, Malvern, UK
pH meter: Jenway 3510	Bibby Scientific, Staffordshire, UK
Pipettes	Gilson Inc., Middleton, WI
Rotor: SW 40 Ti Rotor, swinging bucket, titanium, 6 x 14 ml	Beckman Coulter Life Sciences, Indianapolis, IN, USA
Rotor: SW 60 Ti Rotor, swinging bucket, titanium, 6 x 4 ml	Beckman Coulter Life Sciences, Indianapolis, IN, USA
SEM microscope: Nova NanoSEM 230	FEI, Hillsboro, OR, USA
Shaking incubator: IncoShake	Labotech, Cape Town, South Africa
Sonicator: Virsonic 100 probe	Virtis, Gardiner, NY, USA
SpeedVac™ concentrator: Savant™ SPD131DDA	Thermo Fisher Scientific, Waltham, MA, USA
Sputter coater: Polaron Emitech SC7640	Quorum Technologies, Lewes, UK
TEM microscope: Tecnai G2	Thermo Fisher Scientific, Waltham, MA, USA
Trans-Blot® SD Semi-Dry Transfer Cell	Bio-Rad, Hercules, CA, USA
Ultracentrifuge: Beckman L-80	Beckman Coulter Life Sciences, Indianapolis, IN, USA
Ultracentrifuge: Beckman L8-55M	Beckman Coulter Life Sciences, Indianapolis, IN, USA
Water bath: Grant Y14	Grant Instruments, Cambridge, UK

Table 7.3: General consumables

Product	Producer/Supplier	Product No.
24-well cell culture plate	Costar® by Corning Incorporated, NY, USA	3524
96-well cell culture plate	Costar® by Corning Incorporated, NY, USA	3595
96-well clear, round bottomed, sterile plate, non-tissue culture treated	Nunc®, Thermo Scientific™, Roskilde, Denmark	268200
96-well opaque, flat bottomed, non-sterile	Nunc® MicroWell, Roskilde, Denmark	Z688665
Agar TEM grids 200 mesh copper	Agar Scientific, Essex, UK	04G2220C
Amicon ultra 0.5 ml 100 kDa centrifugal filters	Millipore, Burlington, MA, USA	UFC510096
Amicon ultra 0.5 ml 30 kDa centrifugal filters	Millipore, Burlington, MA, USA	UFC503096
Centrifuge tube (15 ml)	Falcon by BD Biosciences, San Jose, CA, USA	352096
Centrifuge tube (50 ml)	Falcon by BD Biosciences, San Jose, CA, USA	352070
CultureWell 16 chambered cover glasses	Life Technologies, Carlsbad, CA, USA	C-37000
Exosome spin columns (MW 3000)	Invitrogen™, Thermo Fisher Scientific, OR, USA	4484449
Filter, syringe filter unit (0.2 µm)	Abluo™, GVS Lifesciences, Sanford, ME, USA	FJ25ASCCA002DL01
Micro centrifuge tube, flat cap (0.6 ml)	Thermo Scientific QSP, San Diego, CA, USA	502-GRD-Q
Micro centrifuge tube, flat cap (1.5 ml)	Thermo Scientific QSP, San Diego, CA, USA	509-GRD-Q
Micro centrifuge tube, flat locking cap (2.0 ml)	Thermo Scientific QSP, San Diego, CA, USA	L-508GRD-Q
Mr Frosty freezing container	Nalgene, Sigma-Aldrich®, St Louis, MO, USA	C1562
Nitrocellulose membrane Hybond ECL	Amersham Biosciences, Sigma-Aldrich, St Louis, MO, USA	GE10600002
Transwell insert, 6.5 mm with 0.8 µm pore polycarbonate membrane	Corning, NY, USA	3422
Ultracentrifuge tubes for SW 40 Ti, 14 ml, 14 x 95 mm	Beckman Coulter Life Sciences, Indianapolis, IN, USA	331374
Ultracentrifuge tubes for SW 60 Ti, 4 ml, 11 x 60 mm	Beckman Coulter Life Sciences, Indianapolis, IN, USA	328874
Whatman No.1 filter paper	Sigma-Aldrich, St Louis, MO, USA	WHA1001325

REFERENCES

AATONEN, M. T., ÖHMAN, T., NYMAN, T. A., LAITINEN, S., GRÖNHOLM, M. & SILJANDER, P. R.-M. 2014. Isolation and characterization of platelet-derived extracellular vesicles. *Journal of Extracellular Vesicles,* 3.

ABRAMOWICZ, A., MARCZAK, L., WOJAKOWSKA, A., ZAPOTOCZNY, S., WHITESIDE, T. L., WIDLAK, P. & PIETROWSKA, M. 2018. Harmonization of exosome isolation from culture supernatants for optimized proteomics analysis. *Public Library of Science One,* 13**,** e0205496.

ABRAMOWICZ, A., WIDLAK, P. & PIETROWSKA, M. 2016. Proteomic analysis of exosomal cargo: the challenge of high purity vesicle isolation. *Molecular BioSystems,* 12**,** 1407-1419.

ADMYRE, C., GRUNEWALD, J., THYBERG, J., GRIPENBÄCK, S., TORNLING, G., EKLUND, A., SCHEYNIUS, A. & GABRIELSSON, S. 2003. Exosomes with major histocompatibility complex class II and co-stimulatory molecules are present in human BAL fluid. *European Respiratory Journal,* 22**,** 578-583.

ADMYRE, C., JOHANSSON, S. M., QAZI, K. R., FILÉN, J.-J., LAHESMAA, R., NORMAN, M., NEVE, E. P. A., SCHEYNIUS, A. & GABRIELSSON, S. 2007. Exosomes with immune modulatory features are present in human breast milk. *The Journal of Immunology,* 179**,** 1969-1978.

AHMED, T. A., DARE, E. V. & HINCKE, M. 2008. Fibrin: a versatile scaffold for tissue engineering applications. *Tissue Engineering Part B: Reviews,* 14**,** 199-215.

AHMED, Z., RAVANDI, A., MAGUIRE, G. F., KUKSIS, A. & CONNELLY, P. W. 2003. Formation of apolipoprotein AI–phosphatidylcholine core aldehyde Schiff base adducts promotes uptake by THP-1 macrophages. *Cardiovascular Research,* 58**,** 712-720.

ALMQVIST, N., LÖNNQVIST, A., HULTKRANTZ, S., RASK, C. & TELEMO, E. 2008. Serum-derived exosomes from antigen-fed mice prevent allergic sensitization in a model of allergic asthma. *Immunology,* 125**,** 21-27.

ALSER, O. H. & GOUTOS, I. 2018. The evidence behind the use of platelet-rich plasma (PRP) in scar management: a literature review. *Scars, Burns & Healing,* 4**,** 2059513118808773-2059513118808773.

ALVAREZ-ERVITI, L., SEOW, Y., YIN, H., BETTS, C., LAKHAL, S. & WOOD, M. J. 2011. Delivery of siRNA to the mouse brain by systemic injection of targeted exosomes. *Nature Biotechnology,* 29**,** 341.

ALVES, R. & GRIMALT, R. 2018. A review of platelet-rich plasma: History, biology, mechanism of action, and classification. *Skin Appendage Disorders,* 4**,** 18-24.

AMMANN, C. 2011. Stability studies needed to define the handling and transport conditions of sensitive pharmaceutical or biotechnological products. *American Association of Pharmaceutical Scientists,* 12**,** 1264-1275.

AN, M., WU, J., ZHU, J. & LUBMAN, D. M. 2018. Comparison of an optimized ultracentrifugation method versus size-exclusion chromatography for isolation of exosomes from human serum. *Journal of Proteome Research,* 17**,** 3599-3605.

ANDREU, Z., OSHIRO, R. O., REDRUELLO, A., LÓPEZ-MARTÍN, S., GUTIÉRREZ-VÁZQUEZ, C., MORATO, E., MARINA, A. I., GÓMEZ, C. O. & YÁÑEZ-MÓ, M. 2017. Extracellular vesicles as a source for non-invasive biomarkers in bladder cancer progression. *European Journal of Pharmaceutical Sciences,* 98**,** 70-79.

ANDREU, Z., RIVAS, E., SANGUINO-PASCUAL, A., LAMANA, A., MARAZUELA, M., GONZÁLEZ-ALVARO, I., SÁNCHEZ-MADRID, F., DE LA FUENTE, H. & YÁÑEZ-MÓ, M. 2016. Comparative analysis of EV isolation procedures for miRNAs detection in serum samples. *Journal of Extracellular Vesicles,* 5**,** 31655.

ANDREU, Z. & YÁÑEZ-MÓ, M. 2014. Tetraspanins in extracellular vesicle formation and function. *Frontiers in Immunology,* 5**,** 442.

ANGELINI, F., IONTA, V., ROSSI, F., MIRALDI, F., MESSINA, E. & GIACOMELLO, A. 2016. Foetal bovine serum-derived exosomes affect yield and phenotype of human cardiac progenitor cell culture. *BioImpacts,* 6**,** 15.

ANITUA, E., PELACHO, B., PRADO, R., AGUIRRE, J. J., SÁNCHEZ, M., PADILLA, S., ARANGUREN, X. L., ABIZANDA, G., COLLANTES, M. & HERNANDEZ, M. 2015. Infiltration of plasma rich in growth factors enhances in vivo angiogenesis and improves reperfusion and tissue remodeling after severe hind limb ischemia. *Journal of Controlled Release,* 202**,** 31-39.

ARAKAKI, K., KITAMURA, N., FUJIKI, H., KUROKAWA, T., IWAMOTO, M., UENO, M., KANAYA, F., OSADA, Y., GONG, J. P. & YASUDA, K. 2010. Artificial cartilage made from a novel double-network hydrogel: In vivo effects on the normal cartilage and ex vivo evaluation of the friction property. *Journal of Biomedical Materials Research Part A,* 93**,** 1160-1168.

ARSLAN, F., LAI, R. C., SMEETS, M. B., AKEROYD, L., CHOO, A., AGUOR, E. N., TIMMERS, L., VAN RIJEN, H. V., DOEVENDANS, P. A. & PASTERKAMP, G. 2013. Mesenchymal stem cell-derived exosomes increase ATP levels, decrease oxidative stress and activate PI3K/Akt pathway to enhance myocardial viability and prevent adverse remodeling after myocardial ischemia/reperfusion injury. *Stem Cell Research,* 10**,** 301-312.

ASHCROFT, B. A., DE SONNEVILLE, J., YUANA, Y., OSANTO, S., BERTINA, R., KUIL, M. E. & OOSTERKAMP, T. H. 2012. Determination of the size distribution of blood microparticles directly in plasma using atomic force microscopy and microfluidics. *Biomedical Microdevices,* 14**,** 641-649.

ASSOIAN, R. K., KOMORIYA, A., MEYERS, C. A., MILLER, D. M. & SPORN, M. B. 1983. Transforming growth factor-beta in human platelets. Identification of a major storage site, purification, and characterization. *Journal of Biological Chemistry,* 258**,** 7155-7160.

ASWAD, H., JALABERT, A. & ROME, S. 2016. Depleting extracellular vesicles from fetal bovine serum alters proliferation and differentiation of skeletal muscle cells in vitro. *BMC Biotechnology,* 16**,** 32.

AUSPRUNK, D. H. & FOLKMAN, J. 1977. Migration and proliferation of endothelial cells in preformed and newly formed blood vessels during tumor angiogenesis. *Microvascular Research,* 14**,** 53-65.

AYDIN, O., KARACA, G., PEHLIVANLI, F., ALTUNKAYA, C., UZUN, H., ÖZDEN, H., AYDIN, G., ŞAHINER, İ., NIYAZ, M. & GÜLER, O. 2018. Platelet-rich plasma may offer a new hope in suppressed wound healing when compared to mesenchymal stem cells. *Journal of Clinical Medicine,* 7**,** 143.

BABST, M. 2005. A protein's final ESCRT. *Traffic,* 6**,** 2-9.

BACHURSKI, D., SCHULDNER, M., NGUYEN, P.-H., MALZ, A., REINERS, K. S., GRENZI, P. C., BABATZ, F., SCHAUSS, A. C., HANSEN, H. P. & HALLEK, M. 2019. Extracellular vesicle measurements with nanoparticle tracking analysis–An accuracy and repeatability comparison between NanoSight NS300 and ZetaView. *Journal of Extracellular Vesicles,* 8**,** 1596016.

BAIETTI, M. F., ZHANG, Z., MORTIER, E., MELCHIOR, A., DEGEEST, G., GEERAERTS, A., IVARSSON, Y., DEPOORTERE, F., COOMANS, C. & VERMEIREN, E. 2012. Syndecan–syntenin–ALIX regulates the biogenesis of exosomes. *Nature Cell Biology,* 14**,** 677.

BALAJ, L., ATAI, N. A., CHEN, W., MU, D., TANNOUS, B. A., BREAKEFIELD, X. O., SKOG, J. & MAGUIRE, C. A. 2015. Heparin affinity purification of extracellular vesicles. *Scientific Reports,* 5**,** 10266.

BANIZS, A. B., HUANG, T., DRYDEN, K., BERR, S. S., STONE, J. R., NAKAMOTO, R. K., SHI, W. & HE, J. 2014. In vitro evaluation of endothelial exosomes as carriers for small interfering ribonucleic acid delivery. *International Journal of Nanomedicine,* 9**,** 4223.

BANKS, R., FORBES, M., KINSEY, S., STANLEY, A., INGHAM, E., WALTERS, C. & SELBY, P. 1998. Release of the angiogenic cytokine vascular endothelial growth factor (VEGF) from platelets: significance for VEGF measurements and cancer biology. *British Journal of Cancer,* 77**,** 956.

BARANYAI, T., HERCZEG, K., ONÓDI, Z., VOSZKA, I., MÓDOS, K., MARTON, N., NAGY, G., MÄGER, I., WOOD, M. J. & EL ANDALOUSSI, S. 2015. Isolation of exosomes from blood plasma: qualitative and quantitative comparison of ultracentrifugation and size exclusion chromatography methods. *Public Library of Science One,* 10**,** e0145686.

BARILE, L. & VASSALLI, G. 2017. Exosomes: therapy delivery tools and biomarkers of diseases. *Pharmacology & Therapeutics,* 174**,** 63-78.

BASTOS-AMADOR, P., ROYO, F., GONZALEZ, E., CONDE-VANCELLS, J., PALOMO-DIEZ, L., BORRAS, F. E. & FALCON-PEREZ, J. M. 2012. Proteomic analysis of microvesicles from plasma of healthy donors reveals high individual variability. *Journal of Proteomics,* 75**,** 3574-84.

BAUDIN, B., BRUNEEL, A., BOSSELUT, N. & VAUBOURDOLLE, M. 2007. A protocol for isolation and culture of human umbilical vein endothelial cells. *Nature Protocols,* 2**,** 481.

BEACH, A., ZHANG, H.-G., RATAJCZAK, M. Z. & KAKAR, S. S. 2014. Exosomes: an overview of biogenesis, composition and role in ovarian cancer. *Journal of Ovarian Research,* 7**,** 14-14.

BEBAWY, M., ROSEBLADE, A., LUK, F., RAWLING, T., UNG, A. & GRAU, G. E. 2013. Cell-derived microparticles: new targets in the therapeutic management of disease. *Journal of Pharmacy & Pharmaceutical Sciences,* 16**,** 238-253.

BEI, Y., XU, T., LV, D., YU, P., XU, J., CHE, L., DAS, A., TIGGES, J., TOXAVIDIS, V. & GHIRAN, I. 2017. Exercise-induced circulating extracellular vesicles protect against cardiac ischemia–reperfusion injury. *Basic Research in Cardiology,* 112**,** 38.

BEIT-YANNAI, E., TABAK, S. & STAMER, W. D. 2018. Physical exosome: exosome interactions. *Journal of Cellular and Molecular Medicine,* 22**,** 2001-2006.

BELORIBI, S., RISTORCELLI, E., BREUZARD, G., SILVY, F., BERTRAND-MICHEL, J., BERAUD, E., VERINE, A. & LOMBARDO, D. 2012. Exosomal lipids impact notch signaling and induce death of human pancreatic tumoral SOJ-6 cells. *Public Library of Science One,* 7**,** e47480-e47480.

BEYTH, S., BOROVSKY, Z., MEVORACH, D., LIEBERGALL, M., GAZIT, Z., ASLAN, H., GALUN, E. & RACHMILEWITZ, J. 2005. Human mesenchymal stem cells alter antigen-presenting cell maturation and induce T-cell unresponsiveness. *Blood,* 105**,** 2214-2219.

BEZUIDENHOUT, D., DAVIES, N., BLACK, M., SCHMIDT, C., OOSTHUYSEN, A. & ZILLA, P. 2010. Covalent surface heparinization potentiates porous polyurethane scaffold vascularization. *Journal of Biomaterials Applications,* 24**,** 401-418.

BEZUIDENHOUT, D., DAVIES, N. & ZILLA, P. 2002. Effect of well defined dodecahedral porosity on inflammation and angiogenesis. *American Society for Artificial Internal Organs Journal,* 48**,** 465-471.

BHOME, R., DEL VECCHIO, F., LEE, G. H., BULLOCK, M. D., PRIMROSE, J. N., SAYAN, A. E. & MIRNEZAMI, A. H. 2018. Exosomal microRNAs (exomiRs): Small molecules with a big role in cancer. *Cancer Letters,* 420**,** 228-235.

BIAN, S., ZHANG, L., DUAN, L., WANG, X., MIN, Y. & YU, H. 2014. Extracellular vesicles derived from human bone marrow mesenchymal stem cells promote angiogenesis in a rat myocardial infarction model. *Journal of Molecular Medicine,* 92**,** 387-97.

BIOLOGY, A. S. F. B. A. M. 2019. *Required manuscript content and publication guidelines for molecular & cellular proteomics* [Online]. Available: https://www.mcponline.org/content/required-manuscript-content-and-publication-guidelines-molecular-cellular-proteomics [Accessed 18 November 2019].

BLANC, L. & VIDAL, M. 2017. New insights into the function of Rab GTPases in the context of exosomal secretion. *Small GTPases,* 9**,** 95-106.

BOBRIE, A., COLOMBO, M., KRUMEICH, S., RAPOSO, G. & THÉRY, C. 2012. Diverse subpopulations of vesicles secreted by different intracellular mechanisms are present in exosome preparations obtained by differential ultracentrifugation. *Journal of Extracellular Vesicles,* 1**,** 18397.

BÖING, A. N., VAN DER POL, E., GROOTEMAAT, A. E., COUMANS, F. A., STURK, A. & NIEUWLAND, R. 2014. Single-step isolation of extracellular vesicles by size-exclusion chromatography. *Journal of Extracellular Vesicles,* 3.

BOYDEN, S. 1962. The chemotactic effect of mixtures of antibody and antigen on polymorphonuclear leucocytes. *Journal of Experimental Medicine,* 115**,** 453-466.

BRETZ, N. P., RIDINGER, J., RUPP, A. K., RIMBACH, K., KELLER, S., RUPP, C., MARME, F., UMANSKY, L., UMANSKY, V., EIGENBROD, T., SAMMAR, M. & ALTEVOGT, P. 2013. Body fluid exosomes promote secretion of inflammatory cytokines in monocytic cells via Toll-like receptor signaling. *Journal of Biological Chemistry,* 288**,** 36691-702.

BRISSON, A. R., TAN, S., LINARES, R., GOUNOU, C. & ARRAUD, N. 2017. Extracellular vesicles from activated platelets: a semiquantitative cryo-electron microscopy and immuno-gold labeling study. *Platelets,* 28**,** 263-271.

BRUNNER, G., NGUYEN, H., GABRILOVE, J., RIFKIN, D. & WILSON, E. 1993. Basic fibroblast growth factor expression in human bone marrow and peripheral blood cells. *Blood,* 81**,** 631-638.

BRZOZOWSKI, J. S., BOND, D. R., JANKOWSKI, H., GOLDIE, B. J., BURCHELL, R., NAUDIN, C., SMITH, N. D., SCARLETT, C. J., LARSEN, M. R. & DUN, M. D. 2018. Extracellular vesicles with altered tetraspanin CD9 and CD151 levels confer increased prostate cell motility and invasion. *Scientific Reports,* 8**,** 8822.

BURKE, M. C., OEI, M. S., EDWARDS, N. J., OSTRAND-ROSENBERG, S. & FENSELAU, C. 2014. Ubiquitinated proteins in exosomes secreted by myeloid-derived suppressor cells. *Journal of Proteome Research,* 13**,** 5965-5972.

BUSCHMANN, D., KIRCHNER, B., HERMANN, S., MÄRTE, M., WURMSER, C., BRANDES, F., KOTSCHOTE, S., BONIN, M., STEINLEIN, O. K. & PFAFFL, M. W. 2018. Evaluation of serum extracellular vesicle isolation methods for profiling miRNAs by next-generation sequencing. *Journal of Extracellular Vesicles,* 7**,** 1481321.

BUZÁS, E. I., TÓTH, E. Á., SÓDAR, B. W. & SZABÓ-TAYLOR, K. É. Molecular interactions at the surface of extracellular vesicles. Seminars in Immunopathology, 2018. Springer, 453-464.

CAIVANO, A., LA ROCCA, F., SIMEON, V., GIRASOLE, M., DINARELLI, S., LAURENZANA, I., DE STRADIS, A., DE LUCA, L., TRINO, S., TRAFICANTE, A., D'ARENA, G., MANSUETO, G., VILLANI, O., PIETRANTUONO, G., LAURENTI, L., DEL VECCHIO, L. & MUSTO, P. 2017. MicroRNA-155 in serum-derived extracellular vesicles as a potential biomarker for hematologic malignancies - a short report. *Cellular Oncology,* 40**,** 97-103.

CANTIN, R., DIOU, J., BÉLANGER, D., TREMBLAY, A. M. & GILBERT, C. 2008. Discrimination between exosomes and HIV-1: purification of both vesicles from cell-free supernatants. *Journal of Immunological Methods,* 338**,** 21-30.

CARADEC, J., KHARMATE, G., HOSSEINI-BEHESHTI, E., ADOMAT, H., GLEAVE, M. & GUNS, E. 2014. Reproducibility and efficiency of serum-derived exosome extraction methods. *Clinical Biochemistry,* 47**,** 1286-1292.

CARNELL-MORRIS, P., TANNETTA, D., SIUPA, A., HOLE, P. & DRAGOVIC, R. 2017. Analysis of extracellular vesicles using fluorescence nanoparticle tracking analysis. *Methods in Molecular Biology,* 1660**,** 153-173.

CAVALLARI, C., RANGHINO, A., TAPPARO, M., CEDRINO, M., FIGLIOLINI, F., GRANGE, C., GIANNACHI, V., GARNERI, P., DEREGIBUS, M. C. & COLLINO, F. 2017. Serum-derived extracellular vesicles (EVs) impact on vascular remodeling and prevent muscle damage in acute hind limb ischemia. *Scientific Reports,* 7**,** 8180.

CAVALLERI, T., ANGELICI, L., FAVERO, C., DIONI, L., MENSI, C., BAREGGI, C., PALLESCHI, A., RIMESSI, A., CONSONNI, D., BORDINI, L., TODARO, A., BOLLATI, V. & PESATORI, A. C. 2017. Plasmatic extracellular vesicle microRNAs in malignant pleural mesothelioma and asbestos-exposed subjects suggest a 2-miRNA signature as potential biomarker of disease. *Public Library of Science One,* 12**,** e0176680.

CHARGAFF, E. & WEST, R. 1946. The biological significance of the thromboplastic protein of blood. *The Journal of Biological Chemistry,* 166**,** 189-197.

CHEN, C.-H., JIANG, W., VIA, D. P., LUO, S., LI, T.-R., LEE, Y.-T. & HENRY, P. D. 2000. Oxidized low-density lipoproteins inhibit endothelial cell proliferation by suppressing basic fibroblast growth factor expression. *Circulation,* 101**,** 171-177.

CHEN, C., SKOG, J., HSU, C.-H., LESSARD, R. T., BALAJ, L., WURDINGER, T., CARTER, B. S., BREAKEFIELD, X. O., TONER, M. & IRIMIA, D. 2010a. Microfluidic isolation and transcriptome analysis of serum microvesicles. *Lab on a Chip,* 10**,** 505-511.

CHEN, C. W., WANG, L. L., ZAMAN, S., GORDON, J., ARISI, M. F., VENKATARAMAN, C. M., CHUNG, J. J., HUNG, G., GAFFEY, A. C. & SPRUCE, L. A. 2018a. Sustained release of endothelial

progenitor cell-derived extracellular vesicles from shear-thinning hydrogels improves angiogenesis and promotes function after myocardial infarction. *Cardiovascular Research,* 114**,** 1029-1040.

CHEN, L., CHEN, R., KEMPER, S., CONG, M., YOU, H. & BRIGSTOCK, D. R. 2018b. Therapeutic effects of serum extracellular vesicles in liver fibrosis. *Journal of Extracellular Vesicles,* 7**,** 1461505.

CHEN, L., XIANG, B., WANG, X. & XIANG, C. 2017. Exosomes derived from human menstrual blood-derived stem cells alleviate fulminant hepatic failure. *Stem Cell Research & Therapy,* 8**,** 9.

CHEN, T. S., LAI, R. C., LEE, M. M., CHOO, A. B. H., LEE, C. N. & LIM, S. K. 2010b. Mesenchymal stem cell secretes microparticles enriched in pre-microRNAs. *Nucleic Acids Research,* 38**,** 215-224.

CHENG, N.-C., LIN, W.-J., LING, T.-Y. & YOUNG, T.-H. 2017. Sustained release of adipose-derived stem cells by thermosensitive chitosan/gelatin hydrogel for therapeutic angiogenesis. *Acta Biomaterialia,* 51**,** 258-267.

CHING, R. C., WIBERG, M. & KINGHAM, P. J. 2018. Schwann cell-like differentiated adipose stem cells promote neurite outgrowth via secreted exosomes and RNA transfer. *Stem Cell Research & Therapy* 9**,** 266.

CHOI, H. & LEE, D. S. 2016. Illuminating the physiology of extracellular vesicles. *Stem Cell Research & Therapy,* 7**,** 55.

CHOKOZA, C., GUSTAFSSON, C. A., GOETSCH, K. P., ZILLA, P., THIERFELDER, N., PISANO, F., MURA, M., GNECCHI, M., BEZUIDENHOUT, D. & DAVIES, N. H. 2019. Tuning tissue ingrowth into proangiogenic gydrogels via dual modality degradation. *ACS Biomaterials Science & Engineering,* 5**,** 5430-5438.

CHRISTMAN, K. L. & LEE, R. J. 2006. Biomaterials for the treatment of myocardial infarction. *Journal of the American College of Cardiology,* 48**,** 907-913.

CIANCIARUSO, C., PHELPS, E. A., PASQUIER, M., HAMELIN, R., DEMURTAS, D., AHMED, M. A., PIEMONTI, L., HIROSUE, S., SWARTZ, M. A. & DE PALMA, M. 2016. Primary human and rat beta cells release the intracellular autoantigens GAD65, IA-2 and proinsulin in exosomes together with cytokine-induced enhancers of immunity. *Diabetes***,** db160671.

CIUFFREDA, M. C., MALPASSO, G., CHOKOZA, C., BEZUIDENHOUT, D., GOETSCH, K. P., MURA, M., PISANO, F., DAVIES, N. H. & GNECCHI, M. 2018. Synthetic extracellular matrix mimic hydrogel improves efficacy of mesenchymal stromal cell therapy for ischemic cardiomyopathy. *Acta Biomaterialia,* 70**,** 71-83.

CLAYTON, A., COURT, J., NAVABI, H., ADAMS, M., MASON, M. D., HOBOT, J. A., NEWMAN, G. R. & JASANI, B. 2001. Analysis of antigen presenting cell derived exosomes, based on immuno-magnetic isolation and flow cytometry. *Journal of Immunological Methods,* 247**,** 163-74.

COLOMBO, M., MOITA, C., VAN NIEL, G., KOWAL, J., VIGNERON, J., BENAROCH, P., MANEL, N., MOITA, L. F., THÉRY, C. & RAPOSO, G. 2013. Analysis of ESCRT functions in exosome biogenesis, composition and secretion highlights the heterogeneity of extracellular vesicles. *Journal of Cell Science,* 126**,** 5553-5565.

COLOMBO, M., RAPOSO, G. & THÉRY, C. 2014. Biogenesis, secretion, and intercellular interactions of exosomes and other extracellular vesicles. *Annual Review of Cell and Developmental Biology,* 30**,** 255-289.

CONDE-VANCELLS, J., RODRIGUEZ-SUAREZ, E., EMBADE, N., GIL, D., MATTHIESEN, R., VALLE, M., ELORTZA, F., LU, S. C., MATO, J. M. & FALCON-PEREZ, J. M. 2008. Characterization and comprehensive proteome profiling of exosomes secreted by hepatocytes. *Journal of Proteome Research,* 7**,** 5157-66.

CONTRERAS-NARANJO, J. C., WU, H.-J. & UGAZ, V. M. 2017. Microfluidics for exosome isolation and analysis: enabling liquid biopsy for personalized medicine. *Lab on a Chip,* 17**,** 3558-3577.

COUMANS, F. A., BRISSON, A. R., BUZAS, E. I., DIGNAT-GEORGE, F., DREES, E. E., EL-ANDALOUSSI, S., EMANUELI, C., GASECKA, A., HENDRIX, A. & HILL, A. F. 2017. Methodological guidelines to study extracellular vesicles. *Circulation Research,* 120**,** 1632-1648.

CROSS, T. G. & HORNSHAW, M. P. 2016. Can LC and LC-MS ever replace immunoassays? *Journal of Applied Bionalysis,* 2**,** 108.

CUNNINGHAM, C. J., REDONDO-CASTRO, E. & ALLAN, S. M. 2018. The therapeutic potential of the mesenchymal stem cell secretome in ischaemic stroke. *Journal of Cerebral Blood Flow & Metabolism,* 38**,** 1276-1292.

CVJETKOVIC, A., LÖTVALL, J. & LÄSSER, C. 2014. The influence of rotor type and centrifugation time on the yield and purity of extracellular vesicles. *Journal of Extracellular Vesicles,* 3**,** 23111.

DAI, S., WEI, D., WU, Z., ZHOU, X., WEI, X., HUANG, H. & LI, G. 2008. Phase I clinical trial of autologous ascites-derived exosomes combined with GM-CSF for colorectal cancer. *Molecular Therapy,* 16**,** 782-790.

DAI, W. L., ZHOU, A. G., ZHANG, H. & ZHANG, J. 2017. Efficacy of platelet-rich plasma in the treatment of knee osteoarthritis: A meta-analysis of randomized controlled trials. *Arthroscopy,* 33**,** 659-670.e1.

DAVIDSON, S. M., RIQUELME, J. A., TAKOV, K., VICENCIO, J. M., BOI-DOKU, C., KHOO, V., DORETH, C., RADENKOVIC, D., LAVANDERO, S. & YELLON, D. M. 2018a. Cardioprotection mediated by exosomes is impaired in the setting of type II diabetes but can be rescued by the use of non-diabetic exosomes in vitro. *Journal of Cellular and Molecular Medicine,* 22**,** 141-151.

DAVIDSON, S. M., RIQUELME, J. A., ZHENG, Y., VICENCIO, J. M., LAVANDERO, S. & YELLON, D. M. 2018b. Endothelial cells release cardioprotective exosomes that may contribute to ischaemic preconditioning. *Scientific Reports,* 8**,** 15885.

DAVIDSON, S. M. & YELLON, D. M. 2018. Exosomes and cardioprotection - A critical analysis. *Molecular Aspects of Medicine,* 60**,** 104-114.

DAVIES, N., DOBNER, S., BEZUIDENHOUT, D., SCHMIDT, C., BECK, M., ZISCH, A. H. & ZILLA, P. 2008. The dosage dependence of VEGF stimulation on scaffold neovascularisation. *Biomaterials,* 29**,** 3531-3538.

DAVIES, N. H., SCHMIDT, C., BEZUIDENHOUT, D. & ZILLA, P. 2011. Sustaining neovascularization of a scaffold through staged release of vascular endothelial growth factor-A and platelet-derived growth factor-BB. *Tissue Engineering Part A,* 18**,** 26-34.

DE GASSART, A., GÉMINARD, C., FÉVRIER, B., RAPOSO, G. & VIDAL, M. 2003. Lipid raft-associated protein sorting in exosomes. *Blood,* 102**,** 4336-4344.

DE MENEZES-NETO, A., SAEZ, M. J., LOZANO-RAMOS, I., SEGUI-BARBER, J., MARTIN-JAULAR, L., ULLATE, J. M., FERNANDEZ-BECERRA, C., BORRAS, F. E. & DEL PORTILLO, H. A. 2015. Size-

exclusion chromatography as a stand-alone methodology identifies novel markers in mass spectrometry analyses of plasma-derived vesicles from healthy individuals. *Journal of Extracellular Vesicles,* 4**,** 27378.

DEL FATTORE, A., LUCIANO, R., SARACINO, R., BATTAFARANO, G., RIZZO, C., PASCUCCI, L., ALESSANDRI, G., PESSINA, A., PERROTTA, A., FIERABRACCI, A. & MURACA, M. 2015. Differential effects of extracellular vesicles secreted by mesenchymal stem cells from different sources on glioblastoma cells. *Expert Opinion on Biological Therapy,* 15**,** 495-504.

DEREGIBUS, M. C., CANTALUPPI, V., CALOGERO, R., LO IACONO, M., TETTA, C., BIANCONE, L., BRUNO, S., BUSSOLATI, B. & CAMUSSI, G. 2007. Endothelial progenitor cell derived microvesicles activate an angiogenic program in endothelial cells by a horizontal transfer of mRNA. *Blood,* 110**,** 2440-8.

DEREGIBUS, M. C., FIGLIOLINI, F., D'ANTICO, S., MANZINI, P. M., PASQUINO, C., DE LENA, M., TETTA, C., BRIZZI, M. F. & CAMUSSI, G. 2016. Charge-based precipitation of extracellular vesicles. *International Journal of Molecular Medicine,* 38**,** 1359-1366.

DIAGNOSTICS, N. 2011. *Overview of Western Blotting* [Online]. USA. Available: https://www.nationaldiagnostics.com/electrophoresis/article/overview-western-blotting [Accessed 13 August 2019].

DOEPPNER, T. R., HERZ, J., GORGENS, A., SCHLECHTER, J., LUDWIG, A. K., RADTKE, S., DE MIROSCHEDJI, K., HORN, P. A., GIEBEL, B. & HERMANN, D. M. 2015. Extracellular vesicles improve post-stroke neuroregeneration and prevent postischemic immunosuppression. *Stem Cells Translational Medicine,* 4**,** 1131-43.

DOHAN EHRENFEST, D. M., RASMUSSON, L. & ALBREKTSSON, T. 2009. Classification of platelet concentrates: from pure platelet-rich plasma (P-PRP) to leucocyte- and platelet-rich fibrin (L-PRF). *Trends in Biotechnology,* 27**,** 158-67.

DONG, X., GAO, X., DAI, Y., RAN, N. & YIN, H. 2018. Serum exosomes can restore cellular function in vitro and be used for diagnosis in dysferlinopathy. *Theranostics,* 8**,** 1243.

DOYLE, L. M. & WANG, M. Z. 2019. Overview of extracellular vesicles, their origin, composition, purpose, and methods for exosome isolation and analysis. *Cells,* 8**,** 727.

EDGAR, J. R., EDEN, E. R. & FUTTER, C. E. 2014. Hrs- and CD63-dependent competing mechanisms make different sized endosomal intraluminal vesicles. *Traffic,* 15**,** 197-211.

EHRBAR, M., DJONOV, V. G., SCHNELL, C., TSCHANZ, S. A., MARTINY-BARON, G., SCHENK, U., WOOD, J., BURRI, P. H., HUBBELL, J. A. & ZISCH, A. H. 2004. Cell-demanded liberation of VEGF121 from fibrin implants induces local and controlled blood vessel growth. *Circulation Research,* 94**,** 1124-1132.

EITAN, E., ZHANG, S., WITWER, K. W. & MATTSON, M. P. 2015. Extracellular vesicle–depleted fetal bovine and human sera have reduced capacity to support cell growth. *Journal of Extracellular Vesicles,* 4**,** 26373.

EL-ANDALOUSSI, S., LEE, Y., LAKHAL-LITTLETON, S., LI, J., SEOW, Y., GARDINER, C., ALVAREZ-ERVITI, L., SARGENT, I. L. & WOOD, M. J. 2012. Exosome-mediated delivery of siRNA in vitro and in vivo. *Nature Protocols,* 7**,** 2112-26.

ENOKI, C., OTANI, H., SATO, D., OKADA, T., HATTORI, R. & IMAMURA, H. 2010. Enhanced mesenchymal cell engraftment by IGF-1 improves left ventricular function in rats undergoing myocardial infarction. *International Journal of Cardiology* 138**,** 9-18.

ESCUDIER, B., DORVAL, T., CHAPUT, N., ANDRÉ, F., CABY, M.-P., NOVAULT, S., FLAMENT, C., LEBOULAIRE, C., BORG, C. & AMIGORENA, S. 2005. Vaccination of metastatic melanoma patients with autologous dendritic cell (DC) derived-exosomes: results of thefirst phase I clinical trial. *Journal of Translational Medicine,* 3**,** 10.

ETULAIN, J., MENA, H. A., MEISS, R. P., FRECHTEL, G., GUTT, S., NEGROTTO, S. & SCHATTNER, M. 2018. An optimised protocol for platelet-rich plasma preparation to improve its angiogenic and regenerative properties. *Scientific Reports,* 8**,** 1513.

FARHAT, W., HASAN, A., LUCIA, L., BECQUART, F., AYOUB, A. & KOBEISSY, F. 2018. Hydrogels for advanced stem cell therapies: A biomimetic materials approach for enhancing natural tissue function. *IEEE Reviews in Biomedical Engineering,* 12**,** 333-351.

FEINGOLD, K. R. & GRUNFELD, C. 2018. Introduction to lipids and lipoproteins. *Endotext [https://www.ncbi.nlm.nih.gov/books/NBK305896/].* MDText. com, Inc.

FENG, D., ZHAO, W. L., YE, Y. Y., BAI, X. C., LIU, R. Q., CHANG, L. F., ZHOU, Q. & SUI, S. F. 2010. Cellular internalization of exosomes occurs through phagocytosis. *Traffic,* 11**,** 675-687.

FERNANDO, M. R., JIANG, C., KRZYZANOWSKI, G. D. & RYAN, W. L. 2017. New evidence that a large proportion of human blood plasma cell-free DNA is localized in exosomes. *Public Library of Science One,* 12**,** e0183915.

FITZSIMMONS, R. E., MAZUREK, M. S., SOOS, A. & SIMMONS, C. A. 2018. Mesenchymal stromal/stem cells in regenerative medicine and tissue engineering. *Stem Cells International,* 2018.

FOERS, A. D., CHATFIELD, S., DAGLEY, L. F., SCICLUNA, B. J., WEBB, A. I., CHENG, L., HILL, A. F., WICKS, I. P. & PANG, K. C. 2018. Enrichment of extracellular vesicles from human synovial fluid using size exclusion chromatography. *Journal of Extracellular Vesicles,* 7**,** 1490145.

FRANZEN, C. A., SIMMS, P. E., VAN HUIS, A. F., FOREMAN, K. E., KUO, P. C. & GUPTA, G. N. 2014. Characterization of uptake and internalization of exosomes by bladder cancer cells. *BioMed Research International,* 2014**,** 619829-619829.

FRIEDENSTEIN, A. J., GORSKAJA, J. & KULAGINA, N. 1976. Fibroblast precursors in normal and irradiated mouse hematopoietic organs. *Experimental Hematology,* 4**,** 267-274.

FUHRMANN, G., CHANDRAWATI, R., PARMAR, P. A., KEANE, T. J., MAYNARD, S. A., BERTAZZO, S. & STEVENS, M. M. 2018. Engineering extracellular vesicles with the tools of enzyme prodrug therapy. *Advanced Materials,* 30**,** 1706616.

GAMEZ-VALERO, A., MONGUIO-TORTAJADA, M., CARRERAS-PLANELLA, L., FRANQUESA, M., BEYER, K. & BORRAS, F. E. 2016. Size-exclusion chromatography-based isolation minimally alters extracellular vesicles' characteristics compared to precipitating agents. *Scientific Reports,* 6**,** 33641.

GARDINER, C., VIZIO, D. D., SAHOO, S., THÉRY, C., WITWER, K. W., WAUBEN, M. & HILL, A. F. 2016. Techniques used for the isolation and characterization of extracellular vesicles: results of a worldwide survey. *Journal of Extracellular Vesicles,* 5**,** 32945.

GATSON, N. N., WILLIAMS, J. L., POWELL, N. D., MCCLAIN, M. A., HENNON, T. R., ROBBINS, P. D. & WHITACRE, C. C. 2011. Induction of pregnancy during established EAE halts progression of CNS autoimmune injury via pregnancy-specific serum factors. *Journal of Neuroimmunology,* 230**,** 105-113.

GENTILE, P., GARCOVICH, S., BIELLI, A., SCIOLI, M. G., ORLANDI, A. & CERVELLI, V. 2015. The effect of platelet-rich plasma in hair regrowth: A randomized placebo-controlled trial. *Stem Cells Translational Medicine,* 4**,** 1317-23.

GERCEL-TAYLOR, C., ATAY, S., TULLIS, R. H., KESIMER, M. & TAYLOR, D. D. 2012. Nanoparticle analysis of circulating cell-derived vesicles in ovarian cancer patients. *Analytical Biochemistry,* 428**,** 44-53.

GERHARDT, H. 2008. VEGF and endothelial guidance in angiogenic sprouting. *Organogenesis,* 4**,** 241-246.

GERMAIN, R. N. & MARGULIES, D. H. 1993. The biochemistry and cell biology of antigen processing and presentation. *Annual Review of Immunology,* 11**,** 403-450.

GERMAN, J. B., SMILOWITZ, J. T. & ZIVKOVIC, A. M. 2006. Lipoproteins: When size really matters. *Current Opinion in Colloid & Interface Science,* 11**,** 171-183.

GHAI, V., KIM, T.-K., ETHERIDGE, A., NIELSEN, T., HANSEN, T., PEDERSEN, O., GALAS, D. & WANG, K. 2019. Extracellular vesicle encapsulated microRNAs in patients with type 2 diabetes are affected by metformin treatment. *Journal of Clinical Medicine,* 8**,** 617.

GIORDANO, S., ROMEO, M., DI SUMMA, P., SALVAL, A. & LANKINEN, P. 2018. A meta-analysis on evidence of platelet-rich plasma for androgenetic alopecia. *International Journal of Trichology,* 10**,** 1-10.

GOETSCH, K. P., BRACHER, M., BEZUIDENHOUT, D., ZILLA, P. & DAVIES, N. H. 2015. Regulation of tissue ingrowth into proteolytically degradable hydrogels. *Acta Biomater,* 24**,** 44-52.

GOETZL, E. J., GOETZL, L., KARLINER, J. S., TANG, N. & PULLIAM, L. 2016. Human plasma platelet-derived exosomes: effects of aspirin. *The Federation of American Societies for Experimental Biology Journal,* 30**,** 2058-2063.

GONG, M., YU, B., WANG, J., WANG, Y., LIU, M., PAUL, C., MILLARD, R. W., XIAO, D.-S., ASHRAF, M. & XU, M. 2017. Mesenchymal stem cells release exosomes that transfer miRNAs to endothelial cells and promote angiogenesis. *Oncotarget,* 8**,** 45200-45212.

GREENING, D. W., XU, R., JI, H., TAURO, B. J. & SIMPSON, R. J. 2015. A protocol for exosome isolation and characterization: evaluation of ultracentrifugation, density-gradient separation, and immunoaffinity capture methods. *Proteomic Profiling.* Springer.

GRIGOR'EVA, A., DYRKHEEVA, N., BRYZGUNOVA, O., TAMKOVICH, S., CHELOBANOV, B. & RYABCHIKOVA, E. 2017. Contamination of exosome preparations, isolated from biological fluids. *Biochemistry (Moscow), Supplement Series B: Biomedical Chemistry,* 11**,** 265-271.

GUDURIC-FUCHS, J., O'CONNOR, A., CAMP, B., O'NEILL, C. L., MEDINA, R. J. & SIMPSON, D. A. 2012. Selective extracellular vesicle-mediated export of an overlapping set of microRNAs from multiple cell types. *BMC Genomics,* 13**,** 357.

GUO, S.-C., TAO, S.-C., YIN, W.-J., QI, X., YUAN, T. & ZHANG, C.-Q. 2017. Exosomes derived from platelet-rich plasma promote the re-epithelization of chronic cutaneous wounds via activation of YAP in a diabetic rat model. *Theranostics,* 7**,** 81.

GURUNATHAN, S., KANG, M.-H., JEYARAJ, M., QASIM, M. & KIM, J.-H. 2019. Review of the isolation, characterization, biological function, and multifarious therapeutic approaches of exosomes. *Cells,* 8**,** 307.

GUTKIN, A., UZIEL, O., BEERY, E., NORDENBERG, J., PINCHASI, M., GOLDVASER, H., HENICK, S., GOLDBERG, M. & LAHAV, M. 2016. Tumor cells derived exosomes contain hTERT mRNA and transform nonmalignant fibroblasts into telomerase positive cells. *Oncotarget,* 7**,** 59173.

GYORGY, B., PALOCZI, K., KOVACS, A., BARABAS, E., BEKO, G., VARNAI, K., PALLINGER, E., SZABO-TAYLOR, K., SZABO, T. G., KISS, A. A., FALUS, A. & BUZAS, E. I. 2014. Improved circulating microparticle analysis in acid-citrate dextrose (ACD) anticoagulant tube. *Thrombosis Research,* 133**,** 285-92.

HAN, C., ZHOU, J., LIU, B., LIANG, C., PAN, X., ZHANG, Y., ZHANG, Y., WANG, Y., SHAO, L., ZHU, B., WANG, J., YIN, Q., YU, X.-Y. & LI, Y. 2019. Delivery of miR-675 by stem cell-derived exosomes encapsulated in silk fibroin hydrogel prevents aging-induced vascular dysfunction in mouse hindlimb. *Materials Science and Engineering: C,* 99**,** 322-332.

HANNAFON, B. N., GIN, A. L., XU, Y.-F., BRUNS, M., CALLOWAY, C. L. & DING, W.-Q. 2019. Metastasis-associated protein 1 (MTA1) is transferred by exosomes and contributes to the regulation of hypoxia and estrogen signaling in breast cancer cells. *Cell Communication and Signaling,* 17**,** 13.

HANNAFON, B. N., TRIGOSO, Y. D., CALLOWAY, C. L., ZHAO, Y. D., LUM, D. H., WELM, A. L., ZHAO, Z. J., BLICK, K. E., DOOLEY, W. C. & DING, W. Q. 2016. Plasma exosome microRNAs are indicative of breast cancer. *Breast Cancer Res,* 18**,** 90.

HANTGAN, R. R., TAYLOR, R. G. & LEWIS, J. C. 1985. Platelets interact with fibrin only after activation. *Blood,* 65**,** 1299-1311.

HARASZTI, R. A., DIDIOT, M. C., SAPP, E., LESZYK, J., SHAFFER, S. A., ROCKWELL, H. E., GAO, F., NARAIN, N. R., DIFIGLIA, M., KIEBISH, M. A., ARONIN, N. & KHVOROVA, A. 2016. High-resolution proteomic and lipidomic analysis of exosomes and microvesicles from different cell sources. *Journal of Extracellular Vesicles,* 5**,** 32570.

HARDING, C., HEUSER, J. & STAHL, P. 1984. Endocytosis and intracellular processing of transferrin and colloidal gold-transferrin in rat reticulocytes: demonstration of a pathway for receptor shedding. *European Journal of Cell Biology,* 35**,** 256-263.

HARP, D., DRISS, A., MEHRABI, S., CHOWDHURY, I., XU, W., LIU, D., GARCIA-BARRIO, M., TAYLOR, R. N., GOLD, B., JEFFERSON, S., SIDELL, N. & THOMPSON, W. 2016. Exosomes derived from endometriotic stromal cells have enhanced angiogenic effects in vitro. *Cell and Tissue Research,* 365**,** 187-196.

HASHEMI, S. & RAFATI, A. 2016. Comparison between human cord blood serum and platelet-rich plasma supplementation for Human Wharton's Jelly Stem Cells and dermal fibroblasts culture. *Health Sciences,* 5**,** 191-196.

HEATH, N., GRANT, L., OLIVEIRA, T. M., ROWLINSON, R., OSTEIKOETXEA, X., DEKKER, N. & OVERMAN, R. 2018. Rapid isolation and enrichment of extracellular vesicle preparations using anion exchange chromatography. *Scientific Reports,* 8**,** 5730.

HEIJNEN, H. F., SCHIEL, A. E., FIJNHEER, R., GEUZE, H. J. & SIXMA, J. J. 1999. Activated platelets release two types of membrane vesicles: Microvesicles by surface shedding and exosomes derived from exocytosis of multivesicular bodies and alpha-granules. *Blood,* 94**,** 3791-3799.

HEISS, M., HELLSTROM, M., KALEN, M., MAY, T., WEBER, H., HECKER, M., AUGUSTIN, H. G. & KORFF, T. 2015. Endothelial cell spheroids as a versatile tool to study angiogenesis in vitro. *The FASEB Journal,* 29**,** 3076-84.

HOEFNER, D. M., HODEL, S. D., O'BRIEN, J. F., BRANUM, E. L., SUN, D., MEISSNER, I. & MCCONNELL, J. P. 2001. Development of a rapid, quantitative method for LDL subfractionation with use of the Quantimetrix Lipoprint LDL System. *Clinical Chemistry,* 47**,** 266-274.

HOFFMAN, A. S. 2002. Hydrogels for biomedical applications. *Advanced Drug Delivery Reviews,* 54**,** 3-12.

HOLME, I., AASTVEIT, A. H., HAMMAR, N., JUNGNER, I. & WALLDIUS, G. 2009. Lipoprotein components and risk of congestive heart failure in 84 740 men and women in the Apolipoprotein MOrtality RISk study (AMORIS). *European Journal of Heart Failure,* 11**,** 1036-1042.

HOLNESS, C. L. & SIMMONS, D. L. 1993. Molecular cloning of CD68, a human macrophage marker related to lysosomal glycoproteins. *Blood,* 81**,** 1607-13.

HONG, C.-S., FUNK, S., MULLER, L., BOYIADZIS, M. & WHITESIDE, T. L. 2016. Isolation of biologically active and morphologically intact exosomes from plasma of patients with cancer. *Journal of Extracellular Vesicles,* 5**,** 29289.

HONG, P., KOZA, S. & BOUVIER, E. S. P. 2012. Size-exclusion chromatography for the analysis of protein biotherapeutics and their aggregates. *Journal of Liquid Chromatography & Related Technologies,* 35**,** 2923-2950.

HOSSEINI-BEHESHTI, E., CHOI, W., WEISWALD, L.-B., KHARMATE, G., GHAFFARI, M., ROSHAN-MONIRI, M., HASSONA, M. D., CHAN, L., CHIN, M. Y., TAI, I. T., RENNIE, P. S., FAZLI, L. & TOMLINSON GUNS, E. S. 2016. Exosomes confer pro-survival signals to alter the phenotype of prostate cells in their surrounding environment. *Oncotarget,* 7**,** 14639-14658.

HU, Y., RAO, S.-S., WANG, Z.-X., CAO, J., TAN, Y.-J., LUO, J., LI, H.-M., ZHANG, W.-S., CHEN, C.-Y. & XIE, H. 2018. Exosomes from human umbilical cord blood accelerate cutaneous wound healing through miR-21-3p-mediated promotion of angiogenesis and fibroblast function. *Theranostics,* 8**,** 169.

HUANG, C., FISHER, K. P., HAMMER, S. S., NAVITSKAYA, S., BLANCHARD, G. J. & BUSIK, J. V. 2018. Plasma exosomes contribute to microvascular damage in diabetic retinopathy by activating the classical complement pathway. *Diabetes,* 67**,** 1639-1649.

HUANG, L., MA, W., MA, Y., FENG, D., CHEN, H. & CAI, B. 2015. Exosomes in mesenchymal stem cells, a new therapeutic strategy for cardiovascular diseases? *International Journal of Biological Sciences,* 11**,** 238-245.

HUANG, T. & DENG, C.-X. 2019. Current progresses of exosomes as cancer diagnostic and prognostic biomarkers. *International Journal of Biological Sciences,* 15**,** 1-11.

HUNTER, M. P., ISMAIL, N., ZHANG, X., AGUDA, B. D., LEE, E. J., YU, L., XIAO, T., SCHAFER, J., LEE, M.-L. T., SCHMITTGEN, T. D., NANA-SINKAM, S. P., JARJOURA, D. & MARSH, C. B. 2008. Detection of microRNA expression in human peripheral blood microvesicles. *Public Library of Science One,* 3**,** e3694-e3694.

HURLEY, J. H. 2010. The ESCRT complexes. *Critical Reviews in Biochemistry and Molecular Biology,* 45**,** 463-487.

HURWITZ, S. N., NKOSI, D., CONLON, M. M., YORK, S. B., LIU, X., TREMBLAY, D. C. & MECKES, D. G. 2017. CD63 regulates epstein-barr virus LMP1 exosomal packaging, enhancement of vesicle production, and noncanonical NF-κB signaling. *Journal of Virology,* 91**,** e02251-16.

HUSSAIN, M. M., MAXFIELD, F., MAS-OLIVA, J., TABAS, I., JI, Z.-S., INNERARITY, T. & MAHLEY, R. 1991. Clearance of chylomicron remnants by the low density lipoprotein receptor-related protein/alpha 2-macroglobulin receptor. *Journal of Biological Chemistry,* 266**,** 13936-13940.

HUYNH, K., MCMULLEN, J. R., JULIUS, T. L., TAN, J. W., LOVE, J. E., CEMERLANG, N., KIRIAZIS, H., DU, X. J. & RITCHIE, R. H. 2010. Cardiac-specific IGF-1 receptor transgenic expression protects against cardiac fibrosis and diastolic dysfunction in a mouse model of diabetic cardiomyopathy. *Diabetes,* 59**,** 1512-20.

IAVELLO, A., FRECH, V. S., GAI, C., DEREGIBUS, M. C., QUESENBERRY, P. J. & CAMUSSI, G. 2016. Role of Alix in miRNA packaging during extracellular vesicle biogenesis. *International Journal of Molecular Medicine,* 37**,** 958-966.

IBRAHIM, A. & MARBÁN, E. 2016. Exosomes: fundamental biology and roles in cardiovascular physiology. *Annual Review of Physiology,* 78**,** 67-83.

IBRAHIM, A. G., CHENG, K. & MARBAN, E. 2014. Exosomes as critical agents of cardiac regeneration triggered by cell therapy. *Stem Cell Reports,* 2**,** 606-19.

IRVIN, M. W., ZIJLSTRA, A., WIKSWO, J. P. & POZZI, A. 2014. Techniques and assays for the study of angiogenesis. *Experimental Biology and Medicine (Maywood, N.J.),* 239**,** 1476-1488.

JABALEE, J., TOWLE, R. & GARNIS, C. 2018. The role of extracellular vesicles in cancer: Cargo, function, and therapeutic implications. *Cells,* 7**,** 93.

JAMALY, S., RAMBERG, C., OLSEN, R., LATYSHEVA, N., WEBSTER, P., SOVERSHAEV, T., BRÆKKAN, S. K. & HANSEN, J.-B. 2018. Impact of preanalytical conditions on plasma concentration and size distribution of extracellular vesicles using Nanoparticle Tracking Analysis. *Scientific Reports,* 8**,** 17216-17216.

JANMEY, P. A., WINER, J. P. & WEISEL, J. W. 2009. Fibrin gels and their clinical and bioengineering applications. *Journal of the Royal Society Interface,* 6**,** 1-10.

JEON, O., RYU, S. H., CHUNG, J. H. & KIM, B.-S. 2005. Control of basic fibroblast growth factor release from fibrin gel with heparin and concentrations of fibrinogen and thrombin. *Journal of Controlled Release,* 105**,** 249-259.

JIA, H.-L., LIU, C.-W., ZHANG, L., XU, W.-J., GAO, X.-J., BAI, J., XU, Y.-F., XU, M.-G. & ZHANG, G. 2017. Sets of serum exosomal microRNAs as candidate diagnostic biomarkers for Kawasaki disease. *Scientific Reports,* 7**,** 44706.

JIA, L., ZHOU, X., HUANG, X., XU, X., JIA, Y., WU, Y., YAO, J., WU, Y. & WANG, K. 2018. Maternal and umbilical cord serum–derived exosomes enhance endothelial cell proliferation and migration. *The Federation of American Societies for Experimental Biology Journal***,** fj. 201701337RR.

JOHNSTONE, R. M. 1992. The Jeanne Manery-Fisher memorial lecture 1991. Maturation of reticulocytes: formation of exosomes as a mechanism for shedding membrane proteins. *Biochemistry and Cell Biology,* 70**,** 179-90.

JOHNSTONE, R. M., ADAM, M., HAMMOND, J., ORR, L. & TURBIDE, C. 1987. Vesicle formation during reticulocyte maturation. Association of plasma membrane activities with released vesicles (exosomes). *Journal of Biological Chemistry,* 262**,** 9412-9420.

JUNKER, A., KRUMBHOLZ, M., EISELE, S., MOHAN, H., AUGSTEIN, F., BITTNER, R., LASSMANN, H., WEKERLE, H., HOHLFELD, R. & MEINL, E. 2009. MicroRNA profiling of multiple sclerosis lesions identifies modulators of the regulatory protein CD47. *Brain,* 132**,** 3342-3352.

KALANI, A., CHATURVEDI, P., KAMAT, P. K., MALDONADO, C., BAUER, P., JOSHUA, I. G., TYAGI, S. C. & TYAGI, N. 2016. Curcumin-loaded embryonic stem cell exosomes restored neurovascular unit following ischemia-reperfusion injury. *The International Journal of Biochemistry & Cell Biology,* 79**,** 360-369.

KALRA, H., ADDA, C. G., LIEM, M., ANG, C. S., MECHLER, A., SIMPSON, R. J., HULETT, M. D. & MATHIVANAN, S. 2013. Comparative proteomics evaluation of plasma exosome isolation techniques and assessment of the stability of exosomes in normal human blood plasma. *Proteomics,* 13**,** 3354-3364.

KANWAR, S. S., DUNLAY, C. J., SIMEONE, D. M. & NAGRATH, S. 2014. Microfluidic device (ExoChip) for on-chip isolation, quantification and characterization of circulating exosomes. *Lab on a Chip,* 14**,** 1891-1900.

KAPLAN, D. R., CHAO, F. C., STILES, C. D., ANTONIADES, H. N. & SCHER, C. D. 1979. Platelet alpha granules contain a growth factor for fibroblasts. *Blood,* 53**,** 1043-1052.

KAR, B. R. & RAJ, C. 2017. Fractional CO2 laser vs fractional CO2 with topical platelet-rich plasma in the treatment of acne scars: A split-face comparison trial. *Journal of Cutaneous and Aesthetic Surgery,* 10**,** 136-144.

KAREY, K. P. & SIRBASKU, D. A. 1989. Human platelet-derived mitogens. II. Subcellular localization of insulinlike growth factor I to the alpha-granule and release in response to thrombin. *Blood,* 74**,** 1093-1100.

KARIMI, N., CVJETKOVIC, A., JANG, S. C., CRESCITELLI, R., FEIZI, M. A. H., NIEUWLAND, R., LÖTVALL, J. & LÄSSER, C. 2018. Detailed analysis of the plasma extracellular vesicle proteome after separation from lipoproteins. *Cellular and Molecular Life Sciences***,** 1-14.

KARTTUNEN, J., HEISKANEN, M., NAVARRO-FERRANDIS, V., DAS GUPTA, S., LIPPONEN, A., PUHAKKA, N., RILLA, K., KOISTINEN, A. & PITKÄNEN, A. 2018. Precipitation-based extracellular vesicle isolation from rat plasma co-precipitate vesicle-free microRNAs. *Journal of Extracellular Vesicles,* 8**,** 1555410-1555410.

KATAKOWSKI, M., BULLER, B., ZHENG, X., LU, Y., ROGERS, T., OSOBAMIRO, O., SHU, W., JIANG, F. & CHOPP, M. 2013. Exosomes from marrow stromal cells expressing miR-146b inhibit glioma growth. *Cancer Letters,* 335**,** 201-204.

KATSUDA, T., TSUCHIYA, R., KOSAKA, N., YOSHIOKA, Y., TAKAGAKI, K., OKI, K., TAKESHITA, F., SAKAI, Y., KURODA, M. & OCHIYA, T. 2013. Human adipose tissue-derived mesenchymal stem cells secrete functional neprilysin-bound exosomes. *Scientific Reports,* 3**,** 1197.

KHALYFA, A., ALMENDROS, I., GILELES-HILLEL, A., AKBARPOUR, M., TRZEPIZUR, W., MOKHLESI, B., HUANG, L., ANDRADE, J., FARRÉ, R. & GOZAL, D. 2016. Circulating exosomes potentiate tumor malignant properties in a mouse model of chronic sleep fragmentation. *Oncotarget,* 7**,** 54676-54690.

KHAN, M., NICKOLOFF, E., ABRAMOVA, T., JOHNSON, J., VERMA, S. K., KRISHNAMURTHY, P., MACKIE, A. R., VAUGHAN, E., GARIKIPATI, V. N., BENEDICT, C., RAMIREZ, V., LAMBERS, E., ITO, A., GAO, E., MISENER, S., LUONGO, T., ELROD, J., QIN, G., HOUSER, S. R., KOCH, W. J. & KISHORE, R. 2015. Embryonic stem cell-derived exosomes promote endogenous repair mechanisms and enhance cardiac function following myocardial infarction. *Circulation Research,* 117**,** 52-64.

KIM, J., INOUE, K., ISHII, J., VANTI, W. B., VORONOV, S. V., MURCHISON, E., HANNON, G. & ABELIOVICH, A. 2007. A MicroRNA feedback circuit in midbrain dopamine neurons. *Science,* 317**,** 1220-1224.

KIRAZOV, L. P., VENKOV, L. G. & KIRAZOV, E. P. 1993. Comparison of the Lowry and the Bradford protein assays as applied for protein estimation of membrane-containing fractions. *Analytical Biochemistry,* 208**,** 44-8.

KNIPPING, G., ROTHENEDER, M., STRIEGL, G. & ESTERBAUER, H. 1990. Antioxidants and resistance against oxidation of porcine LDL subfractions. *Journal of Lipid Research,* 31**,** 1965-1972.

KOH, Y. Q., ALMUGHLLIQ, F. B., VASWANI, K., PEIRIS, H. N. & MITCHELL, M. D. 2018. Exosome enrichment by ultracentrifugation and size exclusion chromatography. *Frontiers in Bioscience (Landmark Edition),* 23**,** 865-874.

KOL, N., TSVITOV, M., HEVRONI, L., WOLF, S. G., PANG, H. B., KAY, M. S. & ROUSSO, I. 2010. The effect of purification method on the completeness of the immature HIV-1 Gag shell. *Journal of Virological Methods* 169**,** 244-7.

KON, E., FILARDO, G., DI MARTINO, A. & MARCACCI, M. 2011. Platelet-rich plasma (PRP) to treat sports injuries: evidence to support its use. *Knee Surgery, Sports Traumatology, Arthroscopy,* 19**,** 516-527.

KONADU, K. A., HUANG, M. B., ROTH, W., ARMSTRONG, W., POWELL, M., VILLINGER, F. & BOND, V. 2016. Isolation of exosomes from the plasma of HIV-1 positive individuals. *Journal of Visualized Experiments: JoVE*.

KONALA, V. B. R., MAMIDI, M. K., BHONDE, R., DAS, A. K., POCHAMPALLY, R. & PAL, R. 2016. The current landscape of the mesenchymal stromal cell secretome: a new paradigm for cell-free regeneration. *Cytotherapy,* 18**,** 13-24.

KONOSHENKO, M. Y., LEKCHNOV, E. A., VLASSOV, A. V. & LAKTIONOV, P. P. 2018. Isolation of extracellular vesicles: General methodologies and latest trends. *BioMed Research International,* 2018.

KOOIJMANS, S. A., STREMERSCH, S., BRAECKMANS, K., DE SMEDT, S. C., HENDRIX, A., WOOD, M. J., SCHIFFELERS, R. M., RAEMDONCK, K. & VADER, P. 2013. Electroporation-induced siRNA precipitation obscures the efficiency of siRNA loading into extracellular vesicles. *Journal of Controlled Release,* 172**,** 229-238.

KORFF, T. & AUGUSTIN, H. G. 1998. Integration of endothelial cells in multicellular spheroids prevents apoptosis and induces differentiation. *The Journal of Cell Biology,* 143**,** 1341-1352.

KORFF, T. & AUGUSTIN, H. G. 1999. Tensional forces in fibrillar extracellular matrices control directional capillary sprouting. *Journal of Cell Science,* 112 (Pt 19)**,** 3249-58.

KOSAKA, N., IGUCHI, H., HAGIWARA, K., YOSHIOKA, Y., TAKESHITA, F. & OCHIYA, T. 2013. Neutral sphingomyelinase 2 (nSMase2)-dependent exosomal transfer of angiogenic microRNAs regulate cancer cell metastasis. *Journal of Biological Chemistry,* 288**,** 10849-59.

KOTRBOVA, A., STEPKA, K., MASKA, M., PALENIK, J. J., ILKOVICS, L., KLEMOVA, D., KRAVEC, M., HUBATKA, F., DAVE, Z., HAMPL, A., BRYJA, V., MATULA, P. & POSPICHALOVA, V. 2019. TEM ExosomeAnalyzer: a computer-assisted software tool for quantitative evaluation of extracellular vesicles in transmission electron microscopy images. *Journal of Extracellular Vesicles,* 8**,** 1560808.

KOWAL, J., ARRAS, G., COLOMBO, M., JOUVE, M., MORATH, J. P., PRIMDAL-BENGTSON, B., DINGLI, F., LOEW, D., TKACH, M. & THÉRY, C. 2016. Proteomic comparison defines novel markers to characterize heterogeneous populations of extracellular vesicle subtypes. *Proceedings of the National Academy of Sciences of the United States of America,* 113**,** E968-E977.

KOWAL, J., TKACH, M. & THÉRY, C. 2014. Biogenesis and secretion of exosomes. *Current Opinion in Cell Biology,* 29**,** 116-125.

KRAFFT, C., WILHELM, K., EREMIN, A., NESTEL, S., VON BUBNOFF, N., SCHULTZE-SEEMANN, W., POPP, J. & NAZARENKO, I. 2017. A specific spectral signature of serum and plasma-derived extracellular vesicles for cancer screening. *Nanomedicine: Nanotechnology, Biology and Medicine,* 13**,** 835-841.

LAI, R. C., ARSLAN, F., LEE, M. M., SZE, N. S., CHOO, A., CHEN, T. S., SALTO-TELLEZ, M., TIMMERS, L., LEE, C. N., EL OAKLEY, R. M., PASTERKAMP, G., DE KLEIJN, D. P. & LIM, S. K. 2010. Exosome secreted by MSC reduces myocardial ischemia/reperfusion injury. *Stem Cell Research,* 4**,** 214-22.

LAI, R. C. & LIM, S. K. 2019. Membrane lipids define small extracellular vesicle subtypes secreted by mesenchymal stromal cells. *Journal of Lipid Research,* 60**,** 318-322.

LAI, R. C., TAN, S. S., TEH, B. J., SZE, S. K., ARSLAN, F., DE KLEIJN, D. P., CHOO, A. & LIM, S. K. 2012. Proteolytic potential of the MSC exosome proteome: Implications for an exosome-mediated delivery of therapeutic proteasome. *International Journal of Proteomics,* 2012**,** 971907.

LAI, R. C., TAN, S. S., YEO, R. W. Y., CHOO, A. B. H., REINER, A. T., SU, Y., SHEN, Y., FU, Z., ALEXANDER, L. & SZE, S. K. 2016. MSC secretes at least 3 EV types each with a unique permutation of membrane lipid, protein and RNA. *Journal of Extracellular Vesicles,* 5**,** 29828.

LAMICHHANE, T. N., RAIKER, R. S. & JAY, S. M. 2015. Exogenous DNA loading into extracellular vesicles via electroporation is size-dependent and enables limited gene delivery. *Molecular Pharmaceutics,* 12**,** 3650-3657.

LEBERMAN, R. 1966. The isolation of plant viruses by means of “simple” coacervates. *Virology,* 30**,** 341-347.

LEE, J.-K., PARK, S.-R., JUNG, B.-K., JEON, Y.-K., LEE, Y.-S., KIM, M.-K., KIM, Y.-G., JANG, J.-Y. & KIM, C.-W. 2013. Exosomes derived from mesenchymal stem cells suppress angiogenesis by down-regulating VEGF expression in breast cancer cells. *Public Library of Science One,* 8**,** e84256.

LEE, J. W., KIM, B. J., KIM, M. N. & MUN, S. K. 2011. The efficacy of autologous platelet rich plasma combined with ablative carbon dioxide fractional resurfacing for acne scars: a simultaneous split-face trial. *Dermatologic Surgery,* 37**,** 931-8.

LEE, M., BAN, J.-J., IM, W. & KIM, M. 2016. Influence of storage condition on exosome recovery. *Biotechnology and Bioprocess Engineering,* 21**,** 299-304.

LEI, Y., HUANG, S., SHARIF-KASHANI, P., CHEN, Y., KAVEHPOUR, P. & SEGURA, T. 2010. Incorporation of active DNA/cationic polymer polyplexes into hydrogel scaffolds. *Biomaterials,* 31**,** 9106-9116.

LESZCZYNSKA, A., KULKARNI, M., LJUBIMOV, A. V. & SAGHIZADEH, M. 2018. Exosomes from normal and diabetic human corneolimbal keratocytes differentially regulate migration, proliferation and marker expression of limbal epithelial cells. *Scientific Reports,* 8**,** 15173.

LEW, M. 2007. Good statistical practice in pharmacology Problem 2. *British Journal of Pharmacology,* 152**,** 299-303.

LI, D.-B., LIU, J.-L., WANG, W., LUO, X.-M., ZHOU, X., LI, J.-P., CAO, X.-L., LONG, X.-H., CHEN, J.-G. & QIN, C. 2018a. Plasma Exosomal miRNA-122-5p and miR-300-3p as Potential Markers for Transient Ischaemic Attack in Rats. *Frontiers in Aging Neuroscience,* 10.

LI, H., LIAO, Y., GAO, L., ZHUANG, T., HUANG, Z., ZHU, H. & GE, J. 2018b. Coronary serum exosomes derived from patients with myocardial ischemia regulate angiogenesis through the miR-939-mediated nitric oxide signaling pathway. *Theranostics,* 8**,** 2079.

LI, J., CHEN, X., YI, J., LIU, Y., LI, D., WANG, J., HOU, D., JIANG, X., ZHANG, J. & WANG, J. 2016a. Identification and characterization of 293T cell-derived exosomes by profiling the protein, mRNA and microRNA components. *Public Library of Science One,* 11**,** e0163043.

LI, J., LEE, Y., JOHANSSON, H. J., MÄGER, I., VADER, P., NORDIN, J. Z., WIKLANDER, O. P. B., LEHTIÖ, J., WOOD, M. J. A. & ANDALOUSSI, S. E. 2015. Serum-free culture alters the quantity and protein composition of neuroblastoma-derived extracellular vesicles. *Journal of Extracellular Vesicles,* 4**,** 26883-26883.

LI, J. & MOONEY, D. J. 2016. Designing hydrogels for controlled drug delivery. *Nature Reviews Materials,* 1**,** 16071.

LI, J., TAN, M., XIANG, Q., ZHOU, Z. & YAN, H. 2017a. Thrombin-activated platelet-derived exosomes regulate endothelial cell expression of ICAM-1 via microRNA-223 during the thrombosis-inflammation response. *Thrombosis Research,* 154**,** 96-105.

LI, M., KE, Q.-F., TAO, S.-C., GUO, S.-C., RUI, B.-Y. & GUO, Y.-P. 2016b. Fabrication of hydroxyapatite/chitosan composite hydrogels loaded with exosomes derived from miR-126-3p overexpressed synovial mesenchymal stem cells for diabetic chronic wound healing. *Journal of Materials Chemistry B,* 4**,** 6830-6841.

LI, P., KASLAN, M., LEE, S. H., YAO, J. & GAO, Z. 2017b. Progress in exosome isolation techniques. *Theranostics,* 7**,** 789.

LI, P., LIU, Z., XIE, Y., GU, H., DAI, Q., YAO, J. & ZHOU, L. 2018c. Serum exosomes attenuate H2O2-induced apoptosis in rat H9C2 cardiomyocytes via ERK1/2. *Journal of Cardiovascular Translational Research***,** 1-8.

LI, T., YAN, Y., WANG, B., QIAN, H., ZHANG, X., SHEN, L., WANG, M., ZHOU, Y., ZHU, W., LI, W. & XU, W. 2013. Exosomes derived from human umbilical cord mesenchymal stem cells alleviate liver fibrosis. *Stem Cells and Development,* 22**,** 845-854.

LI, Z., MA, Y. Y., WANG, J., ZENG, X. F., LI, R., KANG, W. & HAO, X. K. 2016c. Exosomal microRNA-141 is upregulated in the serum of prostate cancer patients. *OncoTargets and Therapy,* 9**,** 139-48.

LIANG, B., PENG, P., CHEN, S., LI, L., ZHANG, M., CAO, D., YANG, J., LI, H., GUI, T. & LI, X. 2013. Characterization and proteomic analysis of ovarian cancer-derived exosomes. *Journal of Proteomics,* 80**,** 171-182.

LIGA, A., VLIEGENTHART, A., OOSTHUYZEN, W., DEAR, J. & KERSAUDY-KERHOAS, M. 2015. Exosome isolation: a microfluidic road-map. *Lab on a Chip,* 15**,** 2388-2394.

LIN, K.-Y., YANG, C.-C., HSU, C.-J., YEH, M.-L. & RENN, J.-H. 2019. Intra-articular injection of platelet-rich plasma is superior to hyaluronic acid or saline solution in the treatment of mild to moderate knee osteoarthritis: A randomized, double-blind, triple-parallel, placebo-controlled clinical trial. *Arthroscopy: The Journal of Arthroscopic & Related Surgery,* 35**,** 106-117.

LIN, Y., WU, J., GU, W., HUANG, Y., TONG, Z., HUANG, L. & TAN, J. 2018. Exosome–liposome hybrid nanoparticles deliver CRISPR/Cas9 system in MSCs. *Advanced Science,* 5**,** 1700611.

LIU, H., CHEN, L., PENG, Y., YU, S., LIU, J., WU, L., ZHANG, L., WU, Q., CHANG, X., YU, X. & LIU, T. 2017a. Dendritic cells loaded with tumor derived exosomes for cancer immunotherapy. *Oncotarget,* 9**,** 2887-2894.

LIU, J., YELLON, D. M. & DAVIDSON, S. M. 2015. Evaluating early and delayed cardioprotection by plasma exosomes in simulated ischaemia–reperfusion injury. *Bioscience Horizons,* 8**,** hzv001.

LIU, X., HOENE, M., WANG, X., YIN, P., HÄRING, H.-U., XU, G. & LEHMANN, R. 2018a. Serum or plasma, what is the difference? Investigations to facilitate the sample material selection decision making process for metabolomics studies and beyond. *Analytica Chimica Acta,* 1037**,** 293-300.

LIU, X., YANG, Y., LI, Y., NIU, X., ZHAO, B., WANG, Y., BAO, C., XIE, Z., LIN, Q. & ZHU, L. 2017b. Integration of stem cell-derived exosomes with in situ hydrogel glue as a promising tissue patch for articular cartilage regeneration. *Nanoscale,* 9**,** 4430-4438.

LIU, Z., ZHANG, Z., YAO, J., XIE, Y., DAI, Q., ZHANG, Y. & ZHOU, L. 2018b. Serum extracellular vesicles promote proliferation of H9C2 cardiomyocytes by increasing miR-17-3p. *Biochemical and Biophysical Research Communications,* 499**,** 441-446.

LLORENTE, A., SKOTLAND, T., SYLVÄNNE, T., KAUHANEN, D., RÓG, T., ORŁOWSKI, A., VATTULAINEN, I., EKROOS, K. & SANDVIG, K. 2013. Molecular lipidomics of exosomes released by PC-3 prostate cancer cells. *Biochimica et Biophysica Acta-Molecular and Cell Biology of Lipids,* 1831**,** 1302-1309.

LOBB, R. J., BECKER, M., WEN WEN, S., WONG, C. S., WIEGMANS, A. P., LEIMGRUBER, A. & MÖLLER, A. 2015. Optimized exosome isolation protocol for cell culture supernatant and human plasma. *Journal of Extracellular Vesicles,* 4**,** 27031.

LOGOZZI, M., DE MILITO, A., LUGINI, L., BORGHI, M., CALABRO, L., SPADA, M., PERDICCHIO, M., MARINO, M. L., FEDERICI, C., IESSI, E., BRAMBILLA, D., VENTURI, G., LOZUPONE, F., SANTINAMI, M., HUBER, V., MAIO, M., RIVOLTINI, L. & FAIS, S. 2009. High levels of exosomes expressing CD63 and caveolin-1 in plasma of melanoma patients. *Public Library of Science One,* 4**,** e5219.

LOOZE, C., YUI, D., LEUNG, L., INGHAM, M., KALER, M., YAO, X., WU, W. W., SHEN, R.-F., DANIELS, M. P. & LEVINE, S. J. 2009. Proteomic profiling of human plasma exosomes identifies PPARγ as an exosome-associated protein. *Biochemical and Biophysical Research Communications,* 378**,** 433-438.

LOPATINA, T., BRUNO, S., TETTA, C., KALININA, N., PORTA, M. & CAMUSSI, G. 2014. Platelet-derived growth factor regulates the secretion of extracellular vesicles by adipose mesenchymal stem cells and enhances their angiogenic potential. *Cell Communication and Signalling,* 12**,** 26.

LÖTVALL, J., HILL, A. F., HOCHBERG, F., BUZÁS, E. I., DI VIZIO, D., GARDINER, C., GHO, Y. S., KUROCHKIN, I. V., MATHIVANAN, S. & QUESENBERRY, P. 2014. Minimal experimental requirements for definition of extracellular vesicles and their functions: a position statement from the International Society for Extracellular Vesicles. *Journal of Extracellular Vesicles,* 3**,** 26913.

LOZANO-RAMOS, I., BANCU, I., OLIVEIRA-TERCERO, A., ARMENGOL, M. P., MENEZES-NETO, A., DEL PORTILLO, H. A., LAUZURICA-VALDEMOROS, R. & BORRAS, F. E. 2015. Size-exclusion chromatography-based enrichment of extracellular vesicles from urine samples. *Journal of Extracellular Vesicles,* 4**,** 27369.

LU, Z., ZUO, B., JING, R., GAO, X., RAO, Q., LIU, Z., QI, H., GUO, H. & YIN, H. 2017. Dendritic cell-derived exosomes elicit tumor regression in autochthonous hepatocellular carcinoma mouse models. *Journal of Hepatology,* 67**,** 739-748.

LUDWIG, S., SHARMA, P., THEODORAKI, M.-N., PIETROWSKA, M., YERNENI, S. S., LANG, S., FERRONE, S. & WHITESIDE, T. L. 2018. Molecular and functional profiles of exosomes from HPV(+) and HPV(−) head and neck cancer cell lines. *Frontiers in Oncology,* 8.

LUNDBLAD, R. L. 2005. Considerations for the use of blood plasma and serum for proteomic analysis. *The Internet Journal of Genomics and Proteomics,* 1.

LV, L.-L., CAO, Y., LIU, D., XU, M., LIU, H., TANG, R.-N., MA, K.-L. & LIU, B.-C. 2013. Isolation and quantification of microRNAs from urinary exosomes/microvesicles for biomarker discovery. *International Journal of Biological Sciences,* 9**,** 1021-31.

LYNCH, S., SANTOS, S. G., CAMPBELL, E. C., NIMMO, A. M., BOTTING, C., PRESCOTT, A., ANTONIOU, A. N. & POWIS, S. J. 2009. Novel MHC class I structures on exosomes. *The Journal of Immunology,* 183**,** 1884-1891.

MAGALON, J., CHATEAU, A. L., BERTRAND, B., LOUIS, M. L., SILVESTRE, A., GIRAUDO, L., VERAN, J. & SABATIER, F. 2016. DEPA classification: a proposal for standardising PRP use and a retrospective application of available devices. *BMJ Open Sport & Exercise Medicine,* 2**,** e000060.

MALAHIAS, M.-A., MAVROGENIS, A. F., NIKOLAOU, V. S., MEGALOIKONOMOS, P. D., KAZAS, S. T., CHRONOPOULOS, E. & BABIS, G. C. 2019. Similar effect of ultrasound-guided platelet-rich plasma versus platelet-poor plasma injections for chronic plantar fasciitis. *The Foot,* 38**,** 30-33.

MALIK, Z. A., KOTT, K. S., POE, A. J., KUO, T., CHEN, L., FERRARA, K. W. & KNOWLTON, A. A. 2013. Cardiac myocyte exosomes: stability, HSP60, and proteomics. *American Journal of Physiology-Heart and Circulatory Physiology,* 304**,** H954-H965.

MARSHALL, J. 2011. Transwell® invasion assays. *Cell Migration.* Springer.

MARX, R. E. 2004. Platelet-rich plasma: evidence to support its use. *Journal of Oral and Maxillofacial Surgery,* 62**,** 489-496.

MASTORIDIS, S., BERTOLINO, G. M., WHITEHOUSE, G., DAZZI, F., SANCHEZ FUEYO, A. & MARTINEZ-LLORDELLA, M. 2018. Multiparametric analysis of circulating exosomes and other small extracellular vesicles by advanced imaging flow cytometry. *Frontiers in Immunology,* 9**,** 1583.

MATSUZAKI, K., FUJITA, K., JINGUSHI, K., KAWASHIMA, A., UJIKE, T., NAGAHARA, A., UEDA, Y., TANIGAWA, G., YOSHIOKA, I., UEDA, K., HANAYAMA, R., UEMURA, M., MIYAGAWA, Y., TSUJIKAWA, K. & NONOMURA, N. 2017. MiR-21-5p in urinary extracellular vesicles is a novel biomarker of urothelial carcinoma. *Oncotarget,* 8**,** 24668-24678.

MCKELVEY, K. J., POWELL, K. L., ASHTON, A. W., MORRIS, J. M. & MCCRACKEN, S. A. 2015. Exosomes: Mechanisms of uptake. *Journal of Circulating Biomarkers,* 4**,** 7-7.

MCKENZIE, A. J., HOSHINO, D., HONG, N. H., CHA, D. J., FRANKLIN, J. L., COFFEY, R. J., PATTON, J. G. & WEAVER, A. M. 2016. KRAS-MEK signaling controls Ago2 sorting into exosomes. *Cell Reports,* 15**,** 978-987.

MCNAMARA, R. P., CARO-VEGAS, C. P., COSTANTINI, L. M., LANDIS, J. T., GRIFFITH, J. D., DAMANIA, B. A. & DITTMER, D. P. 2018a. Large-scale, cross-flow based isolation of highly pure and endocytosis-competent extracellular vesicles. *Journal of Extracellular Vesicles,* 7**,** 1541396.

MCNAMARA, R. P., COSTANTINI, L. M., MYERS, T. A., SCHOUEST, B., MANESS, N. J., GRIFFITH, J. D., DAMANIA, B. A., MACLEAN, A. G. & DITTMER, D. P. 2018b. Nef secretion into extracellular vesicles or exosomes is conserved across human and simian immunodeficiency viruses. *mBio,* 9**,** e02344-17.

MEAD, B. & TOMAREV, S. 2017. Bone marrow-derived mesenchymal stem cells-derived exosomes promote survival of retinal ganglion cells through miRNA-dependent mechanisms. *Stem Cells Translational Medicine,* 6**,** 1273-1285.

MENARD, J. A., CEREZO-MAGAÑA, M. & BELTING, M. 2018. Functional role of extracellular vesicles and lipoproteins in the tumour microenvironment. *Philosophical Transactions of the Royal Society B,* 373**,** 20160480.

MENG, X., MULLER, V., MILDE-LANGOSCH, K., TRILLSCH, F., PANTEL, K. & SCHWARZENBACH, H. 2016. Diagnostic and prognostic relevance of circulating exosomal miR-373, miR-200a, miR-200b and miR-200c in patients with epithelial ovarian cancer. *Oncotarget,* 7**,** 16923-35.

MERRELL, K., SOUTHWICK, K., GRAVES, S. W., ESPLIN, M. S., LEWIS, N. E. & THULIN, C. D. 2004. Analysis of low-abundance, low-molecular-weight serum proteins using mass spectrometry. *Journal of Biomolecular Techniques,* 15**,** 238-248.

MINCIACCHI, V. R., FREEMAN, M. R. & DI VIZIO, D. 2015. Extracellular vesicles in cancer: exosomes, microvesicles and the emerging role of large oncosomes. *Seminars in Cell & Developmental Biology,* 40**,** 41-51.

MOMEN-HERAVI, F., BALAJ, L., ALIAN, S., TRACHTENBERG, A. J., HOCHBERG, F. H., SKOG, J. & KUO, W. P. 2012. Impact of biofluid viscosity on size and sedimentation efficiency of the isolated microvesicles. *Frontiers in Physiology,* 3**,** 162.

MONTECALVO, A., LARREGINA, A. T., SHUFESKY, W. J., STOLZ, D. B., SULLIVAN, M. L., KARLSSON, J. M., BATY, C. J., GIBSON, G. A., ERDOS, G. & WANG, Z. 2012. Mechanism of transfer of functional microRNAs between mouse dendritic cells via exosomes. *Blood,* 119**,** 756-766.

MORITA, E., COLF, L. A., KARREN, M. A., SANDRIN, V., RODESCH, C. K. & SUNDQUIST, W. I. 2010. Human ESCRT-III and VPS4 proteins are required for centrosome and spindle maintenance. *Proceedings of the National Academy of Sciences of the United States of America,* 107**,** 12889-12894.

MØRK, M., HANDBERG, A., PEDERSEN, S., JØRGENSEN, M. M., BÆK, R., NIELSEN, M. K. & KRISTENSEN, S. R. 2017. Prospects and limitations of antibody-mediated clearing of lipoproteins from blood plasma prior to nanoparticle tracking analysis of extracellular vesicles. *Journal of Extracellular Vesicles,* 6**,** 1308779.

MORSE, M. A., GARST, J., OSADA, T., KHAN, S., HOBEIKA, A., CLAY, T. M., VALENTE, N., SHREENIWAS, R., SUTTON, M. A. & DELCAYRE, A. 2005. A phase I study of dexosome immunotherapy in patients with advanced non-small cell lung cancer. *Journal of Translational Medicine,* 3**,** 9.

MOZAFFARIAN, D., BENJAMIN, E. J., GO, A. S., ARNETT, D. K., BLAHA, M. J., CUSHMAN, M., DE FERRANTI, S., DESPRES, J. P., FULLERTON, H. J., HOWARD, V. J., HUFFMAN, M. D., JUDD, S. E., KISSELA, B. M., LACKLAND, D. T., LICHTMAN, J. H., LISABETH, L. D., LIU, S., MACKEY, R. H., MATCHAR, D. B., MCGUIRE, D. K., MOHLER, E. R., 3RD, MOY, C. S., MUNTNER, P., MUSSOLINO, M. E., NASIR, K., NEUMAR, R. W., NICHOL, G., PALANIAPPAN, L., PANDEY, D. K., REEVES, M. J., RODRIGUEZ, C. J., SORLIE, P. D., STEIN, J., TOWFIGHI, A., TURAN, T. N., VIRANI, S. S., WILLEY, J. Z., WOO, D., YEH, R. W. & TURNER, M. B. 2015. Heart disease and stroke statistics-2015 update: a report from the american heart association. *Circulation,* 131**,** e29-e322.

MULLER, L., HONG, C.-S., STOLZ, D. B., WATKINS, S. C. & WHITESIDE, T. L. 2014. Isolation of biologically-active exosomes from human plasma. *Journal of Immunological Methods,* 411**,** 55-65.

MUNRO, S. 2003. Lipid rafts: elusive or illusive? *Cell,* 115**,** 377-388.

MURGOCI, A. N., CIZKOVA, D., MAJEROVA, P., PETROVOVA, E., MEDVECKY, L., FOURNIER, I. & SALZET, M. 2018. Brain-cortex microglia-derived exosomes: Nanoparticles for glioma therapy. *Chemical Physics and Physical Chemistry,* 19**,** 1205-1214.

MURPHY, A. J. 2013. High density lipoprotein: assembly, structure, cargo, and functions. *ISRN Physiology,* 2013.

MUSTAPIC, M., EITAN, E., WERNER, J. K., JR., BERKOWITZ, S. T., LAZAROPOULOS, M. P., TRAN, J., GOETZL, E. J. & KAPOGIANNIS, D. 2017. Plasma extracellular vesicles enriched for neuronal origin: A potential window into brain pathologic processes. *Frontiers in Neuroscience,* 11**,** 278-278.

MUTSCHELKNAUS, L., PETERS, C., WINKLER, K., YENTRAPALLI, R., HEIDER, T., ATKINSON, M. J. & MOERTL, S. 2016. Exosomes derived from squamous head and neck cancer promote cell survival after ionizing radiation. *Public Library of Science One,* 11**,** e0152213-e0152213.

NAKAMURA, K., JINNIN, M., HARADA, M., KUDO, H., NAKAYAMA, W., INOUE, K., OGATA, A., KAJIHARA, I., FUKUSHIMA, S. & IHN, H. 2016. Altered expression of CD63 and exosomes in scleroderma dermal fibroblasts. *Journal of Dermatological Science,* 84**,** 30-39.

NAKATA, R., SHIMADA, H., FERNANDEZ, G. E., FANTER, R., FABBRI, M., MALVAR, J., ZIMMERMANN, P. & DECLERCK, Y. A. 2017. Contribution of neuroblastoma-derived exosomes to the production of pro-tumorigenic signals by bone marrow mesenchymal stromal cells. *Journal of Extracellular Vesicles,* 6**,** 1332941.

NARAYANASWAMY, R. & TORCHILIN, V. P. 2019. Hydrogels and their applications in targeted drug delivery. *Molecules,* 24**,** 603.

NEDAEINIA, R., MANIAN, M., JAZAYERI, M., RANJBAR, M., SALEHI, R., SHARIFI, M., MOHAGHEGH, F., GOLI, M., JAHEDNIA, S. & AVAN, A. 2017. Circulating exosomes and exosomal microRNAs as biomarkers in gastrointestinal cancer. *Cancer Gene Therapy,* 24**,** 48.

NGUYEN, H. Q., LEE, D., KIM, Y., PAEK, M., KIM, M., JANG, K. S., OH, J., LEE, Y. S., YEON, J. E., LUBMAN, D. M. & KIM, J. 2019. Platelet factor 4 as a novel exosome marker in MALDI-MS analysis of exosomes from human serum. *Analytical Chemistry,* 91**,** 13297-13305.

NIELSEN, T., KRISTENSEN, A. F., PEDERSEN, S., CHRISTIANSEN, G. & KRISTENSEN, S. R. 2018. Investigation of procoagulant activity in extracellular vesicles isolated by differential ultracentrifugation. *Journal of Extracellular Vesicles,* 7**,** 1454777.

NOFER, J.-R., WALTER, M., KEHREL, B., WIERWILLE, S., TEPEL, M., SEEDORF, U. & ASSMANN, G. 1998. HDL3-mediated inhibition of thrombin-induced platelet aggregation and fibrinogen binding occurs via decreased production of phosphoinositide-derived second messengers 1, 2-diacylglycerol and inositol 1, 4, 5-tris-phosphate. *Arteriosclerosis, Thrombosis, and Vascular Biology,* 18**,** 861-869.

NORDIN, J. Z., LEE, Y., VADER, P., MAGER, I., JOHANSSON, H. J., HEUSERMANN, W., WIKLANDER, O. P., HALLBRINK, M., SEOW, Y., BULTEMA, J. J., GILTHORPE, J., DAVIES, T., FAIRCHILD, P. J., GABRIELSSON, S., MEISNER-KOBER, N. C., LEHTIO, J., SMITH, C. I., WOOD, M. J. & EL ANDALOUSSI, S. 2015. Ultrafiltration with size-exclusion liquid chromatography for high yield isolation of extracellular vesicles preserving intact biophysical and functional properties. *Nanomedicine,* 11**,** 879-83.

NOWAK-SLIWINSKA, P., ALITALO, K., ALLEN, E., ANISIMOV, A., APLIN, A. C., AUERBACH, R., AUGUSTIN, H. G., BATES, D. O., VAN BEIJNUM, J. R., BENDER, R. H. F., BERGERS, G., BIKFALVI, A., BISCHOFF, J., BOCK, B. C., BROOKS, P. C., BUSSOLINO, F., CAKIR, B., CARMELIET, P., CASTRANOVA, D., CIMPEAN, A. M., CLEAVER, O., COUKOS, G., DAVIS, G. E., DE PALMA, M., DIMBERG, A., DINGS, R. P. M., DJONOV, V., DUDLEY, A. C., DUFTON, N. P., FENDT, S. M., FERRARA, N., FRUTTIGER, M., FUKUMURA, D., GHESQUIERE, B., GONG, Y., GRIFFIN, R. J., HARRIS, A. L., HUGHES, C. C. W., HULTGREN, N. W., IRUELA-ARISPE, M. L., IRVING, M., JAIN, R. K., KALLURI, R., KALUCKA, J., KERBEL, R. S., KITAJEWSKI, J., KLAASSEN, I., KLEINMANN, H. K., KOOLWIJK, P., KUCZYNSKI, E., KWAK, B. R., MARIEN, K., MELERO-MARTIN, J. M., MUNN, L. L., NICOSIA, R. F., NOEL, A., NURRO, J., OLSSON, A. K., PETROVA, T. V., PIETRAS, K., PILI, R., POLLARD, J. W., POST, M. J., QUAX, P. H. A., RABINOVICH, G. A., RAICA, M., RANDI, A. M., RIBATTI, D., RUEGG, C., SCHLINGEMANN, R. O., SCHULTE-MERKER, S., SMITH, L. E. H., SONG, J. W., STACKER, S. A., STALIN, J., STRATMAN, A. N., VAN DE VELDE, M., VAN HINSBERGH, V. W. M., VERMEULEN, P. B., WALTENBERGER, J., WEINSTEIN, B. M., XIN, H., YETKIN-ARIK, B., YLA-HERTTUALA, S., YODER, M. C. & GRIFFIOEN, A. W. 2018. Consensus guidelines for the use and interpretation of angiogenesis assays. *Angiogenesis,* 21**,** 425-532.

OGAWA, Y., KANAI-AZUMA, M., AKIMOTO, Y., KAWAKAMI, H. & YANOSHITA, R. 2008. Exosome-like vesicles with dipeptidyl peptidase IV in human saliva. *Biological and Pharmaceutical Bulletin* 31**,** 1059-62.

OHSHIMA, K., INOUE, K., FUJIWARA, A., HATAKEYAMA, K., KANTO, K., WATANABE, Y., MURAMATSU, K., FUKUDA, Y., OGURA, S.-I. & YAMAGUCHI, K. 2010. Let-7 microRNA family is selectively secreted into the extracellular environment via exosomes in a metastatic gastric cancer cell line. *Public Library of Science One,* 5**,** e13247.

ONO, M., KOSAKA, N., TOMINAGA, N., YOSHIOKA, Y., TAKESHITA, F., TAKAHASHI, R.-U., YOSHIDA, M., TSUDA, H., TAMURA, K. & OCHIYA, T. 2014. Exosomes from bone marrow mesenchymal stem cells contain a microRNA that promotes dormancy in metastatic breast cancer cells. *Science Signalling,* 7**,** 63.

ONÓDI, Z., PELYHE, C., TERÉZIA NAGY, C., BRENNER, G. B., ALMÁSI, L., KITTEL, Á., MANČEK-KEBER, M., FERDINANDY, P., BUZÁS, E. I. & GIRICZ, Z. 2018. Isolation of high-purity

extracellular vesicles by the combination of iodixanol density gradient ultracentrifugation and bind-elute chromatography from blood plasma. *Frontiers in Physiology,* 9**,** 1479-1479.

OOSTHUYZEN, W., SIME, N. E., IVY, J. R., TURTLE, E. J., STREET, J. M., POUND, J., BATH, L. E., WEBB, D. J., GREGORY, C. D. & BAILEY, M. A. 2013. Quantification of human urinary exosomes by nanoparticle tracking analysis. *The Journal of Physiology,* 591**,** 5833-5842.

ORGANIZATION, W. H. 2009. Stability testing of active pharmaceutical ingredients and finished pharmaceutical products. *World Health Organisation Technical Report Series,* 953**,** 87-130.

OSTI, D., DEL BENE, M., RAPPA, G., SANTOS, M., MATAFORA, V., RICHICHI, C., FALETTI, S., BEZNOUSSENKO, G. V., MIRONOV, A., BACHI, A., FORNASARI, L., BONGETTA, D., GAETANI, P., DIMECO, F., LORICO, A. & PELICCI, G. 2019. Clinical significance of extracellular vesicles in plasma from glioblastoma patients. *Clinical Cancer Research,* 25**,** 266-276.

OSTROWSKI, M., CARMO, N. B., KRUMEICH, S., FANGET, I., RAPOSO, G., SAVINA, A., MOITA, C. F., SCHAUER, K., HUME, A. N., FREITAS, R. P., GOUD, B., BENAROCH, P., HACOHEN, N., FUKUDA, M., DESNOS, C., SEABRA, M. C., DARCHEN, F., AMIGORENA, S., MOITA, L. F. & THERY, C. 2010. Rab27a and Rab27b control different steps of the exosome secretion pathway. *Nature Cell Biology,* 12**,** 19-30; sup pp 1-13.

OTROCK, Z. K., MAHFOUZ, R. A., MAKAREM, J. A. & SHAMSEDDINE, A. I. 2007. Understanding the biology of angiogenesis: review of the most important molecular mechanisms. *Blood Cells, Molecules and Diseases,* 39**,** 212-20.

ØVERBYE, A., SKOTLAND, T., KOEHLER, C. J., THIEDE, B., SEIERSTAD, T., BERGE, V., SANDVIG, K. & LLORENTE, A. 2015. Identification of prostate cancer biomarkers in urinary exosomes. *Oncotarget,* 6**,** 30357-30376.

PALANISAMY, V., SHARMA, S., DESHPANDE, A., ZHOU, H., GIMZEWSKI, J. & WONG, D. T. 2010. Nanostructural and transcriptomic analyses of human saliva derived exosomes. *Public Library of Science One,* 5**,** e8577.

PALHARES, A., SCHELLINI, S. A., PELLIZZON, C. H., PADOVANI, C. R. & DORSA, P. 2009. Evaluation of low intensity laser's action on silicone mammary implant pseudocapsules in rats. *Acta Cirurgica Brasileira,* 24**,** 7-12.

PAN, B.-T. & JOHNSTONE, R. M. 1983. Fate of the transferrin receptor during maturation of sheep reticulocytes in vitro: selective externalization of the receptor. *Cell,* 33**,** 967-978.

PANDYA, M. R. & N, V. C. 2015. *The Techniques of IVF Made Easy*, Jaypee Brothers,Medical Publishers Pvt. Limited.

PARISH, C. R. 1999. Fluorescent dyes for lymphocyte migration and proliferation studies. *Immunology & Cell Biology,* 77**,** 499-508.

PARKER, S. J., RAEDSCHELDERS, K. & VAN EYK, J. E. 2015. Emerging proteomic technologies for elucidating context-dependent cellular signaling events: A big challenge of tiny proportions. *Proteomics,* 15**,** 1486-1502.

PAROLINI, I., FEDERICI, C., RAGGI, C., LUGINI, L., PALLESCHI, S., DE MILITO, A., COSCIA, C., IESSI, E., LOGOZZI, M., MOLINARI, A., COLONE, M., TATTI, M., SARGIACOMO, M. & FAIS, S. 2009. Microenvironmental pH is a key factor for exosome traffic in tumor cells. *The Journal of Biological Chemistry,* 284**,** 34211-22.

PATEL, V. I., PATEL, K. P., MAKADIA, M. G., SHAH, A. D., CHAUDHARI, K. S. & NILAYANGODE, H. N. 2017. Levels of apolipoprotein a1, b100 and lipoprotein (a) in controlled and uncontrolled diabetic patients and in non-diabetic healthy people. *Journal of Clinical and Diagnostic Research: JCDR,* 11**,** BC01.

PATHAN, M., KEERTHIKUMAR, S., CHISANGA, D., ALESSANDRO, R., ANG, C.-S., ASKENASE, P., BATAGOV, A. O., BENITO-MARTIN, A., CAMUSSI, G. & CLAYTON, A. 2017. A novel community driven software for functional enrichment analysis of extracellular vesicles data. *Journal of Extracellular Vesicles,* 6**,** 1321455.

PEINADO, H., ALEČKOVIĆ, M., LAVOTSHKIN, S., MATEI, I., COSTA-SILVA, B., MORENO-BUENO, G., HERGUETA-REDONDO, M., WILLIAMS, C., GARCÍA-SANTOS, G. & GHAJAR, C. M. 2012. Melanoma exosomes educate bone marrow progenitor cells toward a pro-metastatic phenotype through MET. *Nature Medicine,* 18**,** 883.

PHINNEY, D. G. & PITTENGER, M. F. 2017. Concise review: MSC-derived exosomes for cell-free therapy. *Stem Cells,* 35**,** 851-858.

PITT, J. M., ANDRÉ, F., AMIGORENA, S., SORIA, J.-C., EGGERMONT, A., KROEMER, G. & ZITVOGEL, L. 2016. Dendritic cell-derived exosomes for cancer therapy. *The Journal of Clinical Investigation,* 126**,** 1224-1232.

PITTENGER, M. F., MACKAY, A. M., BECK, S. C., JAISWAL, R. K., DOUGLAS, R., MOSCA, J. D., MOORMAN, M. A., SIMONETTI, D. W., CRAIG, S. & MARSHAK, D. R. 1999. Multilineage potential of adult human mesenchymal stem cells. *Science,* 284**,** 143-147.

PLEINES, I., ECKLY, A., ELVERS, M., HAGEDORN, I., ELIAUTOU, S., BENDER, M., WU, X., LANZA, F., GACHET, C. & BRAKEBUSCH, C. 2010. Multiple alterations of platelet functions dominated by increased secretion in mice lacking Cdc42 in platelets. *Blood***,** blood-2009-09-242271.

PROPERZI, F., LOGOZZI, M. & FAIS, S. 2013. Exosomes: the future of biomarkers in medicine. *Biomarkers in Medicine,* 7**,** 769-778.

PUSIC, A. D. & KRAIG, R. P. 2014. Youth and environmental enrichment generate serum exosomes containing miR-219 that promote CNS myelination. *Glia,* 62**,** 284-299.

QI, H., LIU, C., LONG, L., REN, Y., ZHANG, S., CHANG, X., QIAN, X., JIA, H., ZHAO, J. & SUN, J. 2016. Blood Exosomes Endowed with Magnetic and Targeting Properties for Cancer Therapy. *ACS Nano,* 10**,** 3323-3333.

QIAN, Y., HAN, Q., CHEN, W., SONG, J., ZHAO, X., OUYANG, Y., YUAN, W. & FAN, C. 2017. Platelet-rich plasma derived growth factors contribute to stem cell differentiation in musculoskeletal regeneration. *Frontiers in Chemistry,* 5**,** 89.

QUANTIMETRIX. 2005. *Lipoprint® LDL Subfractions Kit* [Online]. 2005 Manhattan Beach Blvd. Redondo Beach CA. Available: https://quantimetrix.com/wp-content/uploads/LipoprintLDLTestKit_English_REF-48-7002.pdf [Accessed 13 August 2019].

RADONS, J. & MULTHOFF, G. 2005. Immunostimulatory functions of membrane-bound and exported heat shock protein 70. *Exercise Immunology Review,* 11**,** 17-33.

RAMASAMY, I. 2014. Recent advances in physiological lipoprotein metabolism. *Clinical Chemistry and Laboratory Medicine* 52**,** 1695-1727.

RAMOS, T. L., SÁNCHEZ-ABARCA, L. I., MUNTIÓN, S., PRECIADO, S., PUIG, N., LÓPEZ-RUANO, G., HERNÁNDEZ-HERNÁNDEZ, Á., REDONDO, A., ORTEGA, R. & RODRÍGUEZ, C. 2016. MSC surface markers (CD44, CD73, and CD90) can identify human MSC-derived extracellular vesicles by conventional flow cytometry. *Cell Communication and Signaling,* 14**,** 2.

RAPOSO, G., NIJMAN, H. W., STOORVOGEL, W., LIEJENDEKKER, R., HARDING, C. V., MELIEF, C. & GEUZE, H. J. 1996. B lymphocytes secrete antigen-presenting vesicles. *Journal of Experimental Medicine,* 183**,** 1161-1172.

REKKER, K., SAARE, M., ROOST, A. M., KUBO, A.-L., ZAROVNI, N., CHIESI, A., SALUMETS, A. & PETERS, M. 2014. Comparison of serum exosome isolation methods for microRNA profiling. *Clinical Biochemistry,* 47**,** 135-138.

REVENFELD, A. L. S., BÆK, R., NIELSEN, M. H., STENSBALLE, A., VARMING, K. & JØRGENSEN, M. 2014. Diagnostic and prognostic potential of extracellular vesicles in peripheral blood. *Clinical Therapeutics,* 36**,** 830-846.

RHEE, J. S., BLACK, M., SCHUBERT, U., FISCHER, S., MORGENSTERN, E., HAMMES, H. P. & PREISSNER, K. T. 2004. The functional role of blood platelet components in angiogenesis. *Journal of Thrombosis and Haemostasis,* 92**,** 394-402.

RICKER, R. & SANDOVAL, L. 1996. Fast, reproducible size-exclusion chromatography of biological macromolecules. *Journal of Chromatography A,* 743**,** 43-50.

RIDKER, P. M., RIFAI, N., COOK, N. R., BRADWIN, G. & BURING, J. E. 2005. Non–HDL cholesterol, apolipoproteins AI and B100, standard lipid measures, lipid ratios, and CRP as risk factors for cardiovascular disease in women. *Journal of the American Medical Association* 294**,** 326-333.

RIKKERT, L., NIEUWLAND, R., TERSTAPPEN, L. & COUMANS, F. 2019. Quality of extracellular vesicle images by transmission electron microscopy is operator and protocol dependent. *Journal of Extracellular Vesicles,* 8**,** 1555419.

RISTORCELLI, E., BERAUD, E., VERRANDO, P., VILLARD, C., LAFITTE, D., SBARRA, V., LOMBARDO, D. & VERINE, A. 2008. Human tumor nanoparticles induce apoptosis of pancreatic cancer cells. *The FASEB Journal,* 22**,** 3358-69.

ROCCARO, A. M., SACCO, A., MAISO, P., AZAB, A. K., TAI, Y.-T., REAGAN, M., AZAB, F., FLORES, L. M., CAMPIGOTTO, F. & WELLER, E. 2013. BM mesenchymal stromal cell–derived exosomes facilitate multiple myeloma progression. *The Journal of Clinical Investigation,* 123**,** 1542-1555.

ROSENBERGER, L., EZQUER, M., LILLO-VERA, F., PEDRAZA, P. L., ORTÚZAR, M. I., GONZÁLEZ, P. L., FIGUEROA-VALDÉS, A. I., CUENCA, J., EZQUER, F., KHOURY, M. & ALCAYAGA-MIRANDA, F. 2019. Stem cell exosomes inhibit angiogenesis and tumor growth of oral squamous cell carcinoma. *Scientific Reports,* 9**,** 663.

ROY, S., HOCHBERG, F. H. & JONES, P. S. 2018. Extracellular vesicles: the growth as diagnostics and therapeutics; a survey. *Journal of Extracellular Vesicles,* 7**,** 1438720.

RYU, J. H., KIM, I.-K., CHO, S.-W., CHO, M.-C., HWANG, K.-K., PIAO, H., PIAO, S., LIM, S. H., HONG, Y. S. & CHOI, C. Y. 2005. Implantation of bone marrow mononuclear cells using injectable fibrin matrix enhances neovascularization in infarcted myocardium. *Biomaterials,* 26**,** 319-326.

SAHOO, S. & LOSORDO, D. W. 2014. Exosomes and cardiac repair after myocardial infarction. *Circulation Research,* 114**,** 333-344.

SALGADO, A. J., SOUSA, J. C., COSTA, B. M., PIRES, A. O., MATEUS-PINHEIRO, A., TEIXEIRA, F., PINTO, L. & SOUSA, N. 2015. Mesenchymal stem cells secretome as a modulator of the neurogenic niche: basic insights and therapeutic opportunities. *Frontiers in Cellular Neuroscience,* 9**,** 249.

SALOMON, C., RYAN, J., SOBREVIA, L., KOBAYASHI, M., ASHMAN, K., MITCHELL, M. & RICE, G. E. 2013. Exosomal signaling during hypoxia mediates microvascular endothelial cell migration and vasculogenesis. *Public Library of Science One,* 8**,** e68451.

SALOMON, C., TORRES, M. J., KOBAYASHI, M., SCHOLZ-ROMERO, K., SOBREVIA, L., DOBIERZEWSKA, A., ILLANES, S. E., MITCHELL, M. D. & RICE, G. E. 2014. A gestational profile of placental exosomes in maternal plasma and their effects on endothelial cell migration. *Public Library of Science One,* 9**,** e98667.

SAN LUCAS, F. A., ALLENSON, K., BERNARD, V., CASTILLO, J., KIM, D. U., ELLIS, K., EHLI, E. A., DAVIES, G. E., PETERSEN, J. L., LI, D., WOLFF, R., KATZ, M., VARADHACHARY, G., WISTUBA, I., MAITRA, A. & ALVAREZ, H. 2016. Minimally invasive genomic and transcriptomic profiling of visceral cancers by next-generation sequencing of circulating exosomes. *Annals of Oncology,* 27**,** 635-41.

SARMA, J. V. & WARD, P. A. 2011. The complement system. *Cell and Tissue Research,* 343**,** 227-235.

SAWAMURA, T., KUME, N., AOYAMA, T., MORIWAKI, H., HOSHIKAWA, H., AIBA, Y., TANAKA, T., MIWA, S., KATSURA, Y. & KITA, T. 1997. An endothelial receptor for oxidized low-density lipoprotein. *Nature,* 386**,** 73.

SCHAGEMAN, J., ZERINGER, E., LI, M., BARTA, T., LEA, K., GU, J., MAGDALENO, S., SETTERQUIST, R. & VLASSOV, A. V. 2013. The complete exosome workflow solution: from isolation to characterization of RNA cargo. *BioMed Research International,* 2013.

SCHMIDT, C., BEZUIDENHOUT, D., BECK, M., VAN DER MERWE, E., ZILLA, P. & DAVIES, N. 2009. Rapid three-dimensional quantification of VEGF-induced scaffold neovascularisation by microcomputed tomography. *Biomaterials,* 30**,** 5959-5968.

SCHWERTZ, H., ROWLEY, J. W., TOLLEY, N. D., CAMPBELL, R. A. & WEYRICH, A. S. 2012. Assessing protein synthesis by platelets. *Platelets and Megakaryocytes.* Springer.

SCLAFANI, A. P. & MCCORMICK, S. A. 2012. Induction of dermal collagenesis, angiogenesis, and adipogenesis in human skin by injection of platelet-rich fibrin matrix. *Archives of Facial Plastic Surgery,* 14**,** 132-136.

SEGURA, E., GUERIN, C., HOGG, N., AMIGORENA, S. & THERY, C. 2007. CD8+ dendritic cells use LFA-1 to capture MHC-peptide complexes from exosomes in vivo. *The Journal of Immunology,* 179**,** 1489-96.

SHARMA, P., LUDWIG, S., MULLER, L., HONG, C. S., KIRKWOOD, J. M., FERRONE, S. & WHITESIDE, T. L. 2018. Immunoaffinity-based isolation of melanoma cell-derived exosomes from plasma of patients with melanoma. *Journal of Extracellular Vesicles,* 7**,** 1435138.

SHARMA, S. & GIMZEWSKI, J. 2012. The quest for characterizing exosomes: circulating nano-sized vesicles. *Journal of Nanomedicine and Nanotechnology,* 3**,** e115.

SHEIKH, A. Y., HUBER, B. C., NARSINH, K. H., SPIN, J. M., VAN DER BOGT, K., DE ALMEIDA, P. E., RANSOHOFF, K. J., KRAFT, D. L., FAJARDO, G. & ARDIGO, D. 2012. In vivo functional and

transcriptional profiling of bone marrow stem cells after transplantation into ischemic myocardium. *Arteriosclerosis, Thrombosis, and Vascular Biology,* 32**,** 92-102.

SHELKE, G. V., LÄSSER, C., GHO, Y. S. & LÖTVALL, J. 2014. Importance of exosome depletion protocols to eliminate functional and RNA-containing extracellular vesicles from fetal bovine serum. *Journal of Extracellular Vesicles,* 3**,** 24783.

SHI, Q., QIAN, Z., LIU, D., SUN, J., WANG, X., LIU, H., XU, J. & GUO, X. 2017. GMSC-derived exosomes combined with a chitosan/silk hydrogel sponge accelerates wound healing in a diabetic rat skin defect model. *Frontiers in Physiology,* 8**,** 904.

SHTAM, T. A., KOVALEV, R. A., VARFOLOMEEVA, E. Y., MAKAROV, E. M., KIL, Y. V. & FILATOV, M. V. 2013. Exosomes are natural carriers of exogenous siRNA to human cells in vitro. *Cell Communication and Signaling,* 11**,** 88.

SILVA, A. M., ALMEIDA, M. I., TEIXEIRA, J. H., MAIA, A. F., CALIN, G. A., BARBOSA, M. A. & SANTOS, S. G. 2017. Dendritic cell-derived extracellular vesicles mediate mesenchymal stem/stromal cell recruitment. *Scientific Reports,* 7**,** 1667.

SIMONSEN, J. B. 2017. What are we looking at? Extracellular vesicles, lipoproteins, or both? *Circulation Research,* 121**,** 920-922.

SIMONSEN, J. B. 2019. Pitfalls associated with lipophilic fluorophore staining of extracellular vesicles for uptake studies. *Journal of Extracellular Vesicles,* 8**,** 1582237.

SINGH, P. P., LI, L. & SCHOREY, J. S. 2015. Exosomal RNA from Mycobacterium tuberculosis-Infected Cells Is Functional in Recipient Macrophages. *Traffic,* 16**,** 555-571.

SKOTLAND, T., EKROOS, K., KAUHANEN, D., SIMOLIN, H., SEIERSTAD, T., BERGE, V., SANDVIG, K. & LLORENTE, A. 2017. Molecular lipid species in urinary exosomes as potential prostate cancer biomarkers. *European Journal of Cancer,* 70**,** 122-132.

SKOTLAND, T., HESSVIK, N. P., SANDVIG, K. & LLORENTE, A. 2019. Exosomal lipid composition and the role of ether lipids and phosphoinositides in exosome biology. *Journal of Lipid Research,* 60**,** 9-18.

SLUIJTER, J. P. G., DAVIDSON, S. M., BOULANGER, C. M., BUZAS, E. I., DE KLEIJN, D. P. V., ENGEL, F. B., GIRICZ, Z., HAUSENLOY, D. J., KISHORE, R. & LECOUR, S. 2017. Extracellular vesicles in diagnostics and therapy of the ischaemic heart: Position Paper from the Working Group on Cellular Biology of the Heart of the European Society of Cardiology. *Cardiovascular Research,* 114**,** 19-34.

SLUIJTER, J. P. G., DAVIDSON, S. M., BOULANGER, C. M., BUZAS, E. I., DE KLEIJN, D. P. V., ENGEL, F. B., GIRICZ, Z., HAUSENLOY, D. J., KISHORE, R., LECOUR, S., LEOR, J., MADONNA, R., PERRINO, C., PRUNIER, F., SAHOO, S., SCHIFFELERS, R. M., SCHULZ, R., VAN LAAKE, L. W., YTREHUS, K. & FERDINANDY, P. 2018. Extracellular vesicles in diagnostics and therapy of the ischaemic heart: Position Paper from the Working Group on Cellular Biology of the Heart of the European Society of Cardiology. *Cardiovascular Research,* 114**,** 19-34.

SOARES MARTINS, T., CATITA, J., MARTINS ROSA, I., A B DA CRUZ E SILVA, O. & HENRIQUES, A. G. 2018. Exosome isolation from distinct biofluids using precipitation and column-based approaches. *Public Library of Science One,* 13**,** e0198820-e0198820.

SÓDAR, B. W., KITTEL, Á., PÁLÓCZI, K., VUKMAN, K. V., OSTEIKOETXEA, X., SZABÓ-TAYLOR, K., NÉMETH, A., SPERLÁGH, B., BARANYAI, T. & GIRICZ, Z. 2016. Low-density lipoprotein mimics

blood plasma-derived exosomes and microvesicles during isolation and detection. *Scientific Reports,* 6**,** 24316.

SOKOLOVA, V., LUDWIG, A.-K., HORNUNG, S., ROTAN, O., HORN, P. A., EPPLE, M. & GIEBEL, B. 2011. Characterisation of exosomes derived from human cells by nanoparticle tracking analysis and scanning electron microscopy. *Colloids and Surfaces B: Biointerfaces,* 87**,** 146-150.

SOO, C. Y., SONG, Y., ZHENG, Y., CAMPBELL, E. C., RICHES, A. C., GUNN-MOORE, F. & POWIS, S. J. 2012. Nanoparticle tracking analysis monitors microvesicle and exosome secretion from immune cells. *Immunology,* 136**,** 192-7.

STAUBACH, S., RAZAWI, H. & HANISCH, F. G. 2009. Proteomics of MUC1-containing lipid rafts from plasma membranes and exosomes of human breast carcinoma cells MCF-7. *Proteomics,* 9**,** 2820-2835.

STUFFERS, S., SEM WEGNER, C., STENMARK, H. & BRECH, A. 2009. Multivesicular endosome biogenesis in the absence of ESCRTs. *Traffic,* 10**,** 925-37.

SUÁREZ, H., GÁMEZ-VALERO, A., REYES, R., LÓPEZ-MARTÍN, S., RODRÍGUEZ, M. J., CARRASCOSA, J. L., CABAÑAS, C., BORRÀS, F. E. & YÁÑEZ-MÓ, M. 2017. A bead-assisted flow cytometry method for the semi-quantitative analysis of extracellular vesicles. *Scientific Reports,* 7**,** 11271.

SUEHIRO, T., MIYAAKI, H., KANDA, Y., SHIBATA, H., HONDA, T., OZAWA, E., MIUMA, S., TAURA, N. & NAKAO, K. 2018. Serum exosomal microRNA-122 and microRNA-21 as predictive biomarkers in transarterial chemoembolization-treated hepatocellular carcinoma patients. *Oncology Letters,* 16**,** 3267-3273.

SUN, A., LAI, Z., ZHAO, M., MU, L. & HU, X. 2019. Native nanodiscs from blood inhibit pulmonary fibrosis. *Biomaterials,* 192**,** 51-61.

SUN, L., LI, D., SONG, K., WEI, J., YAO, S., LI, Z., SU, X., JU, X., CHAO, L. & DENG, X. 2017. Exosomes derived from human umbilical cord mesenchymal stem cells protect against cisplatin-induced ovarian granulosa cell stress and apoptosis in vitro. *Scientific Reports,* 7**,** 2552.

SUNDQUIST, W. I., SCHUBERT, H. L., KELLY, B. N., HILL, G. C., HOLTON, J. M. & HILL, C. P. 2004. Ubiquitin recognition by the human TSG101 protein. *Molecular Cell,* 13**,** 783-9.

SUNG, B. H., KETOVA, T., HOSHINO, D., ZIJLSTRA, A. & WEAVER, A. M. 2015. Directional cell movement through tissues is controlled by exosome secretion. *Nature Communications,* 6**,** 7164.

SVENSSON, K. J., CHRISTIANSON, H. C., WITTRUP, A., BOURSEAU-GUILMAIN, E., LINDQVIST, E., SVENSSON, L. M., MÖRGELIN, M. & BELTING, M. 2013. Exosome uptake depends on ERK1/2-heat shock protein 27 signaling and lipid Raft-mediated endocytosis negatively regulated by caveolin-1. *The Journal of biological chemistry,* 288**,** 17713-17724.

TABET, F., VICKERS, K. C., CUESTA TORRES, L. F., WIESE, C. B., SHOUCRI, B. M., LAMBERT, G., CATHERINET, C., PRADO-LOURENCO, L., LEVIN, M. G., THACKER, S., SETHUPATHY, P., BARTER, P. J., REMALEY, A. T. & RYE, K.-A. 2014. HDL-transferred microRNA-223 regulates ICAM-1 expression in endothelial cells. *Nature Communications,* 5**,** 3292-3292.

TAKASHIMA, A. 1998. Establishment of fibroblast cultures. *Current Protocols in Cell Biology***,** 2.1. 1-2.1. 12.

TAKOV, K., YELLON, D. M. & DAVIDSON, S. M. 2017. Confounding factors in vesicle uptake studies using fluorescent lipophilic membrane dyes. *Journal of Extracellular Vesicles,* 6**,** 1388731.

TAKOV, K., YELLON, D. M. & DAVIDSON, S. M. 2019. Comparison of small extracellular vesicles isolated from plasma by ultracentrifugation or size-exclusion chromatography: yield, purity and functional potential. *Journal of Extracellular Vesicles,* 8**,** 1560809.

TAN, C. Y., LAI, R. C., WONG, W., DAN, Y. Y., LIM, S.-K. & HO, H. K. 2014. Mesenchymal stem cell-derived exosomes promote hepatic regeneration in drug-induced liver injury models. *Stem Cell Research & Therapy,* 5**,** 76.

TAN, M., YAN, H.-B., LI, J.-N., LI, W.-K., FU, Y.-Y., CHEN, W. & ZHOU, Z. 2016. Thrombin stimulated platelet-derived exosomes inhibit platelet-derived growth factor receptor-beta expression in vascular smooth muscle cells. *Cellular Physiology and Biochemistry,* 38**,** 2348-2365.

TAN, S. S., YIN, Y., LEE, T., LAI, R. C., YEO, R. W. Y., ZHANG, B., CHOO, A. & LIM, S. K. 2013. Therapeutic MSC exosomes are derived from lipid raft microdomains in the plasma membrane. *Journal of Extracellular Vesicles,* 2.

TANG, Y.-T., HUANG, Y.-Y., ZHENG, L., QIN, S.-H., XU, X.-P., AN, T.-X., XU, Y., WU, Y.-S., HU, X.-M. & PING, B.-H. 2017. Comparison of isolation methods of exosomes and exosomal RNA from cell culture medium and serum. *International Journal of Molecular Medicine,* 40**,** 834-844.

TAO, S.-C., GUO, S.-C. & ZHANG, C.-Q. 2017a. Platelet-derived extracellular vesicles: An emerging therapeutic approach. *International Journal of Biological Sciences,* 13**,** 828-834.

TAO, S.-C., YUAN, T., RUI, B.-Y., ZHU, Z.-Z., GUO, S.-C. & ZHANG, C.-Q. 2017b. Exosomes derived from human platelet-rich plasma prevent apoptosis induced by glucocorticoid-associated endoplasmic reticulum stress in rat osteonecrosis of the femoral head via the Akt/Bad/Bcl-2 signal pathway. *Theranostics,* 7**,** 733.

TAO, S. C., GUO, S. C., LI, M., KE, Q. F., GUO, Y. P. & ZHANG, C. Q. 2017c. Chitosan wound dressings incorporating exosomes derived from microRNA-126-overexpressing synovium mesenchymal stem cells provide sustained release of exosomes and heal full-thickness skin defects in a diabetic rat model. *Stem Cells Translational Medicine,* 6**,** 736-747.

TAURO, B. J., GREENING, D. W., MATHIAS, R. A., JI, H., MATHIVANAN, S., SCOTT, A. M. & SIMPSON, R. J. 2012. Comparison of ultracentrifugation, density gradient separation, and immunoaffinity capture methods for isolating human colon cancer cell line LIM1863-derived exosomes. *Methods,* 56**,** 293-304.

TCHERPAKOV, M. 2016. Exosome diagnostics and therapeutics: Global markets. *Wellesley, MA: BCC Research*.

THEOS, A. C., TRUSCHEL, S. T., TENZA, D., HURBAIN, I., HARPER, D. C., BERSON, J. F., THOMAS, P. C., RAPOSO, G. & MARKS, M. S. 2006. A lumenal domain-dependent pathway for sorting to intralumenal vesicles of multivesicular endosomes involved in organelle morphogenesis. *Developmental Cell,* 10**,** 343-354.

THÉRY, C., AMIGORENA, S., RAPOSO, G. & CLAYTON, A. 2006. Isolation and characterization of exosomes from cell culture supernatants and biological fluids. *Current Protocols in Cell Biology,* 30**,** 3.22. 1-3.22. 29.

THÉRY, C., WITWER, K. W., AIKAWA, E., ALCARAZ, M. J., ANDERSON, J. D., ANDRIANTSITOHAINA, R., ANTONIOU, A., ARAB, T., ARCHER, F. & ATKIN-SMITH, G. K. 2018. Minimal information for

studies of extracellular vesicles 2018 (MISEV2018): a position statement of the International Society for Extracellular Vesicles and update of the MISEV2014 guidelines. *Journal of Extracellular Vesicles,* 7**,** 1535750.

THORSEN, M., BLONDAL, T. & MOURITZEN, P. 2017. Quantitative RT-PCR for microRNAs in biofluids. *Drug Safety Evaluation.* Springer.

TIAN, T., ZHU, Y. L., ZHOU, Y. Y., LIANG, G. F., WANG, Y. Y., HU, F. H. & XIAO, Z. D. 2014. Exosome uptake through clathrin-mediated endocytosis and macropinocytosis and mediating miR-21 delivery. *Journal of Biological Chemistry,* 289**,** 22258-67.

TIMMERS, L., LIM, S. K., ARSLAN, F., ARMSTRONG, J. S., HOEFER, I. E., DOEVENDANS, P. A., PIEK, J. J., EL OAKLEY, R. M., CHOO, A. & LEE, C. N. 2008. Reduction of myocardial infarct size by human mesenchymal stem cell conditioned medium. *Stem Cell Research,* 1**,** 129-137.

TKACH, M., KOWAL, J. & THÉRY, C. 2017. Why the need and how to approach the functional diversity of extracellular vesicles. *Philosophical Transactions of the Royal Society B: Biological Sciences,* 373**,** 20160479.

TORREGGIANI, E., PERUT, F., RONCUZZI, L., ZINI, N., BAGLIO, S. R. & BALDINI, N. 2014. Exosomes: novel effectors of human platelet lysate activity. *European Cells & Materials,* 28**,** 137-51; discussion 151.

TOWBIN, H., STAEHELIN, T. & GORDON, J. 1979. Electrophoretic transfer of proteins from polyacrylamide gels to nitrocellulose sheets: procedure and some applications. *Proceedings of the National Academy of Sciences,* 76**,** 4350-4354.

TRAJKOVIC, K., HSU, C., CHIANTIA, S., RAJENDRAN, L., WENZEL, D., WIELAND, F., SCHWILLE, P., BRÜGGER, B. & SIMONS, M. 2008. Ceramide triggers budding of exosome vesicles into multivesicular endosomes. *Science,* 319**,** 1244-1247.

TSAO, C. R., LIAO, M. F., WANG, M. H., CHENG, C. M. & CHEN, C. H. 2014. Mesenchymal stem cell derived exosomes: A new hope for the treatment of cardiovascular disease? *Acta Cardiologica Sinica,* 30**,** 395-400.

TSILIONI, I. & THEOHARIDES, T. C. 2018. Extracellular vesicles are increased in the serum of children with autism spectrum disorder, contain mitochondrial DNA, and stimulate human microglia to secrete IL-1β. *Journal of Neuroinflammation,* 15**,** 239.

TSURKAN, M. V., HAUSER, P. V., ZIERIS, A., CARVALHOSA, R., BUSSOLATI, B., FREUDENBERG, U., CAMUSSI, G. & WERNER, C. 2013. Growth factor delivery from hydrogel particle aggregates to promote tubular regeneration after acute kidney injury. *Journal of Controlled Release,* 167**,** 248-255.

TUCKER, R. & PEDRO, A. 2018. Blood-derived non-extracellular vesicle proteins as potential biomarkers for the diagnosis of early ER+ breast cancer and detection of lymph node involvement. *F1000Research,* 7.

TURCHINOVICH, A., TONEVITSKY, A. G., CHO, W. C. & BURWINKEL, B. 2015. Check and mate to exosomal extracellular miRNA: new lesson from a new approach. *Frontiers in Molecular Biosciences,* 2**,** 11.

VALADI, H., EKSTRÖM, K., BOSSIOS, A., SJÖSTRAND, M., LEE, J. J. & LÖTVALL, J. O. 2007. Exosome-mediated transfer of mRNAs and microRNAs is a novel mechanism of genetic exchange between cells. *Nature Cell Biology,* 9**,** 654.

VALENTA, D. T., BULGRIEN, J. J., BANKA, C. L. & CURTISS, L. K. 2006. Overexpression of human ApoAI transgene provides long-term atheroprotection in LDL receptor-deficient mice. *Atherosclerosis,* 189**,** 255-263.

VAN DEN AKKER, F., FEYEN, D. A., VAN DEN HOOGEN, P., VAN LAAKE, L. W., VAN EEUWIJK, E., HOEFER, I., PASTERKAMP, G., CHAMULEAU, S. A., GRUNDEMAN, P. F. & DOEVENDANS, P. A. 2017. Intramyocardial stem cell injection: go (ne) with the flow. *European Heart Journal,* 38**,** 184-186.

VAN DER POL, E., DE ROND, L., COUMANS, F. A., GOOL, E. L., BÖING, A. N., STURK, A., NIEUWLAND, R. & VAN LEEUWEN, T. G. 2018. Absolute sizing and label-free identification of extracellular vesicles by flow cytometry. *Nanomedicine: Nanotechnology, Biology and Medicine,* 14**,** 801-810.

VAN DER POL, E., HOEKSTRA, A. G., STURK, A., OTTO, C., VAN LEEUWEN, T. G. & NIEUWLAND, R. 2010. Optical and non-optical methods for detection and characterization of microparticles and exosomes. *Journal of Thrombosis and Haemostasis,* 8**,** 2596-607.

VAN DEUN, J., MESTDAGH, P., SORMUNEN, R., COCQUYT, V., VERMAELEN, K., VANDESOMPELE, J., BRACKE, M., DE WEVER, O. & HENDRIX, A. 2014. The impact of disparate isolation methods for extracellular vesicles on downstream RNA profiling. *Journal of Extracellular Vesicles,* 3**,** 24858.

VAN MEER, G., VOELKER, D. R. & FEIGENSON, G. W. 2008. Membrane lipids: where they are and how they behave. *Nature Reviews Molecular Cell Biology,* 9**,** 112-24.

VAN NIEL, G., BERGAM, P., DI CICCO, A., HURBAIN, I., CICERO, A. L., DINGLI, F., PALMULLI, R., FORT, C., POTIER, M. C. & SCHURGERS, L. J. 2015. Apolipoprotein E regulates amyloid formation within endosomes of pigment cells. *Cell Reports,* 13**,** 43-51.

VAN NIEL, G., CHARRIN, S., SIMOES, S., ROMAO, M., ROCHIN, L., SAFTIG, P., MARKS, M. S., RUBINSTEIN, E. & RAPOSO, G. 2011. The tetraspanin CD63 regulates ESCRT-independent and -dependent endosomal sorting during melanogenesis. *Developmental Cell,* 21**,** 708-21.

VAN NIEL, G., PORTO-CARREIRO, I., SIMOES, S. & RAPOSO, G. 2006. Exosomes: a common pathway for a specialized function. *The Journal of Biochemistry,* 140**,** 13-21.

VAN POLL, D., PAREKKADAN, B., CHO, C. H., BERTHIAUME, F., NAHMIAS, Y., TILLES, A. W. & YARMUSH, M. L. 2008. Mesenchymal stem cell–derived molecules directly modulate hepatocellular death and regeneration in vitro and in vivo. *Hepatology,* 47**,** 1634-1643.

VAN RENSBURG, A. J., DAVIES, N. H., OOSTHUYSEN, A., CHOKOZA, C., ZILLA, P. & BEZUIDENHOUT, D. 2017. Improved vascularization of porous scaffolds through growth factor delivery from heparinized polyethylene glycol hydrogels. *Acta Biomaterialia,* 49**,** 89-100.

VANCE, J. E. & VANCE, D. E. 2008. *Biochemistry of lipids, lipoproteins and membranes*, Elsevier.

VELLA, L., HILL, A. & CHENG, L. 2016. Focus on extracellular vesicles: exosomes and their role in protein trafficking and biomarker potential in Alzheimer's and Parkinson's disease. *International Journal of Molecular Sciences,* 17**,** 173.

VERBREE-WILLEMSEN, L., ZHANG, Y.-N., GIJSBERTS, C. M., SCHONEVELD, A. H., WANG, J.-W., LAM, C. S., VERNOOIJ, F., BOTS, M. L., PEELEN, L. M. & GROBBEE, D. E. 2018. LDL extracellular vesicle coagulation protein levels change after initiation of statin therapy. Findings from the METEOR trial. *International Journal of Cardiology*.

VERGAUWEN, G., DHONDT, B., VAN DEUN, J., DE SMEDT, E., BERX, G., TIMMERMAN, E., GEVAERT, K., MIINALAINEN, I., COCQUYT, V. & BRAEMS, G. 2017. Confounding factors of ultrafiltration and protein analysis in extracellular vesicle research. *Scientific Reports,* 7**,** 2704.

VERWEIJ, F. J., BEBELMAN, M. P., JIMENEZ, C. R., GARCIA-VALLEJO, J. J., JANSSEN, H., NEEFJES, J., KNOL, J. C., DE GOEIJ-DE HAAS, R., PIERSMA, S. R. & BAGLIO, S. R. 2018. Quantifying exosome secretion from single cells reveals a modulatory role for GPCR signaling. *Journal of Cell Biology***,** jcb. 20170320601192018c.

VERWEIJ, F. J., REVENU, C., ARRAS, G., DINGLI, F., LOEW, D., PEGTEL, D. M., FOLLAIN, G., ALLIO, G., GOETZ, J. G. & ZIMMERMANN, P. 2019. Live tracking of inter-organ communication by endogenous exosomes in vivo. *Developmental Cell,* 48**,** 573-589. e4.

VESTAD, B., LLORENTE, A., NEURAUTER, A., PHUYAL, S., KIERULF, B., KIERULF, P., SKOTLAND, T., SANDVIG, K., HAUG, K. B. F. & OVSTEBO, R. 2017. Size and concentration analyses of extracellular vesicles by nanoparticle tracking analysis: a variation study. *Journal of Extracellular Vesicles,* 6**,** 1344087.

VICENCIO, J. M., YELLON, D. M., SIVARAMAN, V., DAS, D., BOI-DOKU, C., ARJUN, S., ZHENG, Y., RIQUELME, J. A., KEARNEY, J. & SHARMA, V. 2015. Plasma exosomes protect the myocardium from ischemia-reperfusion injury. *Journal of the American College of Cardiology,* 65**,** 1525-1536.

VICKERS, K. C., PALMISANO, B. T., SHOUCRI, B. M., SHAMBUREK, R. D. & REMALEY, A. T. 2011. MicroRNAs are transported in plasma and delivered to recipient cells by high-density lipoproteins. *Nature Cell Biology,* 13**,** 423.

VILLARROYA-BELTRI, C., BAIXAULI, F., MITTELBRUNN, M., FERNÁNDEZ-DELGADO, I., TORRALBA, D., MORENO-GONZALO, O., BALDANTA, S., ENRICH, C., GUERRA, S. & SÁNCHEZ-MADRID, F. 2016. ISGylation controls exosome secretion by promoting lysosomal degradation of MVB proteins. *Nature Communications,* 7**,** 13588.

VILLARROYA-BELTRI, C., GUTIERREZ-VAZQUEZ, C., SANCHEZ-CABO, F., PEREZ-HERNANDEZ, D., VAZQUEZ, J., MARTIN-COFRECES, N., MARTINEZ-HERRERA, D. J., PASCUAL-MONTANO, A., MITTELBRUNN, M. & SANCHEZ-MADRID, F. 2013. Sumoylated hnRNPA2B1 controls the sorting of miRNAs into exosomes through binding to specific motifs. *Nature Communications,* 4**,** 2980.

VILLEDA, S. A., PLAMBECK, K. E., MIDDELDORP, J., CASTELLANO, J. M., MOSHER, K. I., LUO, J., SMITH, L. K., BIERI, G., LIN, K. & BERDNIK, D. 2014. Young blood reverses age-related impairments in cognitive function and synaptic plasticity in mice. *Nature Medicine,* 20**,** 659.

VISHNUBHATLA, I., CORTELING, R., STEVANATO, L., HICKS, C. & SINDEN, J. 2014. The development of stem cell-derived exosomes as a cell-free regenerative medicine. *Journal of Circulating Biomarkers*.

VLASSOV, A. V., MAGDALENO, S., SETTERQUIST, R. & CONRAD, R. 2012. Exosomes: current knowledge of their composition, biological functions, and diagnostic and therapeutic potentials. *Biochimica et Biophysica Acta (BBA)-General Subjects,* 1820**,** 940-948.

WAHLGREN, J., KARLSON, T. D. L., BRISSLERT, M., SANI, F. V., TELEMO, E., SUNNERHAGEN, P. & VALADI, H. 2012. Plasma exosomes can deliver exogenous short interfering RNA to monocytes and lymphocytes. *Nucleic Acids Research***,** gks463.

WALDENSTRÖM, A. & RONQUIST, G. 2014. Role of exosomes in myocardial remodeling. *Circulation Research,* 114**,** 315-324.

WANG, F., LI, L., PIONTEK, K., SAKAGUCHI, M. & SELARU, F. M. 2018a. Exosome miR-335 as a novel therapeutic strategy in hepatocellular carcinoma. *Hepatology,* 67**,** 940-954.

WANG, J.-W., ZHANG, Y.-N., SZE, S., VAN DE WEG, S., VERNOOIJ, F., SCHONEVELD, A., TAN, S.-H., VERSTEEG, H., TIMMERS, L. & LAM, C. 2018b. Lowering low-density lipoprotein particles in plasma using dextran sulphate co-precipitates procoagulant extracellular vesicles. *International Journal of Molecular Sciences,* 19**,** 94.

WANG, J., HENDRIX, A., HERNOT, S., LEMAIRE, M., DE BRUYNE, E., VAN VALCKENBORGH, E., LAHOUTTE, T., DE WEVER, O., VANDERKERKEN, K. & MENU, E. 2014. Bone marrow stromal cell–derived exosomes as communicators in drug resistance in multiple myeloma cells. *Blood,* 124**,** 555-566.

WANG, K., FU, Q., CHEN, X., GAO, Y. & DONG, K. 2012. Preparation and characterization of pH-sensitive hydrogel for drug delivery system. *RSC Advances,* 2**,** 7772-7780.

WANG, T., FANG, L., ZHAO, F., WANG, D. & XIAO, S. 2018c. Exosomes mediate intercellular transmission of porcine reproductive and respiratory syndrome virus. *Journal of Virology,* 92**,** e01734-17.

WANG, T. & TURKO, I. V. 2018. Proteomic toolbox to standardize the separation of extracellular vesicles and lipoprotein particles. *Journal of Proteome Research,* 17**,** 3104-3113.

WANG, X., CHEN, Y., ZHAO, Z., MENG, Q., YU, Y., SUN, J., YANG, Z., CHEN, Y., LI, J. & MA, T. 2018d. Engineered exosomes with ischemic myocardium-targeting peptide for targeted therapy in myocardial infarction. *Journal of the American Heart Association,* 7**,** e008737.

WEBBER, J. & CLAYTON, A. 2013. How pure are your vesicles? *Journal of Extracellular Vesicles,* 2**,** 10.3402/jev.v2i0.19861.

WEI, J. X., LV, L. H., WAN, Y. L., CAO, Y., LI, G. L., LIN, H. M., ZHOU, R., SHANG, C. Z., CAO, J. & HE, H. 2015. Vps4A functions as a tumor suppressor by regulating the secretion and uptake of exosomal microRNAs in human hepatoma cells. *Hepatology,* 61**,** 1284-1294.

WEI, X., LIU, C., WANG, H., WANG, L., XIAO, F., GUO, Z. & ZHANG, H. 2016a. Surface phosphatidylserine is responsible for the internalization on microvesicles derived from hypoxia-induced human bone marrow mesenchymal stem cells into human endothelial cells. *Public Library of Science One,* 11**,** e0147360.

WEI, Z., BATAGOV, A. O., CARTER, D. R. & KRICHEVSKY, A. M. 2016b. Fetal bovine serum RNA interferes with the cell culture derived extracellular RNA. *Scientific Reports,* 6**,** 31175.

WELSH, J. A., HOLLOWAY, J. A., WILKINSON, J. S. & ENGLYST, N. A. 2017. Extracellular vesicle flow cytometry analysis and standardization. *Frontiers in Cell and Developmental Biology,* 5**,** 78.

WELTON, J. L., BRENNAN, P., GURNEY, M., WEBBER, J. P., SPARY, L. K., CARTON, D. G., FALCÓN-PÉREZ, J. M., WALTON, S. P., MASON, M. D., TABI, Z. & CLAYTON, A. 2016. Proteomics analysis of vesicles isolated from plasma and urine of prostate cancer patients using a multiplex, aptamer-based protein array. *Journal of Extracellular Vesicles,* 5**,** 31209-31209.

WELTON, J. L., WEBBER, J. P., BOTOS, L.-A., JONES, M. & CLAYTON, A. 2015. Ready-made chromatography columns for extracellular vesicle isolation from plasma. *Journal of Extracellular Vesicles,* 4**,** 27269.

WERMUTH, P., PIERA-VELAZQUEZ, S. & JIMENEZ, S. 2017. Exosomes isolated from serum of systemic sclerosis patients display alterations in their content of profibrotic and antifibrotic microRNA and

induce a profibrotic phenotype in cultured normal dermal fibroblasts. *Clinical and Experimental Rheumatology,* 35**,** 21-30.

WHITESIDE, T. L. 2016. Tumor-derived exosomes and their role in cancer progression. *Advances in Clinical Chemistry,* 74**,** 103-141.

WIECZOREK, M., ABUALROUS, E. T., STICHT, J., ÁLVARO-BENITO, M., STOLZENBERG, S., NOÉ, F. & FREUND, C. 2017. Major histocompatibility complex (MHC) class I and MHC class II proteins: Conformational plasticity in antigen presentation. *Frontiers in Immunology,* 8.

WIKLANDER, O., BOSTANCIOGLU, B., WELSH, J., ZICKLER, A. M., MURKE, F., FELLDIN, U., HAGEY, D., EVERTSSON, B., LIANG, X.-M. & CORSO, G. 2018. Systematic methodological evaluation of a multiplex bead-based flow cytometry assay for detection of extracellular vesicle surface signatures. *Frontiers in Immunology,* 9**,** 1326.

WILLIAMS, J. L., GATSON, N. N., SMITH, K. M., ALMAD, A., MCTIGUE, D. M. & WHITACRE, C. C. 2013. Serum exosomes in pregnancy-associated immune modulation and neuroprotection during CNS autoimmunity. *Clinical Immunology,* 149**,** 236-243.

WISNIEWSKI, J. R., ZOUGMAN, A., NAGARAJ, N. & MANN, M. 2009. Universal sample preparation method for proteome analysis. *Nature Methods,* 6**,** 359-62.

WOLF, P. 1967. The nature and significance of platelet products in human plasma. *British Journal of Haematology,* 13**,** 269-288.

WOLLERT, T., WUNDER, C., LIPPINCOTT-SCHWARTZ, J. & HURLEY, J. H. 2009. Membrane scission by the ESCRT-III complex. *Nature,* 458**,** 172-7.

WU, J., WANG, Y. & LI, L. 2017. Functional significance of exosomes applied in sepsis: A novel approach to therapy. *Biochimica et Biophysica Acta (BBA)-Molecular Basis of Disease,* 1863**,** 292-297.

WU, M., CHEN, C., WANG, Z., BACHMAN, H., OUYANG, Y., HUANG, P.-H., SADOVSKY, Y. & HUANG, T. J. 2019a. Separating extracellular vesicles and lipoproteins via acoustofluidics. *Lab on a Chip,* 19**,** 1174-1182.

WU, R., GAO, W., YAO, K. & GE, J. 2019b. Roles of exosomes derived from immune cells in cardiovascular diseases. *Frontiers In Immunology,* 10**,** 648.

WU, T., CHEN, Y., DU, Y., TAO, J., ZHOU, Z. & YANG, Z. 2018. Serum exosomal miR-92b-5p as a potential biomarker for acute heart failure caused by dilated cardiomyopathy. *Cellular Physiology and Biochemistry,* 46**,** 1939-1950.

WYSS-CORAY, T. 2016. Ageing, neurodegeneration and brain rejuvenation. *Nature,* 539**,** 180.

XIN, H., LI, Y., BULLER, B., KATAKOWSKI, M., ZHANG, Y., WANG, X., SHANG, X., ZHANG, Z. G. & CHOPP, M. 2012. Exosome-mediated transfer of miR-133b from multipotent mesenchymal stromal cells to neural cells contributes to neurite outgrowth. *Stem Cells,* 30**,** 1556-64.

XU, N., WANG, L., GUAN, J., TANG, C., HE, N., ZHANG, W. & FU, S. 2018. Wound healing effects of a Curcuma zedoaria polysaccharide with platelet-rich plasma exosomes assembled on chitosan/silk hydrogel sponge in a diabetic rat model. *International Journal of Biological Macromolecules,* 117**,** 102-107.

YAMADA, T., INOSHIMA, Y., MATSUDA, T. & ISHIGURO, N. 2012. Comparison of methods for isolating exosomes from bovine milk. *Journal of Veterinary Medical Science***,** 12-0032.

YAMAGUCHI, T., IZUMI, Y., NAKAMURA, Y., YAMAZAKI, T., SHIOTA, M., SANO, S., TANAKA, M., OSADA-OKA, M., SHIMADA, K., MIURA, K., YOSHIYAMA, M. & IWAO, H. 2015. Repeated remote ischemic conditioning attenuates left ventricular remodeling via exosome-mediated intercellular communication on chronic heart failure after myocardial infarction. *Internation Journal of Cardiology,* 178**,** 239-46.

YÁÑEZ-MÓ, M., SILJANDER, P. R.-M., ANDREU, Z., BEDINA ZAVEC, A., BORRÀS, F. E., BUZAS, E. I., BUZAS, K., CASAL, E., CAPPELLO, F. & CARVALHO, J. 2015. Biological properties of extracellular vesicles and their physiological functions. *Journal of Extracellular Vesicles,* 4**,** 27066.

YANG, Y., LIU, Q., LU, J., ADAH, D., YU, S., ZHAO, S., YAO, Y., QIN, L. & CHEN, X. 2017. Exosomes from Plasmodium-infected hosts inhibit tumor angiogenesis in a murine Lewis lung cancer model. *Oncogenesis,* 6**,** e351.

YE, Q., ZÜND, G., BENEDIKT, P., JOCKENHOEVEL, S., HOERSTRUP, S. P., SAKYAMA, S., HUBBELL, J. A. & TURINA, M. 2000. Fibrin gel as a three dimensional matrix in cardiovascular tissue engineering. *European Journal of Cardio-Thoracic Surgery,* 17**,** 587-591.

YE, W., TANG, X., YANG, Z., LIU, C., ZHANG, X., JIN, J. & LYU, J. 2017. Plasma-derived exosomes contribute to inflammation via the TLR9-NF-κB pathway in chronic heart failure patients. *Molecular Immunology,* 87**,** 114-121.

YENTRAPALLI, R., MERL-PHAM, J., AZIMZADEH, O., MUTSCHELKNAUS, L., PETERS, C., HAUCK, S. M., ATKINSON, M. J., TAPIO, S. & MOERTL, S. 2017. Quantitative changes in the protein and miRNA cargo of plasma exosome-like vesicles after exposure to ionizing radiation. *International Journal of Radiation Biology,* 93**,** 569-580.

YEO, R. W., LAI, R. C., ZHANG, B., TAN, S. S., YIN, Y., TEH, B. J. & LIM, S. K. 2013. Mesenchymal stem cell: an efficient mass producer of exosomes for drug delivery. *Advanced Drug Delivery Reviews,* 65**,** 336-41.

YIP, H.-K., CHEN, K.-H., DUBEY, N. K., SUN, C.-K., DENG, Y.-H., SU, C.-W., LO, W.-C., CHENG, H.-C. & DENG, W.-P. 2019. Cerebro-and renoprotective activities through platelet-derived biomaterials against cerebrorenal syndrome in rat model. *Biomaterials***,** 119227.

YOSHIOKA, Y., KONISHI, Y., KOSAKA, N., KATSUDA, T., KATO, T. & OCHIYA, T. 2013. Comparative marker analysis of extracellular vesicles in different human cancer types. *Journal of Extracellular Vesicles,* 2**,** 10.3402/jev.v2i0.20424.

YOU, B., XU, W. & ZHANG, B. 2018. Engineering exosomes: a new direction for anticancer treatment. *American Journal of Cancer Research,* 8**,** 1332-1342.

YU, B., ZHANG, X. & LI, X. 2014. Exosomes derived from mesenchymal stem cells. *International Journal of Molecular Sciences,* 15**,** 4142-4157.

YU, S., LIU, C., SU, K., WANG, J., LIU, Y., ZHANG, L., LI, C., CONG, Y., KIMBERLY, R., GRIZZLE, W. E., FALKSON, C. & ZHANG, H. G. 2007. Tumor exosomes inhibit differentiation of bone marrow dendritic cells. *The Journal of Immunology,* 178**,** 6867-75.

YU, Y. M., GIBBS, K. M., DAVILA, J., CAMPBELL, N., SUNG, S., TODOROVA, T. I., OTSUKA, S., SABAAWY, H. E., HART, R. P. & SCHACHNER, M. 2011. MicroRNA miR-133b is essential for functional recovery after spinal cord injury in adult zebrafish. *European Journal of Neuroscience,* 33**,** 1587-1597.

YUANA, Y., KONING, R. I., KUIL, M. E., RENSEN, P. C., KOSTER, A. J., BERTINA, R. M. & OSANTO, S. 2013. Cryo-electron microscopy of extracellular vesicles in fresh plasma. *Journal of Extracellular Vesicles,* 2.

YUANA, Y., LEVELS, J., GROOTEMAAT, A., STURK, A. & NIEUWLAND, R. 2014. Co-isolation of extracellular vesicles and high-density lipoproteins using density gradient ultracentrifugation. *Journal of Extracellular Vesicles,* 3**,** 23262.

YUANA, Y., OOSTERKAMP, T. H., BAHATYROVA, S., ASHCROFT, B., GARCIA RODRIGUEZ, P., BERTINA, R. M. & OSANTO, S. 2010. Atomic force microscopy: a novel approach to the detection of nanosized blood microparticles. *Journal of Thrombosis and Haemostasis,* 8**,** 315-23.

ZABEO, D., CVJETKOVIC, A., LÄSSER, C., SCHORB, M., LÖTVALL, J. & HÖÖG, J. L. 2017. Exosomes purified from a single cell type have diverse morphology. *Journal of Extracellular Vesicles,* 6**,** 1329476.

ZARJOU, A., KIM, J., TRAYLOR, A. M., SANDERS, P. W., BALLA, J., AGARWAL, A. & CURTIS, L. M. 2010. Paracrine effects of mesenchymal stem cells in cisplatin-induced renal injury require heme oxygenase-1. *American Journal of Physiology-Renal Physiology,* 300**,** F254-F262.

ZHANG, C., ADAMOS, C., OH, M.-J., BARUAH, J., AYEE, M. A., MEHTA, D., WARY, K. K. & LEVITAN, I. 2017. oxLDL induces endothelial cell proliferation via Rho/ROCK/Akt/p27kip1 signaling: opposite effects of oxLDL and cholesterol loading. *American Journal of Physiology-Cell Physiology,* 313**,** C340-C351.

ZHANG, J., GUAN, J., NIU, X., HU, G., GUO, S., LI, Q., XIE, Z., ZHANG, C. & WANG, Y. 2015. Exosomes released from human induced pluripotent stem cells-derived MSCs facilitate cutaneous wound healing by promoting collagen synthesis and angiogenesis. *Journal of Translational Medicine,* 13**,** 1.

ZHANG, K., ZHAO, X., CHEN, X., WEI, Y., DU, W., WANG, Y., LIU, L., ZHAO, W., HAN, Z., KONG, D., ZHAO, Q., GUO, Z., HAN, Z., LIU, N., MA, F. & LI, Z. 2018. Enhanced therapeutic effects of mesenchymal stem cell-derived exosomes with an injectable hydrogel for hindlimb ischemia treatment. *ACS Applied Materials & Interfaces,* 10**,** 30081-30091.

ZHANG, Z., YANG, J., YAN, W., LI, Y., SHEN, Z. & ASAHARA, T. 2016. Pretreatment of cardiac stem cells with exosomes derived from mesenchymal stem cells enhances myocardial repair. *Journal of the American Heart Association,* 5**,** e002856.

ZHENG, T., PU, J., CHEN, Y., MAO, Y., GUO, Z., PAN, H., ZHANG, L., ZHANG, H., SUN, B. & ZHANG, B. 2017. Plasma exosomes spread and cluster around β-amyloid plaques in an animal model of Alzheimer's disease. *Frontiers in Aging Neuroscience,* 9**,** 12.

ZHU, M., LI, Y., SHI, J., FENG, W., NIE, G. & ZHAO, Y. 2012. Exosomes as extrapulmonary signaling conveyors for nanoparticle-induced systemic immune activation. *Small,* 8**,** 404-12.

ZHUANG, X., XIANG, X., GRIZZLE, W., SUN, D., ZHANG, S., AXTELL, R. C., JU, S., MU, J., ZHANG, L. & STEINMAN, L. 2011. Treatment of brain inflammatory diseases by delivering exosome encapsulated anti-inflammatory drugs from the nasal region to the brain. *Molecular Therapy,* 19**,** 1769-1779.

ZISCH, A. H., LUTOLF, M. P., EHRBAR, M., RAEBER, G. P., RIZZI, S. C., DAVIES, N., SCHMOKEL, H., BEZUIDENHOUT, D., DJONOV, V. & ZILLA, P. 2003. Cell-demanded release of VEGF from synthetic, biointeractive cell ingrowth matrices for vascularized tissue growth. *The FASEB Journal,* 17**,** 2260-2262.

ZONNEVELD, M. I., BRISSON, A. R., VAN HERWIJNEN, M. J., TAN, S., VAN DE LEST, C. H., REDEGELD, F. A., GARSSEN, J., WAUBEN, M. H. & NOLTE-'T HOEN, E. N. 2014. Recovery of extracellular vesicles from human breast milk is influenced by sample collection and vesicle isolation procedures. *Journal of Extracellular Vesicles,* 3.

ZOU, J., MO, X., SHI, Z., LI, T., XUE, J., MEI, G. & LI, X. 2016. A prospective study of platelet-rich plasma as biological augmentation for acute achilles tendon rupture repair. *BioMed Research International,* 2016**,** 9364170-9364170.

APPENDICES

Appendix 1: Size exclusion chromatography of fresh fasted serum

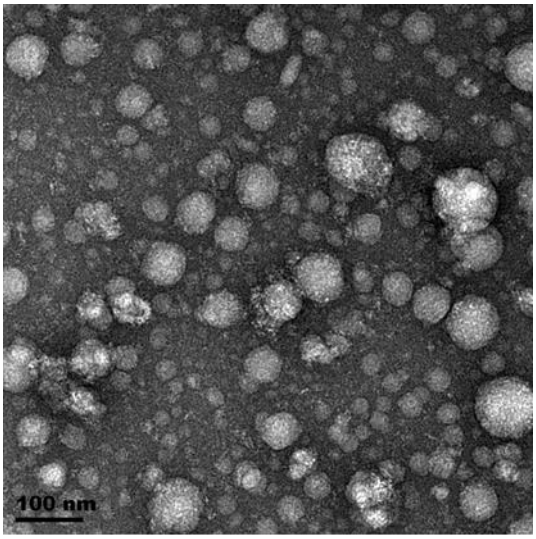

Figure A1: TEM micrograph of exosomes purified from fresh fasted human serum using SEC. Scale bar = 100 nm.

Appendix 2: ExoQuick precipitation followed by size exclusion chromatography

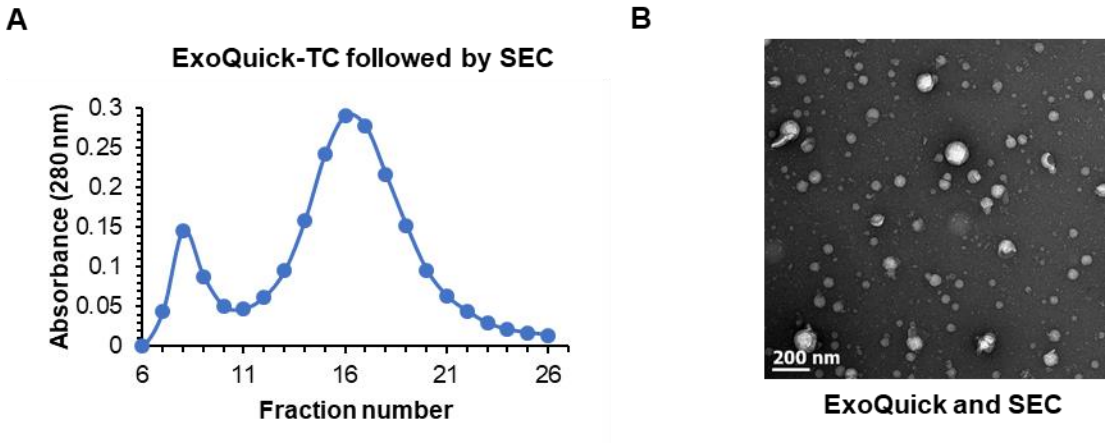

Figure A2: Exosomes purified from pooled human serum using ExoQuick-TC followed by SEC. (A) Absorbance profile of ExoQuick isolated exosomes from 500 µl human serum and the resuspended exosome pellet was loaded onto the SEC column; (B) TEM micrograph of exosomes purified from pooled human serum using ExoQuick-TC followed by SEC. Scale bar = 200 nm.

Appendix 3: Stabilisation of fluorescently labelled exosomes

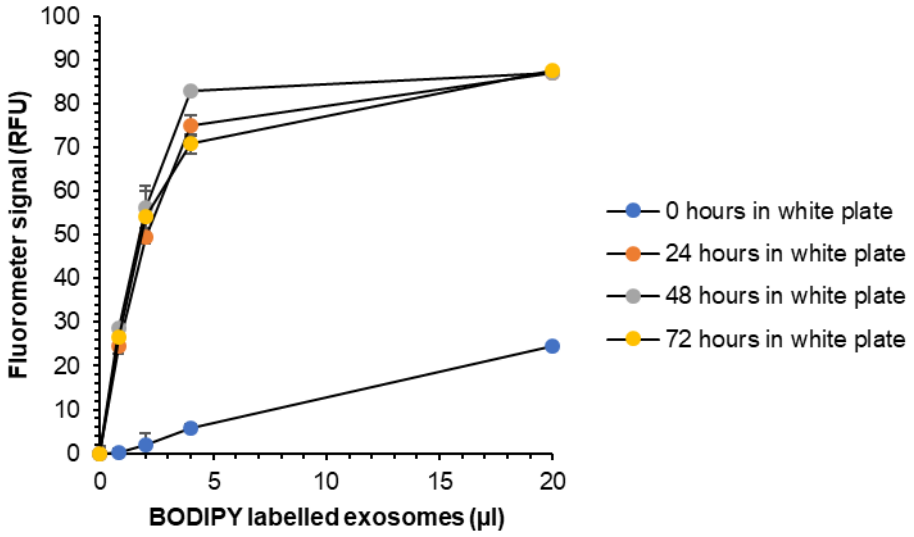

Figure A3: Standardising the standard curve generated from dilutions of BODIPY TR Ceramide labelled SEC-derived exosomes. Fluorescently labelled exosomes required storage for at least 24 prior to stabilising. Three technical repeats.

Appendix 4: TEM analysis of LDL

Table A4: TEM image analysis of LDL

	Average vesicle size (nm)	Min vesicle size (nm)	Max vesicle size (nm)
LDL	21.7 ±2.5	13.9	27.8

Appendix 5: Nanoparticle tracking analysis

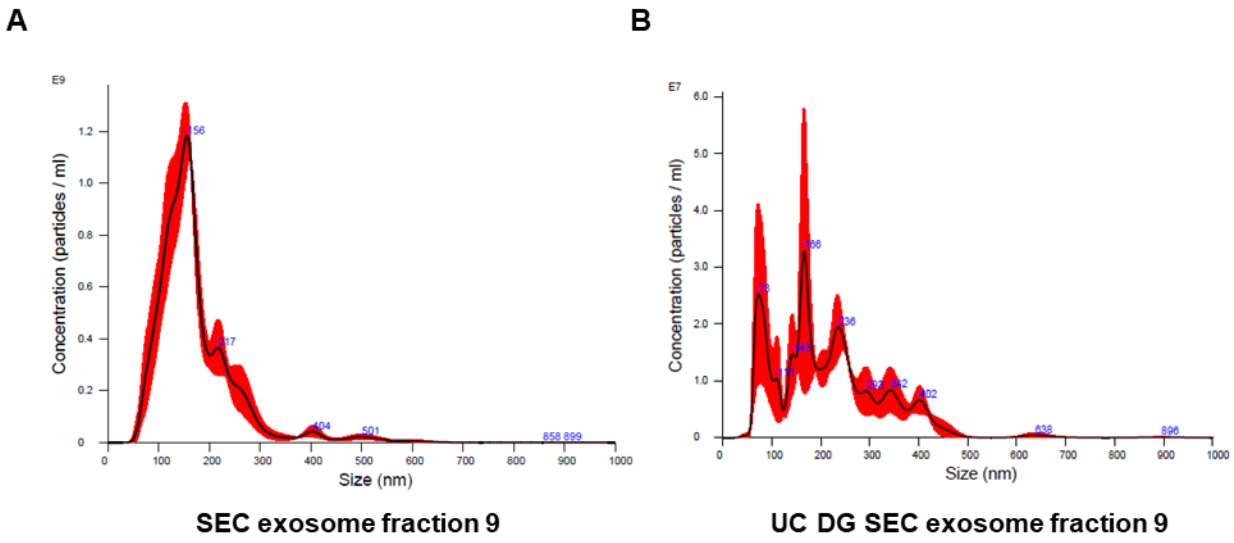

Figure A5: Representative graph of particles/ml vs particle diameter (nm) from a nanoparticle tracking analysis report. (A) SEC exosome fraction 9; (B) UC DG SEC exosome fraction 9. The graph represents the mean of 5 runs measured.

Appendix 6: Mass spectrometry data

Appendix 6: Mass spectrometry data of Funrich analysis (SEC and UC DG SEC), SEC and UC DG SEC proteins and Venn diagram with Karimi *et al.* is found in the database site, see https://zivahub.uct.ac.za/s/2ea2a5888a295dbd50bc

Appendix 7: Flow cytometric analysis of isolated HUVECs

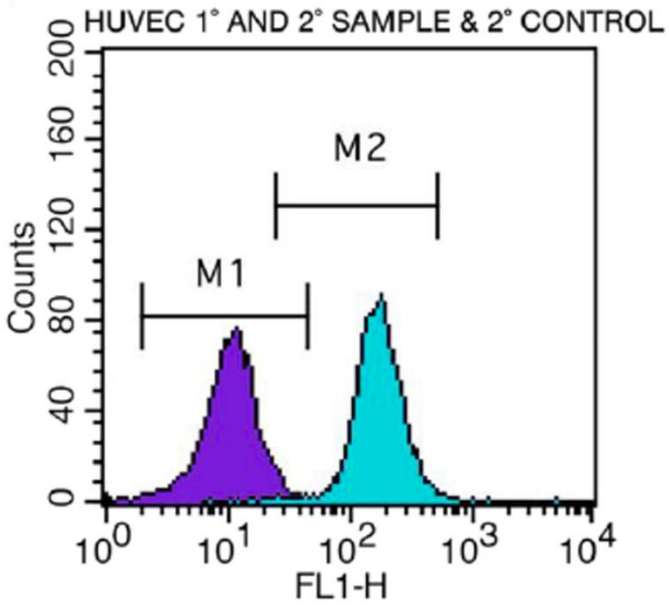

Figure A7: Flow cytometric analysis of isolated HUVECs. Histograms showing secondary (2°) antibody control (2° antibody alone, purple peak) and the primary anti-CD31 antibodies (1°) and 2° antibody sample (1° and 2°, turquoise peak).